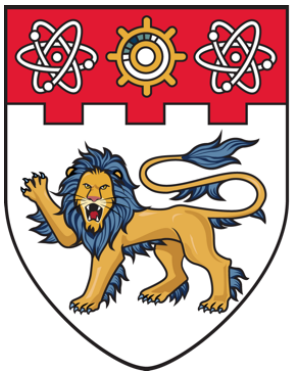

NANYANG TECHNOLOGICAL UNIVERSITY
SINGAPORE

DEVELOPMENT OF PNP PINCER LIGANDS AND THEIR METAL COMPLEXES VIA PD(II)-CATALYZED P(III)-C BOND FORMATION

FOO CE QING

SCHOOL OF PHYSICAL AND MATHEMATICAL SCIENCES

2021

DEVELOPMENT OF PNP PINCER LIGANDS AND THEIR METAL COMPLEXES VIA PD(II)-CATALYZED P(III)-C BOND FORMATION

FOO CE QING

SCHOOL OF PHYSICAL AND MATHEMATICAL SCIENCES

A thesis submitted to the Nanyang Technological University in partial fulfilment of the requirement for the degree of Doctor of Philosophy

2021

Statement of Originality

I hereby certify that the work embodied in this thesis is the result of original research done by me except where otherwise stated in this thesis. The thesis work has not been submitted for a degree or professional qualification to any other university or institution. I declare that this thesis is written by myself and is free of plagiarism and of sufficient grammatical clarity to be examined. I confirm that the investigations were conducted in accord with the ethics policies and integrity standards of Nanyang Technological University and that the research data are presented honestly and without prejudice.

09/08/2021

. . . . . .

Date

. . . . . .

Foo Ce Qing

Supervisor Declaration Statement

I have reviewed the content and presentation style of this thesis and declare it of sufficient grammatical clarity to be examined. To the best of my knowledge, the thesis is free of plagiarism and the research and writing are those of the candidate's except as acknowledged in the Author Attribution Statement. I confirm that the investigations were conducted in accord with the ethics policies and integrity standards of Nanyang Technological University and that the research data are presented honestly and without prejudice.

09/08/2021

. . . . . .

Date

. . . . . .

Leung Pak-Hing

09/08/2021

. . . . . .

Date

. . . . . .

Sumod A. Pullarkat

Authorship Attribution Statement

This thesis contains material from 1 paper published in the following peer-reviewed journal in which I am listed as an author.

Chapter 2 is published as Foo, C. Q.; Sadeer, A.; Li, Y.; Pullarkat, S. A.; Leung, P.-H., Access to C-Stereogenic PN (sp 2) P Pincer Ligands via Phosphapalladacycle Catalyzed Asymmetric Hydrophosphination. *Organometallics* **2021,** *40* (6), 682-692. DOI: 10.1021/acs.organomet.0c00783.

The contributions of the co-authors are as follows:

- Prof. P-H. Leung and Dr. S.A. Pullarkat decided on the research topic and provided supplementary experimental suggestions along the way.
- I prepared the manuscript drafts. The drafts were proofread and revised by Prof. P-H Leung and Dr. S.A. Pullarkat.
- I designed the study together with A. Sadeer through implementing rational experimental improvisations for the optimization of the reaction. All laboratory work were conducted by me at the School of Physical and Mathematical Sciences.
- I synthesized all starting materials required for screening reactions. A. Sadeer provided me with the catalysts.
- All characterization data were gathered by me. A. Sadeer assisted me with the processing and analyses of the collected data to generate the Supporting Information. All NMR, HRMS and XRD data were obtained from the Central Facilities Lab in the School of Physical and Mathematical Sciences.
- Dr. Y. Li performed the X-Ray Diffraction analysis and provided the resolved structural elucidation data files.

09/08/2021

. . . .

Date

Foo Ce Qing

Table of Contents

Dedicated to my dearest grandmother

Abstract

The scene of transition metal catalysis has seen a ubiquitous employment of chiral tertiary phosphines as effective partnering ligand auxiliaries. These are represented in a diverse range of reaction applications, with a plethora of examples illustrating the multifaceted modes of coordination that the phosphine moieties can adopt to suit the requirements of different reactions. To this end, pincer-type tridentate tertiary phosphines have since emerged as a ligand class of its own, facilitating good efficacies in their respective domains of applications yet at the same time providing high stability to the overall complex architecture. Despite these advantageous characteristics, issues associated with their convenient syntheses have remained as a persistent problem particularly for the access towards related asymmetric variants. Herein, asymmetric hydrophosphination is exemplified as a highly viable and effective alternative methodology for the syntheses of optically pure chiral tertiary phosphines, with focus directed specifically at the generation of PN(sp^2)P tridentates that have been considerably elusive in the literature. The synthesized diphosphine adducts are further examined for their compatibility in complexation reactions with various transition metal precursors, and a comprehensive discussion is provided to assess the structural characteristics of the furnished complexes.

Acknowledgements

This journey has been an enriching and humbling experience to which I am fortunate to have had many supporting figures following and guiding me through. My first appreciation goes to my beloved family, for providing unconditional support in everything I do and ensuring me that they are behind my back in all the decisions and choices I make. I am always at ease knowing that they are constantly there for me in whatever circumstances may be.

I am especially thankful to my main supervisor Prof. Leung Pak-Hing, for allowing me to have full reign to venture on my own research ideas, yet at the same time steering me back to the appropriate direction when the need arises. I am grateful for the trust encompassed within this freedom of exploration that he has provided to let me learn and grow on my own.

The same appreciation extends to my co-supervisor Dr. Sumod A. Pullarkat, who kindly provided me with the opportunity to kickstart my research stint in the group as an undergraduate. Not to mention the prompt support that he always offers in all areas of research and school matters, as well as the constant check-ins to make sure that everything is going on track. It was always comforting to be able to receive his warm helping hand whenever and wherever needed.

I would most definitely like to thank my friends in lab – Sadeer, Jia Sheng, Wee Shan, Jeffery and Ronald, for all the help and advice that they have rendered. I am forever indebted to all the times that they have set aside to lend assistance to me despite their own busy schedules. A great adventure is made better with good companions, and I am really glad to have had them alongside me in this journey to make things that much more enjoyable.

A special mention goes to a cherished friend Tiff, who has been a great pillar of support and source of encouragement. Not forgetting the constructive comments that she always provides with vocabulary and grammar corrections in my writings. I am utterly grateful for her unwavering presence and support throughout all this while, especially in times when things may have been a little less easy-going.

Lastly, I would like to express gratitude to my Thesis Advisory Committee members Prof. Leong Weng Kee and Prof. Yan Yaw Kai, for always accommodating their time to listen to my project updates and never failing to give insightful suggestions to improve the research direction. I would also like to thank the staff from the Central Equipment Lab - Ee Ling, Dr. Li Yongxin and Wen Wei for being ever so helpful with their assistance in the various equipment related enquiries and requests I needed from them. Finally, I would like to thank Nanyang Technological University for providing me with a research scholarship to pursue this study programme.

Summary

This thesis documents the development of PN(sp^2)P tertiary diphosphine moieties from their syntheses to complexation as tridentate pincer-type ligands.

Chapter 1 introduces the synthetic relevance and utility of chiral tertiary phosphines in transition metal based catalytic applications. This covers a thorough presentation on the developmental progress of their incorporation as simple monodentates to structurally more defined bi- and tridentates, illustrating the varying properties of these synthons as compatible and effective ligand precursors for different metal mediated reactions. Representative methods for the preparation of chiral tertiary phosphines via catalytic and non-catalytic pathways are also included to reveal certain associated advantages and limitations ascribed to the respective synthetic methodologies. Finally, the underlying aims and objectives are identified to provide the guiding directions for the research outline.

In Chapter 2, the asymmetric hydrophosphination reaction is first shortlisted as a viable alternative method for the generation of chiral tertiary phosphines. This is accompanied with an overview of recent developments and progress in the field, as well as significant achievements accomplished by our group within the research domain. The benefits of the protocol are also highlighted with respect to its record profiles of excellent reactivity and functional group tolerance, coupled with an environmentally sustainable perspective of a one-pot, fully atom economic process. An extension of this procedure employing palladacycle based catalysts unveils a highly enantioselective synthesis of a series of pyridyl based PN(sp^2)P diphosphine adducts bearing central *C*-stereogenicity. Proposals for the reaction mechanism as well as the origins of a stereoselective addition process are discussed based on rationalizations of the catalyst-to-substrate

behaviors. A further expansion of scope with pyrrolyl based analogues is showcased to discern the efficacy of the reaction towards electronically more challenging substrates. Additionally, a preliminary formation of a pyrrolyl based PN(sp^2)P diphosphine palladium(II) complex serves as a proof of concept to decipher the compatibility of the structural motif as suitable ligand auxiliaries.

In Chapter 3, a comprehensive assessment on a selected derivative of the synthesized pyridyl diphosphines as compatible neutral tridentate, pincer-type ligands on various metal centers is uncovered. This comprises of complexation trials with metal precursors from the first to third row of transition metal elements belonging in Group 8, 9 and 10. Detailed discussions on the structural characteristics of individual complexes are provided based on solid and solution state analyses wherever possible. These include certain limitations of the furnished PN(sp^2)P diphosphine moieties as coordinative partners to different metal precursors, and the corresponding adjustments that are implemented to manage these complications. Comparisons made on the furnished complexes reveal unexpected structural distinctions between congeners from the same group, as well as different reactivity characteristics with related examples in the literature. Supplementary experimental efforts to synthesize diastereomerically pure complexes are also exemplified, together with trials to activate pure rhodium(III) complexes for potential utility.

In Chapter 4, an overall perspective of the results hitherto garnered are reiterated to emphasize the accomplishments made towards the targeted research aims and objectives set in Chapter 1. Suggestions for future work based on unfinished endeavors in Chapters 2 and 3 are also briefly stated to outline further potential expansions for the work.

Chapter 1

Introduction

Since its early years of inception, catalysis has continuously remained as a vibrant area of research by chemists worldwide.[1] The phenomenal outcome of incorporating just minute amounts of a chemical additive (i.e. catalyst) in promoting the discovery and modifications of diverse chemical reactions, showcases the remarkable feat that catalysis has displayed in the realm of science. The inherent ability of a catalyst to render reaction progressions at faster rates yet staying chemically unchanged and therefore recyclable at the end of a reaction cycle, further adds to the practicality of catalysis as a cost and time efficient protocol. As such, the prevalence of catalysis today is not just limited to the fields of fundamental research, but also in vast frontiers of modern chemical manufacturing processes such as pharmaceutical,[2] material,[3] and even environmental applications.[4]

Among the different classes of catalyst types, transition metal based complexes represent one of the most extensively studied category of catalysts available in the chemical library.[5] This can be attributed to certain preferential features that such complexes provide, which fulfill either chemical or physical requirements of typical catalytic reactions. In particular, the complementary characteristic of good stability and high reactivity of these compounds enables the ease of their utilization without compromising on reaction rates. Other valuable traits include oxidation state variability as well as specific reaction selectivity, for which have proven to be pivotal in medicinal and biological applications.[6] In conjunction with this, larger emphasis has also been proliferated towards the exploration of asymmetric metal mediated catalysis, in the aims of furnishing new chiral adducts which may be tested for their drug delivery capabilities in existing medical

conditions.[7] With such prospective scientific insights left to be unraveled, transition metal catalysis retains its good position for continual assessment to unveil further potential applications. However, beyond the literal definition of metal mediated catalysis, the bigger picture lies within another equally important component that has yet to be accounted for thus far.

As the term “metal complex” suggests, a transition metal based catalyst consists of more than just the metal center itself. Indeed, as much as a snail is incomplete without its shell, a metal complex would only properly exist with the supplementation of a compatible set of ligands surrounding the metal center. In this aspect, the importance of the presiding ligands cannot be further underscored in the way which they determine the overall chemical state of the metal complex. Aside from providing stability, the more pertinent role that the ligands undertake is their influence on critical factors such as reactivity and selectivity characteristics of the complex.[8] This mainly arises from the steric and electronic properties innate to individual ligand systems,[9] which would eventually be translated to the furnished metal complex when the ligands are affixed onto the metal center. Consequently, ligand compatibility is by default, an essential consideration factor for catalyst design to provide for an optimized metal complex that is both structurally and chemically suitable for reaction. The current molecular library however contains a plethora of ligand types described in the literature, which would be too overly comprehensive to fully cover. In the context of this thesis, the focus would be on phosphorus(III) based ligand systems, with specific attention towards chiral tertiary phosphines of the type PR_3 and their cooperative utility with transition metals for catalyzing asymmetric reactions.

The rise in popularization for the employment of phosphine-metal complexes in catalysis can be credited to certain favorable aspects that phosphine ligands in general, impart onto the metal complex. As previously mentioned, the appropriate combination of both ligand and metal components is imperative to facilitate proper chemical functionality of the resultant complex, and phosphines satisfy this in several ways. Firstly, the presence of a free lone pair of electrons on phosphorus conveys a strong σ-donating capability, which promotes a high affinity mode of coordination. Additionally, phosphines also contain empty σ* orbitals which can accept electrons via backdonation from low valent, electron rich metal centers.[10] This duality feature of phosphines is especially useful for catalytic reactions involving redox processes, in terms of electronic stabilization of metal intermediates adopting variable oxidation states throughout the course of the reaction.[11] In turn, these serve to prevent catalyst deactivation arising from complex decomposition in their highly reactive intermediary states, thereby ensuring constant catalytic activity. Secondly, phosphines display high ligand field strengths, which further aids in stabilizing metals electronically as their d electrons are filled in lower energy orbitals.[12]

In another aspect, steric properties of phosphines also play an evident role in affecting the overall chemical characteristics of the metal complex. The effect would expectedly be more pronounced in tertiary phosphines which are accompanied by three peripheral substituent groups directly on the binding phosphorus atom. Typically, the relative bulkiness of the phosphine ligand can be easily moderated by simply modifying the substituents attached.[13] In the case of chelating phosphines, amending this parameter inherently alters the bite angles associated with the ligand, which again changes the chemical outlook of the metal complex (more elaboration will be provided in a later section of this chapter).[14] Furthermore, inductive electronic differences derived from varying substituent groups would likewise be experienced by the metal complex as the ligand

moieties are modified. In fact, experimental studies conducted to perceive the steric and electronic effects of phosphine based ligands have shown concomitant impacts of both factors on the variation of catalytic functionality.[15] For instance, coupling the typical steric demands of tertiary phosphines together with their exhibition of a fairly high *trans* effect from strong electronic donation, the accommodation of multiple phosphine ligands on the same metal atom is therefore discouraged.[16] Such influences prove vital to a catalytic system as they free up vacant sites on the metal center necessary for substrate coordination and activation. With a wide array of substituted tertiary phosphines available for synthesis and thus limitless avenues for ligand customization, the inexhaustive utility of phosphine based ligand systems presents an enormous potential area for exploration in the field of metal mediated catalysis.

1.1. Monodentate tertiary phosphines

Monodentate phosphines represent the most straightforward class of phosphines in the way which they interact with a metal center, whereby the steric and electronic properties of the phosphine ligand are promptly translated to the metal. For the former, the substrate-metal binding pocket is directly related to the proportional steric bulk of the substituents on the phosphine ligand, which is usually quantified from the determination of its cone angle.[17] In turn, this defines the directionality of how the incoming substrate can interact with the complex, depending on the size and orientation of the substituents. Likewise for the latter, immediate electronic inductive effects from the closely bound substituents also affect the overall electron density of the metal center,[18] consequentially influencing the susceptibilities of the complex to different electronic transition reactions.

The history of tertiary phosphines dates back to the 19th century with initial synthetic discoveries of trimethylphosphine (PMe_3) and triethylphosphine (PEt_3) made by Paul Thenard and Ferdinand Berle respectively.[16, 19] These were synonymously prepared by passing the individual alkylic chloride through a metallic phosphide at heated temperatures, and they represent the first tertiary monophosphines to be synthetically unfounded. Despite this, further experimental explorations towards tertiary phosphine syntheses were however met with lackluster attention before the realization of parallel chemical behaviors that phosphines demonstrate with respect to their amine counterparts. Thereafter in the same timeframe, phosphine complexations to salts of the platinum group metals were subsequently accomplished by the efforts of Hofmann, Cahours and Gal (Figure 1.1).[19-20]

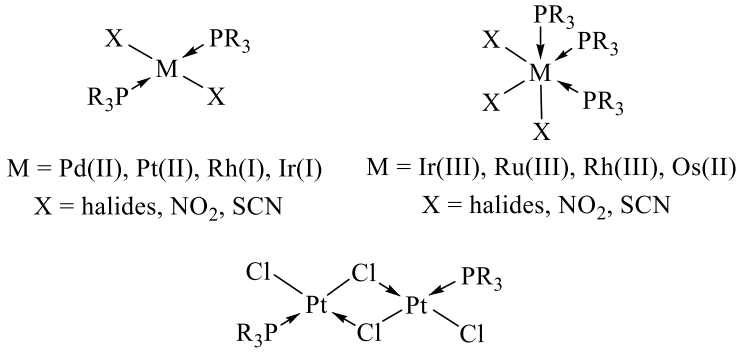

Figure 1.1. Initial examples of phosphine complexation to platinum group metals.

While the next couple of decades then saw increased attention towards tertiary phosphine syntheses and complexation, most of these revolved around structural elucidation and comprehension studies of the furnished compounds.[21] It was only up till the middle of the 20th century whereby the first instances of phosphine-metal complexes showcasing manifestations of catalytic property were disclosed by Reppe and Schweckendiek. Their work introduced the reactivity capacities of various nickel-phosphine complexes in polymerization and cycloaddition

reactions of olefinic substrates, with particular highlight of nickel complexes bearing triphenylphosphine ligands executing comparatively better efficiencies (Scheme 1.1).[16, 22]

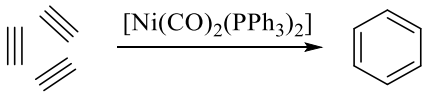

Scheme 1.1. Cycloaddition of alkynes with nickel-PPh_3 complexes.

The onset of this discovery in revealing the catalytic possibilities that can be achieved with metal-phosphine complexes fueled the interest of both academic and industrial institutions alike, thereby setting the stage for intensive research directed at the syntheses of these complexes for catalytic applications.

Following the successful implementation of related complexes in various reactions aside from those stated above,[16] the next major breakthrough that came about for phosphine-metal mediated catalysis was the hydrogenation reaction of alkenes enabled by Wilkinson's catalyst.[23] The significance of this newfound potential of phosphine-metal complexes was further extended when Knowles and Horner reported the first examples of an asymmetric transition metal catalyzed reaction involving the hydrogenation of prochiral olefins (Scheme 1.2).[24]

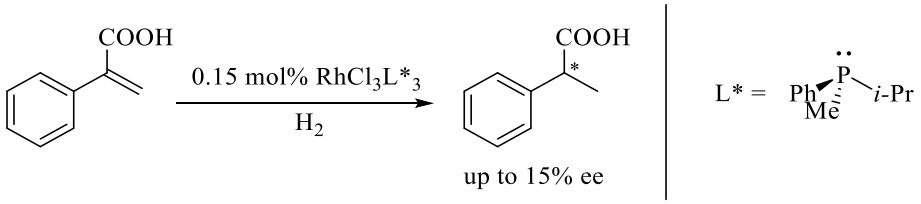

Scheme 1.2. First illustration of asymmetric hydrogenation with a chiral phosphine-metal complex.

In both cases, the tertiary *P*-chiral methylpropylphenylphosphine was used as the chiral auxiliary to mediate the asymmetric reaction, enabling the furnishing of the hydrogenated adduct in up to

15% enantiomeric excess. Apart from granting access to otherwise previously unfounded chiral synthetic pathways, subsequent endeavors of phosphine-metal catalyzed asymmetric reactions built upon these prior works also shed light onto the selectivity properties of such phosphine complexes. This was exemplified by Morrison and co-workers, who noted that the chirogenic center can be localized away from the phosphorus atom onto adjacent parts of the skeletal structure, and still deliver chiral inductions with better effectiveness (Figure 1.2).[25]

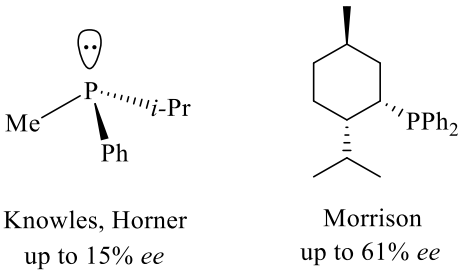

Figure 1.2. Chiral monophosphines used in seminal asymmetric hydrogenation reactions.

Today, developments in the employment of chiral monodentate tertiary phosphines for asymmetric reactions have led to the syntheses of more structurally profound ligands comprised of biaryl components. These represent an extensive library of axially chiral monodentate phosphines which have proven to be highly effective ligands in a multitude of transition metal catalyzed reactions (Figure 1.3).[11, 26]

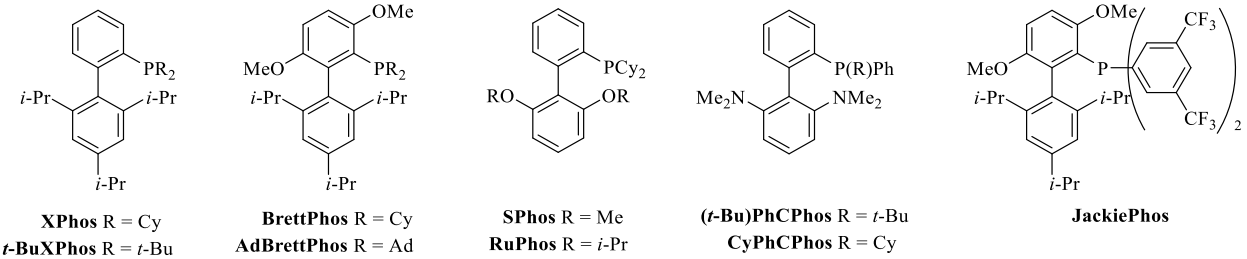

Figure 1.3. Selected examples of axially chiral monodentate tertiary phosphines.

The characteristic feature of such biaryl ligands is largely embodied in the presence of multiple substituent groups situated on both the top and bottom aryl rings. Noticeably, the R groups on the phosphorus atom generally consist of relatively bulky electron donating moieties, which provide various support functionalities that are crucial for optimal reactivity. One such vital functionality derived from these substituents is their ability to facilitate oxidative addition processes by virtue of increasing the electron density on the metal center, yet at the same time promote reductive elimination as a result of their steric hindrance.[27] Furthermore, these steric demands also enhances stability to the ligand itself by retarding the propensity of phosphorus oxidation, which positively contributes to their synthetic practicality as these compounds can be stored and used under ambient conditions.[27]

Other variants of chiral monodentate tertiary phosphines also include ferrocenylphosphines bearing multiple chiral centers incorporating both ferrocenyl planar chirality and substituent based central chirality.[28] This occurs when different substituents are incorporated at the 1,2 positions of the ferrocenyl backbone, which results in the loss of the ferrocenyl plane of symmetry (Figure 1.4).

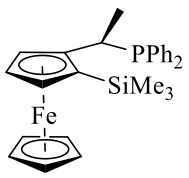

(R_c, S_{pl})

Figure 1.4. Illustration of ferrocenylphosphine ligand bearing both central and planar chirality.

Initial efforts by Hayashi and Kumada produced the first report of a planar chiral ferrocenyl monophosphine ligand, which was successfully exploited in the hydrosilylation reaction of ketones (Scheme 1.3).[29]

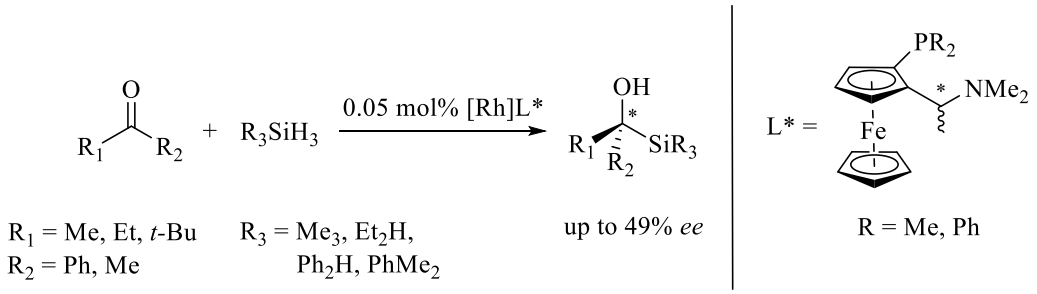

Scheme 1.3. Asymmetric hydrosilylation of ketones using chiral ferrocenyl phosphine ligands.

This milestone discovery kickstarted the venture into chiral ferrocenyl phosphines as plausible partnering moieties in asymmetric reactions, leveraging on the added feature offered by the ferrocene's planar chirality. The establishment of this class of monophosphines as powerful ligands was eventually realized, notably in applications such as cross-coupling as well as allylic substitution reactions.[28a, 30]

The rise in achievements attained from the transitional use of simple to more structurally elaborate monodentate tertiary phosphines are a testament that structural modifications are fundamental for the improvement of ligand potential in catalytic applicability. Thus far, the catalysts in discussion constituted monophosphine complexes that depict only a monodentate form of ligand coordination to the metal center, which may not be the most optimized configuration for certain requirements in the context of asymmetric reactions. One obvious challenge may be pointed to insufficient chiral induction because of limited and inadequate steric enforcements that a monodentate ligand can provide. Another inherent problem can be associated with the larger tendency of monodentates to dissociate from the metal center, which may lead to the occurrence of side reactions such as β-hydride elimination when vacant sites are generated from their departure.[31] Other related complications that can be resulted from such dynamic coordination interactions between monodentate ligands and the metal center is the uncontrollability of the metal

to ligand ratio, which can again cause undesired side reactions that lowers the yields of the intended product.[32] A clear ensuing motivation would therefore be to increase the denticity of the ligands, so that additional functionalities can be encompassed to supplement a more structurally elaborate moiety which may be better catered to satisfy specificity and selectivity needs in a reaction.

1.2. Bidentate tertiary phosphines: Diphosphines & heteronuclear-phosphine chelates

Chelating phosphines are customarily accompanied with defining characteristics associated with their natural bite angle.[33] Besides having a causal effect in the overall spatial allowance for substrate-to-metal interaction, the geometrical flexibilities and constraints limited by the bite angle also enforce certain preferred coordination inclinations onto the ligand.[34] Consequently, rigid conformations adopted from such ligand enforcements can impart several impacts on key reaction steps within a catalytic cycle that involve the stabilization or destabilization of the catalyst in its different chemical transition states.[35] Additional advantages ascribed to such ligand dictated conformational arrangements include the formation of a structurally well-defined motif that can provide selective reactivity, as the complex orientates itself in specific manners which direct chemical reactions onto targeted points within a substrate molecule.[36] Furthermore, the physical tethering of the ligand ensures better likelihood of the chelate to stay in place, hence preventing potential problems arising from coordination site vacancies resulted from ligand dissociation as previously described. Within the classification of bidentate tertiary phosphines, diphosphines dominate as one of the most broadly applied variants, showing marked influences on the chemical preferences of the corresponding ligated complex due to the abovementioned factors.[34b, 37]

The quest to search for more efficient chiral phosphine systems as inspired by the hallmark accomplishments of Knowles and Horner led to the advent of chiral tertiary diphosphines into the scene of asymmetric transition metal catalyzed hydrogenation.[38] Pioneered in the works of Kagan, the chiral diphosphine DIOP performed expeditiously under mild hydrogenation conditions in the asymmetric rhodium(I) catalyzed reduction of *N*-acylaminoacrylic acids, forming the corresponding chiral amino acids with decent optical yields of up to 80% (Scheme 1.4).[39]

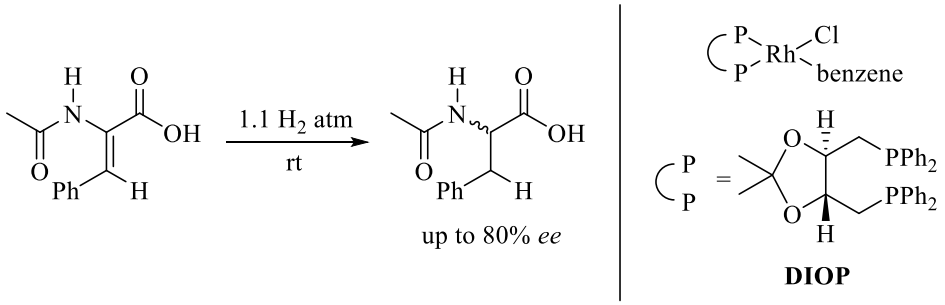

Scheme 1.4. Asymmetric hydrogenation of *N*-acylaminoacrylic acids with rhodium(I)-DIOP complex.

Further developments of analogous C_2-symmetric tertiary diphosphines also revealed their employability in large scale commercial implementations. This was showcased by the Mosanto industrial production of L-DOPA, which utilized a rhodium-DIPAMP complex for the synthesis of the chiral drug that is prescribed for the treatment of Parkinson's disease.[40] The illustrated process was also the first example of an industrial application utilizing asymmetric transition metal catalysis. Since then, other variations of C_2-symmetric diphosphines synthesized for use in asymmetric hydrogenation reactions also showed parallel activity in enabling excellent chiral inductions of up to 99% *ee* (Figure 1.5).[41]

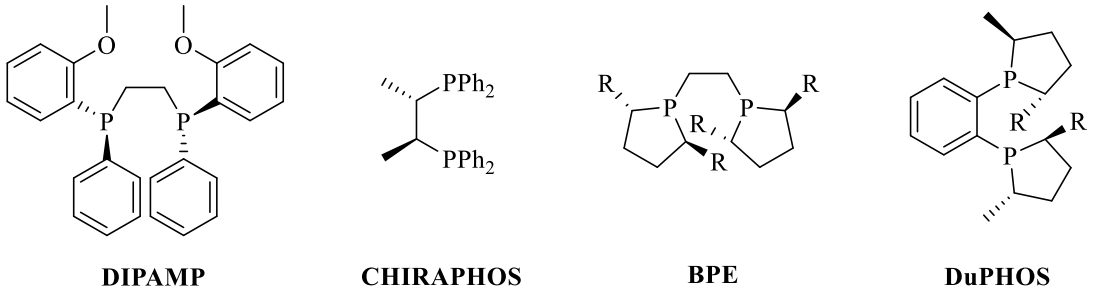

DIPAMP **CHIRAPHOS** **BPE** **DuPHOS**

Figure 1.5. Selected examples of chiral C_2-symmetric tertiary diphosphines.

In general, as with monophosphines, *P*-chirogenic diphosphines are expected to assume better provision of chiral influence as they eliminate possible factors of inefficient secondary chirality transfer.[41d] Aside from that, the chiral induction potential of diphosphines should theoretically be more significant since the steric occupancy arising from the extra skeletal arm also comes into play with imposing additional spatial interactions within the coordination sphere of the complex. Despite such preferential features and the successful application of DIPAMP in the early years, *P*-chiral diphosphines remained starkly uncommon mainly due to the difficulty with their enantioselective syntheses.[42] Nevertheless, while new methodologies and applications were researched upon for *P*-chiral diphosphines,[41d, 43] the efficiencies in asymmetric induction reactions provided by the *C*-chiral equivalents are also not to be understated, as exemplified by representative illustrations of DIOP and CHIRAPHOS based systems.[44]

Until this point, the scope of tertiary diphosphine illustrations has only been limited to those containing point chiralities residing on the ligand backbone or on the phosphorus atom itself. In addition, the display of usefulness of these ancillaries were also largely centered on rhodium mediated reactions. The ensuing section showcases the expansion of diphosphines as compatible chiral auxiliaries and how the ligand class was next taken to greater heights by Noyori and Takaya with their seminal discovery of BINAP (Figure 1.6).

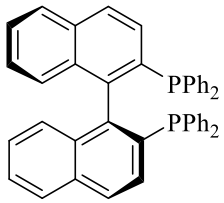

(*S*)-BINAP

Figure 1.6. Illustration of axially chiral diphosphine BINAP.

Endowed with a single element of axial chirality, BINAP exhibited outstanding chiral induction capabilities not only with a variety of different metal centers, but also onto a wider range of substrates encompassing functionalized olefins and ketones for asymmetric hydrogenation.[45] In addition, the versatility of BINAP based metal systems was extended beyond just asymmetric hydrogenation, and included numerous other enantioselective applications like hydroboration,[46] 1,4-disilylation[47] and olefin isomerization.[48]

The revolutionary introduction of BINAP spurred continued attention towards axially chiral diphosphines, with newer generation of variants possessing modifications onto the ring functionality. Other than the usual phenyl or naphthyl make-ups, these also include an array of aromatic heterocyclic groups like pyridine to non-aromatic cyclic ether type derivatives (Figure 1.7).[49] Interestingly in the examples bearing a pyridyl functionality, bulky substituents were deliberately installed at the positions ortho to the nitrogen group so as to prevent their competitive coordination with the phosphine groups to the metal center.[50]

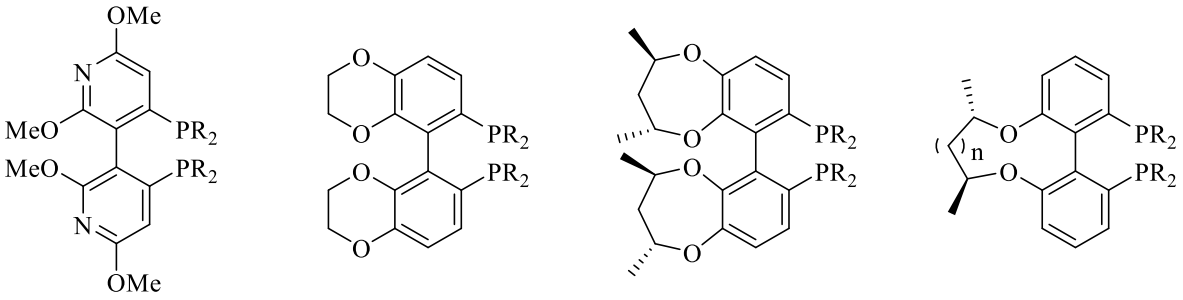

Figure 1.7. Examples of ring functionalized axially chiral diphosphines.

Even more recently, the prevalence of axially chiral diphosphines have also revolved around the syntheses of these ligands containing a spirocyclic framework that imbue high molecular rigidity (Figure 1.8).

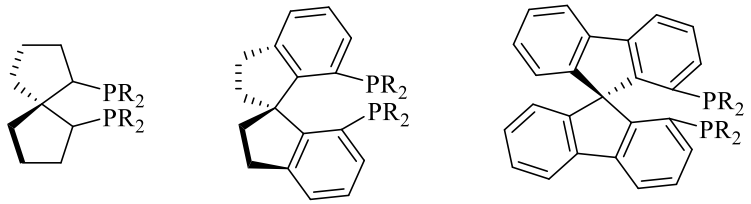

Figure 1.8. Examples of tertiary diphosphines with highly rigid spirocyclic backbones.

Such rigid backbones prove ideal in preventing problems associated with ligand racemization, since this would be virtually impossible with the presence of a quaternary center connected by strong σ-bonding. Furthermore, these were also highlighted to be effective in important fundamental catalytic applications such as C-C bond formation reactions involving coupling, allylation and ring opening pathways.[37]

Similar to their monophosphine counterparts, ferrocenyl diphosphines are also described in innumerable representations in the literature.[28c, 51] Spearheaded by the efforts of Togni and Spindler, the debut of chiral ferrocenyl diphosphines as effective ligands was presented in their work for the successful formation of a chiral amino precursor that is further used for production of the herbicide (*S*)-metolachlor (Scheme 1.5).[52]

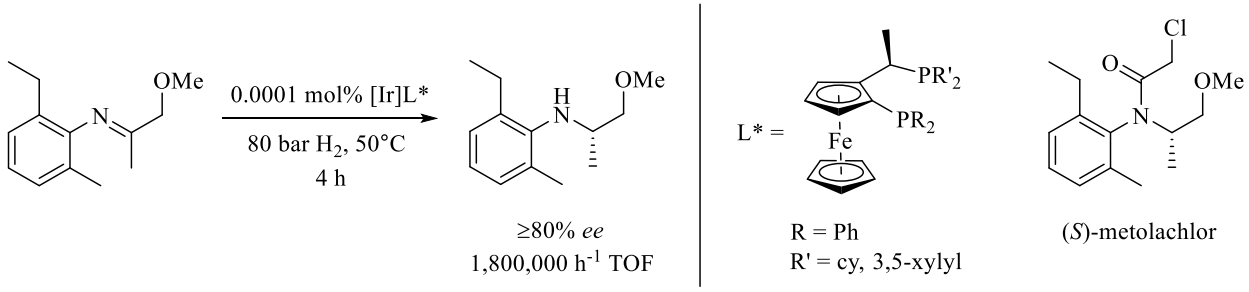

Scheme 1.5. Asymmetric hydrogenation mediated by iridium based ferrocenyl diphosphine complex to form amino precursor for (*S*)-metolachlor synthesis.

Crucial to this synthetic application was the remarkable activity of the associated ferrocenyl diphosphine complex, which could not only catalyze the reaction at fast rates with high turnover frequencies, but were also highly stable to avert chemical decomposition – a huge contrast to other employed catalysts.[52] Among the huge selection of ferrocenyl diphosphines available, these are usually categorized according to two main forms of classifications – a 1,1' or 1,2-disubstituted ferrocenyl diphosphine (Figure 1.9).

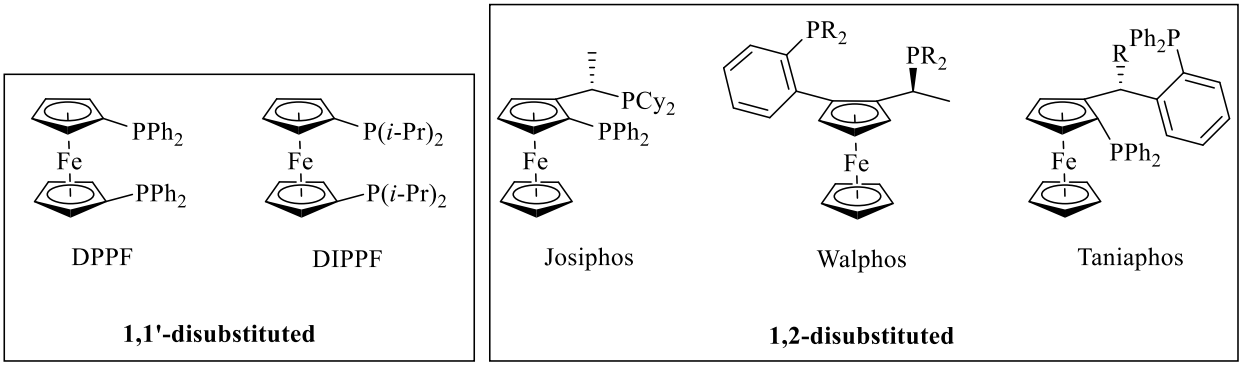

Figure 1.9. Representations of 1,1' and 1,2-disubstituted ferrocenyl diphosphines.

As seen in Figure 1.9, the modularity of ferrocenyl diphosphines is much more enhanced due to the fact that two phosphine groups can be sequentially added onto the same parent ferrocenyl structure with relatively few synthetic steps.[53] In turn, this facilitates the tunable access to variable ferrocenyl diphosphine ligands composed of more distinct steric and electronic differences to fulfill the chemical requirements of specific reactions.[51a, 54]

In another different class of bidentate tertiary phosphine ligands, mixed heteronuclear-phosphine systems consisting of one phosphorus atom tethered to another non-phosphorus atom serve as an alternate means of accessing new phosphorus bidentate ligands. The versatility of such hybrid ligand systems is evidently displayed in vast illustrations of these P-E type bidentates, where E can assume a variety of either neutral or anionic non-phosphorus based donor functionalities. These include a diverse range of classical heterofunctionalized phosphine bidentates incorporating nitrogen, oxygen, or sulfur donors,[55] to more recent examples with carbon based donors like carbenes or olefins,[56] as well as other exotic representations with less commonly utilized donor atoms like silicon[57] and even tellurium (Figure 1.10).[58]

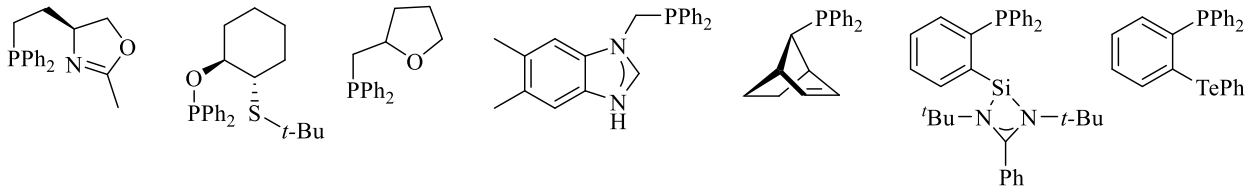

Figure 1.10. Examples of hetero-phosphine bidentate ligands.

An apparent difference resulting from the substitutional use of a heterofunctionalized phosphine bidentate is a significant electronic distinction between both donor atoms, as compared to a traditional diphosphine bidentate containing two similar phosphine donors. This lies with the intrinsic disparity in the hard and softness of the ligating atoms, which can be especially useful in stabilizing changing oxidation states of the metal center during the catalytic cycle.[56g] The added advantage of such a characteristic is the ability to leverage upon the electronic compatibility of each donor atom to respective transitional oxidation states of the metal via a hemilabile mode of coordination during the course of the catalytic reaction, so that reactive metal intermediates can be formed under stabilized control and vacant sites can be opened up to what would otherwise be unavailable in the stable ground state structure of the complex.[59] Further relation with respect to the electronic dissymmetry of the chelating atoms is the inherent difference in their kinetic *trans* effect, which can be important in terms of influencing substrate-to-complex interactions involving substrate adherence for reaction as well as product elimination for regeneration of vacant sites.

1.3. Tridentate tertiary phosphines: Pincer-type diphosphines and mixed hetero-phosphine pincer ligands

More recently, the scope of chelating tertiary phosphines has extended beyond just plain bidentates to even more structurally defined tridentate, pincer-type phosphine ligands. These are usually depicted with a central anchoring moiety (either aryl or alkyl) flanked by two phosphorus donors, or a mixed flanking system comprised of one phosphorus donor and another non-phosphorus donor to form two chelate rings after complexation to a metal center (Figure 1.11).

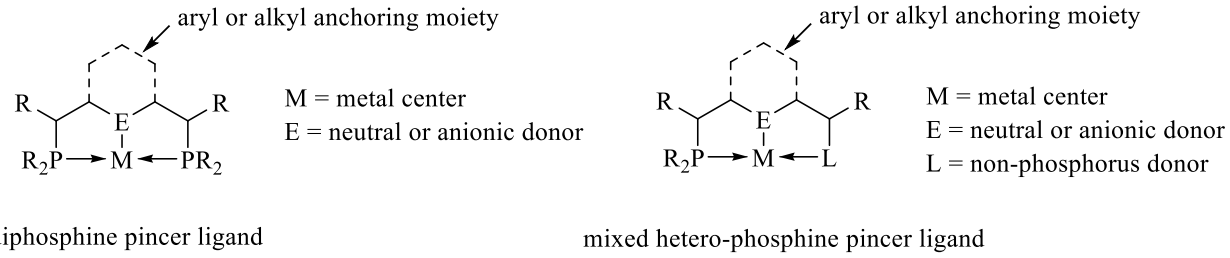

Figure 1.11. General representation of a complex bearing a tridentate pincer-type tertiary phosphine ligand.

Akin to their bidentate counterparts, the additional chelate effect derived from the introduction of a second chelating arm expectedly enhances the stability of ligand coordination to the metal center by a larger extent. Consequently, this confers a strong level of fixity between the ligand and metal center, whereby the tendency for ligand dissociation remains minimal. Accordingly, this also illustrates high thermodynamic and kinetic stability of the ligand, which thus minimizes fluxional behaviors stemming from ligand labilization.[60] The resulting stability of these pincer-type ligand systems is also often manifested in their resistance to thermal decomposition even at extreme elevated temperatures for prolonged periods of time. In certain cases, the furnished pincer complex can even be sublimed under open atmospheric conditions without any form of thermal

degradation.[61] Such robustness prove essential especially for highly endothermic processes, or in reactions requiring the activation of inert bonds under harsh reaction conditions.[62]

In addition, the pincer framework also facilitates the tunable access to ligand systems bearing multiple electronically distinct donor moieties that would otherwise be unsuitable as monodentate ligand units.[60] This again leverages on the stability brought about by the tridentate mode of coordination, which allows preferential binding of such ligand components only when they are part of the pincer architecture. Furthermore as seen from its general structural description shown in Figure 1.11, the degree of modularity with respect to both steric and electronic parameters of the ligand is also proportionally increased with the inclusion of more functionalities on its elaborate backbone. In context, this also permits the feasible incorporation of chiral elements for asymmetric applications. The culmination of all the abovementioned factors typically leads to the formation of a ligand system that possesses a characteristic balance of stability and reactivity, which can be altered in a multitude of fashions via direct modifications to the various functional groups present on the skeletal structure. More importantly, the flexibility of adjustments that can be made to such ligand structures not only opens up a wide range of compatibility to different metal centers of varying electronic properties, but also therefore leads to an unimaginable potential for catalytic applications requiring differing chemical properties of the metal complex. Not surprisingly, the utilization of related tridentate tertiary phosphine pincer complexes has been showcased in a plethora of metal mediated reactions involving myriads of reaction processes with good success since their introduction into the catalytic scene.[63]

1.4. General preparative methods of synthesizing chiral tertiary phosphines

Conventional methods of synthesizing chiral tertiary phosphines typically involve non-catalytic pathways that have been well established in the literature.[64] Amongst the more commonly utilized methodologies, these include a diverse number of protocols ranging from reduction of phosphine oxides or sulfides;[65] substitution reactions between halogenophosphines with organometallic reagents (such as Grignard or organolithium precursors);[66] as well as alkylation of metalated phosphides (Figure 1.12).[67]

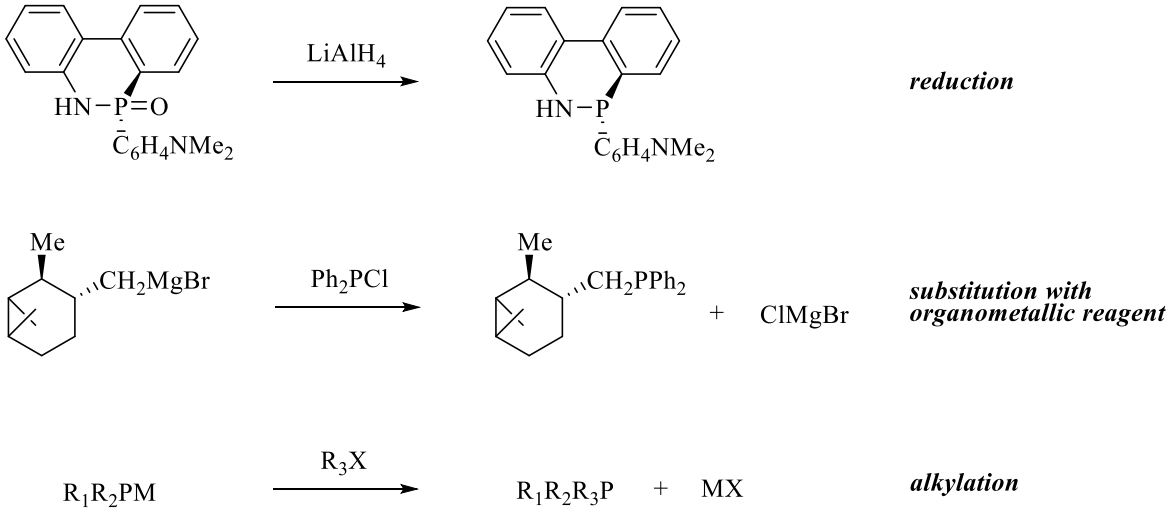

Figure 1.12. Common non-catalytic methods of chiral tertiary phosphine syntheses.

While proven to be effective, certain limitations still exist within these procedures in terms of synthetic practicality and efficiency. One obvious shortcoming of the described practices is the requirement for usage of strong reaction conditions that may lead to adverse complications in generating the desired product with good yields. This is especially so since highly reactive precursors like those shown above naturally exhibit low functional group tolerance, resulting in uncontrolled reactions onto existing functionalities apart from the targeted phosphine group, or otherwise over-reaction to form unwanted side products.[64, 68] Additional detrimental

consequences resulting from the harsh reaction environments are related to stereochemical problems concerning retention of stereochemistry in chiral intermediates. In cases whereby the conditions are inadequately regulated, racemization may be observed leading to a loss of stereogenicity in the final product.[68]

Although improvements have been meted out along the way to mitigate these drawbacks, the implementation of these revised protocols entail extra synthetic manipulations to the already tedious methodology, which can be overly troublesome to perform (such as protection-deprotection with boranes).[69] Furthermore, this again reverts to potential problems associated with loss of product yield as more steps are involved in the overall synthetic preparation. A second evident limitation is the inevitable need for the employment of stoichiometric or even excess amounts of starting materials, which proves to be highly unsustainable in these reactions which are not fully atom economical. This is rendered even more resource wasteful when the precursors in use contain precious chiral auxiliaries (prominently in the syntheses of *P*-chiral phosphines),[70] which may or may not be conveniently accessible. In response, there is greater sense that catalytic preparations to generate chiral tertiary phosphines would suit better to alleviate and circumvent the limitations ascribed to these non-catalytic procedures via carefully designed pathways, as will be described in the following section.

1.5. Organocatalyzed derivation of chiral tertiary phosphines

Where phosphorus-carbon (P-C) bond assembly is concerned, the phospha-Michael reaction represents as one of the most notable organic synthetic approach towards the furnishment of organophosphorus compounds.[71] With respect to the access of chiral phosphines, the synthetic outcome of this methodology bears huge relevance as a plausible pathway for the formation of *C*-stereogenic phosphines, by capitalizing on the nucleophilic nature of phosphines adding on to a prochiral *α, β*-unsaturated olefin moiety. While the syntheses of *C*-chiral phosphines using this strategy have been extensively illustrated to proceed via phosphorus(V) precursors as well, these will not be discussed to limit the scope of content only to carbon-phosphorus(III) bond construction reactions.

In the first example of an asymmetric organocatalyzed synthesis of chiral tertiary phosphines, Melchiorre demonstrated the phospha-Michael addition of secondary phosphines to nitroalkenes in the presence of a cinchona alkaloid, affording the chiral adducts with modest enantioselectivities of up to 67% *ee* (Scheme 1.6).[72]

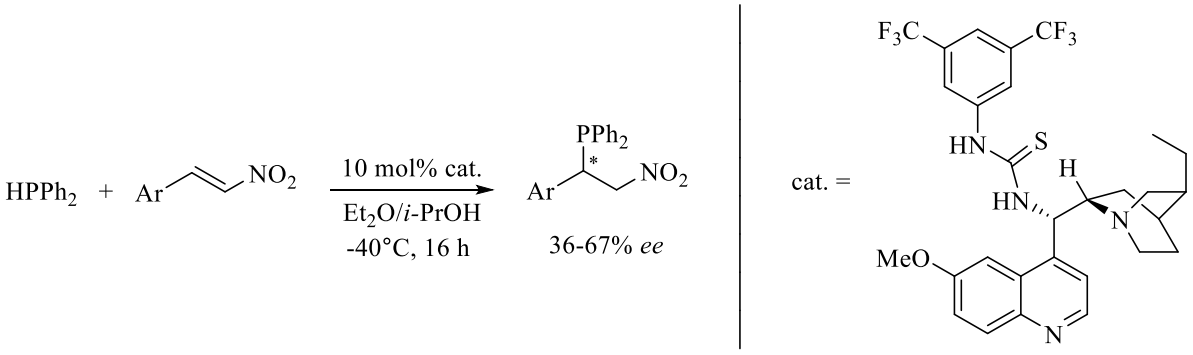

Scheme 1.6. Cinchona alkaloid catalyzed phospha-Michael addition onto nitroolefins.

In other exemplifications of organocatalyzed methods of accessing *C*-chiral phosphines, both Melchiorre and Cordova simultaneously disclosed the efficacious use of chiral secondary amines for the asymmetric addition of diarylphosphines onto enals (Scheme 1.7).[73]

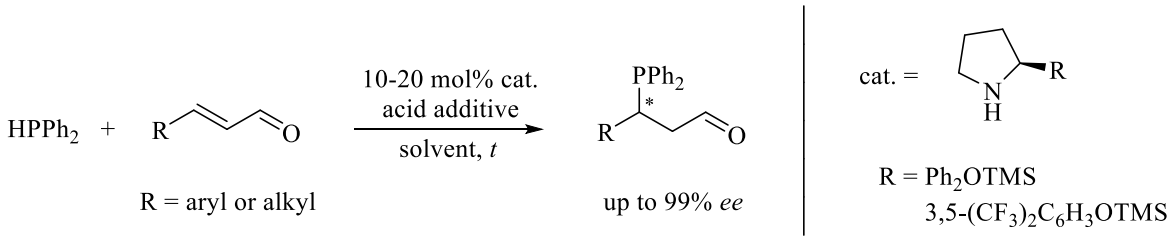

Scheme 1.7. Chiral secondary amine catalyzed phospha-Michael addition onto enals.

The successful employment of organocatalyzed phospha-Michael additions for the generation of *C*-stereogenic phosphines generally lies with the importance of substrate activation, which can be accomplished in a few ways. Firstly, electron withdrawing functionalities as in the case shown in Scheme 1.6, can be encompassed within the substrate backbone to enhance the electrophilicity of the β position and therefore its susceptibility to nucleophilic attack by the phosphine moiety. Secondly, where the reactant is not electronically activated as significantly, the use of less sterically endowed substrates is essential to allow energetically favorable binding interactions with the chiral catalyst to form reactive intermediates, and thereafter to foster an efficient stereo-controlled formation of the chiral adduct. This was well elucidated in mechanistic studies done by Cordova, whereby initial substrate activation via an iminium intermediate[74] and subsequent phosphine addition onto the resultant favorable transition state were highly dependent on optimal proximity interactions between the substrate and catalyst (Figure 1.13).[73b]

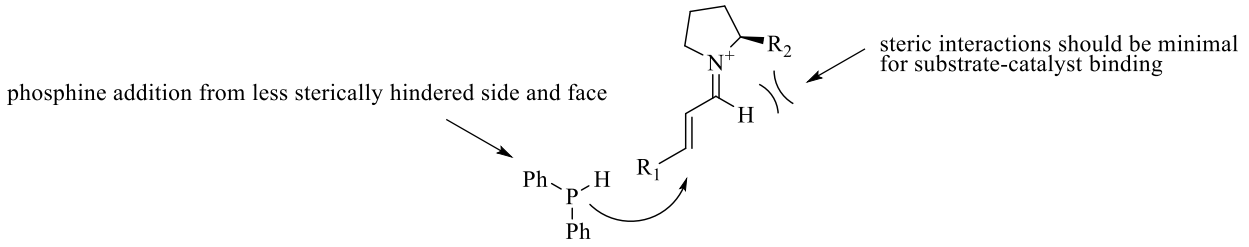

Figure 1.13. Illustration of steric dependency for enantioselective phosphine addition.

In addition to the second point, the ability to achieve good levels of stereodiscrimination in the formation of the phosphine adduct has also been proposed to be accomplished through H-bonding interactions between the phosphine nucleophile and the amine based organocatalyst.[75] This in turn directs the nucleophilic attack selectively onto one of the two enantiotopic faces in the transition state, which however is a lacking phenomenon for phosphorus(III) nucleophiles due to the absence of necessary H-bonding handles. Consequently, this may then lead to less efficient stereocontrol during the addition process and furnished adducts with lower enantioselectivities. Although represented as a viable means to obtain chiral tertiary phosphines, organocatalyzed methodologies remain seemingly less explored due to multiple restrictions in relation to substrate scope as described above. The ensuing solution is therefore to seek for other catalytic systems which can mediate the limitations associated with substrate specificity, so as to allow for easier access to these chiral phosphines.

1.6. Metal catalyzed derivation of chiral tertiary phosphines

The basis of P-C bond construction via a metal catalyzed pathway usually revolves around nucleophilic processes involving the formation of a metal-phosphide (M-P) intermediate through coordination to a metal center, followed by transfer of the highly nucleophilic phosphide onto an electrophilic carbon center.[76] Several advantages are correlated with this associative mechanism, which render the metal catalyzed protocol a robust and reliable alternative for the syntheses of organophosphorus compounds. Firstly, the generation of a phosphide moiety provides for a more nucleophilic species which is activated and hence more reactive for nucleophilic reactions as compared to the uncoordinated free phosphine. Secondly, the additional factor of having the anionic phosphide bound to the metal fragment not only affords convenient utility under neutral conditions, but also ensures high compatibility to functionalities requiring reaction conditions to be held at neutral pH (especially in biological procedures). Thirdly, aside from activating the nucleophilic moiety, the Lewis acidic metal may also aid in the transfer of the phosphide nucleophile via coordination to a Lewis basic element present on the substrate, thereby facilitating concomitant bond cleavage and bond formation processes. (Figure 1.14).[76]

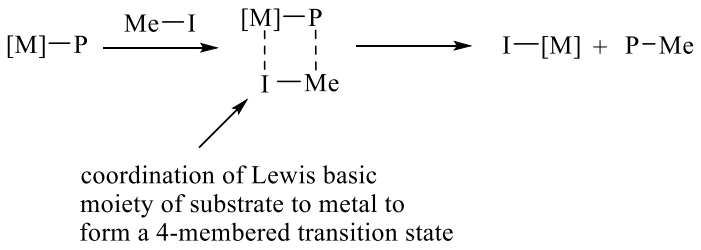

Figure 1.14. General illustration for the transfer of P nucleophile in alkylation reaction via 4-centered transition state.

The dual activation of both nucleophilic and electrophilic components of the reaction also proves to be vital for less reactive substrates such as aryl halides that do not readily undergo nucleophilic substitution. In these cases, the use of low valent metal precursors enables the oxidative addition of the aryl halide, thus bringing the electrophilic aryl center into closer proximity to the coordinated phosphide for more facile reaction.[76] While the existing literature documents a breadth of reports for the catalytic syntheses of phosphines mediated by metal based reagents,[77] only asymmetric procedures will be focused for discussion in this section.

1.6.1 Asymmetric P-C cross-coupling

The current literature today reflects a massive collection of methodologies towards the syntheses of *P*-chiral phosphines using metal catalyzed pathways.[78] Early reports of such protocols have showcased the applicability of asymmetric metal mediated processes such as oxidation and hydrogenation as plausible intermediary steps to synthesize enantiomerically pure precursors which can be further functionalized into the intended chiral phosphine products (Scheme 1.8).[41c, 79]

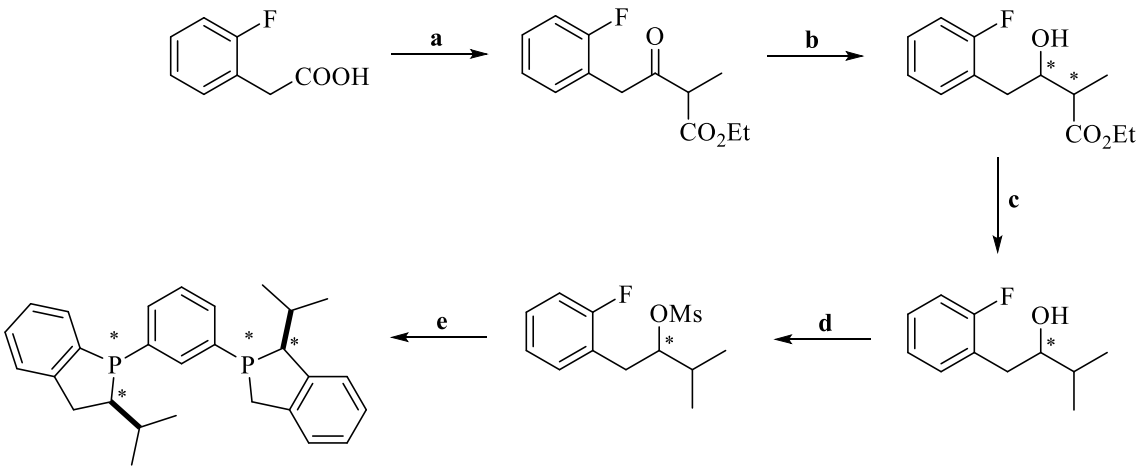

a: i) CDI, ii) $MgCl_2$, $MeCH(CO_2Et)(CO_2K)$

b: H_2, $[\{RuCl((R)\text{-segphos})\}_2(\mu\text{-}Cl)_3][Me_2NH_2]$

c: i) $LiAlH_4$, ii) TsCl, Et_3N, iii) $LiAlH_4$

d: MsCl, Et_3N

e: i) $1,2\text{-}C_6H_4(PHLi)_2$, ii) *n*-BuLi

Scheme 1.8. Synthesis of *P*-chiral diphosphines through formation of chiral intermediates.

These methods however often entail multiple synthetic transformations which require huge amounts of materials and manual effort. In a more streamlined manner of approach to generate *P*-chiral phosphines, the asymmetric metal catalyzed P-C cross-coupling reaction in more recent times, has been established to be an effective substitute method of choice.[80] The first example of an asymmetric P-C bond formation that proceeded through a metal mediated P-C cross-coupling reaction route was introduced by Glueck using *racemic* secondary phosphines with phenyl iodide, catalyzed by a palladium diphosphine complex (Scheme 1.9).[81]

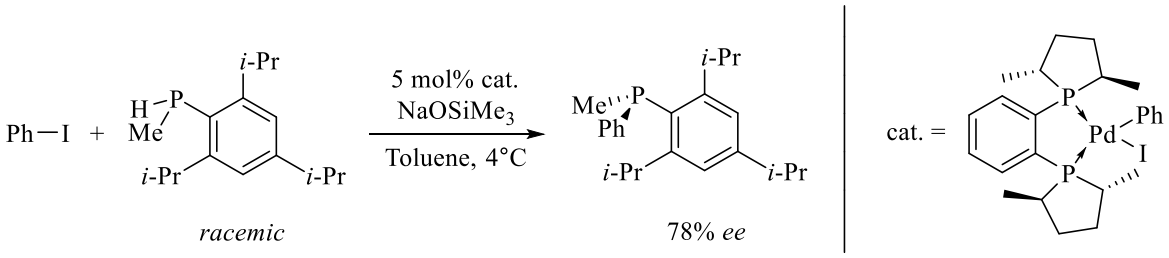

Scheme 1.9. Palladium(II) diphosphine complex catalyzed asymmetric P-C cross-coupling reaction.

Mechanistic insights revealed the key stereoselective step occurring on the metal-phosphido intermediate, relying on dynamic kinetic resolution of the two diastereomeric states to furnish the final *P*-chiral phosphine product in an enantioselective manner. The observed resolution was attributed to the spontaneous pyramidal inversion of configuration on the phosphorus atom when coordinated to a metal, leading to rapid interconversion via equilibrium shift to the more stable and energetically favored diastereomeric form. Additional factors allowing the successful resolution was also driven towards the fact that the rate of interconversion should take place faster than the rate of P-C bond formation (Figure 1.15).

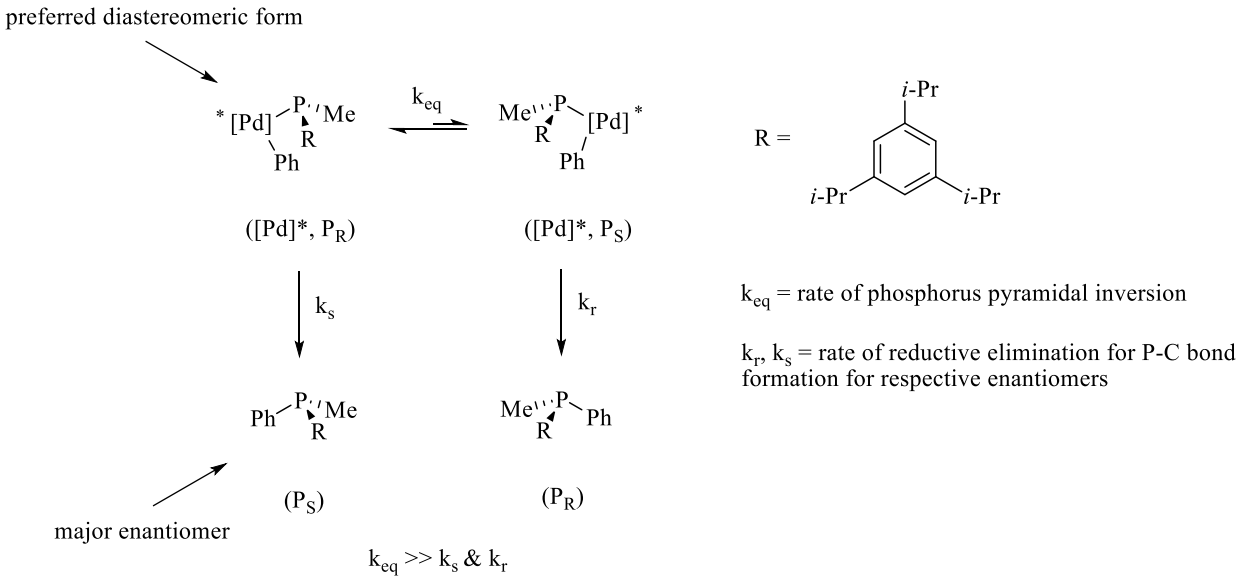

Figure 1.15. Illustration of dynamic kinetic resolution for enantioselective formation of *P*-chiral phosphines.

Accordingly, the imperfect enantiomeric excess obtained is a result of a faster reductive elimination rate of the minor enantiomer with respect to phosphorus interconversion, thereby diluting the overall enantioselectivity of the reaction. Nevertheless, the reaction pathway continues to highlight the significant role of the metal-phosphide intermediate as a necessary component for stereoselective furnishment of the *P*-chiral phosphines.

Further endeavors of asymmetric P-C cross-coupling reactions[80] leveraging on the dynamic kinetic resolution of diastereomeric metal-phosphide mixtures included the use of more convenient in-situ prepared catalysts (Scheme 1.10),[82] silylphosphines as coupling partners (Scheme 1.11),[83] as well as metal precursors featuring platinum[84] and ruthenium[85] centers for the coupling of alkyl halides with secondary phosphines (Scheme 1.12).

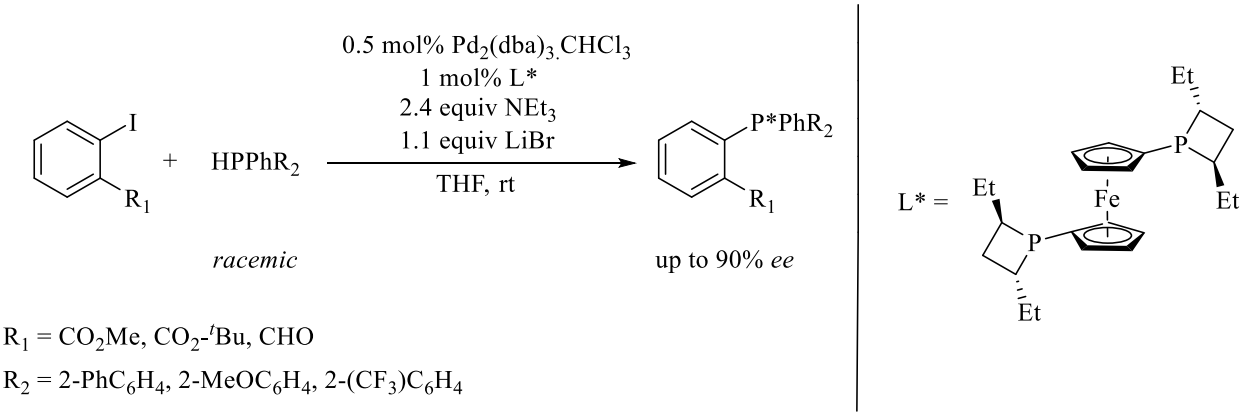

Scheme 1.10. Asymmetric P-C cross-coupling with in-situ prepared palladium(II) ferrocenyl diphosphine catalyst.

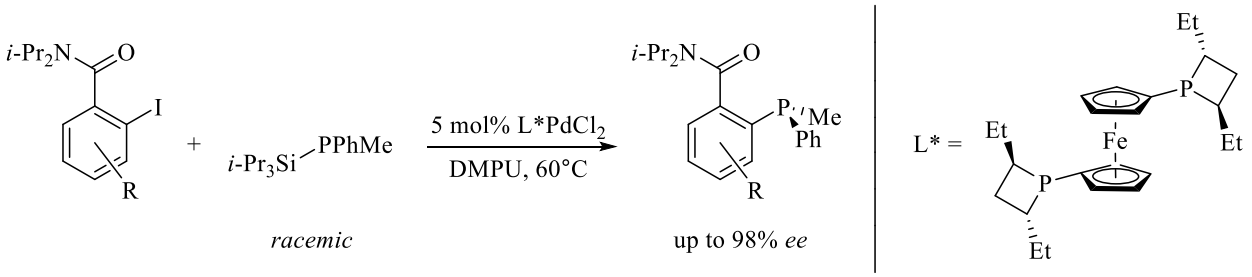

Scheme 1.11. Asymmetric P-C cross-coupling with silylphosphines.

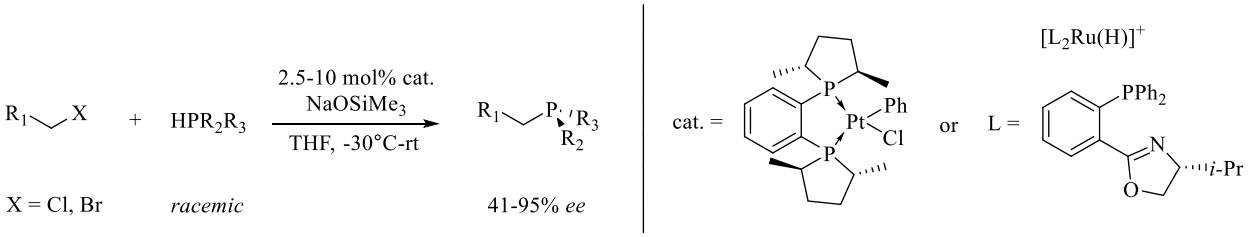

Scheme 1.12. Asymmetric P-C cross-coupling with platinum(II) and ruthenium(II) based metal catalysts using alkyl halides as coupling partners.

1.6.2 Asymmetric allylic phosphination

The development of new P-C bond formation synthetic systems, much like how the synthetic utility of phosphines was discovered based on their nitrogenous amine counterparts, frequently adopts the strategy of emulating parallel reaction pathways and/or mechanisms of N-C bond formation reactions. This has been well highlighted in hydrofunctionalization reactions whereby the hydroaddition of both N and P nucleophiles follow analogous reaction mechanisms under the same catalytic system.[86] The establishment of asymmetric allylic amination as a prominent method for the preparation of chiral amines therefore serves as a highly relevant reference for the synthetic access towards chiral phosphines as well. With this motivation, Togni developed an asymmetric palladium catalyzed allylic phosphination methodology that was able to

furnish *C*-stereogenic tertiary phosphines in decent yields and enantiomeric excess (Scheme 1.13).[87]

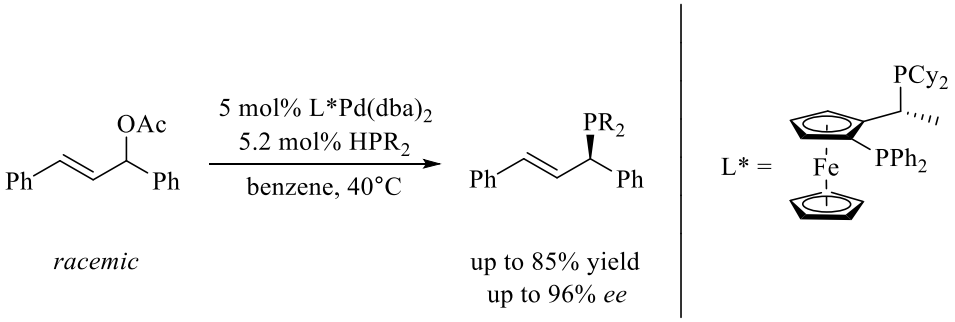

Scheme 1.13. Palladium(II) ferrocenyl diphosphine complex catalyzed asymmetric allylic phosphination.

Despite the good display of stereoselective formation of the chiral phosphine adducts, the overall reaction was still however hampered with issues relating to chemoselectivity, producing undesired side products even under optimized reaction conditions.

1.7. Research aims and objectives

The chemical significance of chiral tertiary phosphines in their utility as potentially effective moieties (either as ligands or synthetic precursors) for fundamentally important processes as accounted for in the above sections, strongly reinforces an existential relevance for continual research to access new and other of such derivatives. To achieve that, methods for their syntheses remain a crucial factor in determining optimized ways to generate these compounds with desirable outcomes, particularly in enantioselective manners. As showcased, the methodologies employed in current literature have seen progressive improvements to fulfill this requirement, outperforming traditional methods of synthesizing chiral tertiary phosphines in multiple ways aside from chemical aspects. With ongoing attention towards sustainable chemistry, it is also imperative that synthetic approaches should in ways or another, encompass less detrimental effects with respect

to environmental and/or economic impacts associated with the reaction process. In light of all these, this thesis serves to document the research aims of expanding the molecular library of chiral tertiary phosphines, as well as to discover the functional compatibility of these newly formed synthons as precursors for complexation onto suitable metal centers, furnishing potentially useful phosphine incorporated complexes via suitable methods of preparations that satisfy the pointers raised above.

References

[1] a) Robertson, A., The early history of catalysis. *Platinum Met. Rev.* **1975**, *19* (2), 64-69; b) Wisniak, J., The history of catalysis. From the beginning to Nobel Prizes. *Educación química* **2010**, *21* (1), 60-69; c) Zecchina, A.; Califano, S., *The development of catalysis: a history of key processes and personas in catalytic science and technology*. John Wiley & Sons: 2017.

[2] Busacca, C. A.; Fandrick, D. R.; Song, J. J.; Senanayake, C. H., The growing impact of catalysis in the pharmaceutical industry. *Adv. Synth. Catal.* **2011**, *353* (11-12), 1825-1864.

[3] Jandeleit, B.; Schaefer, D. J.; Powers, T. S.; Turner, H. W.; Weinberg, W. H., Combinatorial materials science and catalysis. *Angew. Chem. Int. Ed.* **1999**, *38* (17), 2494-2532.

[4] a) Pasinszki, T.; Krebsz, M., Synthesis and application of zero-valent iron nanoparticles in water treatment, environmental remediation, catalysis, and their biological effects. *Nanomaterials* **2020**, *10* (5), 917; b) Pirkanniemi, K.; Sillanpää, M., Heterogeneous water phase catalysis as an environmental application: a review. *Chemosphere* **2002**, *48* (10), 1047-1060.

[5] a) Zhang, H.-H.; Chen, H.; Zhu, C.; Yu, S., A review of enantioselective dual transition metal/photoredox catalysis. *Sci. China Chem* **2020**, *63*, 637-647; b) Aiken III, J. D.; Finke, R. G., A review of modern transition-metal nanoclusters: their synthesis, characterization, and applications in catalysis. *J. Mol. Catal. A: Chem.* **1999**, *145* (1-2), 1-44; c) Jun, C.-H., Transition metal-catalyzed carbon–carbon bond activation. *Chem. Soc. Rev.* **2004**, *33* (9), 610-618.

[6] a) Renfrew, A. K., Transition metal complexes with bioactive ligands: mechanisms for selective ligand release and applications for drug delivery. *Metallomics* **2014**, *6* (8), 1324-1335; b) Fahrni, C. J., Biological applications of X-ray fluorescence microscopy: exploring the subcellular topography and speciation of transition metals. *Curr. Opin. Chem. Biol.* **2007**, *11* (2), 121-127.

[7] a) Sharma, S.; Chauhan, M.; Jamsheera, A.; Tabassum, S.; Arjmand, F., Chiral transition metal complexes: Synthetic approach and biological applications. *Inorg. Chim. Acta* **2017**, *458*, 8-27; b) Abu-Dief, A. M.; Mohamed, I. M., A review on versatile applications of transition metal complexes incorporating Schiff bases. *Beni-suef university journal of basic and applied sciences* **2015**, *4* (2), 119-133.

[8] a) Bligaard, T.; Nørskov, J. K., Ligand effects in heterogeneous catalysis and electrochemistry. *Electrochim. Acta* **2007**, *52* (18), 5512-5516; b) Berrisford, D. J.; Bolm, C.; Sharpless, K. B., Ligand-accelerated catalysis. *Angewandte Chemie International Edition in English* **1995**, *34* (10), 1059-1070.

[9] Durand, D. J.; Fey, N., Computational ligand descriptors for catalyst design. *Chem. Rev.* **2019**, *119* (11), 6561-6594.

[10] a) Marynick, D. S., . pi.-Accepting abilities of phosphines in transition-metal complexes. *J. Am. Chem. Soc.* **1984**, *106* (14), 4064-4065; b) McAuliffe, C. A., *Transition Metal Complexes of Phosphorus, Arsenic & Antimony Ligands*. Macmillan International Higher Education: 2015.

[11] Hayashi, T., Chiral monodentate phosphine ligand MOP for transition-metal-catalyzed asymmetric reactions. *Acc. Chem. Res.* **2000**, *33* (6), 354-362.

[12] Booth, G., Complexes of the transition metals with phosphines, arsines, and stibines. *Advances in Inorganic Chemistry and Radiochemistry* **1964**, *6*, 1-69.

[13] a) Clark, H. C., Steric Demands of Tertiary Phosphine Ligands. *Isr. J. Chem.* **1976**, *15* (3-4), 210-213; b) Brown, T. L.; Lee, K. J., Ligand steric properties. *Coord. Chem. Rev.* **1993**, *128* (1-2), 89-116; c) Wu, K.; Doyle, A. G., Parameterization of phosphine ligands demonstrates enhancement of nickel catalysis via remote steric effects. *Nature chemistry* **2017**, *9* (8), 779.

[14] a) van Leeuwen, P. W.; Kamer, P. C.; Reek, J. N., The bite angle makes the catalyst. *Pure Appl. Chem.* **1999**, *71* (8), 1443-1452; b) van Leeuwen, P. W.; Kamer, P. C.; Reek, J. N.; Dierkes, P., Ligand bite angle effects in metal-catalyzed C− C bond formation. *Chem. Rev.* **2000**, *100* (8), 2741-2770.

[15] a) Romeo, R.; Arena, G.; Monsu Scolaro, L., Steric and electronic factors influencing the reactivity of tertiary phosphines toward platinum (II) complexes. *Inorg. Chem.* **1992**, *31* (23), 4879-4884; b) Freixa, Z.; Van Leeuwen, P. W., Bite angle effects in diphosphine metal catalysts: steric or electronic? *Dalton Transactions* **2003**, (10), 1890-1901.

[16] Pignolet, L. M., *Homogeneous catalysis with metal phosphine complexes*. Springer Science & Business Media: 2013.

[17] Tolman, C. A., Steric effects of phosphorus ligands in organometallic chemistry and homogeneous catalysis. *Chem. Rev.* **1977**, *77* (3), 313-348.

[18] Tolman, C. A., Electron donor-acceptor properties of phosphorus ligands. Substituent additivity. *J. Am. Chem. Soc.* **1970**, *92* (10), 2953-2956.

[19] Hofmann, A. W. V.; Cahours, A., XXVIII. Researches on the phosphorus-bases. *Philosophical Transactions of the Royal Society of London* **1857**, (147), 575-599.

[20] a) Cahours, A.; Gal, H., Untersuchungen über neue Platinderivate der Phosphorbasen. *Justus Liebigs Annalen der Chemie* **1870**, *155* (2), 223-230; b) Malerbi, B., Phosphine Complexes of the Platinum Group Metals. *Platinum Met. Rev.* **1965**, *9* (2), 47-50.

[21] a) Mann, F. G.; Purdie, D., 366. The constitution of complex metallic salts. Part III. The parachors of palladium and mercury in simple and complex compounds. *Journal of the Chemical Society (Resumed)* **1935**, 1549-1563; b) Chatt, J.; Mann, F. G., 366. The constitution of complex

metallic salts. Part VIII. The bridged thio-derivatives of palladous halides with tertiary phosphines. *Journal of the Chemical Society (Resumed)* **1938**, 1949-1954.

[22] Galan, B. R.; Rovis, T., Beyond Reppe: building substituted arenes by [2+ 2+ 2] cycloadditions of alkynes. *Angew. Chem. Int. Ed.* **2009**, *48* (16), 2830-2834.

[23] a) Evans, D.; Osborn, J.; Jardine, F.; Wilkinson, G., Homogeneous hydrogenation and hydroformylation using ruthenium complexes. *Nature* **1965**, *208* (5016), 1203-1204; b) Young, J.; Osborn, J.; Jardine, F.; Wilkinson, G., Hydride intermediates in homogeneous hydrogenation reactions of olefins and acetylenes using rhodium catalysts. *Chemical Communications (London)* **1965**, (7), 131-132.

[24] a) Horner, L.; Siegel, H.; Büthe, H., Asymmetric catalytic hydrogenation with an optically active phosphinerhodium complex in homogeneous solution. *Angewandte Chemie International Edition in English* **1968**, *7* (12), 942-942; b) Knowles, W. S.; Sabacky, M. J., Catalytic asymmetric hydrogenation employing a soluble, optically active, rhodium complex. *Chemical Communications (London)* **1968**, (22), 1445-1446.

[25] Morrison, J. D.; Burnett, R. E.; Aguiar, A. M.; Morrow, C. J.; Phillips, C., Asymmetric homogeneous hydrogenation with rhodium (I) complexes of chiral phosphines. *J. Am. Chem. Soc.* **1971**, *93* (5), 1301-1303.

[26] a) Zapf, A.; Jackstell, R.; Rataboul, F.; Riermeier, T.; Monsees, A.; Fuhrmann, C.; Shaikh, N.; Dingerdissen, U.; Beller, M., Practical synthesis of new and highly efficient ligands for the Suzuki reaction of aryl chlorides. *Chem. Commun.* **2004**, (1), 38-39; b) Singer, R. A.; Doré, M.; Sieser, J. E.; Berliner, M. A., Development of nonproprietary phosphine ligands for the Pd-catalyzed amination reaction. *Tetrahedron Lett.* **2006**, *47* (22), 3727-3731; c) Hartwig, J. F., Evolution of a fourth generation catalyst for the amination and thioetherification of aryl halides.

Acc. Chem. Res. **2008**, *41* (11), 1534-1544; d) So, C. M.; Zhou, Z.; Lau, C. P.; Kwong, F. Y., Palladium-catalyzed amination of aryl mesylates. *Angew. Chem. Int. Ed.* **2008**, *47* (34), 6402-6406; e) Wu, X.-F.; Neumann, H.; Spannenberg, A.; Schulz, T.; Jiao, H.; Beller, M., Development of a general palladium-catalyzed carbonylative Heck reaction of aryl halides. *J. Am. Chem. Soc.* **2010**, *132* (41), 14596-14602; f) Sather, A. C.; Buchwald, S. L., The evolution of Pd0/PdII-catalyzed aromatic fluorination. *Acc. Chem. Res.* **2016**, *49* (10), 2146-2157; g) Qiu, X.; Wang, M.; Zhao, Y.; Shi, Z., Rhodium (I)-Catalyzed Tertiary Phosphine Directed C− H Arylation: Rapid Construction of Ligand Libraries. *Angew. Chem. Int. Ed.* **2017**, *56* (25), 7233-7237.

[27] Ingoglia, B. T.; Wagen, C. C.; Buchwald, S. L., Biaryl monophosphine ligands in palladium-catalyzed C–N coupling: An updated User's guide. *Tetrahedron* **2019**, *75* (32), 4199-4211.

[28] a) Ohno, A.; Yamane, M.; Hayashi, T.; Oguni, N.; Hayashi, M., Preparation and use of chiral ferrocenylphosphines containing new alkyl substituents on the ferrocenylmethyl position. *Tetrahedron: Asymmetry* **1995**, *6* (10), 2495-2502; b) Genov, M.; Almorín, A.; Espinet, P., Microwave assisted asymmetric Suzuki-Miyaura and Negishi cross-coupling reactions: Synthesis of chiral binaphthalenes. *Tetrahedron: Asymmetry* **2007**, *18* (5), 625-627; c) Gomez Arrayas, R.; Adrio, J.; Carretero, J. C., Recent applications of chiral ferrocene ligands in asymmetric catalysis. *Angew. Chem. Int. Ed.* **2006**, *45* (46), 7674-7715.

[29] Hayashi, T.; Yamamoto, K.; Kumada, M., Asymmetric catalytic hydrosilylation of ketones preparation of chiral ferrocenylphosphines as chiral ligands. *Tetrahedron Lett.* **1974**, *15* (49-50), 4405-4408.

[30] a) Jensen, J. F.; Johannsen, M., New air-stable planar chiral ferrocenyl monophosphine ligands: Suzuki cross-coupling of aryl chlorides and bromides. *Org. Lett.* **2003**, *5* (17), 3025-3028; b) Baillie, C.; Zhang, L.; Xiao, J., Ferrocenyl Monophosphine Ligands: Synthesis and

Applications in the Suzuki− Miyaura Coupling of Aryl Chlorides. *The Journal of organic chemistry* **2004**, *69* (22), 7779-7782; c) Zhang, D.; Wang, Q., Palladium catalyzed asymmetric Suzuki–Miyaura coupling reactions to axially chiral biaryl compounds: Chiral ligands and recent advances. *Coord. Chem. Rev.* **2015**, *286*, 1-16.

[31] a) O'Reilly, M. E.; Dutta, S.; Veige, A. S., β-Alkyl elimination: fundamental principles and some applications. *Chem. Rev.* **2016**, *116* (14), 8105-8145; b) Whitesides, G. M.; Gaasch, J. F.; Stedronsky, E. R., Mechanism of thermal decomposition of dibutylbis (triphenylphosphine) platinum (II). *J. Am. Chem. Soc.* **1972**, *94* (15), 5258-5270.

[32] Clevenger, A. L.; Stolley, R. M.; Aderibigbe, J.; Louie, J., Trends in the Usage of Bidentate Phosphines as Ligands in Nickel Catalysis. *Chem. Rev.* **2020**, *120* (13), 6124-6196.

[33] a) Casey, C. P.; Whiteker, G. T., The natural bite angle of chelating diphosphines. *Isr. J. Chem.* **1990**, *30* (4), 299-304; b) Dierkes, P.; van Leeuwen, P. W., The bite angle makes the difference: a practical ligand parameter for diphosphine ligands. *J. Chem. Soc., Dalton Trans.* **1999**, (10), 1519-1530.

[34] a) DeStefano, N.; Johnson, D.; Lane, R.; Venanzi, L., Transition-Metal Complexes with Bidentate Ligands Spanning trans-Positions. I. The synthesis of 2, 11-bis (diphenylphosphinomethyl) benzo [c]-phenanthrene, a ligand promoting the formation of square planar complexes. *Helv. Chim. Acta* **1976**, *59* (8), 2674-2682; b) Kamer, P. C.; van Leeuwen, P. W.; Reek, J. N., Wide bite angle diphosphines: Xantphos ligands in transition metal complexes and catalysis. *Acc. Chem. Res.* **2001**, *34* (11), 895-904; c) Bessel, C. A.; Aggarwal, P.; Marschilok, A. C.; Takeuchi, K. J., Transition-metal complexes containing trans-spanning diphosphine ligands. *Chem. Rev.* **2001**, *101* (4), 1031-1066.

[35] a) Thorn, D. L.; Hoffmann, R., The olefin insertion reaction. *J. Am. Chem. Soc.* **1978**, *100* (7), 2079-2090; b) Dekker, G. P.; Elsevier, C. J.; Vrieze, K.; van Leeuwen, P. W.; Roobeek, C. F., Influence of ligands and anions on the insertion of alkenes into palladium-acyl and palladium-carbomethoxy bonds in the neutral complex (dppp) Pd (C (O) CH3) Cl and the ionic complexes [(P–P) PdR (L)]+ SO3CF3−(P–P= dppe, dppp, dppb; R = C (O) CH3, L= CH3CN, PPh3; R= C (O) OCH3, L= PPh3). *J. Organomet. Chem.* **1992**, *430* (3), 357-372.

[36] Breslow, R.; Belvedere, S.; Gershell, L.; Leung, D., The chelate effect in binding, catalysis, and chemotherapy. *Pure Appl. Chem.* **2000**, *72* (3), 333-342.

[37] Xie, J.-H.; Zhou, Q.-L., Chiral diphosphine and monodentate phosphorus ligands on a spiro scaffold for transition-metal-catalyzed asymmetric reactions. *Acc. Chem. Res.* **2008**, *41* (5), 581-593.

[38] a) Tang, W.; Zhang, X., New chiral phosphorus ligands for enantioselective hydrogenation. *Chem. Rev.* **2003**, *103* (8), 3029-3070; b) Zhang, W.; Chi, Y.; Zhang, X., Developing chiral ligands for asymmetric hydrogenation. *Acc. Chem. Res.* **2007**, *40* (12), 1278-1290.

[39] Kagan, H. B.; Dang, T.-P., Asymmetric catalytic reduction with transition metal complexes. I. Catalytic system of rhodium (I) with (-)-2, 3-0-isopropylidene-2, 3-dihydroxy-1, 4-bis (diphenylphosphino) butane, a new chiral diphosphine. *J. Am. Chem. Soc.* **2002**, *94* (18), 6429-6433.

[40] Knowles, W. S., Application of organometallic catalysis to the commercial production of L-DOPA. *J. Chem. Educ.* **1986**, *63* (3), 222.

[41] a) Fryzuk, M.; Bosnich, B., Asymmetric synthesis. Production of optically active amino acids by catalytic hydrogenation. *J. Am. Chem. Soc.* **1977**, *99* (19), 6262-6267; b) Burk, M. J.; Feaster, J. E., Enantioselective hydrogenation of the C: N group: a catalytic asymmetric reductive

amination procedure. *J. Am. Chem. Soc.* **1992**, *114* (15), 6266-6267; c) Burk, M. J.; Feaster, J. E.; Nugent, W. A.; Harlow, R. L., Preparation and use of C2-symmetric bis (phospholanes): production of. Alpha.-amino acid derivatives via highly enantioselective hydrogenation reactions. *J. Am. Chem. Soc.* **1993**, *115* (22), 10125-10138; d) Crépy, K. V.; Imamoto, T., Recent developments in catalytic asymmetric hydrogenation employing P-chirogenic diphosphine ligands. *Adv. Synth. Catal.* **2003**, *345* (1-2), 79-101.

[42] Pietrusiewicz, K. M.; Zablocka, M., Preparation of scalemic P-chiral phosphines and their derivatives. *Chem. Rev.* **1994**, *94* (5), 1375-1411.

[43] a) Corey, E.; Chen, Z.; Tanoury, G. J., A new and highly enantioselective synthetic route to P-chiral phosphines and diphosphines. *J. Am. Chem. Soc.* **1993**, *115* (23), 11000-11001; b) Imamoto, T.; Tamura, K.; Zhang, Z.; Horiuchi, Y.; Sugiya, M.; Yoshida, K.; Yanagisawa, A.; Gridnev, I. D., Rigid P-chiral phosphine ligands with tert-butylmethylphosphino groups for rhodium-catalyzed asymmetric hydrogenation of functionalized alkenes. *J. Am. Chem. Soc.* **2012**, *134* (3), 1754-1769; c) Yamanoi, Y.; Imamoto, T., Methylene-bridged P-chiral diphosphines in highly enantioselective reactions. *The Journal of organic chemistry* **1999**, *64* (9), 2988-2989.

[44] a) Nishikata, T.; Yamamoto, Y.; Gridnev, I. D.; Miyaura, N., Enantioselective 1, 4-Addition of Ar3Bi,[ArBF3] K, and ArSiF3 to Enones Catalyzed by a Dicationic Palladium (II)− Chiraphos or− Dipamp Complex. *Organometallics* **2005**, *24* (21), 5025-5032; b) Kim, S.-K.; Kim, T.-J.; Chung, J.-H.; Hahn, T.-K.; Chae, S.-S.; Lee, H.-S.; Cheong, M.; Kang, S. O., Bimetallic ethylene tetramerization catalysts derived from chiral DPPDME ligands: syntheses, structural characterizations, and catalytic performance of [(DPPDME) CrCl3] 2 (DPPDME= S, S-and R, R-chiraphos and meso-achiraphos). *Organometallics* **2010**, *29* (22), 5805-5811; c) Akiyama, K.; Wakabayashi, K.; Mikami, K., Enantioselective Heck-Type Reaction Catalyzed by tropos-Pd (II)

Complex with Chiraphos Ligand. *Adv. Synth. Catal.* **2005**, *347* (11-13), 1569-1575; d) Frauenrath, H.; Reim, S.; Wiesner, A., Asymmetric double-bond isomerization of cyclic allyl acetals by using diop and chiraphos modified nickel complexes. *Tetrahedron: Asymmetry* **1998**, *9* (7), 1103-1106.

[45] Noyori, R.; Takaya, H., BINAP: an efficient chiral element for asymmetric catalysis. *Acc. Chem. Res.* **1990**, *23* (10), 345-350.

[46] Hayashi, T.; Matsumoto, Y.; Ito, Y., Catalytic asymmetric hydroboration of styrenes. *J. Am. Chem. Soc.* **1989**, *111* (9), 3426-3428.

[47] Hayashi, T.; Matsumoto, Y.; Ito, Y., Palladium-catalyzed asymmetric 1, 4-disilylation of. alpha.,. beta.-unsaturated ketones: catalytic asymmetric synthesis of. beta.-hydroxy ketones. *J. Am. Chem. Soc.* **1988**, *110* (16), 5579-5581.

[48] Tani, K.; Yamagata, T.; Akutagawa, S.; Kumobayashi, H.; Taketomi, T.; Takaya, H.; Miyashita, A.; Noyori, R.; Otsuka, S., Metal-assisted terpenoid synthesis. 7. Highly enantioselective isomerization of prochiral allylamines catalyzed by chiral diphosphine rhodium (I) complexes. Preparation of optically active enamines. *J. Am. Chem. Soc.* **1984**, *106* (18), 5208-5217.

[49] Li, Y.-M.; Kwong, F.-Y.; Yu, W.-Y.; Chan, A. S., Recent advances in developing new axially chiral phosphine ligands for asymmetric catalysis. *Coord. Chem. Rev.* **2007**, *251* (17-20), 2119-2144.

[50] a) Hu, W.; Chen, C.-C.; Xue, G.; Chan, A. S., Synthesis of (−)-(4R, 5R)-4, 5-bis [di-3′-(2′, 6′-dimethoxypyridyl) phosphinomethyl]-2, 2-dimethyl-1, 3-dioxolane and its application in the Rh-catalyzed asymmetric hydrogenation reactions. *Tetrahedron: Asymmetry* **1998**, *9* (23), 4183-4192; b) Hu, W.; Pai, C. C.; Chen, C. C.; Xue, G.; Chan, A. S., Synthesis of a chiral pyridylphosphine ligand and a comparison of its rhodium complex with the structurally similar

arylphosphine rhodium catalysts in the asymmetric hydrogenation of 2-(6′-methoxy-2′-naphthyl) propenoic acid. *Tetrahedron: Asymmetry* **1998**, *9* (18), 3241-3246.

[51] a) Barbaro, P.; Bianchini, C.; Giambastiani, G.; Parisel, S. L., Progress in stereoselective catalysis by metal complexes with chiral ferrocenyl phosphines. *Coord. Chem. Rev.* **2004**, *248* (21-24), 2131-2150; b) Richards, C. J.; Locke, A. J., Recent advances in the generation of non-racemic ferrocene derivatives and their application to asymmetric synthesis. *Tetrahedron: Asymmetry* **1998**, *9* (14), 2377-2407; c) Atkinson, R. C.; Gibson, V. C.; Long, N. J., The syntheses and catalytic applications of unsymmetrical ferrocene ligands. *Chem. Soc. Rev.* **2004**, *33* (5), 313-328.

[52] Blaser, H.-U.; Spindler, F., Enantioselective catalysis for agrochemicals: the case history of the DUAL MAGNUM® herbicide. *CHIMIA International Journal for Chemistry* **1997**, *51* (6), 297-299.

[53] Blaser, H.-U.; Buser, H.-P.; Häusel, R.; Jalett, H.-P.; Spindler, F., Tunable ferrocenyl diphosphine ligands for the Ir-catalyzed enantioselective hydrogenation of N-aryl imines. *J. Organomet. Chem.* **2001**, *621* (1-2), 34-38.

[54] a) Colacot, T. J., A concise update on the applications of chiral ferrocenyl phosphines in homogeneous catalysis leading to organic synthesis. *Chem. Rev.* **2003**, *103* (8), 3101-3118; b) Wang, D.-Y.; Hu, X.-P.; Hou, C.-J.; Deng, J.; Yu, S.-B.; Duan, Z.-C.; Huang, J.-D.; Zheng, Z., Enantioselective Rh-catalyzed hydrogenation of 3-aryl-2-phosphonomethylpropenoates by a new class of chiral ferrocenyl diphosphine ligands. *Org. Lett.* **2009**, *11* (15), 3226-3229; c) Togni, A.; Breutel, C.; Schnyder, A.; Spindler, F.; Landert, H.; Tijani, A., A novel easily accessible chiral ferrocenyldiphosphine for highly enantioselective hydrogenation, allylic alkylation, and hydroboration reactions. *J. Am. Chem. Soc.* **1994**, *116* (9), 4062-4066; d) Hamann, B. C.; Hartwig,

J. F., Systematic variation of bidentate ligands used in aryl halide amination. Unexpected effects of steric, electronic, and geometric perturbations. *J. Am. Chem. Soc.* **1998**, *120* (15), 3694-3703.

[55] a) Bader, A.; Lindner, E., Coordination chemistry and catalysis with hemilabile oxygen-phosphorus ligands. *Coord. Chem. Rev.* **1991**, *108* (1), 27-110; b) Wassenaar, J.; Reek, J. N., Hybrid bidentate phosphorus ligands in asymmetric catalysis: Privileged ligand approach vs. combinatorial strategies. *Organic & biomolecular chemistry* **2011**, *9* (6), 1704-1713; c) Field, L. D.; Luck, I. J., Synthesis of bidentate mixed donor phosphorus/nitrogen ligands. *Tetrahedron Lett.* **1994**, *35* (7), 1109-1112; d) Kochi, T.; Yoshimura, K.; Nozaki, K., Synthesis of anionic methylpalladium complexes with phosphine–sulfonate ligands and their activities for olefin polymerization. *Dalton Transactions* **2006**, (1), 25-27; e) Bolzati, C.; Tisato, F.; Refosco, F.; Bandoli, G.; Dolmella, A., Uncommon anionic dioxorhenium (V) and neutral monooxorhenium (V) mixed-ligand complexes containing heterofunctionalized phosphine ligands: syntheses and structural characterization. *Inorg. Chem.* **1996**, *35* (21), 6221-6229; f) Tisato, F.; Refosco, F.; Bandoli, G.; Bolzati, C.; Moresco, A., Synthesis and characterization of neutral technetium (III) complexes with mixed S, P-bidentate phosphine–thiolate ligands. Crystal structure of [Tc (SCH 2 CH 2 PPh 2) 2 (SCH 2 CH 2 PPh 2 O)]. *J. Chem. Soc., Dalton Trans.* **1994**, (9), 1453-1461; g) Evans, D. A.; Campos, K. R.; Tedrow, J. S.; Michael, F. E.; Gagne, M. R., Application of chiral mixed phosphorus/sulfur ligands to palladium-catalyzed allylic substitutions. *J. Am. Chem. Soc.* **2000**, *122* (33), 7905-7920; h) Evans, D. A.; Michael, F. E.; Tedrow, J. S.; Campos, K. R., Application of chiral mixed phosphorus/sulfur ligands to enantioselective rhodium-catalyzed dehydroamino acid hydrogenation and ketone hydrosilylation processes. *J. Am. Chem. Soc.* **2003**, *125* (12), 3534-3543.

[56] a) Shintani, R.; Narui, R.; Tsutsumi, Y.; Hayashi, S.; Hayashi, T., Design and synthesis of new chiral phosphorus–olefin bidentate ligands and their use in the rhodium-catalyzed asymmetric addition of organoboroxines to N-sulfonyl imines. *Chem. Commun.* **2011**, *47* (21), 6123-6125; b) García de la Arada, I.; Díez, J.; Gamasa, M. P.; Lastra, E., Organoruthenium Complexes Containing New Phosphorus–Carbon and Phosphorus–Carbon–Sulfur Ligands Generated in the Coordination Sphere by Nucleophilic Addition Reactions. *Organometallics* **2013**, *32* (15), 4342-4352; c) Hahn, F. E.; Naziruddin, A. R.; Hepp, A.; Pape, T., Synthesis, characterization, and H-bonding abilities of ruthenium (II) complexes bearing bidentate NR, NH-carbene/phosphine ligands. *Organometallics* **2010**, *29* (21), 5283-5288; d) Lee, H. M.; Lee, C.-C.; Cheng, P.-Y., Recent development of functionalized N-heterocyclic carbene ligands: coordination chemistry and catalytic applications. *Curr. Org. Chem.* **2007**, *11* (17), 1491-1524; e) Shintani, R.; Duan, W. L.; Nagano, T.; Okada, A.; Hayashi, T., Chiral Phosphine–Olefin Bidentate Ligands in Asymmetric Catalysis: Rhodium-Catalyzed Asymmetric 1, 4-Addition of Aryl Boronic Acids to Maleimides. *Angew. Chem. Int. Ed.* **2005**, *44* (29), 4611-4614; f) Duan, W.-L.; Iwamura, H.; Shintani, R.; Hayashi, T., Chiral Phosphine− Olefin Ligands in the Rhodium-Catalyzed Asymmetric 1, 4-Addition Reactions. *J. Am. Chem. Soc.* **2007**, *129* (7), 2130-2138; g) Field, L. D.; Messerle, B. A.; Vuong, K. Q.; Turner, P., Rhodium (I) and iridium (I) complexes containing bidentate phosphine-imidazolyl donor ligands as catalysts for the hydroamination and hydrothiolation of alkynes. *Dalton Transactions* **2009**, (18), 3599-3614.

[57] Nazish, M.; Siddiqui, M. M.; Sarkar, S. K.; Münch, A.; Legendre, C. M.; Herbst-Irmer, R.; Stalke, D.; Roesky, H. W., Synthesis and Coordination Behavior of a New Hybrid Bidentate Ligand with Phosphine and Silylene Donors. *Chemistry (Weinheim an der Bergstrasse, Germany)* **2021**, *27* (5), 1744.

[58] Gysling, H. J.; Luss, H. R., Synthesis and properties of the hybrid tellurium-phosphorus ligand phenyl o-(diphenylphosphino) phenyl telluride. X-ray structure of [Pt [PhTe (o-(PPh2C6H4)] 2][Pt (SCN) 4]. 2DMF. *Organometallics* **1984**, *3* (4), 596-598.

[59] Braunstein, P.; Naud, F., Hemilability of hybrid ligands and the coordination chemistry of oxazoline-based systems. *Angew. Chem. Int. Ed.* **2001**, *40* (4), 680-699.

[60] Peris, E.; Crabtree, R. H., Key factors in pincer ligand design. *Chem. Soc. Rev.* **2018**, *47* (6), 1959-1968.

[61] Moulton, C. J.; Shaw, B. L., Transition metal–carbon bonds. Part XLII. Complexes of nickel, palladium, platinum, rhodium and iridium with the tridentate ligand 2, 6-bis [(di-t-butylphosphino) methyl] phenyl. *J. Chem. Soc., Dalton Trans.* **1976**, (11), 1020-1024.

[62] Choi, J.; MacArthur, A. H. R.; Brookhart, M.; Goldman, A. S., Dehydrogenation and related reactions catalyzed by iridium pincer complexes. *Chem. Rev.* **2011**, *111* (3), 1761-1779.

[63] Van Der Boom, M. E.; Milstein, D., Cyclometalated phosphine-based pincer complexes: mechanistic insight in catalysis, coordination, and bond activation. *Chem. Rev.* **2003**, *103* (5), 1759-1792.

[64] Honaker, M. T.; Hovland, J. M.; Nicholas Salvatore, R., The synthesis of tertiary and secondary phosphines and their applications in organic synthesis. *Current Organic Synthesis* **2007**, *4* (1), 31-45.

[65] a) Campbell, I.; Way, J., 975. Synthesis and stereochemistry of heterocyclic phosphorus compounds. Part I. Preparation of (+)-and (–)-10-p-dimethylaminophenyl-9, 10-dihydro-9-aza-10-phosphaphenanthrene. *Journal of the Chemical Society (Resumed)* **1960,** 5034-5041; b) Zon, G.; DeBruin, K. E.; Naumann, K.; Mislow, K., Stereospecific desulfurization of acyclic phosphine

sulfides with hexachlorodisilane and the alkaline hydrolysis of monoalkoxy-and monoalkylthiophosphonium salts. *J. Am. Chem. Soc.* **1969**, *91* (25), 7023-7027.

[66] a) Brunner, H.; Leyerer, H., Asymmetrische Katalysen: XXXV. Neue optisch aktive, einzähnige Phosphine aus α-Pinen und Mannit. Rhodium-Komplexe und enantioselektive Katalysen. *J. Organomet. Chem.* **1987**, *334* (3), 369-376; b) Kaesz, H.; Stone, F., Preparation and Characterization of Vinyldichlorophosphine, Vinyldimethylphosphine, and Ethyldimethylphosphine1, 2. *The Journal of Organic Chemistry* **1959**, *24* (5), 635-637.

[67] a) Aguiar, A.; Beisler, J.; Mills, A., Lithium diphenylphosphide: A convenient source and some reactions. *The Journal of Organic Chemistry* **1962**, *27* (3), 1001-1005; b) Aguiar, A.; Giacin, J.; Mills, A., A novel reaction leading to (1, 2-diphenylethyl) diphenylphosphine. *The Journal of Organic Chemistry* **1962**, *27* (2), 674-676.

[68] Campbell, I.; Way, J., 406. Synthesis and stereochemistry of heterocyclic phosphorus compounds. Part II. Loss of optical activity in the reduction of (+)-2-carboxy-9-phenyl-9-phosphafluorene 9-oxide. *Journal of the Chemical Society (Resumed)* **1961**, 2133-2141.

[69] a) Ballot, S.; Noiret, N., Synthesis of new C60 based phosphines. *Tetrahedron Lett.* **2003**, *44* (49), 8811-8814; b) Imamoto, T.; Kikuchi, S.-i.; Miura, T.; Wada, Y., Stereospecific reduction of phosphine oxides to phosphines by the use of a methylation reagent and lithium aluminum hydride. *Org. Lett.* **2001**, *3* (1), 87-90; c) Marsi, K. L., Phenylsilane reduction of phosphine oxides with complete stereospecificity. *The Journal of Organic Chemistry* **1974**, *39* (2), 265-267.

[70] Kolodiazhnyi, O. I., Recent developments in the asymmetric synthesis of P-chiral phosphorus compounds. *Tetrahedron: Asymmetry* **2012**, *23* (1), 1-46.

[71] Enders, D.; Saint-Dizier, A.; Lannou, M. I.; Lenzen, A., The Phospha-Michael addition in organic synthesis. *Eur. J. Org. Chem.* **2006**, *2006* (1), 29-49.

[72] Bartoli, G.; Bosco, M.; Carlone, A.; Locatelli, M.; Mazzanti, A.; Sambri, L.; Melchiorre, P., Organocatalytic asymmetric hydrophosphination of nitroalkenes. *Chem. Commun.* **2007**, (7), 722-724.

[73] a) Carlone, A.; Bartoli, G.; Bosco, M.; Sambri, L.; Melchiorre, P., Organocatalytic asymmetric hydrophosphination of α, β-unsaturated aldehydes. *Angew. Chem. Int. Ed.* **2007**, *46* (24), 4504-4506; b) Ibrahem, I.; Hammar, P.; Vesely, J.; Rios, R.; Eriksson, L.; Cordova, A., Organocatalytic Asymmetric Hydrophosphination of α, β-Unsaturated Aldehydes: Development, Mechanism and DFT Calculations. *Adv. Synth. Catal.* **2008**, *350* (11-12), 1875-1884.

[74] Lelais, G.; MacMillan, D. W., Modern strategies in organic catalysis: the advent and development of iminium activation. *Aldrichimica Acta* **2006**, *39* (3), 79-87.

[75] Dzięgielewski, M.; Pięta, J.; Kamińska, E.; Albrecht, Ł., Organocatalytic synthesis of optically active organophosphorus compounds. *Eur. J. Org. Chem.* **2015**, *2015* (4), 677-702.

[76] Glueck, D. S., Metal-catalyzed nucleophilic carbon–heteroatom (C–X) bond formation: the role of M–X intermediates. *Dalton Transactions* **2008**, (39), 5276-5286.

[77] Baillie, C.; Xiao, J., Catalytic synthesis of phosphines and related compounds. *Curr. Org. Chem.* **2003**, *7* (5), 477-514.

[78] Glueck, D. S., Metal-catalyzed asymmetric synthesis of P-stereogenic phosphines. *Synlett* **2007**, *2007* (17), 2627-2634.

[79] a) Hoge, G., Synthesis of both enantiomers of a P-chirogenic 1, 2-bisphospholanoethane ligand via convergent routes and application to rhodium-catalyzed asymmetric hydrogenation of CI-1008 (pregabalin). *J. Am. Chem. Soc.* **2003**, *125* (34), 10219-10227; b) Shimizu, H.; Saito, T.; Kumobayashi, H., Synthesis of novel chiral benzophospholanes and their application in asymmetric hydrogenation. *Adv. Synth. Catal.* **2003**, *345* (1-2), 185-189.

[80] Tappe, F. M.; Trepohl, V. T.; Oestreich, M., Transition-metal-catalyzed CP cross-coupling reactions. *Synthesis* **2010**, *2010* (18), 3037-3062.

[81] Moncarz, J. R.; Laritcheva, N. F.; Glueck, D. S., Palladium-catalyzed asymmetric phosphination: Enantioselective synthesis of a P-chirogenic phosphine. *J. Am. Chem. Soc.* **2002**, *124* (45), 13356-13357.

[82] Korff, C.; Helmchen, G., Preparation of chiral triarylphosphines by Pd-catalysed asymmetric P–C cross-coupling. *Chem. Commun.* **2004**, (5), 530-531.

[83] Chan, V. S.; Bergman, R. G.; Toste, F. D., Pd-catalyzed dynamic kinetic enantioselective arylation of silylphosphines. *J. Am. Chem. Soc.* **2007**, *129* (49), 15122-15123.

[84] a) Scriban, C.; Glueck, D. S., Platinum-catalyzed asymmetric alkylation of secondary phosphines: enantioselective synthesis of P-stereogenic phosphines. *J. Am. Chem. Soc.* **2006**, *128* (9), 2788-2789; b) Scriban, C.; Glueck, D. S.; Golen, J. A.; Rheingold, A. L., Platinum-catalyzed asymmetric alkylation of a secondary phosphine: mechanism and origin of enantioselectivity. *Organometallics* **2007**, *26* (7), 1788-1800; c) Anderson, B. J.; Glueck, D. S.; DiPasquale, A. G.; Rheingold, A. L., Substrate and Catalyst Screening in Platinum-Catalyzed Asymmetric Alkylation of Bis (secondary) Phosphines. Synthesis of an Enantiomerically Pure C 2-Symmetric Diphosphine. *Organometallics* **2008**, *27* (19), 4992-5001.

[85] Chan, V. S.; Stewart, I. C.; Bergman, R. G.; Toste, F. D., Asymmetric catalytic synthesis of P-stereogenic phosphines via a nucleophilic ruthenium phosphido complex. *J. Am. Chem. Soc.* **2006**, *128* (9), 2786-2787.

[86] a) Kawaoka, A. M.; Douglass, M. R.; Marks, T. J., Homoleptic lanthanide alkyl and amide precatalysts efficiently mediate intramolecular hydrophosphination/cyclization. Observations on scope and mechanism. *Organometallics* **2003**, *22* (23), 4630-4632; b) Takaki, K.; Komeyama, K.;

Takehira, K., Synthesis of lanthanide (II)–imine complexes and their use in carbon–carbon and carbon–nitrogen unsaturated bond transformation. *Tetrahedron* **2003**, *59* (52), 10381-10395.

[87] Butti, P.; Rochat, R.; Sadow, A. D.; Togni, A., Palladium-Catalyzed Enantioselective Allylic Phosphination. *Angew. Chem. Int. Ed.* **2008**, *47* (26), 4878-4881.

Chapter 2

Enantioselective synthesis of *C*-stereogenic PN(sp^2)P pincer ligands *via* catalytic asymmetric hydrophosphination

2.1. Introduction

The furnishment of organophosphorus compounds has ubiquitously proceeded through the construction of a P-C bond assembly. Amongst other synthetic options available as described previously, the net addition of a P-H bond across a C-C or C-X (where X can be N, O or S) multiple bond has been popularized as a strategic method of choice for the abovementioned purpose.[1] Referred to as hydrophosphination, the process typically involves the addition of trivalent secondary phosphines to substrate molecules bearing an electron withdrawing group (EWG) together with the said unsaturated functionality in the presence of an added catalyst (Scheme 2.1).

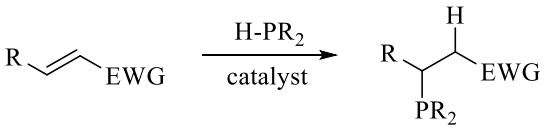

Scheme 2.1. General schematic illustration of hydrophosphination reaction.

Classical conducts of hydrophosphination have included the use of acids,[2] bases[3] and free radicals[4] as catalytic precursors to mediate the reaction. However due to the strength in reactivity of these additives, reaction outcomes are often plagued with problems associated with uncontrolled reaction and low selectivity, leading to the formation of undesired side products. In view of these limitations on an otherwise synthetically viable protocol to access organophosphines, the route towards finding more controlled methods has thus led to the advent of metal catalyzed

hydrophosphination as an alternative approach.[1] Since the introductory use of metal based catalysts, the scene of hydrophosphination has seen extensive developments in exploring the increased efficiencies that can be achieved with the newly minted methodology. Over the past few decades, progress in the field was vastly represented in countless examples showcasing the successful performance of different metal precursors including lanthanide[5] and alkaline-earth metals[6] for the intra- and intermolecular hydrophosphination of a diverse substrate scope incorporating aldehydes,[7] olefins,[6b, 8] carbodiimides,[9] imines[10] and heterocumulenes.[11]

Based on the working principle behind this methodology, the extension of catalytic hydrophosphination employed under asymmetric conditions presents great potential for the provision of chiral tertiary phosphines. Analogous to how the asymmetric organocatalyzed phospha-Michael addition reaction functions to generate optically active phosphine adducts, the synthetic motivation behind asymmetric hydrophosphination (AHP) likewise follows similarly in functionalizing prochiral carbons into chiral centers. Leveraging on the enhanced nucleophilicity of the phosphine moiety manifested in the metal-phosphide intermediate, the metal catalyzed asymmetric hydrophosphination in comparison to the organocatalyzed phospha-Michael addition reaction, has exhibited better reactivity with a larger scope of substrates (apart from those already mentioned above) that are less electrophilically activated, as will be illustrated in the following section. More importantly, it has also demonstrated to exude better robustness in terms of producing the chiral adducts with optimal enantioselectivities, the most vital component in asymmetric syntheses.

2.2. Metal complex catalyzed asymmetric hydrophosphination

An initial report of metal mediated AHP was reported by Glueck, carried out using a platinum(0) precursor with methacrylonitrile as described below (Scheme 2.2).[12]

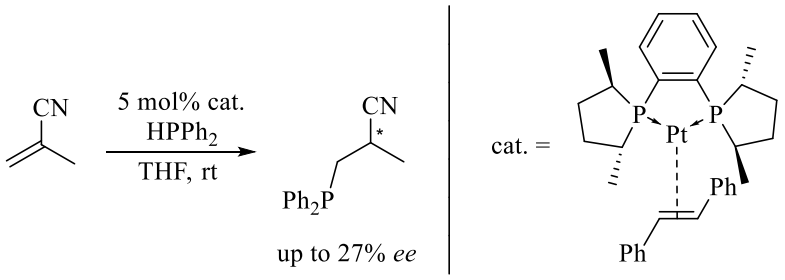

Scheme 2.2. Platinum(0) catalyzed AHP of methacrylonitrile.

Despite the modest levels of enantioselectivity attained, experimental insights gathered from this work revealed the mechanistic principles and corresponding implications governing the enantioselective process. In general, the main procedures of the catalytic cycle involve oxidative addition of the secondary phosphine, followed by insertion of the olefin and finally reductive elimination to release the product. Essentially, the insertion step holds two functional consequences for reaction. Firstly, the diastereoselective nature of this step (due to an additional point of chirality derived from the ligand) represents the key to generate the enantioenriched product. In order to facilitate successful asymmetric induction, it is therefore crucial that the ligand remains bound to the metal center during this phase, especially in the presence of other coordinative species participating in the catalytic cycle. In this case, the Me-Duphos ligand was carefully selected for utilization due to its rigid structure and strong bonding with platinum in comparison to other related diphosphine chelated Pt complexes. Secondly, it also moderates the

compatibility of the system to the phosphine substrate, with bulkier substituted phosphines working less favorably due to probable steric inhibition for olefin approach.[1]

Subsequent examples of metal catalyzed AHP by Togni showcased the use of a non-zero valent nickel precursor to mediate the addition reaction (Scheme 2.3).[13]

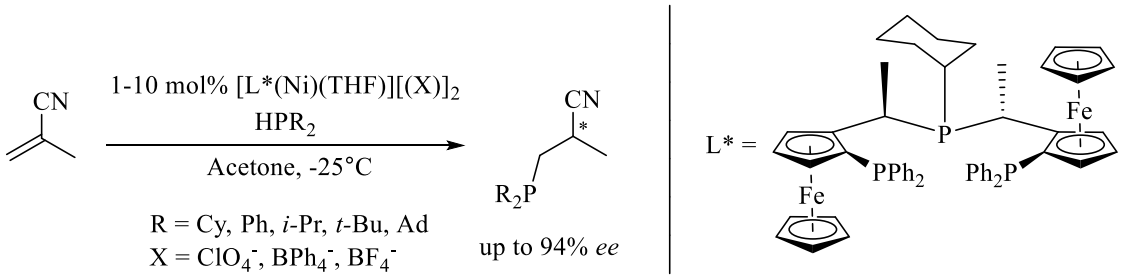

Scheme 2.3. Nickel(II) catalyzed AHP of methacrylonitrile.

Unlike the previous case, the nickel(II) system initiates the reaction through olefin coordination, which activates the substrate for intermolecular nucleophilic attack by the phosphine. At this stage, the formation of an axially chiral aza-allenyl phosphonium intermediate coordinated to the chiral metal template results in the generation of a diastereomeric mixture, which further undergoes a stereospecific proton transfer to yield the α-stereogenic adduct enantioselectively (Scheme 2.4).

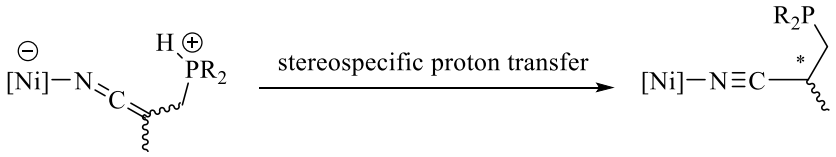

Scheme 2.4. Formation of diastereomeric nickel(II) transition state consisting of an axially chiral aza-allenyl phosphonium intermediate to generate enantioenriched adduct via stereospecific proton transfer.

Judging from the difference in mechanistic pathways for phosphine addition, it may be discerned that the improved tolerance for bulkier phosphine substrates in this scenario could be attributed to a better steric accommodation as compared to the earlier process involving an insertion step.

2.3. Palladacycle catalyzed asymmetric hydrophosphination

With the mechanistic understanding and preliminary results obtained from these works, the foundation was thus set for further developments in metal catalyzed AHP to employ more fine-tuned systems to improve reaction outcomes. To this end, pivotal efforts by Leung and Pullarkat have revolutionized the use of deliberately synthesized palladacycles as highly promising candidates for the catalytic facilitation of AHP with remarkable effectiveness (Figure 2.1).[14]

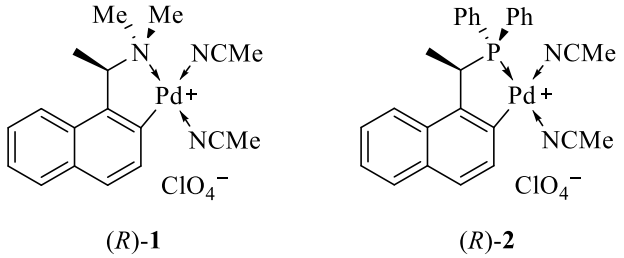

(*R*)-**1** (*R*)-**2**

Figure 2.1. Palladacycles developed for use in AHP by Leung and Pullarkat.

As with typical asymmetric metal complex catalysis depending on a chiral promoter, the stereochemical integrity of the ligand inherently plays an apparent role in providing for a stereospecific chiral inducing step. In this case, the chiral auxiliaries as showcased in Figure 2.1 fulfill this factor via a unique stereochemical feature arising from the five-membered chelate ring.[15] Structural investigations of related complexes of **1** have elucidated the rigid fixation of the chelate ring in either an absolute λ or δ conformation (for (*S*) and (*R*) configuration respectively) in both solid and solution states.[16] This has been identified as a consequential effect resulting

from steric repulsion between the methyl group on the chiral center and a proximal naphthalene proton, which not only prevents ring fluxionality but also in turn enforces the N-methyl moieties to remain in their respective axial and equatorial positions (Figure 2.2).[17]

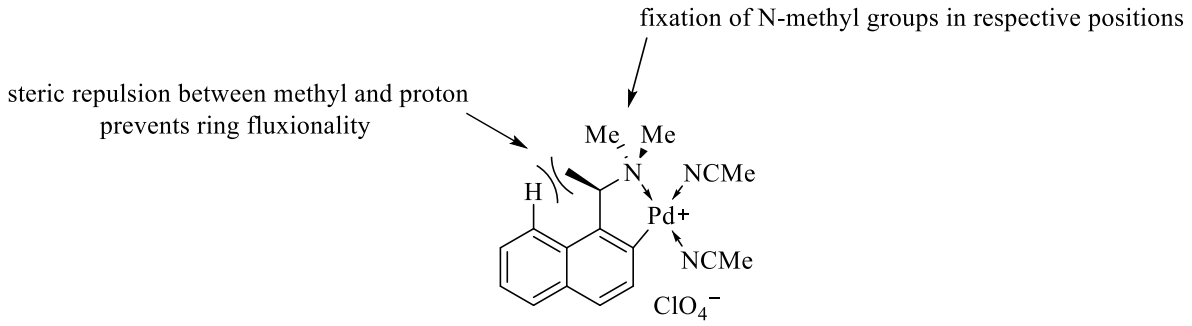

Figure 2.2. Illustration of structural enforcements within the chiral auxiliary of (*R*)-**1**.

The combination of these structural enforcements creates a well-defined chiral environment for effective stereochemical induction during the AHP reaction, which can be visually illustrated in the square planar intermediate below (Figure 2.3).

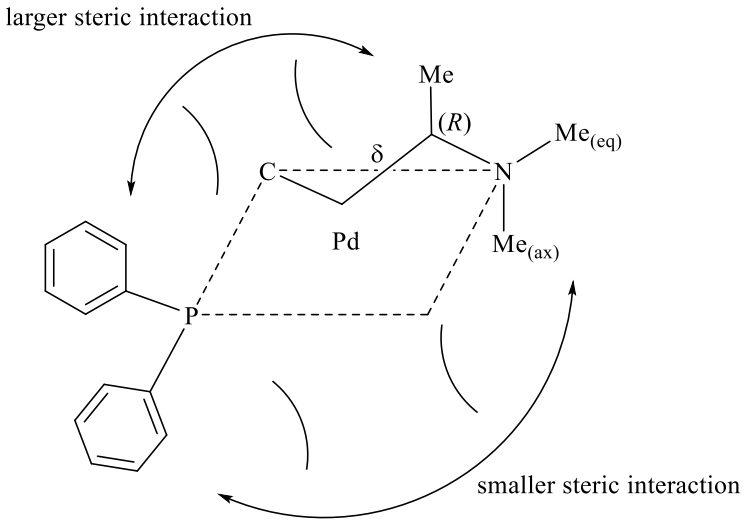

Figure 2.3. Representation of square planar intermediate during AHP reaction for δ-locked palladacycle.

As seen, steric influences by the three projecting methyl groups dictate the coordination of the incoming phosphine moiety in an orientation that renders the least steric repulsion. Relations drawn from structural modelling studies have also revealed the stereo-projection from the methyl substituent on the stereogenic carbon as the larger contributor towards the enantio-determination of the final product.[15a] In addition to that, the ligand also features distinct electronic characteristics between the ligating atoms which provide for a regioselective coordination process. Preferential coordination of phosphine *trans* to the N/P atoms and parallel inclination of the harder donors (usually oxygen or nitrogen from the α-unsaturated functionality) coordinating *trans* to the π-acidic naphthyl group results in the specific attachment of both nucleophilic and electrophilic components onto the metal center for intramolecular reaction.[18]

2.4. Pincer metal complex catalyzed asymmetric hydrophosphination

A more recent generation of catalysts embodying a chiral pincer backbone have also been introduced as suitable complexes for AHP. These were concomitantly developed by the groups of Duan and Leung, which generally bears a PCP type ligand architecture as shown in Figure 2.4.

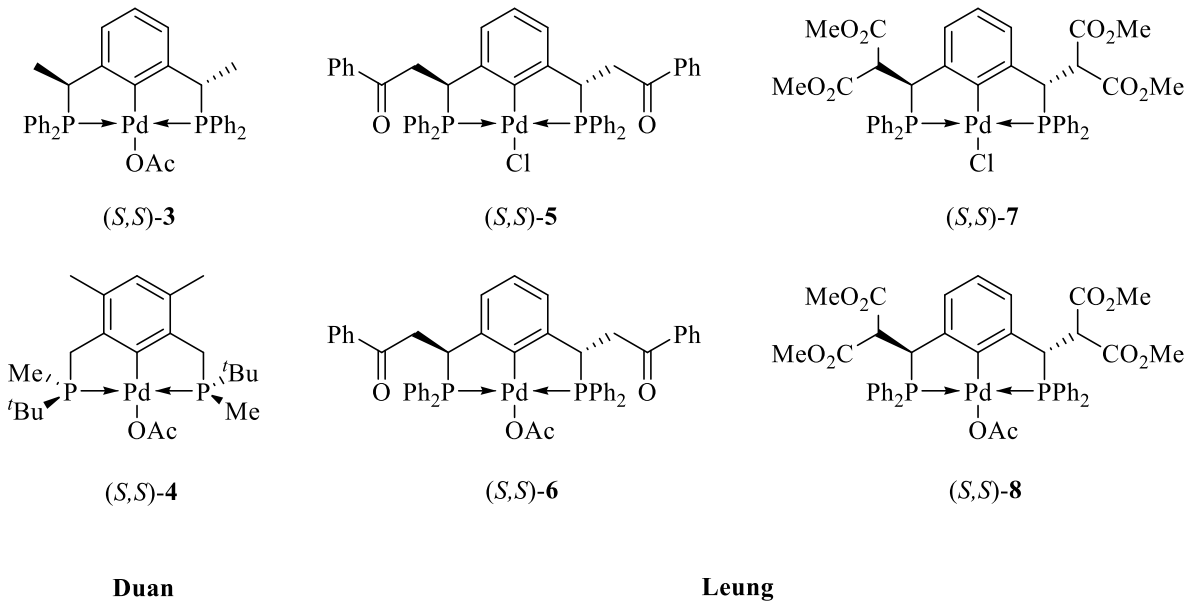

Figure 2.4. PCP pincer complexes developed for use in AHP by Duan and Leung.

In contrast to complexes **1** and **2**, the pincer complexes mediate the reaction through an intermolecular pathway because of only one possible vacant site. Nevertheless, the stereo-induction capability of these complexes does not fall short in comparison to their predecessors.[14a, 14c] Again, structural resolutions performed for **7** uncovered the stereochemical outlook of the pincer complex.[19] Based on X-ray analysis, the solid state structure showed axial orientation for the CO_2Me substituents, which understandably minimizes their steric interferences with both the central anchor ring as well as the PPh_2 groups that lie closely adjacent to them. This steric phenomenon was also verified to exist for the complex in solution state, which thus locks the two

five-membered chelate rings similarly in either an absolute λ or δ conformation (Figure 2.5). Ring interconversion was additionally explained and confirmed by NMR to be prevented by inhibition of bond rotation about the chiral center, due to steric hindrance from the equatorial Ph groups.

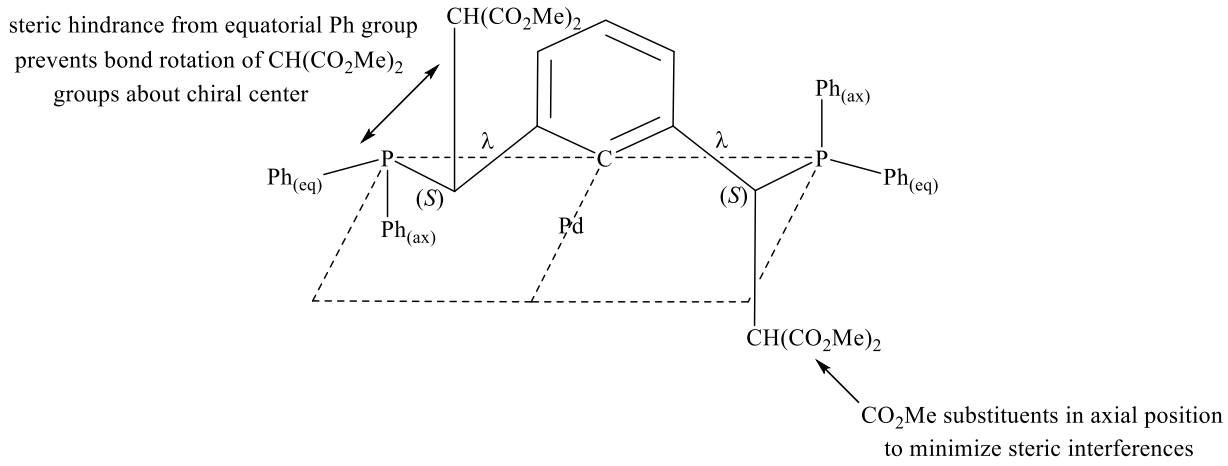

Figure 2.5. Stereochemical projections of substituents present in pincer complex (*S*,*S*)-**7.**

In essence, the stereochemical information derived from the design of these complexes converge to provide the necessary enforcements for effective chiral induction. This goes back to emphasize the intricacies of proper ligand design as a strong determinant and important factor for enantio-induction in the context of asymmetric applications.

2.5. Recent and current efforts with catalytic asymmetric hydrophosphination

Thus far, we have seen the progress of catalytic hydrophosphination as a plausible method to obtain organophosphorus compounds, to the asymmetric application of this protocol for the potential furnishment of new chiral tertiary phosphines. In the aim towards more sustainable approaches of synthesizing these chiral moieties, catalytic hydrophosphination serves as a highly favorable alternative due to the atom economical nature of the reaction (as with typical addition processes). Moreover, extensive achievements have been accomplished in the field of metal catalyzed AHP, with a plethora of chiral phosphine motifs synthesized under optimized utilization of the intricately designed metal complexes **1-7** and their derivatives, additionally showcasing the versatility of this reaction in its tolerance towards varying functional groups.[1]

Having these motivations in hand, our group has continuously invested in the expansion of chiral phosphine analogues via the use of catalytic AHP to survey their potential as compatible motifs for ligands in asymmetric applications and even biological processes.[14a, 14b, 20] Over the past decade, we have successfully implemented the reaction for the formation of new chiral tertiary phosphine derivatives with good yields and selectivity, utilizing the in-house catalysts that we have synthesized.[21] The following diagram depicts selected examples of the abovementioned, encompassing a range of synthesized phosphine synthons that have been subsequently employed as ligands or otherwise furnished as unique phosphine based adducts to showcase the added functionality of AHP as a plausible method to access specialized chiral phosphines that may be further investigated for potential utility (Figure 2.6).

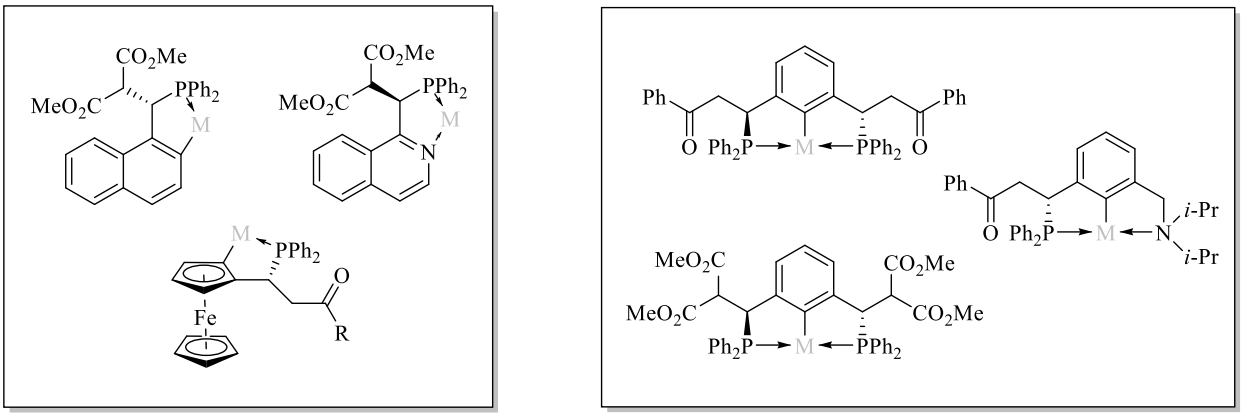

Asymmetric Hydrophosphination

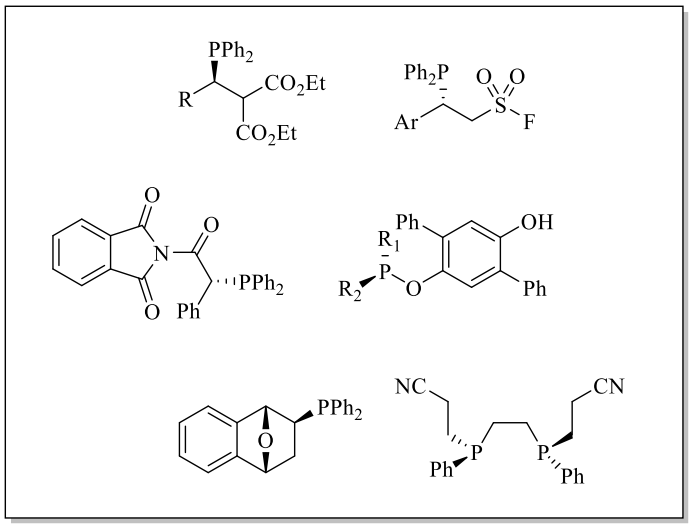

Figure 2.6. Selected illustrations of chiral tertiary phosphine derivatives obtained with AHP by our research group.

In particular, the more recent development of the PC(sp^2)P pincer scaffolds that were synthesized and affixed onto complexes **5-8** proved to be a landmark accomplishment, with these resultant complexes displaying excellent efficiencies in their respective applications.[14b, 22] Riding on the preliminary success exhibited by these new tridentate phosphine derivatives, we were curious to explore deeper into analogous pincer frameworks with regard to the comparative potentials in terms of their chemical syntheses and utility.

2.6. Illustrations of chiral pyridyl based PN(sp^2)P ligands in the literature

Coincidentally, a quick search in the literature revealed surprisingly that asymmetric constructions of chiral pyridyl based PN(sp^2)P moieties, in comparison to their phenyl based PC(sp^2)P counterparts, have been less extensively portrayed. In fact, it was only in the later 1990s wherein separate efforts by Zhang and Osborn showcased the first instances of these chiral phosphine tridentates (Figure 2.7).[23]

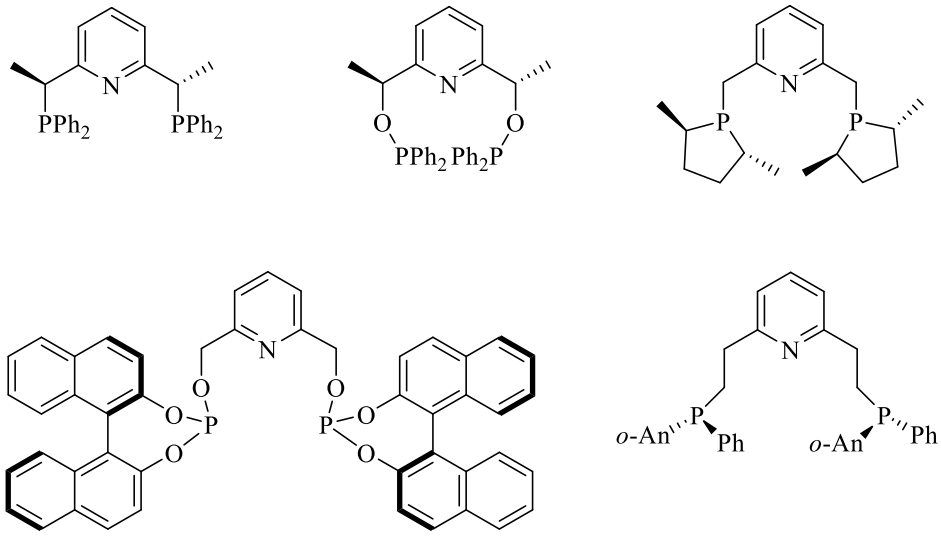

Figure 2.7. First examples of chiral pyridyl based PN(sp^2)P tridentates.

To the best of our knowledge, despite these earlier synthetic appearances, asymmetric representations of these derivatives remain especially rare, with the next single illustration featured only recently by Mezzetti and coworkers.[24] We thus turned our attention towards the ways that these phosphine motifs have been conventionally synthesized, and realized that a possible explanation to their scarcity may be drawn to the impediments accompanying their synthetic preparations.

2.7. General methods of synthesizing chiral pyridyl PN(sp^2)P tridentates

The generation of a chiral pyridyl PN(sp^2)P pincer ligand typically revolves around installing chiral elements either on the skeletal framework or functionalizing the prochiral substituents on the phosphorus atoms. Based on literature, these usually adopt three generic synthetic pathways namely; (a) asymmetric functionalization of the benzylic carbon,[23a, 23b, 25] (b) substitution with pre-defined chiral units drawn from existing chiral pools,[26] as well as (c) affixation of pre-synthesized *P*-stereogenic ligands[24, 27] (Figure 2.8).

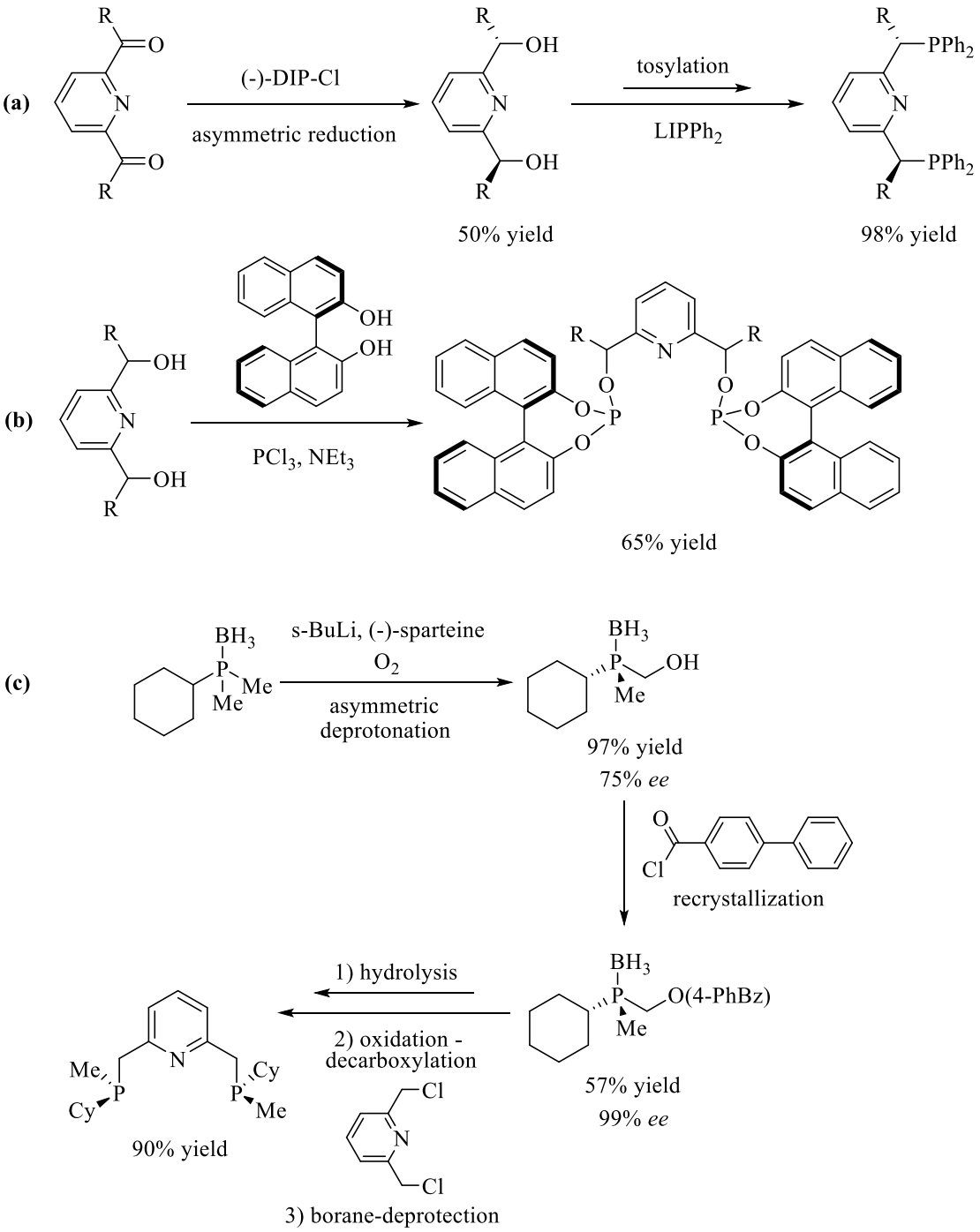

Figure 2.8. General methods of chiral PN(sp^2)P ligand synthesis.

As seen in Figure 2.8, the synthetic complexities borne within the existing methods of accessing chiral pyridyl PN(sp^2)P motifs could be the immediate reason for the lackluster display of these ligands in the literature. Aside from that, various drawbacks stemming from these methodologies may also hinder the willingness for experimentalists to commit to these preparative techniques. Firstly, the accessibility to enantiomerically pure *P*-chiral phosphines has been contemporarily regarded as a synthetically challenging process. Even in the described methodology, recrystallization had to be performed which is a highly time consuming and unpredictable process. That being said, certain difficulties also exist in the making of the *C*-stereogenic analogues in terms of introducing chirality onto the structure. Often, heteroatomic amino or hydroxyl groups are included as spacers at the ortho positions of the central ring (as described in method (b)), so that chirality can be established via a direct substitution with halogenophosphines derived from chiral pools.[28] The resulting effect of this is a further situation of the *C*-chirogenic center along the skeletal arm, which then extrapolates to an enhanced degree of secondary relay and probable less efficient transfer of chiral information. Secondly, the need to undergo multi-step processes involving cumbersome synthetic manipulations generally leads to low yields of the intended product. Thirdly, stoichiometric amounts of chiral starting materials or resolving agents are required which is wasteful in terms of atom economy.

2.8. Asymmetric hydrophosphination as an alternative method

The associated limitations in the access towards chiral pyridyl PN(sp^2)P tridentates as described above present as an apparent synthetic problem which remains to be resolved. In combination with the prior accomplishments we have made in the syntheses of chiral PC(sp^2)P tridentates, the corresponding formulation of the PN(sp^2)P analogues with AHP as a convenient synthetic method at our disposal would thoroughly complement the research objectives that we have set out to do as previously mentioned. Furthermore, this would also serve as a potential alternative to circumvent otherwise synthetically challenging pathways for the preparation of these motifs. On this basis, an investigation towards the syntheses of *C*-stereogenic, pyridyl based PN(sp^2)P diphosphine pincer ligands via catalytic asymmetric hydrophosphination was thus carried out.

2.9. Results and Discussions

Initial experiments were conducted with the use of 2,6-disubstituted pyridyl dienone **9a** as the standard substrate, together with 2.1 equivalents of diphenylphosphine ($HPPh_2$) in dichloromethane (DCM). For the facilitation of work-up procedures and characterizations, the generated isomeric tertiary phosphine adducts were sulfurized with elemental sulfur to form air stable phosphine sulfides that can be conveniently handled under open atmosphere (Table 2.1).

Table 2.1. Optimization screenings for AHP on standard substrate **9a**.[a]

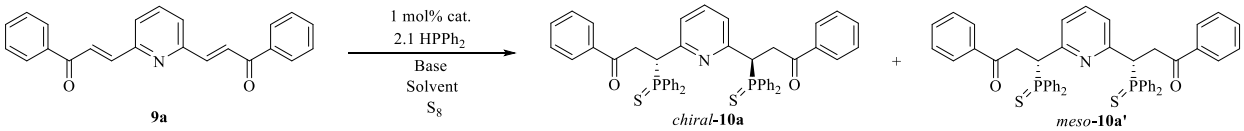

Entry	Cat.	Solvent	Base	*T* (°C)	Conv. (%)[d]	*de* (%)[e]	*ee* (%)[f]
1	-	DCM	NEt_3	rt	11/31	n.d	-
2[b]	(*S*)-**2**	DCM	NEt_3	rt	90/2	13	43
3[b]	(*S*)-**2**	DCM	NEt_3	-60	44/45	n.d	49
4	(*S*,*S*)-**6**	DCM	-	rt	59/18	38	57
5	(*S*,*S*)-**6**	DCM	-	-60	30/34	30	93
6	(*S*,*S*)-**8**	DCM	-	rt	70/15	43	>99
7	(*S*,*S*)-**8**	DCM	-	-60	0/48	-	-
8	(*S*,*S*)-**8**	Acetone	-	rt	95/4	37	>99
9	(*S*,*S*)-**8**	Toluene	-	rt	76/13	18	>99
10	(*S*,*S*)-**8**	THF	-	rt	38/33	17	88
11	(*S*,*S*)-**8**	EtOAc	-	rt	75/13	36	98
12	(*S*,*S*)-**8**	MeOH	-	rt	>99/0	17	18
13[c]	(*S*,*S*)-**8**	DCM	-	0	25/27	13	n.d
14[c]	(*S*,*S*)-**8**	Acetone	-	0	>99/0	72	>99

[a] Reaction conditions: 1 equiv. of **9a**, 2.1 equiv. of $HPPh_2$, 1 mol% of catalyst and 2.1 equiv. of base (where necessary) in 2 mL solvent at stipulated temperature for 24 hours. [b] 2.5 mol% of catalyst used. [c] Reaction conducted for 48 hours. [d] Determined from $^{31}P\{^1H\}$ NMR. Expressed as a ratio of diphosphinated/monophosphinated product. [e] Determined from $^{31}P\{^1H\}$ NMR with chiral **10a** as the major stereoisomer. [f] Determined by chiral HPLC after isolation of the sulfurized chiral isomer.

Trials began with a control experiment conducted in the absence of a catalyst at room temperature (Table 2.1, Entry 1). The reaction was regularly monitored via $^{31}P\{^{1}H\}$ NMR spectroscopy of the crude mixture and it was observed that the uncatalyzed hydrophosphination reaction proceeded negligibly to afford only 11% of the intended diphosphine product after 24 hours. Under similar reaction conditions, a separate trial incorporating the use of (*S*)-**2** on the other hand, afforded the targeted product in 90% conversion albeit with poor diastereo- and enantioselectivities (Table 2.1, Entry 2). A further reaction run conducted at -60°C revealed the inefficiency of (*S*)-**2** as a catalyst owing to low reactivity and insignificant improvements to selectivity (Table 2.1, Entry 3).

Interestingly, the results obtained provided a supplementary finding to the catalytic reactivity of (*S*)-**2** in comparison to a previous study employing the monosubstituted 2-pyridyl enone **11** as the substrate.[22] With the availability of two active catalytic vacant sites, the (*S*)-**2** palladacycle promotes the reaction through an intramolecular mechanism in which simultaneous coordination of both the substrate and $HPPh_2$ onto the Pd center allows for a highly stereoselective addition process. In the case of substrate **11**, this unfortunately led to catalyst poisoning as a consequence of strong and irreversible P-N chelation. Concurringly, the occurrence of catalyst poisoning is also probable for **9a**, but this was evidently disproved by the observed positive conversions to the diphosphine product. It may perhaps be deduced that repulsion between the more sterically demanding disubstituted substrate with the PPh_2 auxiliary on (*S*)-**2** prevented the P-N chelation, thereby permitting reaction progression by facilitating a fast product elimination process (Scheme 2.5).

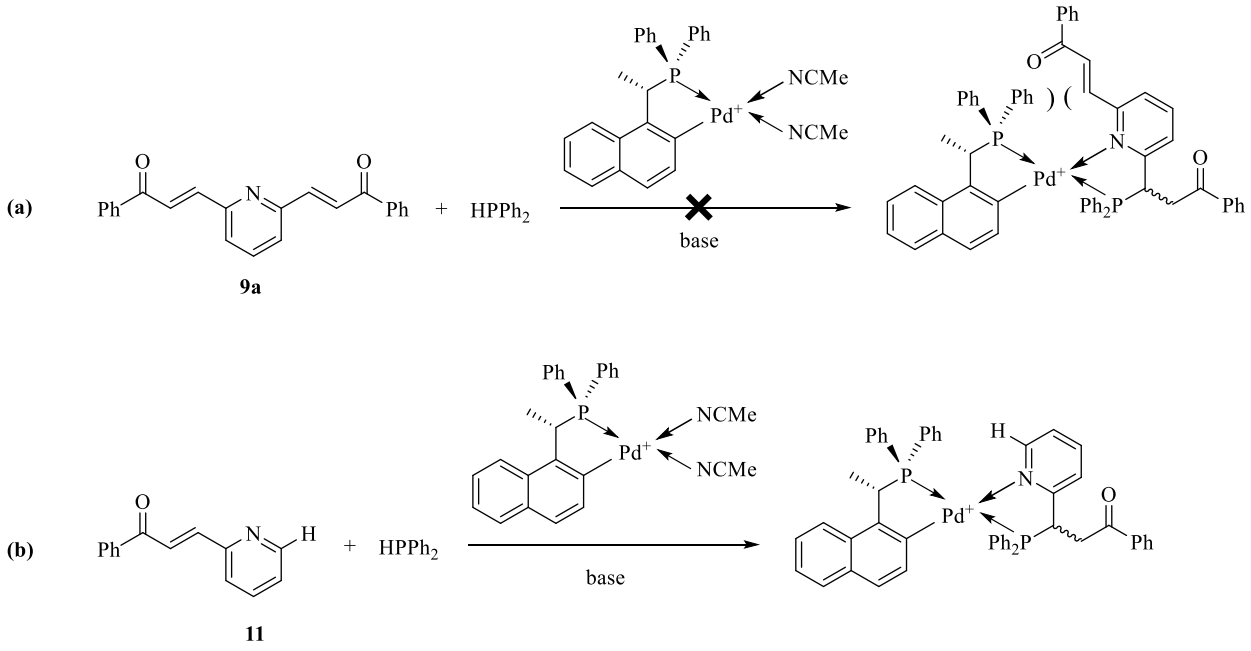

Scheme 2.5. Illustration of **(a)** steric induced prevention of catalyst poisoning and **(b)** catalyst poisoning due to P-N chelation.

Subsequent attempts were therefore focused on raising selectivity levels whilst ensuring decent conversions by replacing the choice of catalyst to the pincer complexes (*S*,*S*)-**6** and (*S*,*S*)-**8**. Additionally, it was envisaged that the presence of only a single active vacant site in these complexes would exclude complications arising from catalyst poisoning. Comparatively, both pincer complexes outperformed (*S*)-**2** in terms of generating the product with much improved selectivity at room temperature, with (*S*,*S*)-**8** impressively providing the chiral diastereomeric adduct in almost absolute enantiopurity (Table 2.1, Entries 4 and 6). To determine if the diastereoselectivity could be further improved at lower temperature, both (*S*,*S*)-**6** and (*S*,*S*)-**8** were also evaluated at -60°C, but these runs proved to be unsuccessful with lower conversions achieved in both cases and with even no signs of the intended diphosphine product observed in the trial with (*S*,*S*)-**8** (Table 2.1, Entries 5 and 7). A correlation may therefore be derived whereby while the more sterically defined pincer complexes imbue better stereochemical induction, their chemical

reactivities are inadvertently reduced at lower temperatures, especially for the case of the relatively bulkier ester-functionalized (*S*,*S*)-**8** complex.

Despite this, the favorable *de* and *ee* values obtained with (*S*,*S*)-**8** at room temperature still justified its selection as the catalyst of choice for further optimization reactions. Apart from methanol, solvent optimization trials generally displayed good toleration to an appreciable range of less polar to highly polar solvents to provide the furnished product with decent conversions and excellent enantioselectivities (Table 2.1, Entries 8-12). Since there were little discrepancies in *ee* values between various solvent options, both DCM and acetone were further analyzed for low temperature screenings in view of the preferential *de* values obtained at room temperature (Table 2.1, Entries 6 and 8). The results of these studies revealed a stark disparity between the two chosen solvents. While the run with acetone yielded the product with significant enrichment of diastereoselectivity (from 37% to 72%), the experiment conducted using DCM conversely showed a drastic decrease in *de* value (from 43% to 13%) and a considerable loss of product conversion. (Table 2.1, Entries 13 and 14). Nevertheless, the reaction with acetone managed to preserve both the levels of conversion as well as enantioselectivity, and it was thus chosen as the optimized solvent of choice. Notably, trials to further improve the diastereoselectivity of the product by subjecting the reaction to temperatures below 0°C proved to be ineffective, owing to adverse implications on reaction rates and corresponding yields.

With the selected catalyst and optimized conditions in hand, a series of functionalized moieties of **9** were then synthesized for the assessment of substrate scope (Table 2.2).

Table 2.2. Screenings for AHP on functionalized substrates **9**.[a]

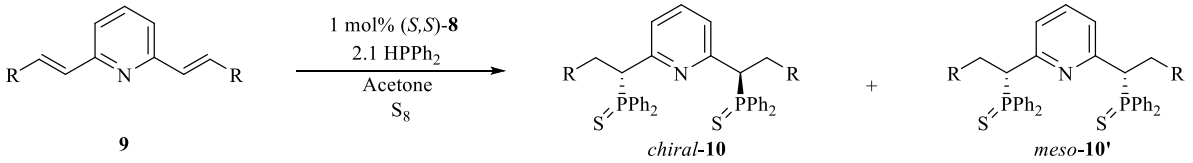

Entry	Substrate	R	T (h)	*T* (°C)	Product	Conv. (%)[d]	*de* (%)[e]	*ee* (%)[f]
1	**9a**	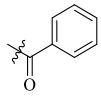	48	0	**10a**	>99	72	>99
2[b]	**9b**	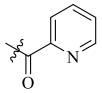	108	rt	**10b**	>99	36	84
3[b]	**9c**		144	rt	**10c**	87	2	89
4[b]	**9d**	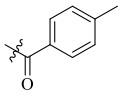	24	rt	**10d**	>99	20	>99
5[b]	**9e**	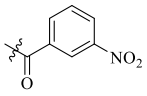	24	rt	**10e**	>99	34	99
6	**9f**	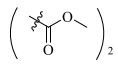	24	rt	**10f**	>99	12[g]	3

Table 2.2. continued

Entry	Substrate	R	T (h)	*T* (°C)	Product	Conv. (%)[d]	*de* (%)[e]	*ee* (%)[f]
7[c]	**9f**		24	rt	**10f**	>99	5[g]	-
8	**9f**	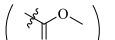	24	0	**10f**	>99	7[g]	5
9	**9f**		180	-40	**10f**	>99[h]	-	-

[a] Reaction conditions: 1 equiv. of substrate **9**, 2.1 equiv. of $HPPh_2$ and 1 mol% of (*S*,*S*)-**8** in 2 mL acetone at the indicated temperature for the stipulated timing. [b] 4 mL of acetone used. [c] (*S*,*S*)-**8** not added. NaOAc used as external base. [d] Determined from $^{31}P\{^1H\}$ NMR. [e] Determined from $^{31}P\{^1H\}$ NMR with *chiral* **10** as the major stereoisomer. [f] Determined by chiral HPLC after isolation of the sulfurized chiral isomer. [g] *Meso* product obtained as major stereoisomer. [h] Only 20% of converted product constitutes to diphosphines **10**. The other 80% of the converted product remains as the monophosphine adduct.

It should be noted that adjustments were made to carry out the reactions at room temperature in certain cases due to the inherent lower reactivities of the functionalized substrates arising from solubility issues. Attempts to perform the reactions at the optimized temperature of 0°C led to poor conversions even after employing twice the optimized reaction time of 48 hours. Despite the increase in temperature, the enantio-induction ability of the catalyst was remarkably unimpaired. As shown in Table 2.2, both electron donating 4-Me and electron withdrawing 3-NO_2 functionalities were very well tolerated, providing adducts with substantial conversions and near absolute enantiopurities (Table 2.2, Entries 4 and 5). Substrates bearing heterocyclic groups at the

terminal ends of the backbone were also modestly tolerated, although longer reaction times were required (Table 2.2, Entries 2 and 3). This could be attributed to the presence of additional donor atoms on the substrate backbone which may have participated in transient coordinative interactions with the Pd center, thereby hindering the full operating capacity of the metal complex. On another note, the slightly diminished conversion obtained in the case of **9c** could also be accorded to the much stronger electron donating capability of the furyl functionality, thereby reducing the electrophilicity of the *β*-carbon and its corresponding reactivity for phosphine addition.

On the other hand, reaction with the highly electron withdrawing, tetra ester functionalized substrate **9f** seemingly proceeded almost entirely without the influence of the catalyst, as can be seen by the meagre *de* and *ee* values attained at room temperature (Table 2.2, Entry 6). This prompted an investigation into a possible background uncatalyzed reaction pathway, which was subsequently verified with a trial reaction under similar reaction conditions but without the incorporation of (*S,S*)-**8**. As postulated, the reaction yielded the intended diphosphine products in full conversion despite the absence of the catalyst (Table 2.2, Entry 7). Upon this realization, further experiments were conducted at reduced temperatures in the aim of lowering the rate of background reaction to enhance selectivity. Unfortunately, the efforts proved futile as no substantial improvements to enantioselectivity were observed despite a drop in reaction temperature to 0°C (Table 2.2, Entry 8). A successive attempt with an even lower reaction temperature of -40°C eventually slowed the rate of product formation too excessively, with only 20% of the converted product constituting to the intended diphosphine adduct after more than a week of elapsed reaction time (Table 2.2, Entry 9). Evidently, a necessary balance had to be achieved by the catalyst for the accommodation of the relative steric bulk of the substrate and the

simultaneous mediation of the reaction at low temperatures to avert background reaction arising from the increased reactivity of the substrate.

With respect to diastereoselectivity, the attained *de* values were modest at best. This was expectedly so since prior optimization studies with the standard substrate **9a** have revealed its temperature dependence, with lower temperatures affording higher differentials. The sulfurized crude mixture can however be separated via silica chromatography to solely afford the isomerically pure forms of each diastereomer, notwithstanding a certain loss in yield. The selectivity of the reaction was indicated to be (*R*,*R*) on both chiral centers, as determined from the absolute configuration of the isolated phosphine sulfide **10a** via its single crystal diffraction analysis shown below (Figure 2.9).

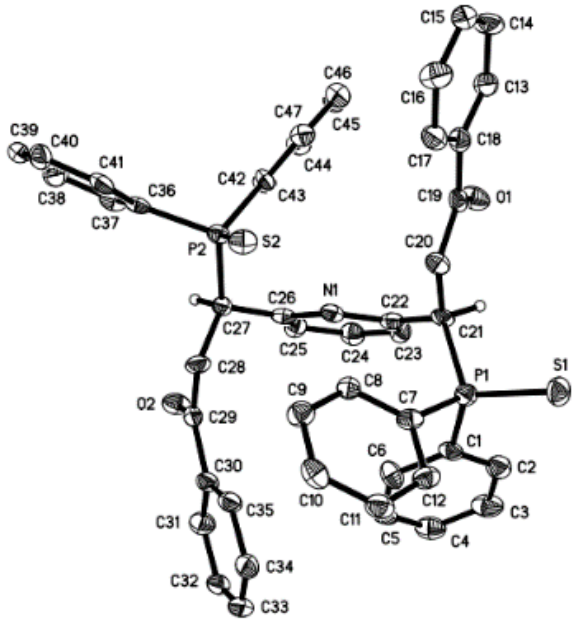

Figure 2.9. ORTEP representation of phosphine sulfide (*R*,*R*)-**10a** with thermal ellipsoids drawn at 50% probability level. Hydrogen atoms (except those on chiral carbons) are omitted for clarity.

2.10. Proposed reaction mechanism

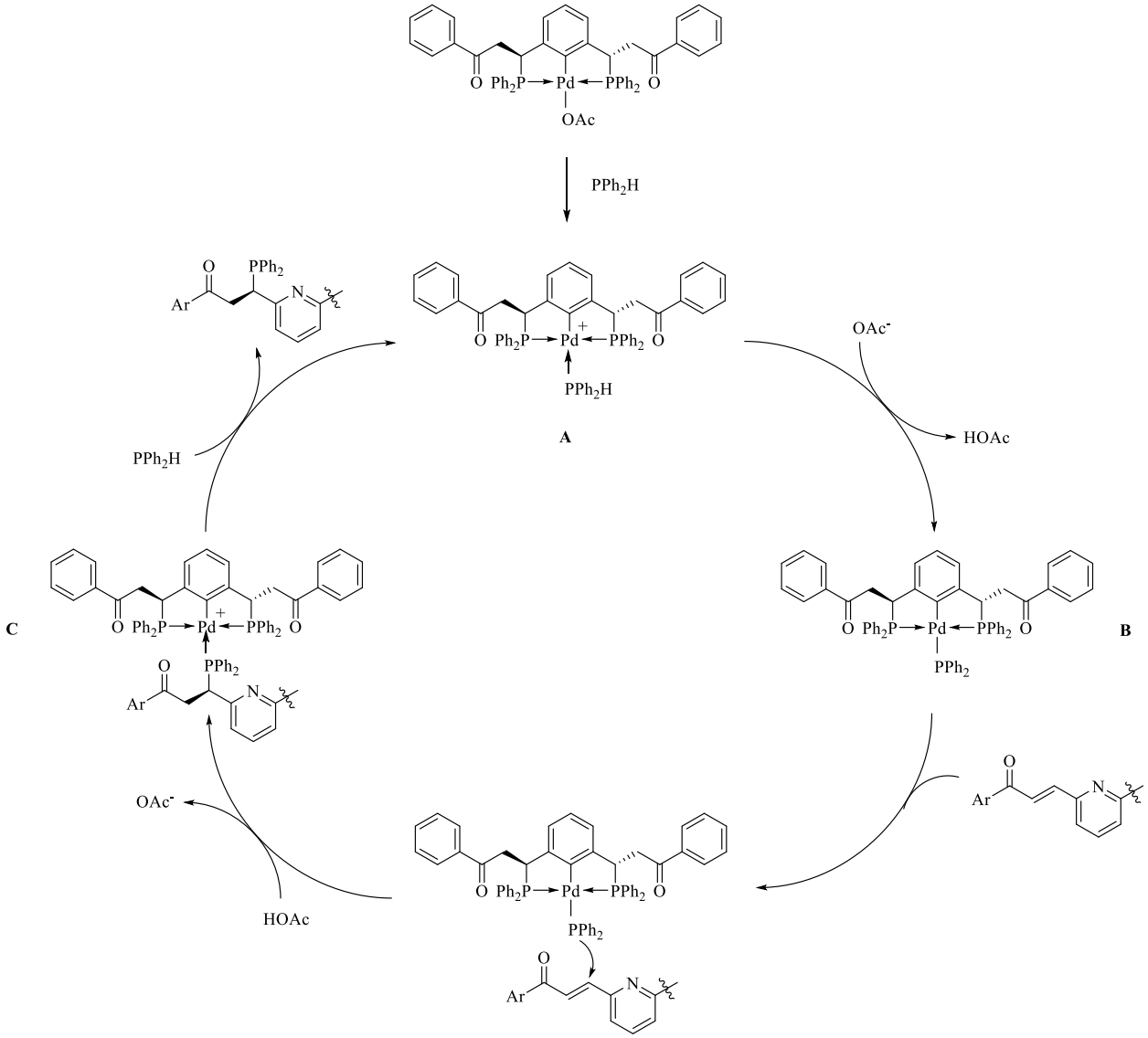

Figure 2.10. Mechanistic proposal for the AHP reaction.

The proposed mechanistic pathway for the reaction is described in Figure 2.10 above. In the initial phase, the acetate ligand gets readily displaced by a $HPPh_2$ moiety to form intermediate **A**. The liberated acetate anion in turn acts as an external base to deprotonate the coordinated phosphine, generating the active nucleophilic phosphide species **B** which adds intermolecularly to a proximal substrate molecule, thus resulting in the first stereogenic P-C bond formation. Protonolysis then ensues to regenerate the acetate anion and provide the monophosphine adduct **C**. Due to steric demands induced between the formed monophosphine and the auxiliaries present on the catalyst, the Pd-P bond is rendered kinetically labile to enable facile product elimination, thereby freeing up the vacant site on Pd for the coordination of a subsequent $HPPh_2$ moiety to facilitate the second addition process. The high levels of enantiomeric excess achieved in the eventual furnished products suggests an underlying efficient stereochemical control by the chiral catalyst. On the other hand, the diastereoselectivity of the reaction which is determined during the second addition process, is subjected to probable conflicting stereochemical influence from both the catalyst as well as the chiral intermediate from the first addition.[29] This may have resulted in a less selective formation of diastereomers, which could explain for the disparity in the levels of diastereoselectivity observed in comparison to the enantioselectivity of the overall reaction. Nevertheless, the effectiveness of this metal catalyzed protocol is still well exhibited by its ability to generate near enantiomerically pure pyridyl PN(sp^2)P adducts.

2.11. Proposed discussion for stereoselectivity

As previously mentioned, the stereoinduction step occurs during the P-C bond formation process, whereby the optically active auxiliary from the metal complex exerts a chiral influence on the incoming substrate for selective bond construction. However in the case presented here, the involvement of a sequential addition procedure may be assumed to raise the complexity of the chiral induction process due to the generation of an additional chiral stimulus from the initial monophosphinated adduct. Consequently, two possible modes of stereoinduction can happen; 1) catalyst-controlled or 2) substrate-controlled.[29] This can be more clearly elaborated in the following illustration (Figure 2.11).

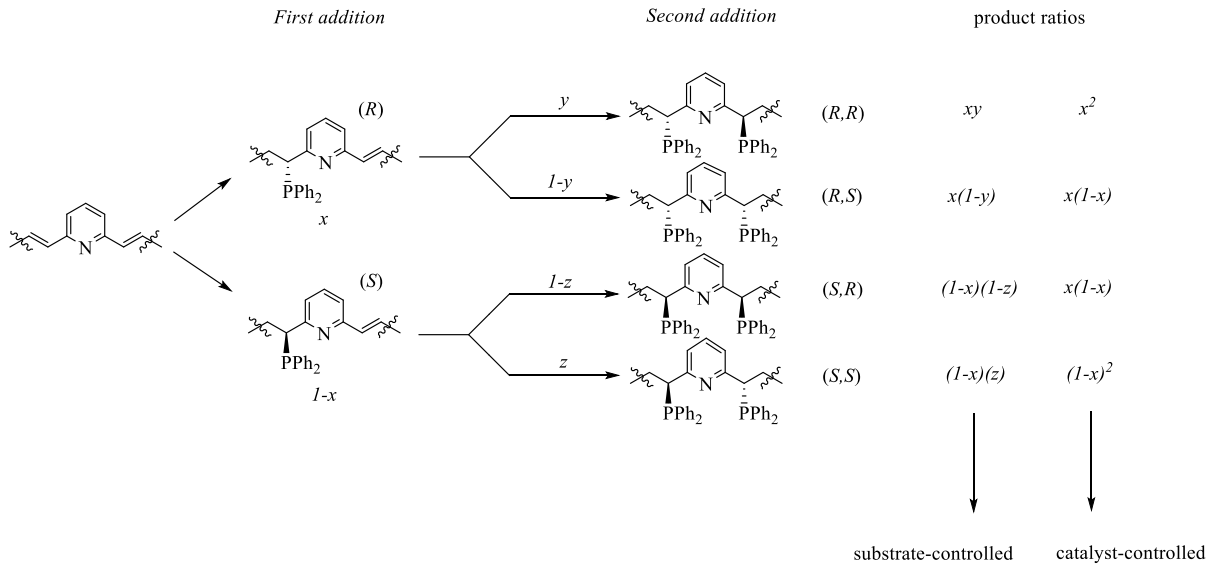

Figure 2.11. Proposed stereoinduction pathways for the AHP reaction.

In an ideal scenario whereby the catalyst provides good enantiodiscrimination and is selective enough to garner absolute chiral control, the reaction should in general produce the enantiomeric products with high diastereo- and enantioselectivities. Following the flowchart under the catalyst-controlled pathway, the attainment of products with absolute enantiomerical excess would theoretically mean the formation of only either one of the two conformers throughout the entire process. Additionally, this would also lead to a perfect diastereomeric ratio skewed solely towards the chiral diastereomer.

With respect to this, several noteworthy correlations can be presented. Firstly, based on the non-absolute diastereomeric excess obtained in our scenario, it is evident that the enantio-discretion process veers towards the other pathway relating to a substrate-controlled mechanism. This in turn justifies the assumption raised above that changes in the substrate affect subsequent catalytic selectivity, in which both chiral intermediates (*R*)-X and (*S*)-X corresponding to the enantiomeric forms of the monophosphinated adduct, are inequivalently recognized by the catalyst on a stereochemical viewpoint upon approach for the second addition step. Secondly, the end state accomplishment of perfect enantiomeric excess for the reaction thus reflects absolute selectivity in either one of the two hydrophosphination steps. Thirdly, the favoring of the chiral diastereomer with a corresponding (*R,R*) configuration (as indicated by X-ray crystallography of the enantiopure product) suggests a stereoselective bias towards the formation of *R*-enantiomer in both addition steps. Having these in mind, we thus attempt to discern the origins for stereoselectivity in the reaction, using the proposed chiral inducing pathways as described in the next diagram (Figure 2.12).

.

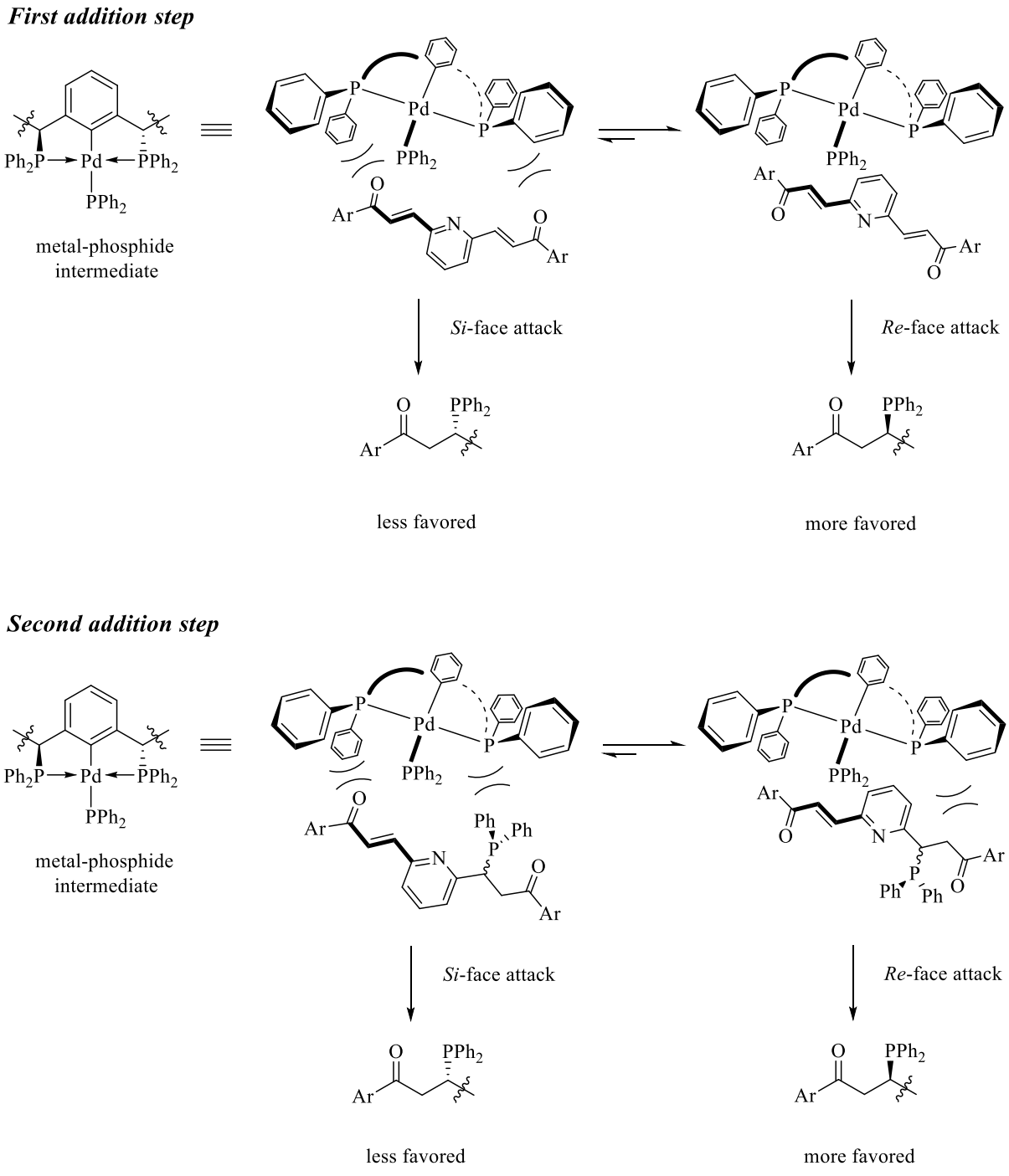

Figure 2.12. Proposed stereoselective formation of product.

With reference to our proposed mechanism, the stereoselective P-C bond assembly should accordingly take place between the substrate and the metal-phosphide intermediate **B**. Figure 2.12 shows a truncated representation of the chiral metal-phosphido complex, with attention directed at the stereoprojecting PPh_2 groups as part of the main determinant factors for the controlled approach of the substrate. The general inclination for (*R*)-formation on the prochiral carbon center may be attributed to the spatial interactions between the substrate and catalyst, which predict a more favorable orientation for *Re*-face attack due to a minimization of steric repulsion when the substituents on the substrate are pointed away from the stereoprojection of the PPh_2 moieties. This steric phenomenon holds through for both addition steps as depicted, but is unlikely the only constituting factor for stereoinduction in the second step. With plausible stereochemical interactions arising from the newly installed chiral center from the previous addition step, a few potential scenarios may surface to influence the selectivity of the second hydrophosphination process.

*In the case whereby the first addition is **not** absolutely selective;*

1) The inclusion of a substantially bulky PPh_2 group increases the existing steric interactions between substrate and catalyst, leading to enhanced preference for *Re*-face attack and rendering it the sole selective pathway.

2) The catalyst identifies the enantiomeric monophosphine intermediates stereochemically as individually unique moieties and processes the second addition differently to form the corresponding chiral and *meso* products for each stereoisomer. Accordingly in the event of a perfectly enantioselective reaction outcome, the value of *z* has to be zero (with respect to the (*R*,*R*)

configuration obtained) while the three remaining numerical parameters may take random values not necessarily equaling to zero.

In the case whereby the first addition is absolutely selective;

3) With additional steric bulk and stereo-influence from the incorporation of the first PPh_2, the different diastereomeric transition states become less energetically distinguishable during the second addition, resulting in a less selective formation of the subsequent P-C bond to generate both *chiral* and *meso* adducts.

In another aspect, the diastereoselective preference for the formation of the final product may also be rationalized using the Masamune diastereomeric match or mismatch effect.[30] For this to be done, we refer specifically to the second addition process wherein the stereochemistry of the monophosphine adduct contributes an influence to the determination of the diastereomeric match or mismatch pairs between the metal-phosphide intermediate and the incoming monophosphinated substrate (Figures 2.13 and 2.14).

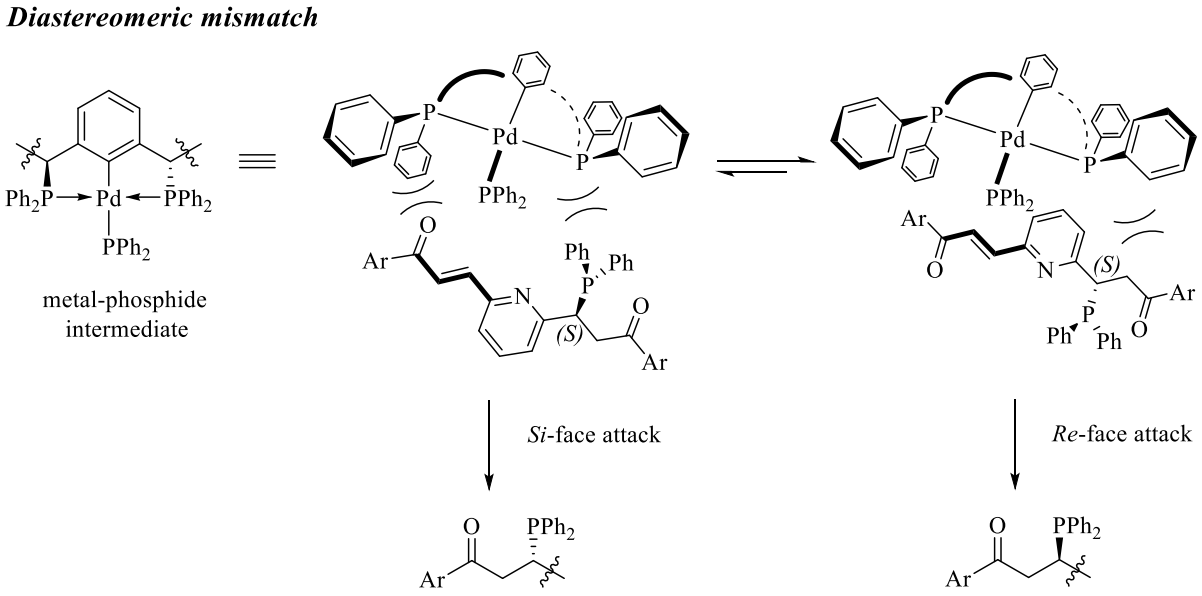

Figure 2.13. Proposed diastereomeric mismatch between (*S*)-monophosphine and (*S*,*S*)-metal-phosphide intermediate to generate reduced selectivity of *Re*-face product.

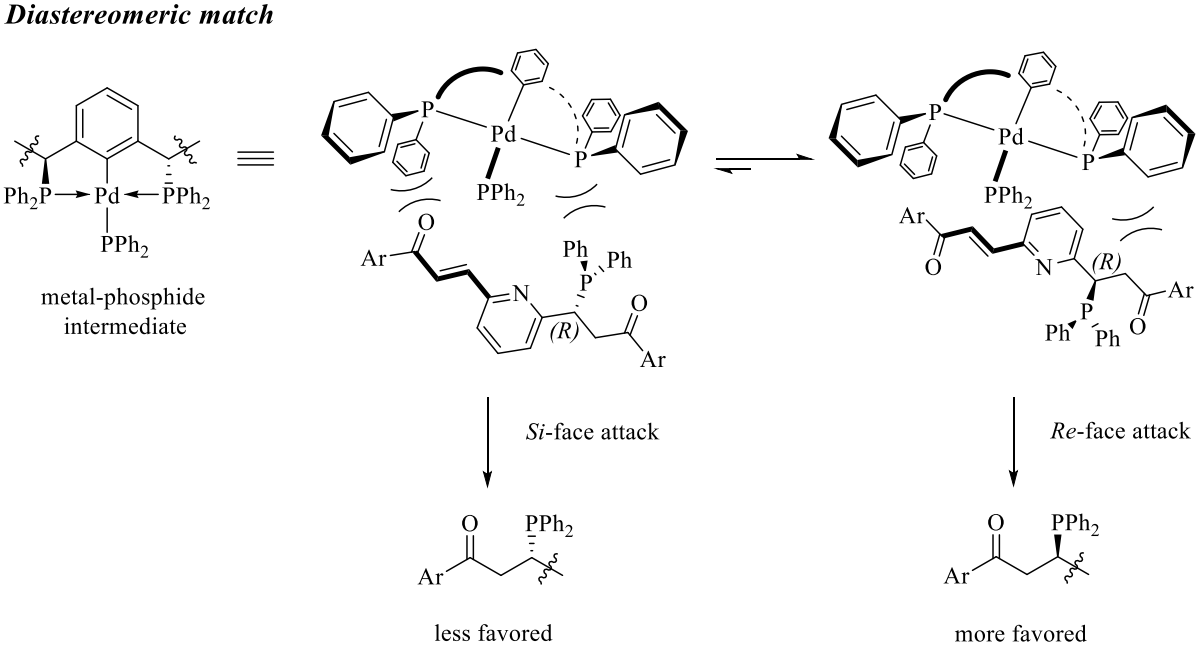

Figure 2.14. Proposed diastereomeric match between (*R*)-monophosphine and (*S*,*S*)-metal-phosphide intermediate to generate enhanced selectivity of *Re*-face product.

With the stereoconfiguration of the metal complex fixed at (*S*,*S*), the resultant prompts for diastereofacial selectivity in the reaction aside from the original steric considerations already taken into account from the interaction drawings above, rests mainly upon the stereoprojection of the added PPh_2 group and its interference with the direction of approach by the next PPh_2 moiety. From the illustrations shown above, it is evident that if the first PPh_2 substituent adopts an (*S*) configuration, additional steric interactions occurring between the bottom face approach of the metal-phosphide intermediate and the downward facing PPh_2 group on the substrate would likely result in a less selective formation of the *Re*-face adduct. Correspondingly, this leads to a lowered diastereoselectivity ratio between *Re* and *Si* products and hence establishes a diastereomeric mismatch pair of reacting molecules constituting of the (*S*)-monophosphine and (*S*,*S*)-metal-phosphide intermediate. On the other hand, an (*R*) conformation on the monophosphinated adduct would predict an opposite effect from the abovementioned, whereby the upward projection of the PPh_2 substituent promotes a more favorable *Re*-face attack due to less steric inhibition, in addition to the other existing steric interactions which also support the *Re*-face addition product. In turn, this corresponds to an enhanced selectivity towards the *R*e-face product and hence describe a diastereomerically matched pair of reacting molecules constituting of the (*R*)-monophosphine and (*S*,*S*)-metal-phosphide intermediate. The following predicted consequence follows the selective formation of the (*R*,*R*)-diphosphine product as corroborated by its crystal structure and thus provides an apparent plausibility for the Masamune diastereomeric match/mismatch effect to be part of the determinant factors in the observed stereochemical outcome.

While we were unable to ascertain the step which confers absolute selectivity, conclusions acquired from the above proposed explanations point towards a more probable reason for the first addition to be the associated step in generating enantiomerically pure monophosphinated adducts, that eventually leads to formation of the enantiomerically pure diphosphines despite a non-perfect diastereomeric ratio. This takes into account the combination of both steric and stereochemical considerations, in which the planarity of the initial substrate molecule in conjunction with the absence of any additional stereochemical influence lies in line with the *Re*-face attack as the only plausible preferred mode of addition. Nevertheless, the overall stereoselective outcome still highlights the underlying adeptness of the catalyst in providing a well-defined stereochemical induction to facilitate the reaction via a highly selective process.

2.12. Extended scope with pyrrolyl based substrates

Based on the results presented above, it may be observed that the reaction was highly tolerant to electronic differences present within the scope of substrates listed in Table 2.2. In this aspect, the scope of reaction was thus extended to include pyrrolyl based substrates bearing a direct electronic functionalization on the central nitrogen moiety, to examine the adaptability of the reaction towards substrates with more distinct electronic disparities in comparison to substrates **9**. The attempted experimental trials with respect to the abovementioned are illustrated in the following sections. Additionally, two previously unmentioned palladacycle catalysts (*S*)-**12** and (*S*)-**13** which are utilized for reaction will be first introduced here for illustrative purposes later (Figure 2.15).

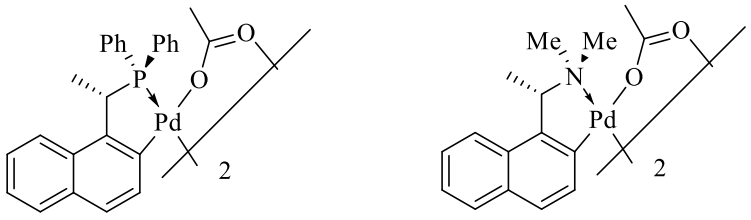

(*S*)-**12** (*S*)-**13**

Figure 2.15. Illustration of catalysts (*S*)-**12** and (*S*)-**13**.

Preliminary trials were conducted using **14a**, which corresponds to the pyrrole variant of the standard substrate **9a** as shown in Table 2.3 below. Reaction progressions were monitored by $^{31}P\{^{1}H\}$ NMR analysis of the crude mixture for the concomitant determination of $HPPh_2$ conversion and product formation. Likewise, the obtained products were sulfurized upon reaction termination to facilitate work-up and characterization processes under open air conditions.

Table 2.3. Condition screenings for attempted AHP on substrate **14a**.[a]

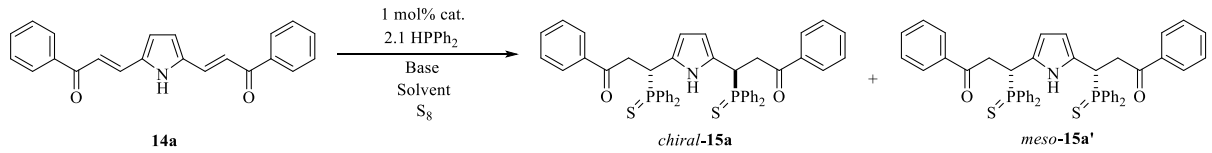

Entry	Cat.	Solvent	Base	Additive[c]	Time (h)	*T* (°C)	Conv. (%)[d]
1	-	DCM	NEt_3	-	48	rt	-
2[b]	(*S*)-**2**	DCM	NEt_3	-	48	rt	0/24
3[b]	(*S*)-**2**	DCM	NEt_3	-	96	50	22/35
4	(*S*,*S*)-**8**	DCM	-	-	96	50	0/7
5	(*S*,*S*)-**8**	Acetone	-	-	48	rt	-
6	(*S*,*S*)-**8**	Acetone	-	-	192	50	25/30
7[b]	(*S*,*S*)-**8**	Acetone	-	-	144	50	30/5
8[b]	(*S*)-**12**	Toluene	-	AcOH	120	100	0/31
9[b]	(*S*)-**13**	Toluene	-	AcOH	120	100	21/34

[a] Reaction conditions: 1 equiv. of **14a**, 2.1 equiv. of $HPPh_2$, 1 mol% of catalyst and 2.1 equiv. of base (where necessary) in 2 mL solvent. [b] 2.5 mol% of catalyst used. [c] Added in 1 equiv. [d] Determined from $^{31}P\{^1H\}$ NMR. Expressed as a ratio of diphosphinated/monophosphinated product.

A primary attempt made to discern the ability of the reaction to proceed in the absence of a catalyst revealed a negative result, with absolutely no indications of any formed products after the stipulated reaction time (Table 2.3, Entry 1). Similar reaction conditions adopted based on those employed in the initial optimization screenings of **9a** showed a glaring difference in the reactivity of **14a**, with the observed levels of product conversion incomparable to those achieved

with the pyridyl based substrate (Table 2.3, Entries 2 to 4). Further efforts emulating the optimized catalyzed conditions for **9a** were similarly ineffective in generating the intended products with appreciable conversions even under elevated temperatures and prolonged reaction durations (Table 2.3, Entries 5 and 6). In all cases, either a complete stagnation or negligible progression was realized despite further conduct of the reaction after the stipulated time. Both diastereo- and enantioselectivities of the reaction were omitted due to the difficulty in their accurate quantification from the modest amounts of diphosphine product attained.

The evident lack of reactivity in **14a** as denoted by the obtained results pointed towards a likely reason based on the default structure of the substrate. With the main driving factor for reaction dependent on the electrophilicity of the β-carbon, it is imperative that substrate activation specific to that position is reasonably sufficient for promotion of the addition process. In the case of **14a**, a resonance donation of electrons into the enone functionality via delocalization of the lone pair of electrons from the pyrrole nitrogen is possible to render the targeted reaction site more electron rich and less electrophilically activated than desired (Scheme 2.6).

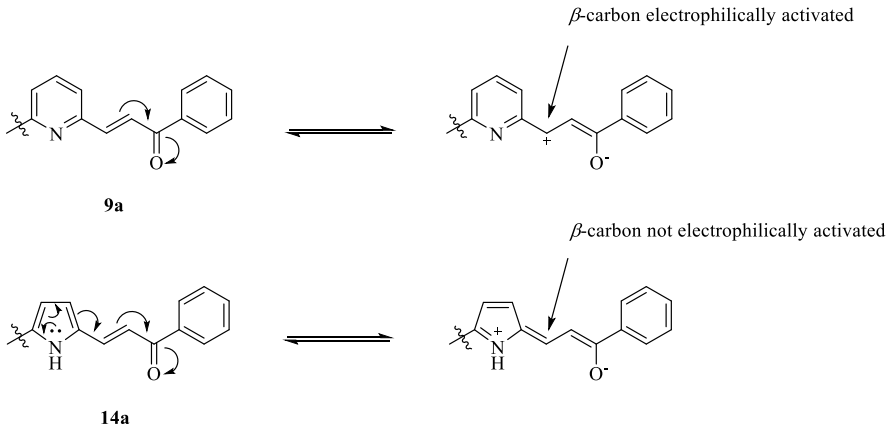

Scheme 2.6. Illustration of electronical difference of the β-carbon between substrates **9a** and **14a**.

On the contrary, such a phenomenon is electronically not possible for **9a**, which therefore supports for the related observations for the comparatively lower reactivities of **14a**. This is in line with the fact that the β-carbon center in the former substrate is electronically more primed for the nucleophilic addition reaction due to a lower containment of electron density from the delocalization effect.

Judging from the results obtained, it can be noticed that the experimental run using (*S*)-**2** granted the better outcome in terms of product conversion within a shorter reaction duration (Table 2.3, Entry 2). Nevertheless, comparable conversions could also be ultimately achieved with the use of (*S,S*)-**8** albeit requiring a considerably longer reaction time (Table 2.3, Entry 6). Increasing the loading of (*S,S*)-**8** was also uneventful in enhancing the rate of reaction (Table 2.3, Entry 7). This can probably be explained with reference to the difference in the mediation of the reaction pathway by the catalysts, which is outlined in the diagram below (Figure 2.16).

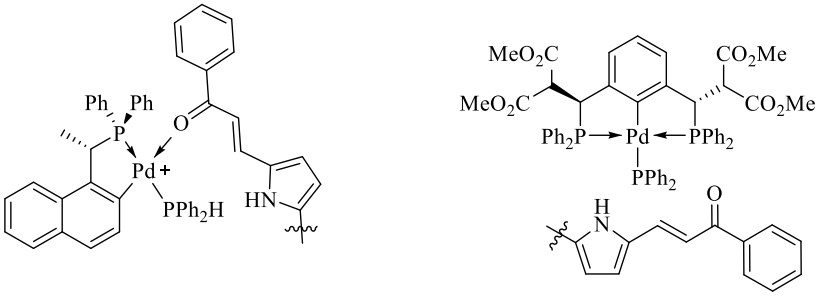

(*S*)-**2** (*S,S*)-**8**

Figure 2.16. Reaction mediation pathways by catalysts (*S*)-**2** and (*S,S*)-**8**.

As seen in Figure 2.16, the presence of two vacant sites in (*S*)-**2** allows for the simultaneous accommodation of both the enone and phosphine substrates onto the metal auxiliary, with the enone coordinated via its carbonyl O atom to the Lewis acidic palladium(II) center. Such a

coordination interaction would result in an enhanced electron withdrawing behavior by the carbonyl functionality, thereby causing the *β*-carbon to be more effectively electrophilic for facile reaction. On the other hand, the single vacant site present in (*S*,*S*)-**8** would preferentially allow coordination of the PPh_2^- moiety, prohibiting any form of possible substrate activation by the metal complex. In conjunction with the natural low reactivity of the substrate, the reaction progression would expectedly be comparatively less enhanced.

In retrospect, it may be hypothesized with regard to the mechanistic mode of reaction for (*S*)-**2** that the relative steric bulk stemming from the substrate could have limited its approach to displace the bound $HPPh_2$ for its own coordination to allow for more optimal reaction. Acknowledging this plausibility, subsequent experimental trials were therefore conducted with derivatized variants of (*S*)-**2** using the acetate-bridged catalysts (*S*)-**12** and (*S*)-**13**. The use of these acetate-incorporated catalysts was deliberate in the hopes that the acetate ligand would prevent the persistent binding of $HPPh_2$ on the coordination site intended for substrate adherence. To further facilitate this, an extra addition of acetic acid (AcOH) as an additive was included with the understanding that the concentration of $HPPh_2$ would be present in larger excess as compared to that of acetate, which is dependent on the catalyst loading. The reactions were also performed in non-coordinating toluene to avert complications arising from competitive solvent binding. Comparatively, the reaction using (*S*)-**13** furnished a better product conversion as compared to (*S*)-**12**, highlighting a possible influence from the difference in steric properties of both catalysts (Table 2.3, Entries 7 and 8). Unfortunately, the results obtained in terms of product formation could only at best be matched to that achieved by (*S*)-**2**, reverting us back to the consensus that the substrate is essentially too inherently unreactive for the addition reaction.

With the low conversion rates obtained with the catalyzed reaction pathway, a separate experiment was conducted under *racemic* conditions in the aim of acquiring structural elucidations of the addition product (Scheme 2.7).

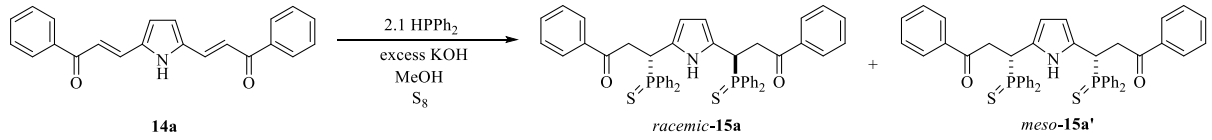

Scheme 2.7. *Racemic* hydrophosphination of **14a**.

Subjecting **14a** to a methanolic solution with excess KOH managed to provide an eventual complete conversion of the substrate to the *racemic* and *meso* adducts **15,** albeit with a long reaction time as well. This could be ascribed to the possibility of a deprotonation occurrence of the mildly acidic pyrrolyl proton within a strongly basic reaction environment, together with the fact that KOH was present in large stoichiometry. Consequently, the formation of an anionic species on the nitrogen atom cascades into a greater electron donating propensity by the pyrrole group via the delocalization effect as proposed in Scheme 2.6, thereby leading to decreased reactivity on the substrate for nucleophilic addition. On a side note, the observations gathered from this experiment provided an additional insight with respect to the sensitivity of the reaction towards base additives, suggesting a higher level of incompatibility with more basic reaction conditions. Attempts to purify the sulfurized crude mixture were unsuccessful due to the inseparability of the diastereomeric isomers on silica chromatography. Slow recrystallization of the partially purified fractions containing both diastereomeric adducts in DCM/*n*-hexane however managed to afford single crystals of X-ray quality corresponding to *meso* **15a'** as shown in the ORTEP diagram below (Figure 2.17).

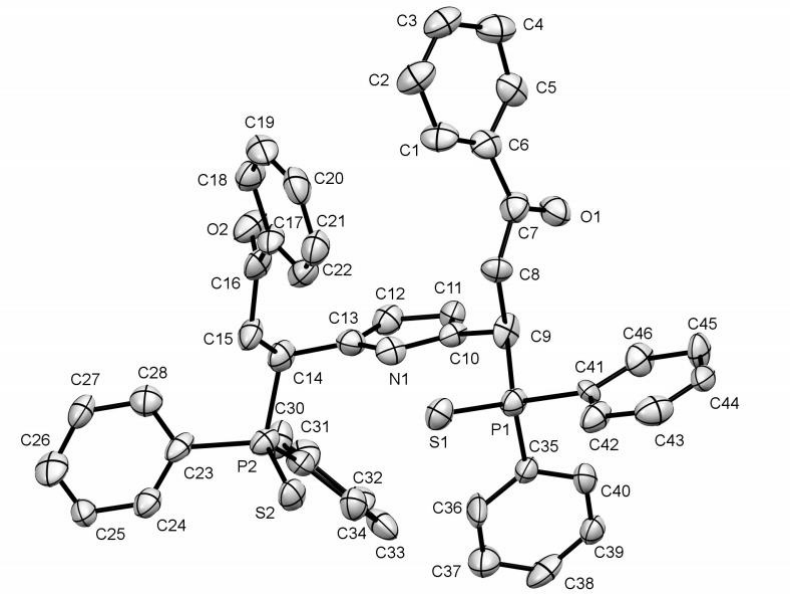

Figure 2.17. ORTEP representation of *meso* phosphine sulfide **15a'** with thermal ellipsoids drawn at 50% probability level. Hydrogen atoms are omitted for clarity.

With the important notion of electronic activation for this class of substrate, we next proceeded to probe the compatibility of the electronically more reactive substrate **14b** in the AHP reaction (Table 2.4). Substrate **14b** is adapted from its pyridyl counterpart **9f** that was previously described to undergo the hydrophosphination reaction in full completion without catalyst influence. As such, **14b** was deliberately designed in a bid to resolve both issues by capitalizing on the difference in reactivity between the pyrrole center and the diester functionalities, to hopefully provide for a balance in reactivity level of the overall substrate with the aim of promoting a controlled selective reaction process.

Table 2.4. Condition screenings for attempted AHP on substrate **14b**.[a]

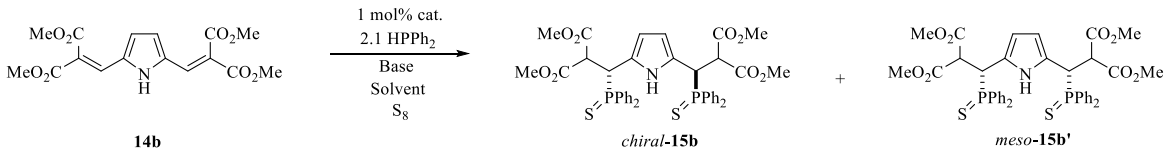

Entry	Cat.	Solvent	Base	Time (h)	*T* (°C)	Conv. (%)[d]	*de* (%)[e]	*ee* (%)[f]
1	-	DCM/MeOH	NaOAc	96	rt	81/11	4	-
2[b]	(*S*)-**1**	DCM	NEt_3	96	rt	39/15	15	7
3[b]	(*S*)-**2**	DCM	NEt_3	96	rt	51/15	5	70
4	(*S*,*S*)-**8**	DCM	-	96	rt	trace	-	-
5[c]	(*S*,*S*)-**8**	DCM	-	288	rt	43/30	3	0
6	(*S*)-**2**	MeOH	NEt_3	96	rt	91/9	14	9
7	(*S*)-**2**	Acetone	NEt_3	96	rt	38/18	10	20

[a] Reaction conditions: 1 equiv. of **14b**, 2.1 equiv. of $HPPh_2$, 1 mol% of catalyst and 2.1 equiv. of base (where necessary) in 2 mL solvent. [b] 2.5 mol% of catalyst used. [c] 5 mol% of catalyst used. [d] Determined from $^{31}P\{^1H\}$ NMR. Expressed as a ratio of diphosphinated/monophosphinated product. [e] Determined from $^{31}P\{^1H\}$ NMR with chiral **15b** as the major stereoisomer. [f] Determined by chiral HPLC after isolation of the sulfurized chiral isomer.

An initial conduct of a control reaction without the addition of catalyst established the possibility of an uncatalyzed reaction pathway, which saw almost complete conversion of $HPPh_2$ to generate the intended diphosphine adducts **15b/b'** in a major proportion (Table 2.4, Entry 1). Trials conducted under standard reaction conditions previously employed for **14a** revealed a stark difference in the results observed as expected due to the increase in substrate reactivity (Table 2.4, Entries 2 and 3). In general, similar to better product conversions were accomplished under milder reaction conditions within the same timeframe. Most notably, implementing (*S*)-**2** as catalyst

managed to furnish the diphosphine product with a decent enantioselectivity of 70% *ee*. Reaction with (*S*,*S*)-**8** however proceeded much more sluggishly with trace amounts of product attained after similar durations at room temperature (Table 2.4, Entry 4). A repeat experiment with increased loading of the catalyst to 5 mol% also displayed slow reaction to only provide comparable conversions with respect to the experimental runs using (*S*)-**2** even after a significant extension of reaction time (Table 2.4, Entry 5). Furthermore, formation of the products entailed negligible levels of selectivity, indicating an absolute unapparent influence by the catalyst. These results however align with those hitherto obtained with the analogous pyridyl substrate **9f**, suggestive of possible steric hindrances experienced between both bulky substrate and catalyst moieties which might have prevented the occurrence of effective mutual stereochemical interactions.

A concise solvent screening was next commenced with (*S*)-**2** selected as the catalyst of choice based on its superior performance from the optimization screenings. In an aim to improve the reaction rates, methanol was first screened under the presumption that a protic solvent would facilitate the protonolysis process and thus speed up the reaction in that aspect. As observed, complete consumption of $HPPh_2$ was accomplished under the same reaction duration and the intended diphosphine product was formed as the major product albeit with unimpressive selectivity (Table 2.4, Entry 6). A secondary trial with acetone as solvent (given its optimal compatibility with **9a**) paled in comparison in terms of conversion rates although slight improvements were observed with selectivity (Table 2.4, Entry 7). Further efforts with the motivation to improve reaction selectivity by running low temperature experiments were unfortunately accosted with significant deteriorations in reactivity, giving negligible amounts of product formation.

Purifications of the crude mixture containing the sulfurized diphosphine adducts were only partially achieved due to the inseparability of the diastereomeric isomers on silica chromatography.

Attempts at recrystallization of the diastereomeric mixture were also unsuccessful in providing crystals for structural determination. In turn, a separate experiment was performed to complex the furnished diphosphine adducts onto a selected palladium(II) precursor based on general trends whereby complexed diastereomers tend to be better separated on silica chromatography. At the same time, a preliminary investigation towards the compatibility of the synthesized adducts as potential ligand ancillaries could also be unfounded from the complexation trial (Scheme 2.8).

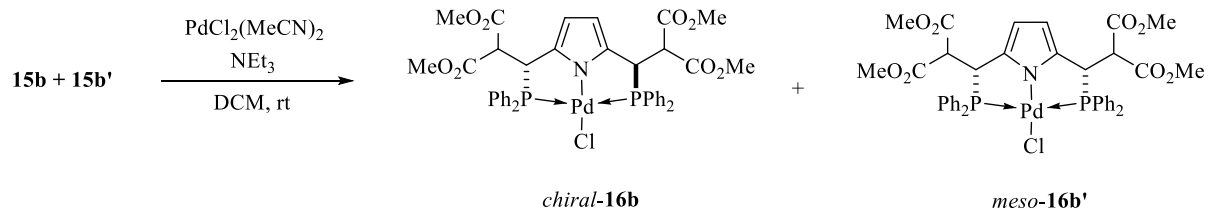

Scheme 2.8. Complexation of diphosphines **15b** and **15b'** to $PdCl_2(MeCN)_2$.

Complexation of the diastereomeric mixture of **15b** and **15b'** proceeded based on the reaction conditions illustrated in Scheme 2.8, and analysis via $^{31}P\{^1H\}$ NMR of the crude mixture revealed distinct coordination shifts at 46.6 ppm and 46.8 ppm. The signals were represented by clear sharp singlets indicative of the chemical equivalence of the two phosphorus atoms. Unfortunately, attempts to purify the crude mixture were again met with difficulties in separation of the diastereomeric isomers, providing a partially purified mixture containing both isomeric products. Nevertheless, slow fractional recrystallization of this mixture in DCM/*n*-hexane were successful in the provision of X-ray quality single crystals, which were subsequently resolved to depict the structural illustration of *racemic* **16b** (Figure 2.18). Efforts to obtain chiral crystals of **16b** were unsuccessful even after repeated attempts at recrystallization with modified solvent combinations.

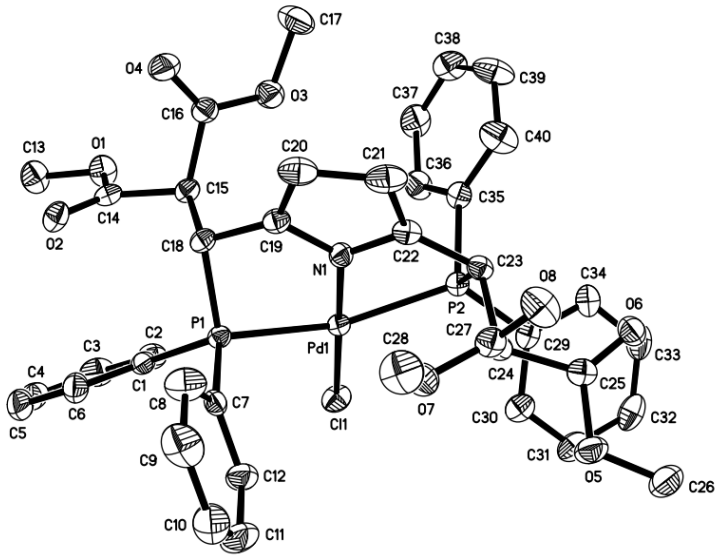

Figure 2.18. ORTEP representation of *racemic* pyrrolyl PNP palladium(II) complex **16b** with thermal ellipsoids drawn at 50% probability level. Hydrogen atoms are omitted for clarity.

Complex **16b** adopts a distorted square planar configuration as illustrated by its diagrammatical representation above. The selected bond lengths and bond angles of the complex are listed as follows. Bond lengths: Pd1-N1 = 1.984 Å, Pd1-P1 = 2.311 Å, Pd1-P2 = 2.314 Å, Pd1-Cl1 = 2.327 Å. Bond angles: P1-Pd1-P2 = 156.41º, N1-Pd1-P1 = 78.10º, N1-Pd1-P2 = 78.36º, P1-Pd1-Cl1 = 101.98º, P2-Pd1-Cl1 = 101.57º. References drawn to analogous pyrrolyl based PNP complexes showcased a greater extent of distortion in complex **16b** towards the pyrrole ring.[31] This is identified by the more acute P-Pd-P bond angle as compared to reported values in the literature (156.41º versus 162.28º), illustrating a larger twisting of the complex about the P-Pd-P bond axis likely due to the intense steric demands imposed by the four bulky projecting CO_2Me substituents. The direction of distortion towards the pyrrole ring is usual as a result of steric strain arising from the chelation of the tridentate ligand. No other notable deviations of bond length and bond angles values were observed, with the stated values above falling in close resemblance to those reported in the literature.[31]

2.13. Conclusion

In conclusion, we have positively showcased the employment of catalytic asymmetric hydrophosphination as an expeditious pathway for the synthetic access to *C*-stereogenic, pyridyl based PN(sp^2)P diphosphine adducts. This protocol has displayed several beneficial traits from the perspective of synthesis, offering a one-pot direct access to these chiral phosphines with excellent selectivity and atom economy. Most substantially, these enantiomerically pure tertiary phosphines were synthesized under mild reaction conditions, starting with completely achiral substrates. Furthermore, the described methodology has also surmounted the traditional synthetic difficulties related to current known methods in the literature, opening up new avenues towards more suitable and convenient access to otherwise synthetically elusive chiral pyridyl PN(sp^2)P tridentates that may be evaluated further for asymmetric applications.

An extension of the reaction protocol was also performed to include pyrrolyl based substrates to test the tolerance of the reaction towards the electronically more demanding class of compound. While the results obtained were modest in comparison to its pyridyl counterparts, valuable insights were gathered which could be useful for further optimizations of the AHP reaction towards more electronically challenging substrates. Nonetheless, the preliminary findings accomplished with the syntheses as well as complexation of the pyrrolyl based PN(sp^2)P diphosphine adducts revealed a good indication for the applicability of these synthons as potential ligand frameworks onto compatible metal centers. In turn, these may be additionally probed for plausible reaction applications and uses.

Experimental and Methods

General information

Unless otherwise stated, all reactions were carried out under a positive pressure of nitrogen using standard Schlenk techniques. Solvents were purchased from their respective companies (MeOH: Fulltime Reagent, DCM, EA: Fisher Chemicals, Toluene, n-hexane: Avantor, THF: Schedelco, Acetone: VWR Chemicals) and used as supplied. Prior to use, all solvents intended for air sensitive reactions were dried and distilled or degassed where necessary. A PSL-1820 Low Temp Pairstirrer was used for conducting low temperature reactions. Thin layer chromatography (TLC) was done using Merck silica gel 60 F254 aluminum supported plates. Flash column chromatography was performed using Merck silica gel 60. NMR spectra were obtained using Bruker AV 300 (^{1}H at 300 MHz, ^{13}C{^{1}H} at 75 MHz, ^{31}P{^{1}H} at 121 MHz); AV 400 (^{1}H at 400 MHz, ^{13}C{^{1}H} at 100 MHz, ^{31}P{^{1}H} at 162 MHz) and AV 500 (^{1}H at 500 MHz, ^{13}C{^{1}H} at 125 MHz, ^{31}P{^{1}H} at 202 MHz) spectrometers. Chemical shifts were reported in ppm and referenced to an internal $SiMe_4$ standard at δ 0 ppm, or to the residual proton signals of the respective deuterated solvents for ^{1}H and ^{13}C{^{1}H} NMR. Chiral high-performance liquid chromatography (HPLC) data were acquired using an Agilent Technologies 1200 Series HPLC machine with Daicel CHIRALPAK I-series columns. Optical rotations were measured with a JASCO P-1030 Polarimeter in the specified solvent and concentration in a 0.1 dm cell at 25.0^{o}C. High resolution mass spectrometry (HRMS) was conducted via the electrospray ionization (ESI) method using a Waters Q-Tof Premier spectrometer.

Materials

Syntheses of the substrate precursors; pyridine-2,6-dicarbaldehyde **17**[32], pyrrole-2,5-dicarbaldehyde **18**[33] and respective Wittig reagents **19**[19] were performed according to literature methods. Subsequent syntheses of substrates **9a**,[34] **9b**,[35] **9c**,[36] **9d**,[2] **9e**,[2] **9f**,[4] proceeded via slight modifications to reported procedures. Catalysts (*S*)-**2,** (*S*,*S*)-**6,** (*S*,*S*)-**8**,[21a, 37] $PdCl_2(MeCN)_2$[38] and diphenylphosphine[39] were also prepared according to literature methods. All other reagents were procured from Sigma Aldrich and used directly as supplied.

General procedure for the syntheses of substrates 9a-c

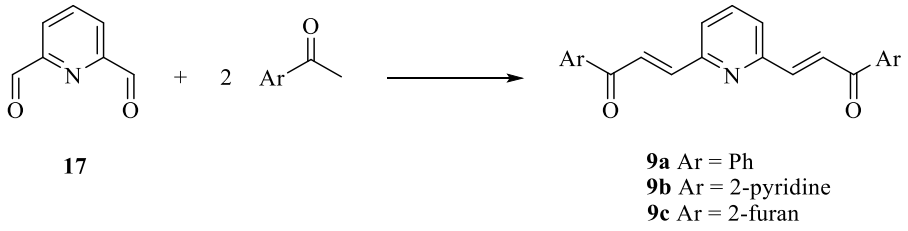

17

9a Ar = Ph
9b Ar = 2-pyridine
9c Ar = 2-furan

Scheme 2.9. Synthetic outline for substrates **9a-c**.

Synthesis of substrate 9a

A 50 mL round-bottomed flask was charged with NaOH (10 mL, 10% w/w in water) and di-aldehyde **17** (0.2 g, 1.48 mmol, 1 equiv.) in methanol (12 mL). Following which, acetophenone (0.36 g, 2.96 mmol, 2 equiv.) dissolved in methanol (3 mL) was added dropwise slowly into the mixture placed in an ice bath. The resultant mixture was left to stir for 24 h at room temperature for the formation of a suspension. Volatiles were removed under vacuum and the crude mixture was re-dissolved in DCM. Extraction was performed using water (2 x 10 mL) and the collected organic layer was dried over $MgSO_4$. Filtration of the mixture and subsequent removal of DCM

afforded the crude product which was further purified via precipitation in DCM/*n*-hexane to obtain pure **9a**.

Synthesis of substrate 9b

A 50 mL round-bottomed flask was charged with Na_2CO_3 (39.2 mg, 0.37 mmol, 0.25 equiv.), 2-acetylpyridine (0.36 g, 2.96 mmol, 2 equiv.) and di-aldehyde **17** (0.2 g, 1.48 mmol, 1 equiv.) in water (20 mL). The resultant mixture was heated at 70°C and stirred for 5 h for the formation of a suspension. The crude mixture was filtered with thorough washing using cold water, and the collected residue was purified via silica gel chromatography in DCM/EA to afford pure **9b**.

Synthesis of substrate 9c

A 100 mL round-bottomed flask was charged with KOH (2.4 mL. 85% w/w in water) and di-aldehyde **17** (0.2 g, 1.48 mmol, 1 equiv.) in methanol (50 mL) and water (10 mL) at 0°C. Following which, 2-acetylfuran (0.33 g, 2.96 mmol, 2 equiv.) was added and the resultant mixture was left to stir for 16 h at 0°C for the formation of a suspension. Volatiles were removed under vacuum and the crude mixture was re-dissolved in DCM. Extraction was performed using water (2 x 10 mL) and the collected organic layer was dried over $MgSO_4$. Filtration of the mixture and subsequent removal of DCM afforded the crude product which was purified via silica gel chromatography in DCM/EA to give pure **9c**.

General procedure for the syntheses of substrates 9d-e

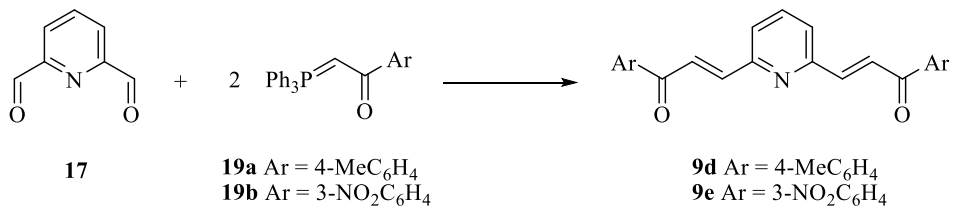

17 **19a** Ar = 4-MeC_6H_4
19b Ar = 3-$NO_2C_6H_4$
9d Ar = 4-MeC_6H_4
9e Ar = 3-$NO_2C_6H_4$

Scheme 2.10. Synthetic outline for substrates **9d-e.**

A 25 mL Schlenk tube was charged with di-aldehyde **17** (0.2 g, 1.48 mmol, 1 equiv.) and the respective phosphonium ylides **19a** and **19b** (2.96 mmol, 2 equiv.) in toluene (10 mL). The resultant mixture was refluxed under nitrogen for 24 h for the formation of a suspension. Volatiles were removed under vacuum and the crude mixture was purified via silica gel chromatography in DCM/*n*-hexane to afford pure **9d** and **9e.**

General procedure for the synthesis of substrate 9f

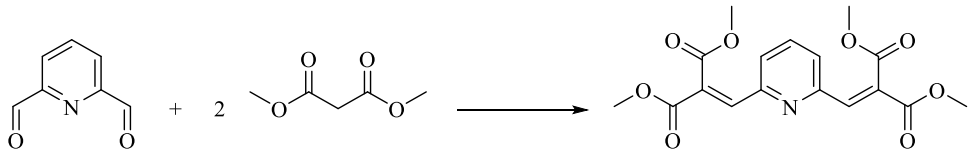

17 **9f**

Scheme 2.11. Synthetic outline for substrate **9f**.

A 25 mL round-bottomed flask was charged with dimethyl malonate (0.39 g, 2.96 mmol, 2 equiv.) and piperidine (50.4 mg, 0.59 mmol, 0.4 equiv.) in n-heptane (10 mL). Following which, di-aldehyde **17** (0.2 g, 1.48 mmol, 1 equiv.) was added and the resultant mixture was refluxed at 140°C under Dean-Stark conditions for 24 h. Volatiles were removed under vacuum and the crude mixture was re-dissolved in DCM. Extraction was performed using water (2 x 10 mL) and the

collected organic layer was dried over $MgSO_4$. Filtration of the mixture and subsequent removal of DCM afforded the crude product which was re-dissolved in DCM/*n*-hexane for recrystallization to obtain pure **9f**.

General procedure for the synthesis of substrate 14a

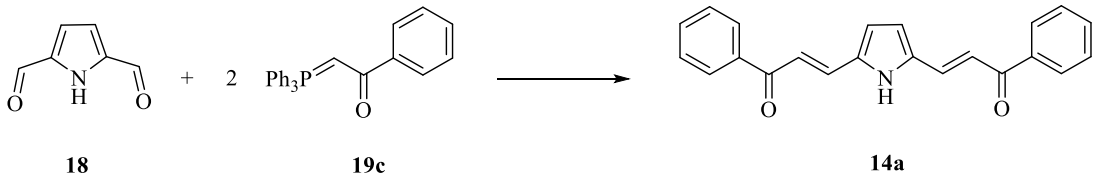

18 **19c** **14a**

Scheme 2.12. Synthetic outline for substrate **14a**.

A 25 mL Schlenk tube was charged with di-aldehyde **18** (0.2 g, 1.48 mmol, 1 equiv.) and phosphonium ylide **19c** (2.96 mmol, 2 equiv.) in toluene (10 mL). The resultant mixture was refluxed under nitrogen for 24 h for the formation of a suspension. The crude mixture was purified via direct filtration and the collected solids were further washed in toluene before being subjected to oven-drying under 60ºC overnight to afford pure **14a**.

General procedure for the synthesis of substrate 14b

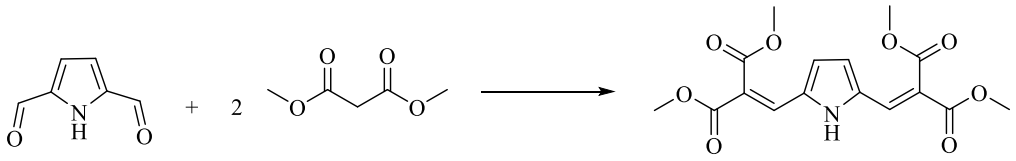

18 **14b**

Scheme 2.13. Synthetic outline for substrate **14b**.

A 25 mL round-bottomed flask was charged with dimethyl malonate (0.39 g, 2.96 mmol, 2 equiv.) and piperidine (50.4 mg, 0.59 mmol, 0.4 equiv.) in n-heptane (10 mL). Following which, di-aldehyde **18** (0.2 g, 1.48 mmol, 1 equiv.) was added and the resultant mixture was refluxed at 140°C under Dean-Stark conditions for 48 h. Volatiles were removed under vacuum and the crude mixture was re-dissolved in DCM. Extraction was performed using water (2 x 10 mL) and the collected organic layer was dried over $MgSO_4$. Filtration of the mixture and subsequent removal of DCM afforded the crude product which was purified via silica gel chromatography in DCM/*n*-hexane to afford pure **14b**.

Characterization data of substrates 9 and 14

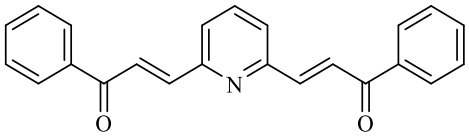

9a. White solid. Yield: 261 mg, 0.77 mmol, 52%. ^{1}H NMR ($CDCl_3$, 400 MHz): δ 7.49-7.56 (m, 6H, Ar), 7.61-7.64 (m, 2H, Ar), 7.77-7.82 (m, 3H, C(O)CHCHCCHC*H* overlapped with C(O)CHC*H*), 8.09-8.11 (m, 4H, Ar), 8.16 (d, 2H, $^3J_{HH}$ = 15.4 Hz, C(O)C*H*); ^{13}C{^{1}H} NMR (CD_2Cl_2, 100 MHz): δ 125.4-153.5 (21C, Ar and vinylic), 190.3 (s, 2C, *C*(O)). HRMS (ESI) m/z: $(M + H)^+$ calcd for $C_{23}H_{18}NO_2$, 340.1338; found, 340.1340.

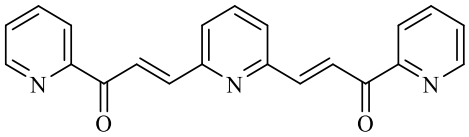

9b. White solid. Yield: 93.5 mg, 0.28 mmol, 19%. ^{1}H NMR ($CDCl_3$, 400 MHz): δ 7.50-7.53 (m, 2H, Ar), 7.62-7.64 (d, 2H, $^{3}J_{HH}$ = 7.7 Hz, C(O)CHCHCC*H*), 7.78-7.81 (t, 1H, $^{3}J_{HH}$ = 7.7 Hz, C(O)CHCHCCHC*H*), 7.88-7.92 (m, 2H, Ar), 7.98 (d, 2H, $^{3}J_{HH}$ = 15.8 Hz, C(O)C*H*), 8.19-8.21 (m, 2H, Ar), 8.72 (d, 2H, $^{3}J_{HH}$ = 15.9 Hz, C(O)CHC*H*), 8.79-8.80 (m, 2H, Ar); ^{13}C{^{1}H} NMR (CD_2Cl_2, 100 MHz): δ 122.7-137.1 (10C, Ar and vinylic), 137.5 (s, 1C, C(O)CHCHCCH*C*H), 142.6-154.0 (8C, Ar and vinylic), 189.7 (s, 2C, *C*(O)). HRMS (ESI) m/z: $(M + H)^+$ calcd for $C_{21}H_{16}N_3O_2$, 342.1243; found, 342.1242.

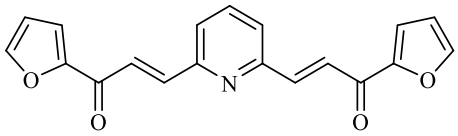

9c. Off-white solid. Yield: 165 mg, 0.52 mmol, 35%. ^{1}H NMR ($CDCl_3$, 400 MHz): δ 6.63-6.65 (m, 2H, Ar), 7.43-7.44 (m, 2H, Ar), 7.51 (d, 2H, $^{3}J_{HH}$ = 7.7 Hz, C(O)CHCHCC*H*), 7.71-7.72 (m, 2H, Ar), 7.80 (t, 1H, $^{3}J_{HH}$ = 7.7 Hz, C(O)CHCHCCHC*H*), 7.88 (d, 2H, $^{3}J_{HH}$ = 15.4 Hz, C(O)C*H*), 8.02 (d, 2H, $^{3}J_{HH}$ = 15.4 Hz, C(O)CHC*H*); ^{13}C{^{1}H} NMR (CD_2Cl_2, 100 MHz): δ 112.5 (s, 2C, Ar), 118.2 (s, 2C, Ar), 125.6-125.8 (4C, Ar and vinylic), 137.7 (s, 1C, C(O)CHCHCCH*C*H), 141.6-153.6 (8C, Ar and vinylic), 177.6 (s, 2C, *C*(O)). HRMS (ESI) m/z: $(M + H)^+$ calcd for $C_{19}H_{14}NO_4$, 320.0923; found, 320.0926.

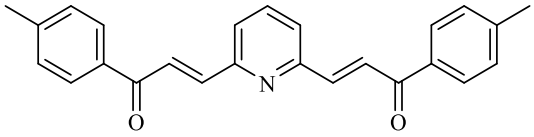

9d. White solid. Yield: 262 mg, 0.71 mmol, 48%. ^{1}H NMR ($CDCl_3$, 400 MHz): δ 2.46 (s, 6H, C*H*$_3$), 7.34 (d, 4H, $^{3}J_{HH}$ = 8.1 Hz, Ar), 7.49 (d, 2H, $^{3}J_{HH}$ = 7.7 Hz, C(O)CHCHCC*H*), 7.76-7.81 (m, 3H, C(O)CHCHCCHC*H* overlapped with C(O)CHC*H*), 8.01 (d, 4H, $^{3}J_{HH}$ = 8.1 Hz, Ar), 8.15 (d, 2H, $^{3}J_{HH}$ = 15.4 Hz, C(O)C*H*); ^{13}C{^{1}H} NMR (CD_2Cl_2, 100 MHz): δ 21.4 (s, 2C, *C*H$_3$), 125.2-153.6 (21C, Ar and vinylic), 189.8 (s, 2C, C(O)). HRMS (ESI) m/z: $(M + H)^+$ calcd for $C_{25}H_{22}NO_2$, 368.1651; found, 368.1644.

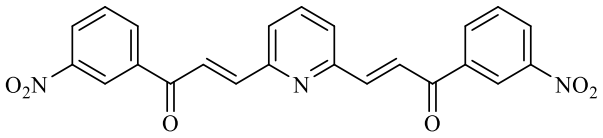

9e. White solid. Yield: 345 mg, 0.80 mmol, 54%. ^{1}H NMR (CD_2Cl_2, 400 MHz): δ 7.60 (pseudo d, 2H, $^{3}J_{HH}$ = 7.7 Hz, Ar), 7.81 (t, H, $^{3}J_{HH}$ = 7.9 Hz, C(O)CHCHCCHC*H*), 7.87-7.91 (m, 3H, C(O)CHCHCC*H* overlapped with C(O)CHC*H*), 8.26 (d, 2H, $^{3}J_{HH}$ = 15.2 Hz C(O)C*H*), 8.47 (pseudo t, 4H, $^{3}J_{HH}$ = 7.7 Hz, Ar), 8.92 (br s, 2H, Ar); ^{13}C{^{1}H} NMR (CD_2Cl_2, 100 MHz): δ 123.4-134.2 (12C, Ar and vinylic), 138.1 (s, 1C, C(O)CHCHCCH*C*H), 139.1-153.1 (8C, Ar and vinylic), 188.1 (s, 2C, *C*(O)). HRMS (ESI) m/z: $(M + H)^+$ calcd for $C_{23}H_{16}N_3O_6$, 430.1039; found, 430.1036.

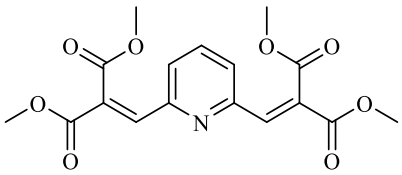

9f. White solid. Yield: 172 mg, 0.47 mmol, 32%. ^{1}H NMR ($CDCl_3$, 400 MHz): δ 3.86 (s, 6H, OC*H*$_3$), 3.87 (s, 6H, OC*H*$_3$), 7.41 (d, 2H, $^{3}J_{HH}$ = 7.8 Hz, C(O)CCHCC*H*), 7.69 (s, 2H, C*H*), 7.75 (t, 1H, $^{3}J_{HH}$ = 7.8 Hz, C(O)CCHCCHC*H*); ^{13}C{^{1}H} NMR (CD_2Cl_2, 100 MHz): δ 52.4 (s, 2C, O*C*H$_3$), 52.8 (s, 2C, O*C*H$_3$), 125.3-129.5 (4C, Ar and vinylic), 137.8 (s, 1C, C(O)CCHCCH*C*H), 140.1-151.7 (4C, Ar and vinylic), 164.0 (s, 2C, *C*(O)), 165.9 (s, 2C, *C*(O)). HRMS (ESI) m/z: (M + H)$^+$ calcd for $C_{17}H_{18}NO_8$, 364.1032; found, 364.1029.

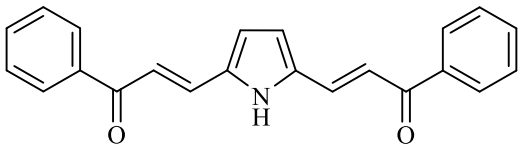

14a. Pink solid. Yield: 183 mg, 0.56 mmol, 38%. ^{1}H NMR ($CDCl_3$, 400 MHz): δ 6.78 (s, 2H, NCC*H*), 7.31 (d, 2H, C(O)C*H*, $^{3}J_{HH}$ = 15.7 Hz), 7.48-7.60 (m, 7H, Ar), 7.71 (d, 2H, C(O)CHC*H*, $^{3}J_{HH}$ = 15.6 Hz), 8.00-8.02 (m, 3H, Ar), 9.13 (br s, 1H, N*H*); The carbon spectrum was unable to be obtained due to the insolubility of **14a** in most organic solvents. Attempts to dissolve **14a** in more polar solvents such as MeOH and DMSO resulted in a change in structural integrity of the compound as observed by ^{1}H NMR analysis. HRMS (ESI) m/z: (M + H)$^+$ calcd for $C_{22}H_{18}NO_2$, 327.1259; found, 327.1262.

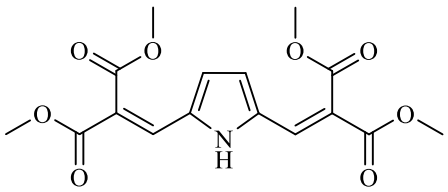

14b. Yellow solid. Yield: 119 mg, 0.34 mmol, 23%. ^{1}H NMR (CD_2Cl_2, 400 MHz): δ 3.81 (s, 6H, COC*H*$_3$), 3.95 (s, 6H, COC*H*$_3$), 6.69 (s, 2H, NCC*H*), 7.56 (s, 2H, C(O)CC*H*), 11.55 (br s, 1H, N*H*); ^{13}C{^{1}H} NMR (CD_2Cl_2, 100 MHz): δ 52.4 (s, 2C, O*C*H$_3$), 52.9 (s, 2C, O*C*H$_3$), 119.2 (s, 2C, C(O)*C*CH), 121.3 (s, 2C, NC*C*H), 131.6 (s, 2C, N*C*), 133.6 (s, 2C, C(O)C*C*H), 165.5 (s, 2C, *C*(O)), 167.2 (s, 2C, *C*(O)). HRMS (ESI) m/z: $(M + H)^+$ calcd for $C_{16}H_{18}NO_8$, 351.0954; found, 351.0953.

General procedure for the syntheses of phosphine sulfides 10

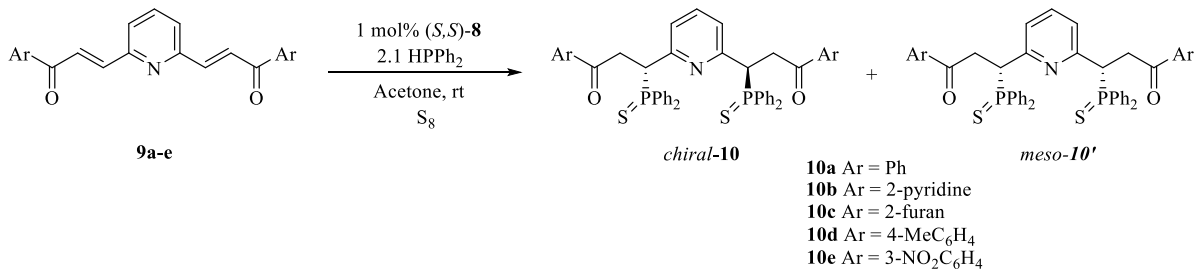

Scheme 2.14. Synthetic outline for pyridyl keto-phosphine sulfides **10a-e**.

Substrates **9a-e** (0.027 mmol, 1.0 equiv.) and catalyst (*S*,*S*)-**8** (0.49 mg, 0.547 μmol, 1 mol %) were added into a 10 mL storage tube and dissolved in acetone (2-4 mL). The mixture was stirred for 1 minute before diphenylphosphine (10.7 mg, 0.057 mmol, 2.1 equiv.) was added with washing using another portion of acetone (0.5-1 mL). The resultant mixture was left to stir at room temperature for the stipulated reaction time or until complete consumption of the substrate as monitored by TLC. Sulfur (2.64 mg, 0.082 mmol, 3.0 equiv.) was subsequently added and the mixture was stirred for another 1 h. Solvents were then removed via rotary evaporation and the crude mixture was purified via silica gel chromatography to afford the pure phosphine sulfide adducts **10a-e**.

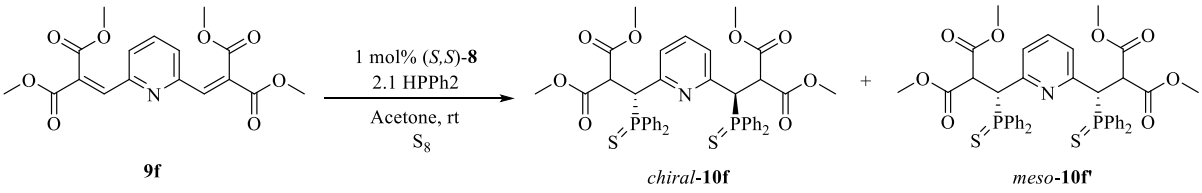

Scheme 2.15. Synthetic outline for pyridyl ester-phosphine sulfides **10f**.

The procedure for the synthesis of phosphine sulfides **10f** follows the same as the abovementioned protocol for the syntheses of **12a-e**.

General procedure for the syntheses of phosphine sulfides 15

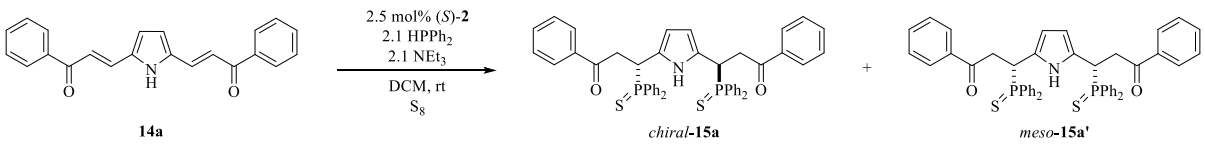

Scheme 2.16. Synthetic outline for pyrrolyl keto-phosphine sulfides **15a**.

Substrate **14a** (0.027 mmol, 1.0 equiv.) and catalyst (*S*)-**2** (0.858 mg, 1.37 μmol, 2.5 mol %) were added into a 10 mL storage tube and dissolved in DCM (2-4 mL). The mixture was stirred for 1 minute before diphenylphosphine (10.7 mg, 0.057 mmol, 2.1 equiv.) and triethylamine (5.77 mg, 0.057 mmol, 2.1 equiv.) were added successively with washing using another portion of DCM (0.5-1 mL). The resultant mixture was then left to stir at room temperature for the stipulated reaction time. Sulfur (2.64 mg, 0.082 mmol, 3.0 equiv.) was subsequently added and the mixture was stirred for another 1 h. Solvents were then removed via rotary evaporation and the crude mixture was partially purified via preparative TLC in DCM/*n*-hexane to afford a diastereomeric mixture of phosphine sulfides **15a** and **15a'** which could not be further separated.

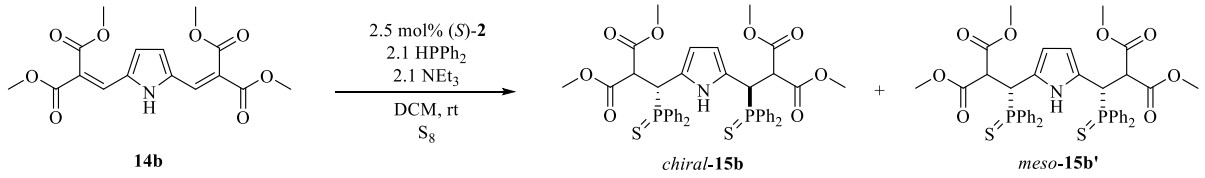

Scheme 2.17. Synthetic outline for pyrrolyl ester-phosphine sulfides **15b**.

The procedure for the synthesis of phosphine sulfides **15b** follows the same as the abovementioned protocol for the synthesis of **15a**. The crude mixture was likewise partially purified via preparative TLC in DCM/*n*-hexane to afford a diastereomeric mixture of phosphine sulfides **15b** and **15b'** which could not be further separated.

Characterization data of phosphine sulfides 10 and 15

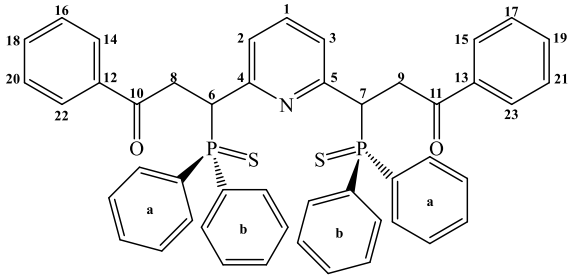

Figure 2.19. General labelling of carbon atoms for phosphine sulfides **10a** and **10a'**.

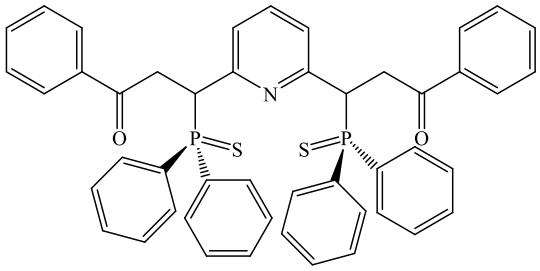

10a. White solid. Yield: 11.0 mg, 14.2 μmol, 53%. The *ee* was determined on a Daicel CHIRALPAK IC column with *n*-hexane/2-propanol = 75/25, flow = 1.0 mL/min, temperature = 23°C, wavelength = 210 nm. Retention times: 8.8 min (minor), 21.2 min (major). $[\alpha]_D^{25}$ = +118.0 (*c* = 0.35, $CHCl_3$). ^{1}H NMR (CD_2Cl_2, 400 MHz): δ 3.50 (ddd, 2H, $^2J_{HH}$ = 18.3 Hz, $^3J_{HP}$ = 13.3 Hz, $^3J_{HH}$ = 2.1 Hz, PCHC*H*), 4.56 (ddd, 2H, $^2J_{HH}$ = 18.4 Hz, $^3J_{HH}$ = 9.9 Hz, $^3J_{HP}$ = 4.9 Hz, PCHC*H*), 4.84 (pseudo ddd, 2H, $^2J_{HP}$ = 13.5 Hz, $^3J_{HH}$ = 10.0 Hz, $^3J_{HH}$ = 2.1 Hz, PC*H*), 6.69 (pseudo d, 2H, $^3J_{HP}$ = 7.7 Hz, PCHCC*H*), 6.94 (t, 1H, $^3J_{HH}$ = 7.7 Hz, PCHCCHC*H*), 7.18-7.22 (m, 4H, Ar), 7.27-7.31 (m, 2H, Ar), 7.34-7.46 (m, 10H, Ar), 7.52-7.60 (m, 6H, Ar), 7.84-7.91 (m, 8H, Ar); ^{31}P{^{1}H} NMR (CD_2Cl_2, 162 MHz): δ 50.8; ^{13}C{^{1}H} NMR (CD_2Cl_2, 100 MHz): δ 39.0 (d, 2C, $^2J_{CP}$ = 2.5 Hz, C8 and C9), 45.2 (d, 2C, $^1J_{CP}$ = 51.6 Hz, C6 and C7), 123.7 (s, 2C, C2 and C3), 128.1 (d, 4C, $^3J_{CP}$ = 12.3 Hz, Ca^{meta}), 128.2 (s, 4C, C16, C17, C20 and C21), 128.42 (s, 4C, C14, C15, C22 and

C23), 128.49 (d, 4C, $^{3}J_{CP}$ = 12.4 Hz, Cb^{meta}), 131.1 (d, 2C, $^{4}J_{CP}$ = 2.8 Hz, Ca^{para}), 131.5 (d, 2C, $^{4}J_{CP}$ = 2.7 Hz, Cb^{para}), 131.63 (d, 2C, $^{1}J_{CP}$ = 80.3 Hz, Ca^{ipso}), 131.66 (d, 4C, $^{2}J_{CP}$ = 9.6 Hz, Ca^{ortho}), 131.67 (d, 2C, $^{1}J_{CP}$ = 77.9 Hz, Cb^{ipso}), 131.8 (d, 4C, $^{2}J_{CP}$ = 10.1 Hz, Cb^{ortho}), 133.2 (s, 2C, C18 and C19), 135.3 (s, 1C, C1), 136.4 (s, 2C, C12 and C13), 155.0 (s, 2C, C4 and C5), 196.6 (d, 2C, $^{3}J_{CP}$ = 14.3 Hz, C10 and C11). HRMS (ESI) m/z: $(M + H)^{+}$ calcd for $C_{47}H_{40}NO_2P_2S_2$, 776.1976; found, 776.1977.

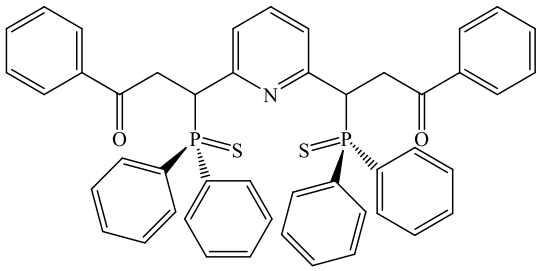

10a'. White solid. Yield: 4.8 mg, 6.13 µmol, 23%. ^{1}H NMR (CD_2Cl_2, 400 MHz): δ 3.44 (ddd, 2H, $^{2}J_{HH}$ = 18.0 Hz, $^{3}J_{HP}$ = 13.0 Hz, $^{3}J_{HH}$ = 2.7 Hz, PCHC*H*), 3.93 (ddd, 2H, $^{2}J_{HH}$ = 18.0 Hz, $^{3}J_{HH}$ = 10.0 Hz, $^{3}J_{HP}$ = 6.1 Hz, PCHC*H*), 4.84 (pseudo ddd, 2H, $^{2}J_{HP}$ = 15.7 Hz, $^{3}J_{HH}$ = 10.1 Hz, $^{3}J_{HH}$ = 2.6 Hz, PC*H*), 6.80 (pseudo d, 2H, $^{3}J_{HP}$ = 7.8 Hz, PCHCC*H*), 7.06 (t, 1H, $^{3}J_{HH}$ = 7.8 Hz, PCHCCHC*H*), 7.28-7.53 (m, 18H, Ar), 7.68-7.70 (m, 4H, Ar), 7.77-7.82 (m, 4H, Ar), 7.89-7.93 (m, 4H, Ar); ^{31}P{^{1}H} NMR (CD_2Cl_2, 162 MHz): δ 50.7; ^{13}C{^{1}H} NMR (CD_2Cl_2, 100 MHz): δ 38.1 (d, 2C, $^{2}J_{CP}$ = 2.8 Hz, C8 and C9), 45.9 (d, 2C, $^{1}J_{CP}$ = 50.4 Hz, C6 and C7), 123.5 (s, 2C, C2 and C3), 128.0 (s, 4C, C16, C17, C20 and C21), 128.1 (d, 4C, $^{3}J_{CP}$ = 12.4 Hz, Ca^{meta}), 128.49 (s, 4C, C14, C15, C22 and C23), 128.50 (d, 4C, $^{3}J_{CP}$ = 12.3 Hz, Cb^{meta}), 131.0 (d, 2C, $^{1}J_{CP}$ = 79.5 Hz, Ca^{ipso}), 131.38 (d, 2C, $^{1}J_{CP}$ = 78.7 Hz, Cb^{ipso}), 131.39 (d, 2C, $^{4}J_{CP}$ = 2.7 Hz, Ca^{para}), 131.6 (d, 2C, $^{4}J_{CP}$ = 2.8 Hz, Cb^{para}), 131.9 (d, 4C, $^{2}J_{CP}$ = 9.6 Hz, Ca^{ortho}), 132.4 (d, 4C, $^{2}J_{CP}$ = 10.1 Hz, Cb^{ortho}), 133.1 (s, 2C, C18 and C19), 135.5 (s, 1C, C1), 136.4 (s, 2C, C12 and C13), 154.9 (s, 2C, C4 and

C5), 196.4 (d, 2C, $^{3}J_{CP}$ = 14.1 Hz, C10 and C11). HRMS (ESI) m/z: $(M + H)^{+}$ calcd for $C_{47}H_{40}NO_2P_2S_2$, 776.1976; found, 776.1979.

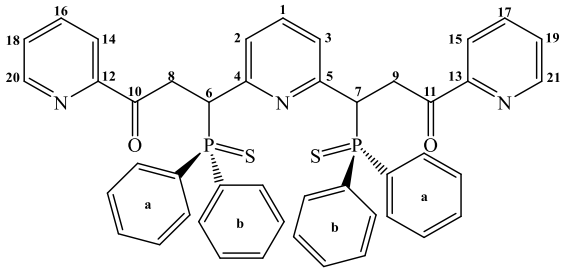

Figure 2.20. General labelling of carbon atoms for phosphine sulfides **10b** and **10b'**.

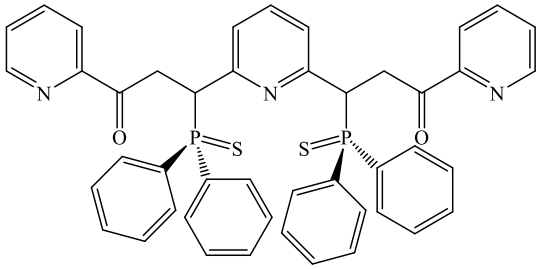

10b. White solid. Yield: 9.7 mg, 12.5 μmol, 46%. The *ee* was determined on a Daicel CHIRALPAK IB column with *n*-hexane/2-propanol = 85/15, flow = 0.8 mL/min, temperature = 20°C, wavelength = 210 nm. Retention times: 31.2 min (minor), 35.8 min (major). $[\alpha]_D^{25}$ = +82.7 (*c* = 0.55, $CHCl_3$). ^{1}H NMR (CD_2Cl_2, 400 MHz): δ 3.72 (ddd, 2H, $^2J_{HH}$ = 18.8 Hz, $^3J_{HP}$ = 13.0 Hz, $^3J_{HH}$ = 2.9 Hz, PCHC*H*), 4.38 (ddd, 2H, $^2J_{HH}$ = 18.8 Hz, $^3J_{HH}$ = 10.2 Hz, $^3J_{HP}$ = 6.8 Hz, PCHC*H*), 4.80 (pseudo ddd, 2H, $^2J_{HP}$ = 14.7 Hz, $^3J_{HH}$ = 10.2 Hz, $^3J_{HH}$ = 2.8 Hz, PC*H*), 6.88 (pseudo d, 2H, $^3J_{HP}$ = 7.7 Hz, PCHCC*H*), 7.05 (t, 1H, $^3J_{HH}$ = 7.7 Hz, PCHCCHC*H*), 7.22-7.30 (m, 6H, Ar), 7.37-7.48 (m, 8H, Ar), 7.60-7.65 (m, 4H, Ar), 7.74-7.80 (m, 4H, Ar), 7.89-7.94 (m, 4H, Ar), 8.66-8.67 (m, 2H, Ar); ^{31}P{^{1}H} NMR (CD_2Cl_2, 162 MHz): δ 50.7; ^{13}C{^{1}H} NMR (CD_2Cl_2, 100 MHz): δ 38.1 (d, 2C, $^2J_{CP}$ = 3.0 Hz, C8 and C9), 45.2 (d, 2C, $^1J_{CP}$ = 50.5 Hz, C6 and C7), 121.5 (s, 2C, C2 and C3), 123.3 (s, 2C, C14 and C15), 127.2 (s, 2C, C18 and C19), 128.1 (d, 4C, $^3J_{CP}$ = 12.3 Hz, Ca^{meta}), 128.4 (d, 4C, $^3J_{CP}$ = 12.2 Hz, Cb^{meta}), 131.1 (d, 2C, $^4J_{CP}$ = 2.5 Hz, Ca^{para}), 131.4 (d, 2C, $^4J_{CP}$ = 2.5 Hz, Cb^{para}), 131.5 (d, 2C, $^1J_{CP}$ = 78.8 Hz, Ca^{ipso}), 131.6 (d, 2C, $^1J_{CP}$ = 77.8 Hz, Cb^{ipso}),

131.8 (d, 4C, $^{2}J_{CP}$ = 10.1 Hz, Ca^{ortho}), 131.9 (d, 4C, $^{2}J_{CP}$ = 10.0 Hz, Cb^{ortho}), 135.3 (s, 1C, C1), 136.7 (s, 2C, C16 and C17), 149.0 (s, 2C, C20 and C21), 153.0 (s, 2C, C12 and C13), 154.9 (s, 2C, C4 and C5), 198.2 (d, 2C, $^{3}J_{CP}$ = 14.3 Hz, C10 and C11). HRMS (ESI) m/z: $(M + H)^{+}$ calcd for $C_{45}H_{38}N_3O_2P_2S_2$, 778.1881; found, 778.1885.

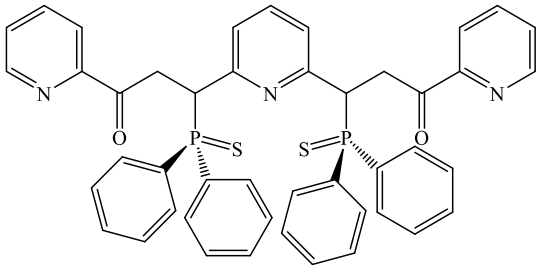

10b'. White solid. Yield: 4.6 mg, 5.90 μmol, 22%. ^{1}H NMR (CD_2Cl_2, 400 MHz): δ 3.78 (ddd, 2H, $^{2}J_{HH}$ = 18.6 Hz, $^{3}J_{HP}$ = 12.9 Hz, $^{3}J_{HH}$ = 2.9 Hz, PCHC*H*), 4.04 (ddd, 2H, $^{2}J_{HH}$ = 18.6 Hz, $^{3}J_{HH}$ = 10.4 Hz, $^{3}J_{HP}$ = 6.8 Hz, PCHC*H*), 4.79 (pseudo ddd, 2H, $^{2}J_{HP}$ = 16.4 Hz, $^{3}J_{HH}$ = 10.3 Hz, $^{3}J_{HH}$ = 2.9 Hz, PC*H*), 6.89 (pseudo d, 2H, $^{3}J_{HP}$ = 7.8 Hz, PCHCC*H*), 7.11 (t, 1H, $^{3}J_{HH}$ = 7.8 Hz, PCHCCHC*H*), 7.14-7.24 (m, 6H, Ar), 7.37-7.47 (m, 8H, Ar), 7.71-7.82 (m, 8H, Ar), 7.89-7.94 (m, 4H, Ar), 8.63-8.64 (m, 2H, Ar); ^{31}P{^{1}H} NMR (CD_2Cl_2, 162 MHz): δ 51.0; ^{13}C{^{1}H} NMR (CD_2Cl_2, 100 MHz): δ 37.7 (d, 2C, $^{2}J_{CP}$ = 2.4 Hz, C8 and C9), 46.3 (d, 2C, $^{1}J_{CP}$ = 49.9 Hz, C6 and C7), 121.5 (s, 2C, C2 and C3), 123.6 (s, 2C, C14 and C15), 127.3 (s, 2C, C18 and C19), 128.0 (d, 4C, $^{3}J_{CP}$ = 12.3 Hz, Ca^{meta}), 128.4 (d, 4C, $^{3}J_{CP}$ = 12.5 Hz, Cb^{meta}), 131.0 (d, 2C, $^{1}J_{CP}$ = 79.9 Hz, Ca^{ipso}), 131.2 (d, 2C, $^{4}J_{CP}$ = 2.6 Hz, Ca^{para}), 131.43 (d, 2C, $^{4}J_{CP}$ = 2.6 Hz, Cb^{para}), 131.45 (d, 2C, $^{1}J_{CP}$ = 78.5 Hz, Cb^{ipso}), 132.0 (d, 4C, $^{2}J_{CP}$ = 9.8 Hz, Ca^{ortho}), 132.4 (d, 4C, $^{2}J_{CP}$ = 10.1 Hz, Cb^{ortho}), 135.4 (s, 1C, C1), 136.8 (s, 2C, C16 and C17), 148.9 (s, 2C, C20 and C21), 152.7 (s, 2C, C12 and C13), 155.0 (s, 2C, C4 and C5), 198.2 (d, 2C, $^{3}J_{CP}$ = 14.2 Hz, C10 and C11). HRMS (ESI) m/z: $(M + H)^{+}$ calcd for $C_{45}H_{38}N_3O_2P_2S_2$, 778.1881; found, 778.1882.

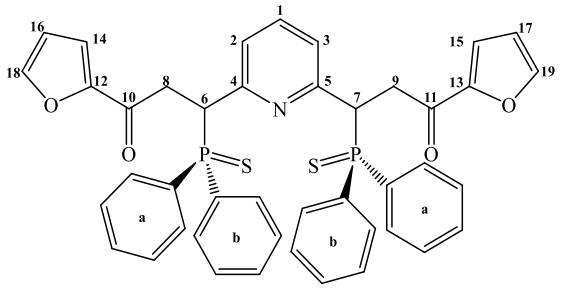

Figure 2.21. General labelling of carbon atoms for phosphine sulfides **10c** and **10c'**.

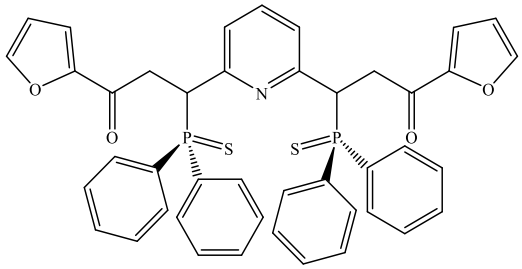

10c. White solid. Yield: 4.3 mg, 5.73 μmol, 21%. The *ee* was determined on a Daicel CHIRALPAK IA column with *n*-hexane/2-propanol = 85/15, flow = 1.0 mL/min, temperature = 20°C, wavelength = 230 nm. Retention times: 30.1 min (minor), 43.0 min (major). $[\alpha]_D^{25}$ = +243.1 (*c* = 0.13, $CHCl_3$). ^{1}H NMR (CD_2Cl_2, 400 MHz): δ 3.34 (ddd, 2H, $^2J_{HH}$ = 18.0 Hz, $^3J_{HP}$ = 13.3 Hz, $^3J_{HH}$ = 2.6 Hz, PCHC*H*), 4.25 (ddd, 2H, $^2J_{HH}$ = 18.1 Hz, $^3J_{HH}$ = 10.0 Hz, $^3J_{HP}$ = 5.7 Hz, PCHC*H*), 4.79 (pseudo ddd, 2H, $^2J_{HP}$ = 14.2 Hz, $^3J_{HH}$ = 10.0 Hz, $^3J_{HH}$ = 2.5 Hz, PC*H*), 6.49-6.50 (m, 2H, Ar), 6.72 (pseudo d, 2H, $^3J_{HP}$ = 7.8 Hz, PCHCC*H*), 6.96 (t, 1H, $^3J_{HH}$ = 7.7 Hz, PCHCCHC*H*), 7.15-7.16 (m, 2H, Ar), 7.22-7.33 (m, 6H, Ar), 7.39-7.49 (m, 6H, Ar), 7.55-7.62 (m, 6H, Ar), 7.88-7.93 (m, 4H, Ar); ^{31}P{^{1}H} NMR (CD_2Cl_2, 162 MHz): δ 50.71; ^{13}C{^{1}H} NMR (CD_2Cl_2, 100 MHz): δ 38.4 (d, 2C, $^2J_{CP}$ = 2.9 Hz, C8 and C9), 44.7 (d, 2C, $^1J_{CP}$ = 51.3 Hz, C6 and C7), 112.1 (s, 2C, C16 and C17), 117.7 (s, 2C, C14 and C15), 123.6 (s, 2C, C2 and C3), 128.1 (d, 4C, $^3J_{CP}$ = 12.0 Hz, Ca^{meta}), 128.5 (d, 4C, $^3J_{CP}$ = 12.1 Hz, Cb^{meta}), 131.2 (d, 2C, $^4J_{CP}$ = 3.0 Hz, Ca^{para}), 131.47 (d, 2C, $^1J_{CP}$ = 80.7 Hz, Ca^{ipso}), 131.51 (d, 2C, $^1J_{CP}$ = 79.0 Hz, Cb^{ipso}), 131.6 (d, 2C, $^4J_{CP}$ = 2.9 Hz, Cb^{para}),

131.7 (d, 4C, $^{2}J_{CP}$ = 9.8 Hz, Ca^{ortho}), 131.9 (d, 4C, $^{2}J_{CP}$ = 10.1 Hz, Cb^{ortho}), 135.4 (s, 1C, C1), 146.5 (s, 2C, C18 and C19), 152.1 (s, 2C, C12 and C13), 154.8 (s, 2C, C4 and C5), 185.5 (d, 2C, $^{3}J_{CP}$ = 14.9 Hz, C10 and C11). HRMS (ESI) m/z: $(M + H)^{+}$ calcd for $C_{43}H_{36}NO_4P_2S_2$, 756.1561; found, 756.1560.

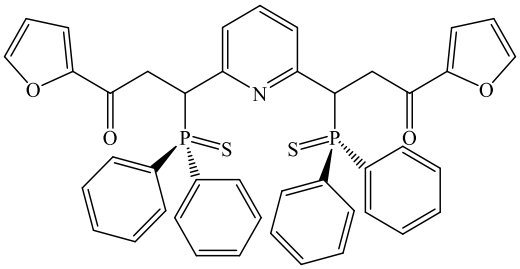

10c'. White solid. Yield: 2.4 mg, 3.18 μmol, 12%. ^{1}H NMR (CD_2Cl_2, 400 MHz): δ 3.34 (ddd, 2H, $^{2}J_{HH}$ = 17.8 Hz, $^{3}J_{HP}$ = 13.1 Hz, $^{3}J_{HH}$ = 3.0 Hz, PCHC*H*), 3.72 (ddd, 2H, $^{2}J_{HH}$ = 17.8 Hz, $^{3}J_{HH}$ = 10.1 Hz, $^{3}J_{HP}$ = 6.7 Hz, PCHC*H*), 4.77 (pseudo ddd, 2H, $^{2}J_{HP}$ = 16.1 Hz, $^{3}J_{HH}$ = 10.0 Hz, $^{3}J_{HH}$ = 3.0 Hz, PC*H*), 6.48-6.49 (m, 2H, Ar), 6.83 (pseudo d, 2H, $^{3}J_{HP}$ = 7.8 Hz, PCHCC*H*), 7.02-7.03 (m, 2H, Ar), 7.08 (t, 1H, $^{3}J_{HH}$ = 7.7 Hz, PCHCCHC*H*), 7.27-7.31 (m, 6H, Ar), 7.40-7.54 (m, 8H, Ar), 7.74-7.80 (m, 4H, Ar), 7.88-7.93 (m, 4H, Ar); ^{31}P{^{1}H} NMR (CD_2Cl_2, 162 MHz): δ 50.68; ^{13}C{^{1}H} NMR (CD_2Cl_2, 100 MHz): δ 38.0 (d, 2C, $^{2}J_{CP}$ = 2.3 Hz, C8 and C9), 45.7 (d, 2C, $^{1}J_{CP}$ = 50.5 Hz, C6 and C7), 112.1 (s, 2C, C16 and C17), 117.3 (s, 2C, C14 and C15), 123.5 (s, 2C, C2 and C3), 128.0 (d, 4C, $^{3}J_{CP}$ = 12.3 Hz, Ca^{meta}), 128.4 (d, 4C, $^{3}J_{CP}$ = 12.2 Hz, Cb^{meta}), 131.0 (d, 2C, $^{1}J_{CP}$ = 79.9 Hz, Ca^{ipso}), 131.28 (d, 2C, $^{4}J_{CP}$ = 2.5 Hz, Ca^{para}), 131.35 (d, 2C, $^{1}J_{CP}$ = 78.5 Hz, Cb^{ipso}), 131.5 (d, 2C, $^{4}J_{CP}$ = 2.4 Hz, Cb^{para}), 131.9 (d, 4C, $^{2}J_{CP}$ = 9.8 Hz, Ca^{ortho}), 132.4 (d, 4C, $^{2}J_{CP}$ = 10.2 Hz, Cb^{ortho}), 135.5 (s, 1C, C1), 146.4 (s, 2C, C18 and C19), 152.2 (s, 2C, C12 and C13), 154.8 (s, 2C, C4 and C5), 185.4 (d, 2C, $^{3}J_{CP}$ = 14.3 Hz, C10 and C11). HRMS (ESI) m/z: $(M + H)^{+}$ calcd for $C_{43}H_{36}NO_4P_2S_2$, 756.1561; found, 756.1565.

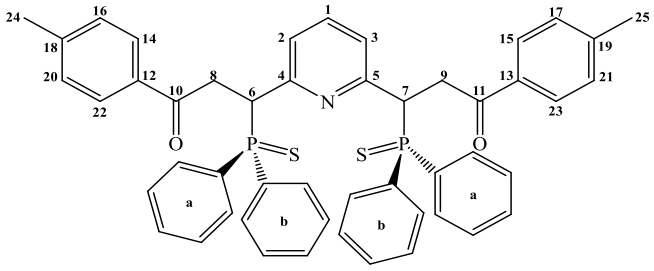

Figure 2.22. General labelling of carbon atoms for phosphine sulfides **10d** and **10d'**.

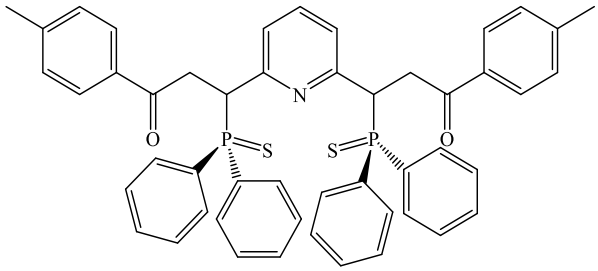

10d. White solid. Yield: 9.2 mg, 11.4 μmol, 42%. The *ee* was determined on a Daicel CHIRALPAK IA column with *n*-hexane/2-propanol = 75/25, flow = 1.0 mL/min, temperature = 20°C, wavelength = 230 nm. Retention times: 47.2 min (major), 60.2 min (minor). $[\alpha]_D^{25}$ = +214.1 (*c* = 0.92, $CHCl_3$). ^{1}H NMR (CD_2Cl_2, 400 MHz): δ 2.36 (s, 6H, C*H*$_3$), 3.50 (ddd, 2H, $^2J_{HH}$ = 18.3 Hz, $^3J_{HP}$ = 13.8 Hz, $^3J_{HH}$ = 1.8 Hz, PCHC*H*), 4.56 (ddd, 2H, $^2J_{HH}$ = 18.3 Hz, $^3J_{HH}$ = 9.8 Hz, $^3J_{HP}$ = 4.7 Hz, PCHC*H*), 4.87 (pseudo ddd, 2H, $^2J_{HP}$ = 13.6 Hz, $^3J_{HH}$ = 9.6 Hz, $^3J_{HH}$ = 1.6 Hz, PC*H*), 6.69 (pseudo d, 2H, $^3J_{HP}$ = 7.7 Hz, PCHCC*H*), 6.90 (t, 1H, $^3J_{HH}$ = 7.7 Hz, PCHCCHC*H*), 7.16-7.25 (m, 10H, Ar), 7.30-7.35 (m, 4H, Ar), 7.38-7.42 (m, 2H, Ar), 7.58-7.63 (m, 4H, Ar), 7.79-7.91 (m, 8H, Ar); ^{31}P{^{1}H} NMR ($CDCl_3$, 162 MHz): δ 51.1; ^{13}C{^{1}H} NMR (CD_2Cl_2, 100 MHz): δ 21.4 (s, 2C, C24 and C25), 38.9 (d, 2C, $^2J_{CP}$ = 2.2 Hz, C8 and C9), 45.4 (d, 2C, $^1J_{CP}$ = 51.6 Hz, C6 and C7), 123.7 (s, 2C, C2 and C3), 128.1 (d, 4C, $^3J_{CP}$ = 12.0 Hz, Ca^{meta}), 128.3 (s, 4C, C16, C17, C20 and C21), 128.5 (d, 4C, $^3J_{CP}$ = 11.8 Hz, Cb^{meta}), 129.1 (s, 4C, C14, C15, C22 and C23), 131.1 (d, 2C, $^4J_{CP}$ = 2.6 Hz, Ca^{para}), 131.5 (d, 2C, $^4J_{CP}$ = 2.8 Hz, Cb^{para}), 131.65 (d, 4C, $^2J_{CP}$ = 9.6 Hz, Ca^{ortho}),

131.68 (d, 2C, $^{1}J_{CP}$ = 79.7 Hz, Ca^{ipso}), 131.7 (d, 2C, $^{1}J_{CP}$ = 78.2 Hz, Cb^{ipso}), 131.9 (d, 4C, $^{2}J_{CP}$ = 9.7 Hz, Cb^{ortho}), 133.9 (s, 2C, C12 and C13), 135.3 (s, 1C, C1), 144.2 (s, 2C, C18 and C19), 155.1 (s, 2C, C4 and C5), 196.1 (d, 2C, $^{3}J_{CP}$ = 14.0 Hz, C10 and C11). HRMS (ESI) m/z: $(M + H)^{+}$ calcd for $C_{49}H_{44}NO_2P_2S_2$, 804.2289; found, 804.2292.

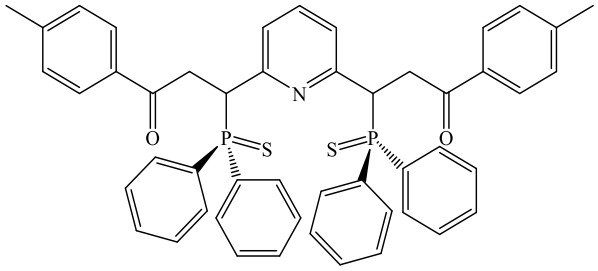

10d'. White solid. Yield: 5.0 mg, 6.21 μmol, 23%. ^{1}H NMR (CD_2Cl_2, 400 MHz): δ 2.37 (s, 6H, C*H*$_3$), 3.41 (ddd, 2H, $^{2}J_{HH}$ = 17.9 Hz, $^{3}J_{HP}$ = 13.1 Hz, $^{3}J_{HH}$ = 2.6 Hz, PCHC*H*), 3.91 (ddd, 2H, $^{2}J_{HH}$ = 17.9 Hz, $^{3}J_{HH}$ = 10.1 Hz, $^{3}J_{HP}$ = 6.1 Hz, PCHC*H*), 4.82 (pseudo ddd, 2H, $^{2}J_{HP}$ = 13.1 Hz, $^{3}J_{HH}$ = 10.1 Hz, $^{3}J_{HH}$ = 2.6 Hz, PC*H*), 6.77 (pseudo d, 2H, $^{3}J_{HP}$ = 7.8 Hz, PCHCC*H*), 7.04 (t, 1H, $^{3}J_{HH}$ = 7.7 Hz, PCHCCHC*H*), 7.12-7.20 (m, 4H, Ar), 7.26-7.29 (m, 6H, Ar), 7.38-7.49 (m, 6H, Ar), 7.57-7.59 (m, 4H, Ar), 7.78-7.94 (m, 8H, Ar); ^{31}P{^{1}H} NMR ($CDCl_3$, 162 MHz): δ 50.7; ^{13}C{^{1}H} NMR (CD_2Cl_2, 100 MHz): δ 21.4 (s, 2C, C24 and C25), 37.9 (d, 2C, $^{2}J_{CP}$ = 2.3 Hz, C8 and C9), 46.1 (d, 2C, $^{1}J_{CP}$ = 50.1 Hz, C6 and C7), 123.5 (s, 2C, C2 and C3), 128.09 (d, 4C, $^{3}J_{CP}$ = 12.3 Hz, Ca^{meta}), 128.10 (s, 4C, C16, C17, C20 and C21), 128.5 (d, 4C, $^{3}J_{CP}$ = 12.1 Hz, Cb^{meta}), 129.1 (s, 4C, C14, C15, C22 and C23), 131.0 (d, 2C, $^{1}J_{CP}$ = 79.4 Hz, Ca^{ipso}), 131.38 (d, 2C, $^{4}J_{CP}$ = 2.4 Hz, Ca^{para}), 131.44 (d, 4C, $^{1}J_{CP}$ = 78.9 Hz, Cb^{ipso}), 131.5 (d, 2C, $^{4}J_{CP}$ = 2.5 Hz, Cb^{para}), 131.9 (d, 2C, $^{2}J_{CP}$ = 9.9 Hz, Ca^{ortho}), 132.5 (d, 4C, $^{2}J_{CP}$ = 10.0 Hz, Cb^{ortho}), 133.9 (s, 2C, C12 and C13), 135.4 (s, 1C, C1), 144.0 (s, 2C, C18 and C19), 155.0 (s, 2C, C4 and C5), 196.0 (d, 2C, $^{3}J_{CP}$ = 14.0 Hz, C10 and C11). HRMS (ESI) m/z: $(M + H)^{+}$ calcd for $C_{49}H_{44}NO_2P_2S_2$, 804.2289; found, 804.2289.

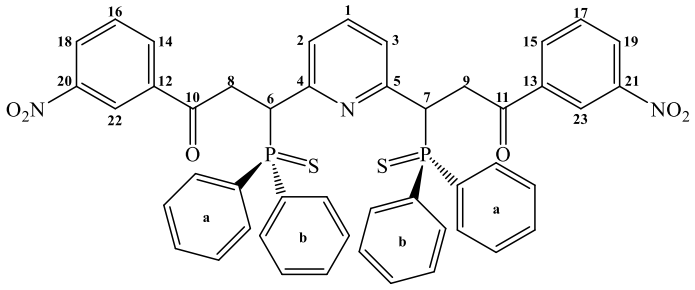

Figure 2.23. General labelling of carbon atoms for phosphine sulfides **10e** and **10e'**.

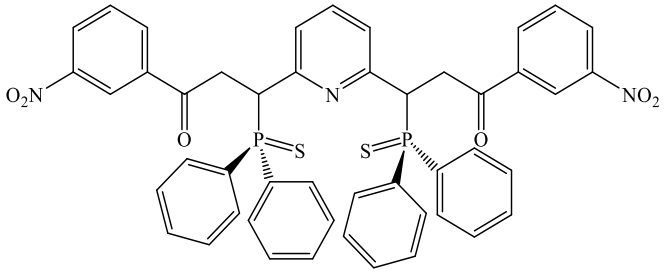

10e. White solid. Yield: 8.6 mg, 9.93 µmol, 37%. The *ee* was determined on a Daicel CHIRALPAK IA column with *n*-hexane/2-propanol = 85/15, flow = 1.0 mL/min, temperature = 20°C, wavelength = 230 nm. Retention times: 35.2 min (minor), 72.3 min (major). $[\alpha]_D^{25}$ = +258.6 (*c* = 0.86, $CHCl_3$). ^{1}H NMR (CD_2Cl_2, 400 MHz): δ 3.37-3.45 (m, 2H, C*H*), 4.79-4.89 (m, 4H, C*H*), 6.57 (pseudo d, 2H, $^3J_{HP}$ = 7.7 Hz, PCHCC*H*), 6.91 (t, 1H, $^3J_{HH}$ = 7.7 Hz, PCHCCHC*H*), 7.18-7.23 (m, 4H, Ar), 7.29-7.33 (m, 2H, Ar), 7.36-7.52 (m, 10H, Ar), 7.66-7.70 (m, 2H, Ar), 7.94-7.99 (m, 4H, Ar), 8.32-8.34 (m, 2H, Ar), 8.37-8.40 (m, 2H, Ar), 8.71-8.72 (m, 2H, Ar); ^{31}P{^{1}H} NMR (CD_2Cl_2, 162 MHz): δ 50.1; ^{13}C{^{1}H} NMR (CD_2Cl_2, 100 MHz): δ 38.9 (d, 2C, $^2J_{CP}$ = 2.7 Hz, C8 and C9), 43.9 (d, 2C, $^1J_{CP}$ = 51.4 Hz, C6 and C7), 122.9 (s, 2C, C22 and C23), 123.7 (s, 2C, C2 and C3), 127.3 (s, 2C, C18 and C19), 128.0 (d, 4C $^3J_{CP}$ = 12.4 Hz, Ca^{meta}), 128.6 (d, 4C, $^3J_{CP}$ = 12.5 Hz, Cb^{meta}), 129.8 (s, 2C, C16 and C17), 131.2 (d, 2C, $^1J_{CP}$ = 78.3 Hz, Ca^{ipso}), 131.30 (d, 2C, $^1J_{CP}$ = 81.5 Hz, Cb^{ipso}), 131.32 (d, 2C, $^4J_{CP}$ = 2.6 Hz, Ca^{para}), 131.5 (d, 4C, $^2J_{CP}$ = 10.1 Hz, Ca^{ortho}), 131.7 (d, 4C, $^2J_{CP}$ = 9.5 Hz, Cb^{ortho}), 131.8 (d, 2C, $^4J_{CP}$ = 2.6 Hz, Cb^{para}), 134.2 (s, 2C, C14 and

C15), 135.1 (s, 1C, C1), 137.8 (s, 2C, C12 and C13), 148.4 (s, 2C, C20 and C21), 153.9 (s, 2C, C4 and C5), 195.3 (d, 2C, $^{3}J_{CP}$ = 15.1 Hz, C10 and C11). HRMS (ESI) m/z: $(M + H)^{+}$ calcd for $C_{47}H_{38}N_3O_6P_2S_2$, 866.1677; found, 866.1675.

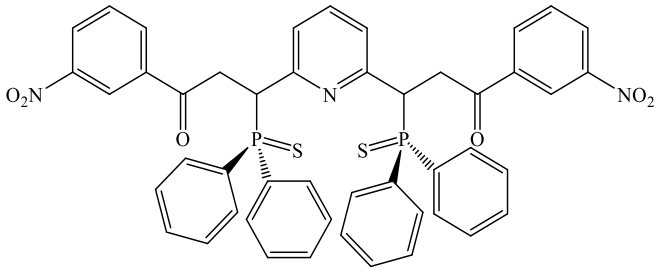

10e'. White solid. Yield: 4.5 mg, 5.20 μmol, 19%. ^{1}H NMR (CD_2Cl_2, 400 MHz): δ 3.46 (ddd, 2H, $^{2}J_{HH}$ = 18.1 Hz, $^{3}J_{HP}$ = 12.2 Hz, $^{3}J_{HH}$ = 2.9 Hz, PCHC*H*), 3.98 (ddd, 2H, $^{2}J_{HH}$ = 18.0 Hz, $^{3}J_{HH}$ = 9.9 Hz, $^{3}J_{HP}$ = 7.3 Hz, PCHC*H*), 4.83 (pseudo ddd, 2H, $^{2}J_{HP}$ = 15.6 Hz, $^{3}J_{HH}$ = 9.9 Hz, $^{3}J_{HH}$ = 3.0 Hz, PC*H*), 6.75 (pseudo d, 2H, $^{3}J_{HP}$ = 7.8 Hz, PCHCC*H*), 7.08 (t, 1H, $^{3}J_{HH}$ = 7.9 Hz, PCHCCHC*H*), 7.31-7.55 (m, 14H, Ar), 7.77-7.82 (m, 4H, Ar), 7.91-7.96 (m, 4H, Ar), 8.00-8.02 (m, 2H, Ar), 8.27-8.29 (m, 2H, Ar), 8.41-8.42 (m, 2H, Ar); ^{31}P{^{1}H} NMR (CD_2Cl_2, 162 MHz): δ 50.3; ^{13}C{^{1}H} NMR (CD_2Cl_2, 100 MHz): δ 38.3 (d, 2C, $^{2}J_{CP}$ = 3.1 Hz, C8 and C9), 45.8 (d, 2C, $^{1}J_{CP}$ = 50.2 Hz, C6 and C7), 122.5 (s, 2C, C22 and C23), 123.7 (s, 2C, C2 and C3), 127.3 (s, 2C, C18 and C19), 128.3 (d, 4C $^{3}J_{CP}$ = 12.3 Hz, Ca^{meta}), 128.6 (d, 4C, $^{3}J_{CP}$ = 12.0 Hz, Cb^{meta}), 129.8 (s, 2C, C16 and C17), 130.7 (d, 2C, $^{1}J_{CP}$ = 80.0 Hz, Ca^{ipso}), 131.0 (d, 2C, $^{1}J_{CP}$ = 78.6 Hz, Cb^{ipso}), 131.6 (d, 2C, $^{4}J_{CP}$ = 2.9 Hz, Ca^{para}), 131.8 (d, 2C, $^{4}J_{CP}$ = 3.1 Hz, Cb^{para}), 131.9 (d, 4C, $^{2}J_{CP}$ = 9.8 Hz, Ca^{ortho}), 132.4 (d, 4C, $^{2}J_{CP}$ = 10.1 Hz, Cb^{ortho}), 133.6 (s, 2C, C14 and C15), 135.6 (s, 1C, C1), 137.4 (s, 2C, C12 and C13), 148.3 (s, 2C, C20 and C21), 154.5 (s, 2C, C4 and C5), 194.6 (d, 2C, $^{3}J_{CP}$ = 14.2 Hz, C10 and C11). HRMS (ESI) m/z: $(M + H)^{+}$ calcd for $C_{47}H_{38}N_3O_6P_2S_2$, 866.1677; found, 866.1682.

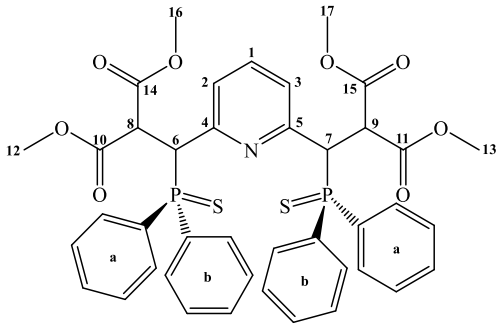

Figure 2.24. General labelling of carbon atoms for phosphine sulfides **10f** and **10f'**.

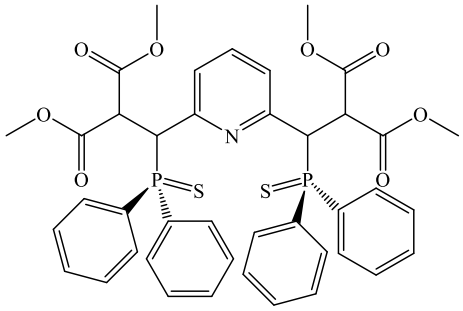

10f. White solid. Yield: 9.4 mg, 11.7 µmol, 43%. The *ee* was determined on a Daicel CHIRALPAK IA column with *n*-hexane/2-propanol = 75/25, flow = 1.0 mL/min, temperature = 23°C, wavelength = 254 nm. Retention times: 14.4 min (major), 62.1 min (minor). $[\alpha]_D^{25}$ = +5.7 (*c* = 0.49, $CHCl_3$). ^{1}H NMR (CD_2Cl_2, 400 MHz): δ 3.35 (s, 12H, OC*H*$_3$), 4.42 (pseudo dd, 2H, $^2J_{HP}$ = 11.5 Hz, $^3J_{HH}$ = 10.8 Hz, PC*H*), 5.05 (pseudo dd, 2H, $^3J_{HH}$ = 10.6 Hz, $^3J_{HP}$ = 10.3 Hz, PCHC*H*), 6.84 (pseudo d, 2H, $^3J_{HP}$ = 7.8 Hz, PCHCC*H*), 6.98 (t, 1H, $^3J_{HH}$ = 7.8 Hz, PCHCCHC*H*), 7.23-7.27 (m, 4H, Ar), 7.35-7.39 (m, 2H, Ar), 7.45-7.56 (m, 6H, Ar), 7.59-7.64 (m, 4H, Ar), 7.94-7.99 (m, 4H, Ar); ^{31}P{^{1}H} NMR (CD_2Cl_2, 162 MHz): δ 48.6; ^{13}C{^{1}H} NMR (CD_2Cl_2, 75 MHz): δ 48.5 (d, 2C, $^1J_{CP}$ = 47.6 Hz, C6 and C7), 52.6 (d, 2C, $^2J_{CP}$ = 30.7 Hz, C8 and C9), 54.0 (s, 4C, C12, C13, C16 and C17), 124.2 (s, 2C, C2 and C3), 128.1 (d, 4C, $^3J_{CP}$ = 12.4 Hz, Ca^{meta}), 128.3 (d, 4C, $^3J_{CP}$ = 12.4 Hz, Cb^{meta}), 130.5 (d, 2C, $^1J_{CP}$ = 82.2 Hz, Ca^{ipso}), 130.7 (d, 2C, $^1J_{CP}$ = 79.6 Hz, Cb^{ipso}), 131.4 (d, 2C, $^4J_{CP}$ = 3.2 Hz, Ca^{para}), 131.6 (d, 2C, $^4J_{CP}$ = 3.0 Hz, Cb^{para}), 132.2 (d, 2C, $^2J_{CP}$ = 9.8 Hz,

Ca^{ortho}), 132.4 (d, 4C, $^{2}J_{CP}$ = 9.8 Hz, Cb^{ortho}), 134.9 (s, 1C, C1), 153.8 (s, 2C, C4 and C5), 167.2 (d, 4C, $^{3}J_{CP}$ = 15.7 Hz, C10, C11, C14 and C15). HRMS (ESI) m/z: $(M + H)^{+}$ calcd for $C_{41}H_{40}NO_8P_2S_2$, 800.1671; found, 800.1675.

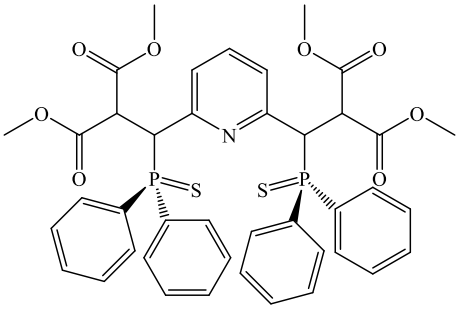

10f'. White solid. Yield: 7.7 mg, 9.63 μmol, 36%. ^{1}H NMR (CD_2Cl_2, 400 MHz): δ 3.17 (s, 6H, OC*H*$_3$), 3.45 (s, 6H, OC*H*$_3$), 4.89 (pseudo dd, 2H, $^{2}J_{HP}$ = 11.1 Hz, $^{3}J_{HH}$ = 10.8 Hz, PC*H*), 5.03 (pseudo dd, 2H, $^{3}J_{HH}$ = 10.7 Hz, $^{3}J_{HP}$ = 9.4 Hz, PCHC*H*), 6.63 (pseudo d, 2H, $^{3}J_{HP}$ = 7.8 Hz, PCHCC*H*), 6.80 (t, 1H, $^{3}J_{HH}$ = 7.8 Hz, PCHCCHC*H*), 7.23-7.27 (m, 4H, Ar), 7.33-7.36 (m, 2H, Ar), 7.49-7.59 (m, 10H, Ar), 8.09-8.14 (m, 4H, Ar); ^{31}P{^{1}H} NMR (CD_2Cl_2, 162 MHz): δ 48.8; ^{13}C{^{1}H} NMR (CD_2Cl_2, 100 MHz): δ 48.2 (d, 2C, $^{1}J_{CP}$ = 47.3 Hz, C6 and C7), 52.5 (d, 2C, $^{2}J_{CP}$ = 30.5 Hz, C8 and C9), 53.8 (s, 4C, C12, C13, C16 and C17), 123.9 (s, 2C, C2 and C3), 128.3 (d, 8C, $^{3}J_{CP}$ = 12.4 Hz, Ca^{meta} overlapped with Cb^{meta}), 130.8 (d, 2C, $^{1}J_{CP}$ = 79.3 Hz, Ca^{ipso}), 131.2 (d, 2C, $^{1}J_{CP}$ = 82.7 Hz, Cb^{ipso}), 131.3 (d, 2C, $^{4}J_{CP}$ = 2.9 Hz, Ca^{para}), 131.7 (d, 2C, $^{4}J_{CP}$ = 3.0 Hz, Cb^{para}), 132.1 (d, 2C, $^{2}J_{CP}$ = 9.9 Hz, Ca^{ortho}), 132.5 (d, 4C, $^{2}J_{CP}$ = 10.0 Hz, Cb^{ortho}), 134.5 (s, 1C, C1), 153.5 (s, 2C, C4 and C5), 167.7 (d, 4C, $^{3}J_{CP}$ = 16.0 Hz, C10, C11, C14 and C15). HRMS (ESI) m/z: $(M + H)^{+}$ calcd for $C_{41}H_{40}NO_8P_2S_2$, 800.1671; found, 800.1672.

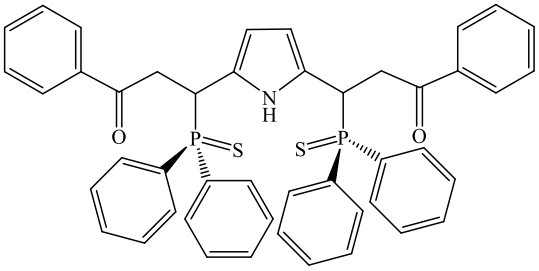

15a/15a' (reported as an inseparable diastereomeric mixture). Yellow solid. ^{1}H NMR ($CDCl_3$, 400 MHz): δ 3.02 (ddd, $^{2}J_{HH}$ = 17.5 Hz, $^{3}J_{HH}$ = 11.3 Hz, $^{3}J_{HP}$ = 2.2 Hz, PCHC*H*), 3.11 (ddd, $^{2}J_{HH}$ = 17.8 Hz, $^{3}J_{HH}$ = 11.7 Hz, $^{3}J_{HP}$ = 2.1 Hz, PCHC*H*), 3.58 (ddd, $^{2}J_{HH}$ = 17.8 Hz, $^{3}J_{HH}$ = 10.2 Hz, $^{3}J_{HP}$ = 4.5 Hz, PCHC*H*), 4.02 (ddd, $^{2}J_{HH}$ = 17.6 Hz, $^{3}J_{HH}$ = 10.4 Hz, $^{3}J_{HP}$ = 4.4 Hz, PCHC*H*), 4.78-4.87 (m, overlap of both isomers' PC*H*), 5.56 (s, NCC*H*), 5.70 (s, NCC*H*), 6.88-8.07 (m, Ar), 9.57 (br s, N*H*), 10.13 (br s, N*H*); ^{31}P{^{1}H} NMR ($CDCl_3$, 162 MHz): δ 48.1, 48.4; HRMS (ESI) m/z: $(M + H)^+$ calcd for $C_{46}H_{40}NO_2P_2S_2$, 763.1897; found, 763.1893.

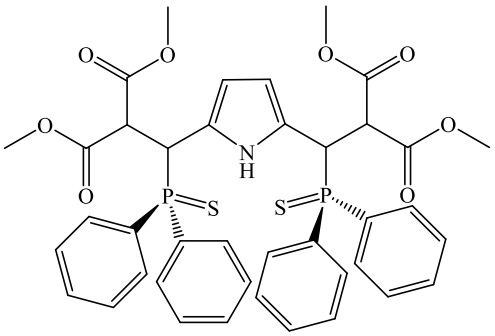

15b/15b' (reported as an inseparable diastereomeric mixture). Yellow solid. ^{1}H NMR (CD_2Cl_2, 400 MHz): δ 3.14 (s, C(O)CH_3), 3.16 (s, C(O)CH_3), 3.26 (s, C(O)CH_3), 3.31 (s, C(O)CH_3), 4.26-4.33 (m, overlap of both isomers' PCHC*H*), 4.81-4.91 (m, overlap of both isomers' PC*H*), 5.70 (s, NCC*H*), 5.79 (s, NCC*H*), 7.23-7.93 (m, Ar), 10.08 (br s, N*H*), 10.18 (br s, N*H*); ^{31}P{^{1}H} NMR (CD_2Cl_2, 162 MHz): δ 45.8, 46.0; HRMS (ESI) m/z: $(M + H)^+$ calcd for $C_{40}H_{40}NO_8P_2S_2$, 787.1592; found, 787.1587.

General procedure for the syntheses of pyrrolyl PNP complexes 16

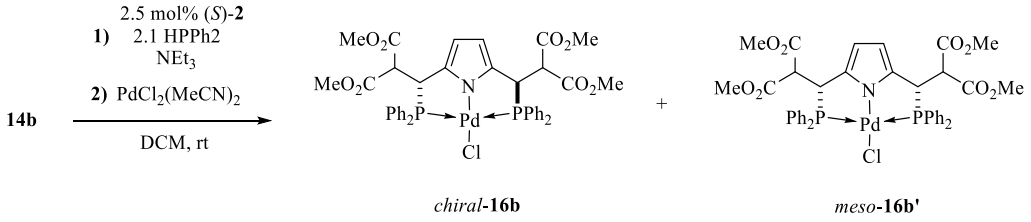

Scheme 2.18. Synthetic outline for complexation of diphosphines **15b** and **15b'** to $PdCl_2(MeCN)_2$.

Substrate **14b** (0.082 mmol, 1.0 equiv.) and catalyst (*S*)-**2** (2.57 mg, 1.37 μmol, 2.5 mol %) were added into a 10 mL storage tube and dissolved in DCM (2-4 mL). The mixture was stirred for 1 minute before diphenylphosphine (32.1 mg, 0.171 mmol, 2.1 equiv.) and triethylamine (17.3 mg, 0.171 mmol, 2.1 equiv.) were added successively with washing using another portion of DCM (0.5-1 mL). The resultant mixture was then left to stir at room temperature until stagnation of reaction as monitored by $^{31}P\{^{1}H\}$ NMR analysis of the crude mixture. Following which a portion of $PdCl_2(MeCN)_2$ (0.082 mmol, 1.0 equiv.) was added in-situ to the generated pot of diphosphines **15b** and **15b'** and the resultant mixture was continued to stir for 24 h to form a dark yellow solution. Solvent removal was performed via rotary evaporation and the crude mixture was purified using silica gel chromatography in DCM/EA to furnish a partially purified mixture containing both diastereomeric isomers. Further attempts to purify this mixture were unsuccessful due to the inseparability of the diastereomers on the mobile phase.

Characterization data of pyrrolyl PNP complexes 16

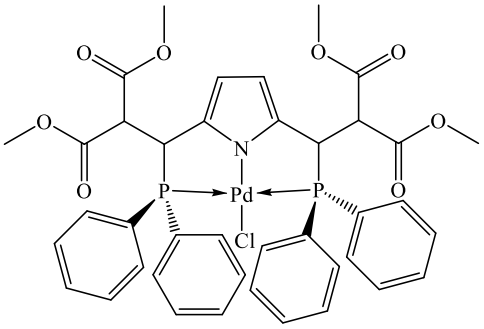

16a/16a' (reported as an inseparable diastereomeric mixture). Yellow solid. ^{1}H NMR (CD_2Cl_2, 400 MHz): δ 3.18 (s, C(O)C*H*$_3$), 3.24 (s, C(O)C*H*$_3$), 3.26 (s, C(O)C*H*$_3$), 3.52 (s, C(O)C*H*$_3$), 3.65-3.70 (m, overlap of both isomers' PCHC*H*), 4.78-4.86 (m, overlap of both isomers' PC*H*), 5.87 (s, NCC*H*), 5.99 (s, NCC*H*), 7.44-7.57 (m, Ar), 7.78-7.90 (m, Ar), 8.10-8.14 (m, Ar); ^{31}P{^{1}H} NMR (CD_2Cl_2, 162 MHz): δ 46.6, 46.8; HRMS (ESI) m/z: $(M + H)^+$ calcd for $C_{40}H_{39}ClNO_8P_2Pd$, 863.0796; found, 863.0792.

Reprinted with permission from “Foo, C. Q.; Sadeer, A.; Li, Y.; Pullarkat, S. A.; Leung, P.-H., Access to C-Stereogenic PN (sp 2) P Pincer Ligands via Phosphapalladacycle Catalyzed Asymmetric Hydrophosphination. *Organometallics* **2021,** *40* (6), 682-692.” Copyright 2021 American Chemical Society.[40]

References

[1] Koshti, V.; Gaikwad, S.; Chikkali, S. H., Contemporary avenues in catalytic PH bond addition reaction: A case study of hydrophosphination. *Coord. Chem. Rev.* **2014**, *265*, 52-73.

[2] Chikkali, S.; Gudat, D., Hydrophosphanation of Phenolic Aldehydes as Facile Synthetic Approach to Catechol-Functionalized Phosphane Oxides and Phosphanes. Wiley Online Library: 2006.

[3] Rauhut, M.; Hechenbleikner, I.; Currier, H. A.; Schaefer, F.; Wystrach, V., The cyanoethylation of phosphine and phenylphosphine. *J. Am. Chem. Soc.* **1959**, *81* (5), 1103-1107.

[4] Berger, H.-O.; Nöth, H., Beiträge zur chemie des bors: 132. 1-phospha-und 1-arsa-4-bora-cyclohexadiene-2, 5. *J. Organomet. Chem.* **1983**, *250* (1), 33-48.

[5] a) Trifonov, A.; Basalov, I.; Kissel, A., Use of organolanthanides in the catalytic intermolecular hydrophosphination and hydroamination of multiple C–C bonds. *Dalton Transactions* **2016**, *45* (48), 19172-19193; b) Douglass, M. R.; Stern, C. L.; Marks, T. J., Intramolecular hydrophosphination/cyclization of phosphinoalkenes and phosphinoalkynes catalyzed by organolanthanides: scope, selectivity, and mechanism. *J. Am. Chem. Soc.* **2001**, *123* (42), 10221-10238.

[6] a) Liu, B.; Roisnel, T.; Carpentier, J. F.; Sarazin, Y., Heteroleptic alkyl and amide iminoanilide alkaline earth and divalent rare earth complexes for the catalysis of hydrophosphination and (cyclo) hydroamination reactions. *Chemistry–A European Journal* **2013**, *19* (40), 13445-13462; b) Crimmin, M. R.; Barrett, A. G.; Hill, M. S.; Hitchcock, P. B.; Procopiou, P. A., Calcium-catalyzed intermolecular hydrophosphination. *Organometallics* **2007**, *26* (12), 2953-2956.

[7] Chen, Y.-R.; Duan, W.-L., Palladium-catalyzed 1, 4-addition of diarylphosphines to α, β-unsaturated aldehydes. *Org. Lett.* **2011**, *13* (21), 5824-5826.

[8] Ghebreab, M. B.; Bange, C. A.; Waterman, R., Intermolecular Zirconium-Catalyzed Hydrophosphination of Alkenes and Dienes with Primary Phosphines. *J. Am. Chem. Soc.* **2014**, *136* (26), 9240-9243.

[9] a) Crimmin, M. R.; Barrett, A. G.; Hill, M. S.; Hitchcock, P. B.; Procopiou, P. A., Heavier group 2 element catalyzed hydrophosphination of carbodiimides. *Organometallics* **2008**, *27* (4), 497-499; b) Zhang, W. X.; Nishiura, M.; Mashiko, T.; Hou, Z., Half-Sandwich o-N, N-Dimethylaminobenzyl Complexes over the Full Size Range of Group 3 and Lanthanide Metals. Synthesis, Structural Characterization, and Catalysis of Phosphine P□ H Bond Addition to Carbodiimides. *Chemistry–A European Journal* **2008**, *14* (7), 2167-2179.

[10] Li, J.; Lamsfus, C. A.; Song, C.; Liu, J.; Fan, G.; Maron, L.; Cui, C., Samarium-Catalyzed Diastereoselective Double Addition of Phenylphosphine to Imines and Mechanistic Studies by DFT Calculations. *ChemCatChem* **2017**, *9* (8), 1368-1372.

[11] a) Behrle, A. C.; Schmidt, J. A., Insertion reactions and catalytic hydrophosphination of heterocumulenes using α-metalated N, N-dimethylbenzylamine rare-earth-metal complexes. *Organometallics* **2013**, *32* (5), 1141-1149; b) Zhang, Y.; Qu, L.; Wang, Y.; Yuan, D.; Yao, Y.; Shen, Q., Neutral and cationic zirconium complexes bearing multidentate aminophenolato ligands for hydrophosphination reactions of alkenes and heterocumulenes. *Inorg. Chem.* **2018**, *57* (1), 139-149.

[12] Kovacik, I.; Wicht, D. K.; Grewal, N. S.; Glueck, D. S.; Incarvito, C. D.; Guzei, I. A.; Rheingold, A. L., Pt (Me-Duphos)-catalyzed asymmetric hydrophosphination of activated olefins: enantioselective synthesis of chiral phosphines. *Organometallics* **2000**, *19* (6), 950-953.

[13] a) Sadow, A. D.; Haller, I.; Fadini, L.; Togni, A., Nickel (II)-catalyzed highly enantioselective hydrophosphination of methacrylonitrile. *J. Am. Chem. Soc.* **2004**, *126* (45),

14704-14705; b) Sadow, A. D.; Togni, A., Enantioselective addition of secondary phosphines to methacrylonitrile: catalysis and mechanism. *J. Am. Chem. Soc.* **2005**, *127* (48), 17012-17024.

[14] a) Pullarkat, S. A., Recent progress in palladium-catalyzed asymmetric hydrophosphination. *Synthesis* **2016**, *48* (4), 493-503; b) Chew, R. J.; Leung, P. H., Our odyssey with functionalized chiral phosphines: from optical resolution to asymmetric synthesis to catalysis. *The Chemical Record* **2016**, *16* (1), 141-158; c) Pullarkat, S. A.; Leung, P.-H., Chiral metal complex-promoted asymmetric hydrophosphinations. In *Hydrofunctionalization*, Springer: 2011; pp 145-166.

[15] a) Chen, S.; Ng, J. K.-P.; Pullarkat, S. A.; Liu, F.; Li, Y.; Leung, P.-H., Asymmetric synthesis of new diphosphines and pyridylphosphines via a kinetic resolution process promoted and controlled by a chiral palladacycle. *Organometallics* **2010**, *29* (15), 3374-3386; b) Corey, E.; Bailar Jr, J. C., The Stereochemistry of Complex Inorganic Compounds. XXII. Stereospecific Effects in Complex Ions1. *J. Am. Chem. Soc.* **1959**, *81* (11), 2620-2629.

[16] Aw, B.-H.; Selvaratnam, S.; Leung, P.-H.; Rees, N. H.; McFarlane, W., NMR assignment of absolute configuration of a P-chiral diphosphine and mechanics of its stereoselective formation. *Tetrahedron: Asymmetry* **1996**, *7* (6), 1753-1762.

[17] a) Chooi, S. Y.; Tan, M.; Leung, P.-H.; Mok, K., Stereochemical investigation of bis (bidentate)-palladium (II) complexes. Transmission of ring chiralities between chelating amine ligands via their prochiral N-methyl substituents. *Inorg. Chem.* **1994**, *33* (14), 3096-3103; b) Alcock, N. W.; Hulmes, D. I.; Brown, J. M., Contrasting behaviour of related palladium complex-derived resolving agents. 8-H conformational locking of the 1-naphthyl side-chain. *J. Chem. Soc., Chem. Commun.* **1995**, (3), 395-397.

[18] a) Leung, P.-H., Asymmetric synthesis and organometallic chemistry of functionalized phosphines containing stereogenic phosphorus centers. *Acc. Chem. Res.* **2004**, *37* (3), 169-177; b)

Jia, Y.-X.; Li, B.-B.; Li, Y.; Pullarkat, S. A.; Xu, K.; Hirao, H.; Leung, P.-H., Stereoelectronic and catalytic properties of chiral cyclometalated phospha-palladium and-platinum complexes. *Organometallics* **2014**, *33* (21), 6053-6058.

[19] Yang, X.-Y.; Tay, W. S.; Li, Y.; Pullarkat, S. A.; Leung, P.-H., Asymmetric 1, 4-conjugate addition of diarylphosphines to α, β, γ, δ-unsaturated ketones catalyzed by transition-metal pincer complexes. *Organometallics* **2015**, *34* (20), 5196-5201.

[20] a) Subramanian, G.; Sadeer, A.; Mukherjee, K.; Kojima, T.; Tripathi, P.; Naidu, R.; Tay, S. W.; Pang, J. H.; Pullarkat, S. A.; Chandramohanadas, R., Evaluation of ferrocenyl phosphines as potent antimalarials targeting the digestive vacuole function of Plasmodium falciparum. *Dalton Transactions* **2019**, *48* (3), 1108-1117; b) Verma, N. K.; Sadeer, A.; Kizhakeyil, A.; Pang, J. H.; Chiu, Q. Y. A.; Tay, S. W.; Kumar, P.; Pullarkat, S. A., Screening of ferrocenyl–phosphines identifies a gold-coordinated derivative as a novel anticancer agent for hematological malignancies. *RSC advances* **2018**, *8* (51), 28960-28968; c) Li, B.-B.; Jia, Y.-X.; Zhu, P.-C.; Chew, R. J.; Li, Y.; Tan, N. S.; Leung, P.-H., Highly selective anti-cancer properties of ester functionalized enantiopure dinuclear gold (I)-diphosphine. *European journal of medicinal chemistry* **2015**, *98*, 250-255.

[21] a) Huang, Y.; Chew, R. J.; Li, Y.; Pullarkat, S. A.; Leung, P.-H., Direct synthesis of chiral tertiary diphosphines via Pd (II)-catalyzed asymmetric hydrophosphination of dienones. *Org. Lett.* **2011**, *13* (21), 5862-5865; b) Huang, Y.; Pullarkat, S. A.; Li, Y.; Leung, P.-H., Palladacycle-catalyzed asymmetric hydrophosphination of enones for synthesis of C*-and P*-chiral tertiary phosphines. *Inorg. Chem.* **2012**, *51* (4), 2533-2540; c) Xu, C.; Jun Hao Kennard, G.; Hennersdorf, F.; Li, Y.; Pullarkat, S. A.; Leung, P.-H., Chiral Phosphapalladacycles as Efficient Catalysts for the Asymmetric Hydrophosphination of Substituted Methylidenemalonate Esters: Direct Access

to Functionalized Tertiary Chiral Phosphines. *Organometallics* **2012**, *31* (8), 3022-3026; d) Gan, K.; Sadeer, A.; Xu, C.; Li, Y.; Pullarkat, S. A., Asymmetric construction of a ferrocenyl phosphapalladacycle from achiral enones and a demonstration of its catalytic potential. *Organometallics* **2014**, *33* (19), 5074-5076; e) Yang, X.-Y.; Gan, J. H.; Li, Y.; Pullarkat, S. A.; Leung, P.-H., Palladium catalyzed asymmetric hydrophosphination of α, β-and α, β, γ, δ-unsaturated malonate esters–efficient control of reactivity, stereo-and regio-selectivity. *Dalton Transactions* **2015**, *44* (3), 1258-1263; f) Sadeer, A.; Ong, Y. J.; Kojima, T.; Foo, C. Q.; Li, Y.; Pullarkat, S. A.; Leung, P. H., Desymmetrization of Achiral Heterobicyclic Alkenes through Catalytic Asymmetric Hydrophosphination. *Chemistry–An Asian Journal* **2018**, *13* (19), 2829-2833; g) Katona, D. v.; Lu, Y.; Li, Y.; Pullarkat, S. A.; Leung, P.-H., Catalytic Approach toward Chiral P, N-Chelate Complexes Utilizing the Asymmetric Hydrophosphination Protocol. *Inorg. Chem.* **2020**, *59* (6), 3874-3886; h) Teo, R. H. X.; Chen, H. J.; Li, Y.; Pullarkat, S. A.; Leung, P. H., Asymmetric Catalytic 1, 2-Dihydrophosphination of Secondary 1, 2-Diphosphines–Direct Access to Free P*-and P*, C*-Diphosphines. *Adv. Synth. Catal.* **2020**, *362* (12), 2373-2378.

[22] Yang, X.-Y.; Jia, Y.-X.; Tay, W. S.; Li, Y.; Pullarkat, S. A.; Leung, P.-H., Mechanistic insights into the role of PC-and PCP-type palladium catalysts in asymmetric hydrophosphination of activated alkenes incorporating potential coordinating heteroatoms. *Dalton Transactions* **2016**, *45* (34), 13449-13455.

[23] a) Sablong, R.; Osborn, J. A., The asymmetric hydrogenation of imines using tridentate C2 diphosphine complexes of iridium (I) and rhodium (I). *Tetrahedron Lett.* **1996**, *37* (28), 4937-4940; b) Sablong, R.; Newton, C.; Dierkes, P.; Osborn, J. A., Chiral tridentate C2 diphosphine ligands for enantioselective catalysis. *Tetrahedron Lett.* **1996**, *37* (28), 4933-4936; c) Jiang, Q.; Van Plew, D.; Murtuza, S.; Zhang, X., Synthesis of (1R, 1R′)-2, 6-bis [1-(diphenylphosphino) ethyl] pyridine

and its application in asymmetric transfer hydrogenation. *Tetrahedron Lett.* **1996**, *37* (6), 797-800; d) Zhu, G.; Terry, M.; Zhang, X., Asymmetric allylic alkylation catalyzed by palladium complexes with new chiral ligands. *Tetrahedron Lett.* **1996**, *37* (26), 4475-4478; e) Zhu, G.; Terry, M.; Zhang, X., Asymmetric hydrosilylation of ketones catalyzed by ruthenium complexes with chiral tridentate ligands. *J. Organomet. Chem.* **1997**, *547* (1), 97-101.

[24] Huber, R.; Passera, A.; Mezzetti, A., Iron (II)-catalyzed hydrogenation of acetophenone with a chiral, pyridine-based PNP pincer ligand: support for an outer-sphere mechanism. *Organometallics* **2018**, *37* (3), 396-405.

[25] a) Gorla, F.; Venanzi, L. M.; Albinati, A., Synthesis of (1R, 1'S)-and (1S, 1'S),(1R, 1'R)-bis [1-(diphenylphosphino) ethyl] benzene derivatives and their cyclometalation reactions with platinum (II) compounds. The x-ray crystal structures of [2, 6-bis [(diphenylphosphino) methyl] phenyl] chloropalladium (II),[(1R, 1'S)-2, 6-bis [1-(diphenylphosphino) ethyl] phenyl] chloroplatinum (II), and [(1R, 1'R),(1S, 1'S)-2, 6-bis [1-(diphenylphosphino) ethyl] phenyl] chloroplatinum (II). *Organometallics* **1994**, *13* (1), 43-54; b) Jiang, Q.; Van Plew, D.; Murtuza, S.; Zhang, X., Synthesis of (13, lg')-2, 6-Bis [1-(diphenylphosphino) ethyl] pyridine and its Application in Asymmetric Transfer Hydrogenation. *Studies* **1996**, *6* (1), 8; c) Longmire, J. M.; Zhang, X.; Shang, M., Synthesis and X-ray Crystal Structures of Palladium (II) and Platinum (II) Complexes of the PCP-Type Chiral Tridentate Ligand (1 R, 1 'R)-1, 3-Bis [1-(diphenylphosphino) ethyl] benzene. Use in the Asymmetric Aldol Reaction of Methyl Isocyanoacetate and Aldehydes. *Organometallics* **1998**, *17* (20), 4374-4379.

[26] a) Wallner, O. A.; Olsson, V. J.; Eriksson, L.; Szabó, K. J., Synthesis of new chiral pincer-complex catalysts for asymmetric allylation of sulfonimines. *Inorg. Chim. Acta* **2006**, *359* (6), 1767-1772; b) Aydin, J.; Kumar, K. S.; Sayah, M. J.; Wallner, O. A.; Szabó, K. J., Synthesis and

Catalytic Application of Chiral 1, 1 '-Bi-2-naphthol-and Biphenanthrol-Based Pincer Complexes: Selective Allylation of Sulfonimines with Allyl Stannane and Allyl Trifluoroborate. *The Journal of organic chemistry* **2007**, *72* (13), 4689-4697; c) Aydin, J.; Conrad, C. S.; Szabo, K. J., Stereoselective pincer-complex catalyzed ch functionalization of benzyl nitriles under mild conditions. An efficient route to β-aminonitriles. *Org. Lett.* **2008**, *10* (22), 5175-5178.

[27] a) Medici, S.; Gagliardo, M.; Williams, S. B.; Chase, P. A.; Gladiali, S.; Lutz, M.; Spek, A. L.; van Klink, G. P.; van Koten, G., Novel P-Stereogenic PCP Pincer-Aryl Ruthenium (II) Complexes and Their Use in the Asymmetric Hydrogen Transfer Reaction of Acetophenone. *Helv. Chim. Acta* **2005**, *88* (3), 694-705; b) Ding, B.; Zhang, Z.; Xu, Y.; Liu, Y.; Sugiya, M.; Imamoto, T.; Zhang, W., P-Stereogenic PCP pincer–Pd complexes: synthesis and application in asymmetric addition of diarylphosphines to nitroalkenes. *Org. Lett.* **2013**, *15* (21), 5476-5479; c) Arenas, I.; Boutureira, O.; Matheu, M. I.; Díaz, Y.; Castillón, S., Synthesis of a P-Stereogenic PNPtBu, Ph Ruthenium Pincer Complex and Its Application in Asymmetric Reduction of Ketones. *Eur. J. Org. Chem.* **2015**, *2015* (17), 3666-3669; d) Xu, Y.; Yang, Z.; Ding, B.; Liu, D.; Liu, Y.; Sugiya, M.; Imamoto, T.; Zhang, W., Asymmetric Michael addition of diphenylphosphine to β, γ-unsaturated α-keto esters catalyzed by a P-stereogenic pincer-Pd complex. *Tetrahedron* **2015**, *71* (38), 6832-6839; e) Yang, Z.; Liu, D.; Liu, Y.; Sugiya, M.; Imamoto, T.; Zhang, W., Synthesis and Structural Characterization of Nickel Complexes Possessing P-Stereogenic Pincer Scaffolds and Their Application in Asymmetric Aza-Michael Reactions. *Organometallics* **2015**, *34* (7), 1228-1237; f) Yang, Z.; Wei, X.; Liu, D.; Liu, Y.; Sugiya, M.; Imamoto, T.; Zhang, W., P-Stereogenic pincer iridium complexes: synthesis, structural characterization and application in asymmetric hydrogenation. *J. Organomet. Chem.* **2015**, *791*, 41-45; g) Yang, Z.; Xia, C.; Liu, D.; Liu, Y.; Sugiya, M.; Imamoto, T.; Zhang, W., P-stereogenic PNP pincer-Pd catalyzed intramolecular

hydroamination of amino-1, 3-dienes. *Organic & biomolecular chemistry* **2015**, *13* (9), 2694-2702; h) Pietrusiewicz, K. M.; Zablocka, M., Preparation of scalemic P-chiral phosphines and their derivatives. *Chemical reviews* **1994**, *94* (5), 1375-1411.

[28] a) Morales-Morales, D., Recent applications of phosphinite POCOP pincer complexes towards organic transformations. *Mini-Reviews in Organic Chemistry* **2008**, *5* (2), 141-152; b) Benito-Garagorri, D.; Kirchner, K., Modularly designed transition metal PNP and PCP pincer complexes based on aminophosphines: synthesis and catalytic applications. *Acc. Chem. Res.* **2008**, *41* (2), 201-213; c) Leforestier, B.; Gyton, M. R.; Chaplin, A. B., Synthesis and group 9 complexes of macrocyclic PCP and POCOP pincer ligands. *Dalton Transactions* **2020**, *49* (7), 2087-2101; d) Benito-Garagorri, D.; Becker, E.; Wiedermann, J.; Lackner, W.; Pollak, M.; Mereiter, K.; Kisala, J.; Kirchner, K., Achiral and chiral transition metal complexes with modularly designed tridentate PNP pincer-type ligands based on N-heterocyclic diamines. *Organometallics* **2006**, *25* (8), 1900-1913.

[29] Glueck, D. S., Selectivity via catalyst or substrate control in catalytic asymmetric transformations of bifunctional symmetrical substrates. *Catalysis Science & Technology* **2011**, *1* (7), 1099-1108.

[30] Masamune, S.; Choy, W.; Petersen, J. S.; Sita, L. R., Double asymmetric synthesis and a new strategy for stereochemical control in organic synthesis. *Angew. Chem. Int. Ed.* **1985**, *24* (1), 1-30.

[31] Kumar, S.; Mani, G.; Mondal, S.; Chattaraj, P. K., Pyrrole-based new diphosphines: Pd and Ni complexes bearing the PNP pincer ligand. *Inorg. Chem.* **2012**, *51* (22), 12527-12539.

[32] Alam, M. M., Template synthesis of new type of macrocyclic molecule derived from pyridine-2, 6-decarboxaldehyde and 1, 2-bis (2-Aminoethoxy) ethane. *Journal of Bangladesh Academy of Sciences* **2011**, *35* (1), 61-65.

[33] Peters, G. M.; Winegrad, J. B.; Gau, M. R.; Imler, G. H.; Xu, B.; Ren, S.; Wayland, B. B.; Zdilla, M. J., Synthesis and structure of 2, 5-bis [N-(2, 6-mesityl) iminomethyl] pyrrolylcobalt (II): evidence for one-electron-oxidized, redox noninnocent ligand behavior. *Inorg. Chem.* **2017**, *56* (6), 3377-3385.

[34] Yang, X.-Y.; Tay, W. S.; Li, Y.; Pullarkat, S. A.; Leung, P.-H., Versatile Syntheses of Optically Pure PCE Pincer Ligands: Facile Modifications of the Pendant Arms and Ligand Backbones. *Organometallics* **2015**, *34* (8), 1582-1588.

[35] Zhang, Z.; Dong, Y.-W.; Wang, G.-W., Efficient and clean aldol condensation catalyzed by sodium carbonate in water. *Chem. Lett.* **2003**, *32* (10), 966-967.

[36] Basnet, A.; Thapa, P.; Karki, R.; Na, Y.; Jahng, Y.; Jeong, B.-S.; Jeong, T. C.; Lee, C.-S.; Lee, E.-S., 2, 4, 6-Trisubstituted pyridines: synthesis, topoisomerase I and II inhibitory activity, cytotoxicity, and structure–activity relationship. *Biorg. Med. Chem.* **2007**, *15* (13), 4351-4359.

[37] Ng, J. K.-P.; Tan, G.-K.; Vittal, J. J.; Leung, P.-H., Optical resolution and the study of ligand effects on the ortho-metalation reaction of resolved (±)-diphenyl [1-(1-naphthyl) ethyl] phosphine and its arsenic analogue. *Inorg. Chem.* **2003**, *42* (23), 7674-7682.

[38] Luu, H.-T.; Wiesler, S.; Frey, G.; Streuff, J., A titanium (III)-catalyzed reductive umpolung reaction for the synthesis of 1, 1-disubstituted tetrahydroisoquinolines. *Org. Lett.* **2015**, *17* (10), 2478-2481.

[39] Gulyás, H.; Benet-Buchholz, J.; Escudero-Adan, E. C.; Freixa, Z.; van Leeuwen, P. W., Ionic interaction as a powerful driving force for the formation of heterobidentate assembly ligands. *Chemistry–A European Journal* **2007**, *13* (12), 3424-3430.

[40] Foo, C. Q.; Sadeer, A.; Li, Y.; Pullarkat, S. A.; Leung, P.-H., Access to C-Stereogenic PN (sp 2) P Pincer Ligands via Phosphapalladacycle Catalyzed Asymmetric Hydrophosphination. *Organometallics* **2021**, *40* (6), 682-692.

Chapter 3

Preparations of PNP pincer complexes with Group 8, 9 and 10 transition metal elements

3.1. Introduction

Pioneering works by Shaw and Moulton have introduced the field of pincer chemistry into the organometallic scene.[1] Reputed for their characteristic ability to form immensely stable yet reactive coordination complexes, pincer ligands have since emerged as attractive versatile frameworks for the syntheses and application of associated metal compounds.[2] As it turns out, these privileged ligand scaffolds and their corresponding metal complexes have proven to be effective in widespread applications; including the likes of chemical sensors,[3] nano materials,[4] as well as in catalysis.[5] Apart from stability, the allure of pincer ligands as cooperative partners in metal mediated reactions is also largely credited to their high levels of modularity as previously illustrated in Chapter 1. The diagram below expresses the extent to which various modes of modifications may be incorporated into the ligand backbone and how they can affect the overall chemical disposition of the ligand (Figure 3.1).

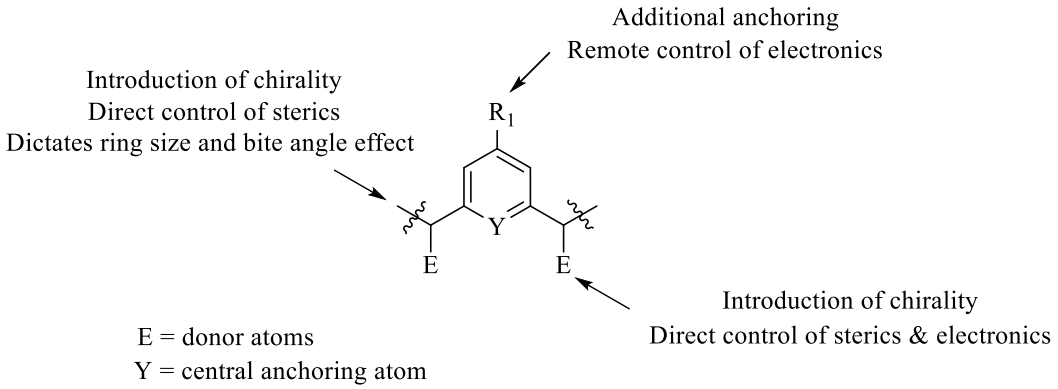

Figure 3.1. Illustration of typical modes of modulations onto a pincer ligand.

To add on to this, the electronic diversity that can be attained from the integration of multiple different donor atoms remains as a highly relevant factor of consideration in the design of compatible systems for metal association. Since its first appearance, the attention of pincer ligands has mainly been centered on the syntheses and applications of variants consisting of a central aromatic ring.[6] In fact, the definition of a pincer ligand back then was specific only to tridentates containing monoanionic C^- donors as the central anchor (i.e. a phenyl group). As the domain of pincer-related chemistry evolved, the quest to search for more specialized pincer ligands that can provide a suitable chemical fit for intended applications have led to the founding and expansion of new pincer systems with varying electronic backbones.[7]

Amongst the extensive variety of pincer ligands available in the current molecular library, those featuring phosphorus atoms as donor groups on both pendant arms remain markedly as one of the more commonly utilized variants, especially in the context of fundamental applications.[5a, 8] To this end, C_2-symmetrical PC(sp^2)P based tridentates have been widely established as successful pincer systems.[5a, 8d, 9] In turn, this serves as a reasonable motivation for exploration into other analogous pincer frameworks built upon the generic structural make-up of these antecedents. To date, the library of pincer ligands describes an almost inexhaustive list of these diphosphine based derivatives. Therefore to limit the content that will be accounted for, the discussion in this chapter will only delve specifically into C_2-symmetrical PN(sp^2)P type pincer ligands bearing a central pyridyl anchor, which would appropriately be the closest analogue for comparison purposes to the phenyl based PC(sp^2)P variant.

With all other structural peripherals remaining constant, the change in electronic properties derived from this adaptation of pincer ligands rests mainly upon the pyridine auxiliary. Albeit seemingly subtle, the chemical disparities observed between themselves and their phenyl based

PC(sp^2)P counterparts are by no means insignificant. Experiments involving comparative studies between structurally and isoelectronically analogous PCP and PNP ligated complexes have discerned stark differences corresponding to reactivity, stability and even the thermodynamics and kinetics for their respective syntheses.[8a, 8b, 10] Evidently, these findings reinforce a positive leap towards the further development of PN(sp^2)P ligands as complementary keys to unlock unrealized potentials and applications by their PC(sp^2)P analogues.

3.2. Achiral pyridyl PN(sp^2)P pincer complexes in the literature

Comparatively, the formation of pyridyl based PN(sp^2)P pincer complexes follow a much more uncomplicated process involving displacement of pre-existing labile ligands on the metal precursor to result in direct metalation. Illustrations of these pincer complexes have been apparent in the literature as viable systems for numerous applications, and these mostly comprise of related achiral derivatives which display multiple modes of complex activation to mediate reactions in different manners.[8a-c, 11] Among these, several examples highlight the leverage that is derived from the use of such a ligand system to facilitate reactions that may have otherwise been more difficult to achieve.

One such exemplification is in the electrophilic activation of olefins, which has been traditionally accomplished by coordination of the alkene to Lewis acidic metal centers.[12] Due to the neutrality of the PN(sp^2)P auxiliary, resultant complexes ligated with these pincer ligands often end up as ionic compounds bearing at least one coordinated anionic ligand. In order to liberate a vacant site for substrate adhesion, a simple metathesis reaction with a silver salt additive containing weakly or non-coordinating counter-anions is typically performed. Consequently, this leads to the formation of a doubly cationic complex which is highly electron deficient and thus able to execute

substantial activation for non-electron poor olefins. Showcases of this chemical display by related PN(sp^2)P pincer complexes have been illustrated in reports revolving coupling and hydrofunctionalization reactions of unactivated alkenes (Schemes 3.1 and 3.2).[13]

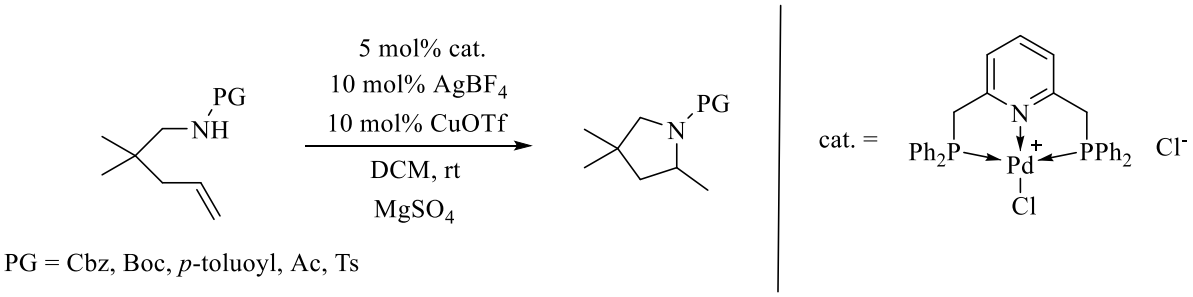

Scheme 3.1. PN(sp^2)P palladium(II) complex catalyzed intramolecular hydroamination of amidoalkenes.

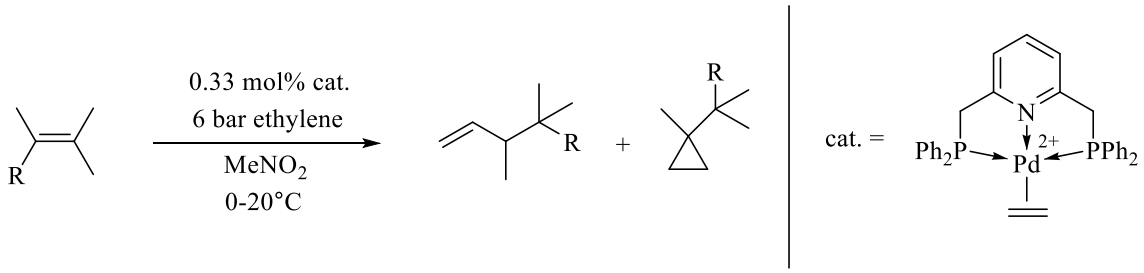

Scheme 3.2. PN(sp^2)P palladium(II) complex catalyzed coupling of ethylene to internal olefins.

As seen, both examples utilized either preformed or in-situ generated charged palladium(II) species as catalysts, which allowed the enhancement of electrophilicity and subsequent functionalization of olefins that are considerably less reactive for nucleophilic attack under relatively mild reaction conditions. In the latter example, the increase in reactivity of the olefinic substrate even led to the unexpected formation of an intramolecular cyclization product, arising from activation of a more internally situated and electron rich carbon center by the metal complex.

Another notable implementation of pyridyl PN(sp^2)P ligands extends to a more interesting method of application involving ligand cooperative catalysis.[8c, 14] In such cases, certain fragments of the ligand participate as non-innocent moieties which contribute to part of a reaction step within the catalytic cycle. With respect to this particular ligand system, such a phenomenon is usually observed from the ability of the central aromatic ring to undergo dearomatization-rearomatization processes.[15] This typically occurs among pyridyl PN(sp^2)P complexes bearing methylene spacers, whereby transfer of their benzylic protons leads to dearomatization of the pyridine ring. Correspondingly, these dearomatized complexes have been largely employed in X-H type activation reactions (where X = H, O, N, etc), which concomitantly allows rearomatization for regeneration of the catalyst.

Catalytic applications engaging this metal-ligand cooperation have been extensively demonstrated by Milstein and co-workers,[15-16] with initial discoveries of this mechanism derived from the use of related ruthenium PN(sp^2)P pincer complexes (Scheme 3.3).[8c, 14]

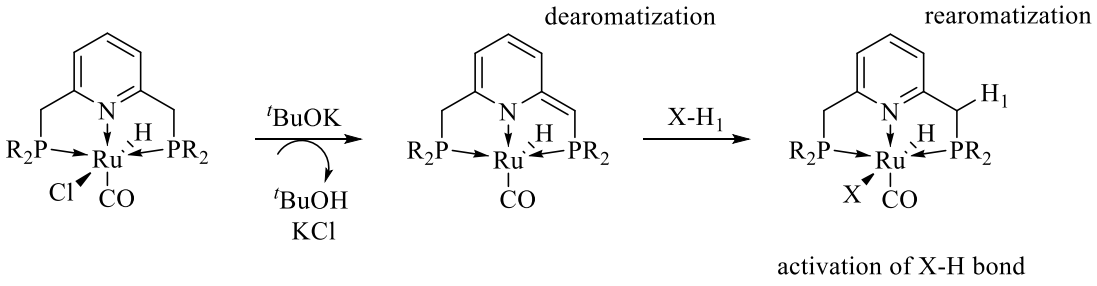

Scheme 3.3. Illustration of dearomatization-rearomatization process in pyridyl PN(sp^2)P ruthenium complexes.

Representative illustrations capitalizing on the reversible dearomatization property of such a ligand system were prominently displayed in acceptorless dehydrogenation reactions of alcohols.[14, 17] Mechanistic discussions proposed the abovementioned dearomatization occurrence for O-H activation of the alcohol, followed by intramolecular β-H elimination resulting in removal of the

subsequent proton on the substrate to furnish the dehydrogenated product. To illustrate extended synthetic applicability, the newly formed oxidized intermediates could also be further in-situ functionalized into other derivatives such as esters, amides and imines. [14, 17] In a similar but converse manner, the application of this system has also seen effective employments in hydrogenation reactions by iron based catalysts on a myriad of carbonyl precursors including ketones, aldehydes, esters and even carbon dioxide under mild reaction conditions with excellent turnovers.[18] Congruent examples exploiting the same chemical reactivity of these PN(sp^2)P ligands were also featured with other metal centers including rhodium,[19] iridium,[20] nickel[21] and copper.[22] Today, this method of approach has established itself as a new paradigm in catalytic bond activation reactions.[14-16, 18]

3.3. Chiral pyridyl PN(sp^2)P pincer complexes in the literature

On the other hand, asymmetric implementations of chirally constructed pyridyl PN(sp^2)P complexes have only been limited to a handful of reported illustrations. This could be principally attributed to the difficult and tedious syntheses of the chiral ligand as highlighted in Chapter 2. Nevertheless, they have been detailed to proceed with decent effectiveness in several applications. While the enantioselectivities obtained in the final products were not stellar, the applications highlighted the versatility of PN(sp^2)P ligand systems not just in a series of different reactions, but also their compatibility with a diverse range of platinum group metals. These were represented accordingly in reactions involving asymmetric allylic alkylation, transfer hydrogenation as well as hydrofunctionalizations using in-situ palladium, ruthenium and iridium based metal catalysts (Schemes 3.4 to 3.7). [10c, 23] In certain examples, the PN(sp^2)P ligated complex even proved to be more efficient in stereoinduction when compared to its exact PC(sp^2)P analogue or other well-established ligand systems such as BINAP.[10c]

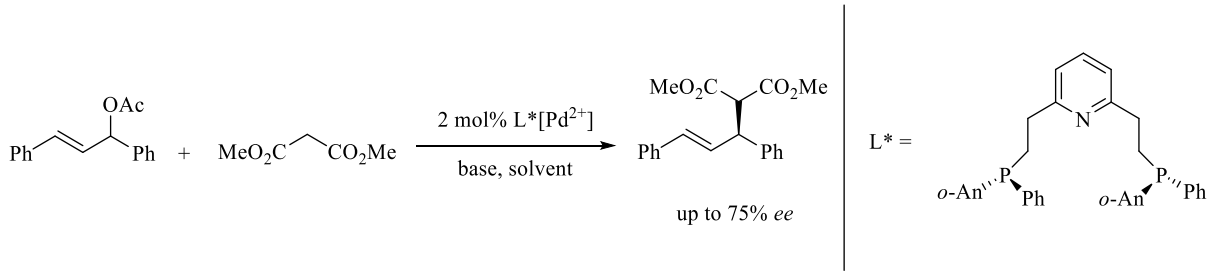

Scheme 3.4. Asymmetric allylic alkylation using chiral PN(sp^2)P palladium(II) complex.

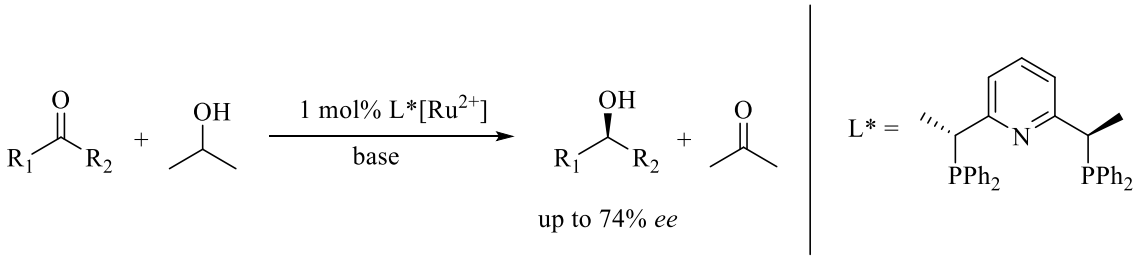

Scheme 3.5. Asymmetric transfer hydrogenation with chiral PN(sp^2)P ruthenium(II) complex.

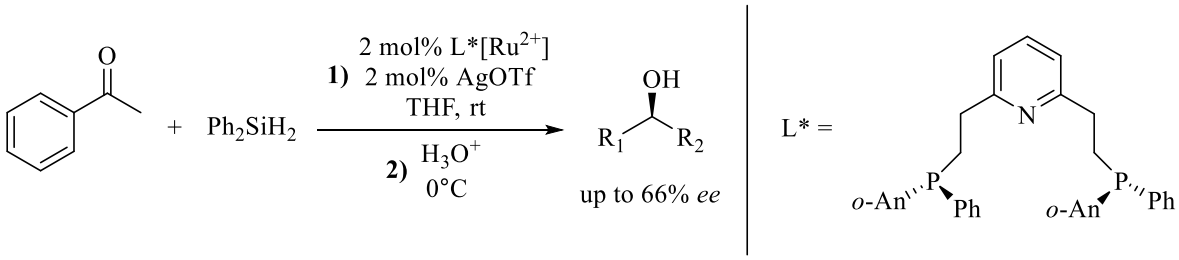

Scheme 3.6. Asymmetric hydrosilylation using chiral PN(sp^2)P ruthenium(II) complex.

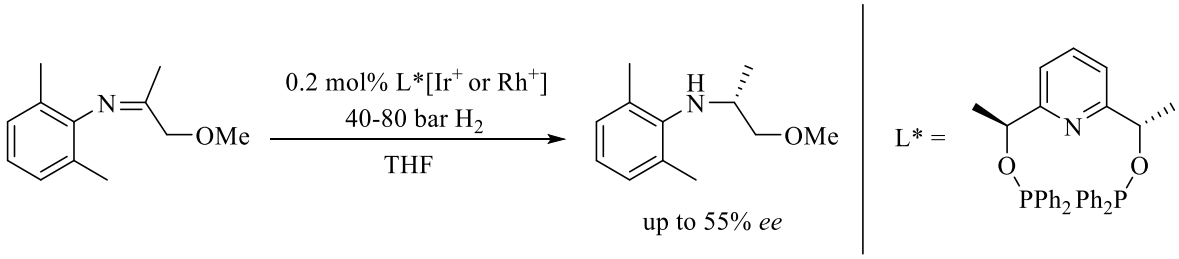

Scheme 3.7. Asymmetric hydrogenation using chiral PN(sp^2)P iridium(I) and rhodium(I) complexes.

More recently, the scope of utility for chiral pyridyl PN(sp^2)P ligands has also been extended to applications in cooperative catalysis using related *P*-chiral analogues. This was exemplified by Mezzetti and co-workers in an asymmetric hydrogenation reaction mediated by a *P*-chiral pyridyl PN(sp^2)P ligated iron complex (Scheme 3.8).[24]

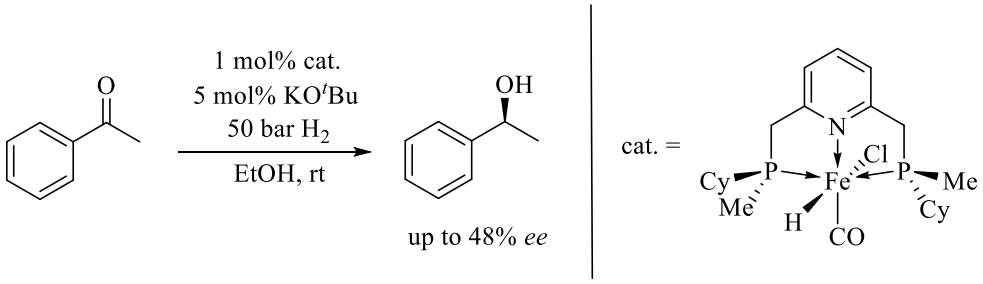

Scheme 3.8. *P*-chiral iron(II) PN(sp^2)P complex catalyzed asymmetric hydrogenation.

Mechanistic probing revealed the earlier described non-innocent nature of the PN(sp^2)P ligand, but in this case the benzylic proton transfers as a hydridic (instead of protic) moiety onto the carbonyl group of the substrate for dearomatization of the pyridine ring. Protonolysis by ethanol ensues to generate the alcohol product and the catalyst is regenerated via rearomatization of the ring under the hydrogen atmosphere.

The abovementioned examples have emphasized several advantages ascribed to pyridyl based PN(sp^2)P ligands, which make them highly valuable synthons for prospective synthetic evaluations. Firstly, they have displayed compatibility to a variety of transition metals, thereby highlighting their level of applicability in terms of electronic adaptability. More significantly, the exhibition of certain chemical characteristics such as metal-ligand cooperation via dearomatization-rearomatization, is a feature that is distinctly unique to such a system with respect to all other aromatic pincer systems containing non-pyridyl central rings. Clearly, the Achilles heel hindering the progress in development of this ligand system, especially in asymmetric applications, lies with the lack of convenient synthetic accessibility to these chiral PN(sp^2)P ligand motifs.

In the previous chapter, we have showcased the use of asymmetric hydrophosphination as an effective and viable means of overcoming the primary problem associated with synthesizing chiral PN(sp^2)P ligands. More importantly, enantiomerically pure PN(sp^2)P adducts could be obtained which would be aptly relevant for further experimental trials in metal complexation and possibly onto asymmetric applications thereafter. With this motivation in play coupled with the accomplishments achieved by related PN(sp^2)P ligands in the literature, these newly furnished chiral tridentates were thus subjected to in-situ metal complexation reactions in the aim of generating and expanding the library of chiral PN(sp^2)P pincer complexes. In the next section, we will uncover the compatibility of these synthesized diphosphine adducts for complexation onto various metal centers for both internal comparisons with other synthesized congeners, as well as external comparisons to related analogues in the literature. Methods of syntheses using selected metal precursors belonging to Group 8, 9 and 10 will be illustrated, and the results of their syntheses (including certain limitations) will also be discussed to elucidate distinctive characteristics and structural differentiations associated with the respective metal used for complexation.

3.4. Results and Discussions

All complexation trials were initiated under *racemic* conditions using the model substrate **9a** to first identify if the PN(sp^2)P adduct is compatible with the respective metal precursors. In-situ metalation was also performed due to the air sensitivity of the free diphosphine. It has to be noted that NMR representations of the crude mixture for all complexation trials that will be discussed will contain both diastereomeric isomers of the *racemic* and *meso* products unless otherwise stated. A further section on the trials performed for separation of the diastereomeric

diphosphines prior to metalation will be included to explain the conduct of complexation trials via the use of both diastereomeric isomers.

The *racemic* preparation of the ligand precursors **10a** and **10a'** can be conveniently accomplished by subjecting enone **9a** to a methanolic solution containing excess KOH (Scheme 3.9).

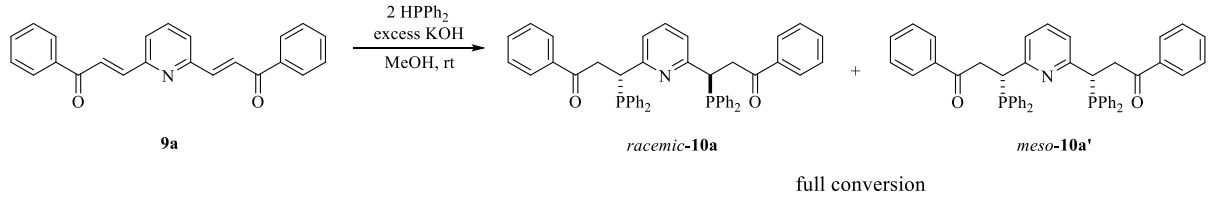

9a *racemic*-**10a** + *meso*-**10a'**

Scheme 3.9. *Racemic* preparation of ligand precursors **10a** and **10a'** for complexation trials.

Diphosphines **10a** and **10a'** form an insoluble suspension of white solids in methanol, which upon completion of reaction is evacuated under vacuum for removal of solvent. Degassed toluene is added to redissolve the solids and a preliminary purification via cannula extraction is performed with washing using degassed water to remove the residual KOH from the crude mixture. The existing diphosphine mixture in toluene is either used directly for metalation or vacuumed dry for the addition of another suitable solvent depending on the metal precursor used or the requirements of the complexation reaction. On an additional note, it is worth mentioning from this synthetic methodology that the diphosphine adducts have proven to be stable in highly alkaline conditions given the synthetic outline above.

3.5. Iron

As with conventional methods of complexing neutral based ligands to iron, initial trials were attempted with the use of commonly available iron(II) salts, in this case anhydrous iron(II) chloride and iron(II) bromide (Scheme 3.10). The following discussion represents the findings for both precursors as they yielded similar experimental results and observations. The outcome of reaction drawn in the schematic represents only the postulated products as will be explained in the following section.

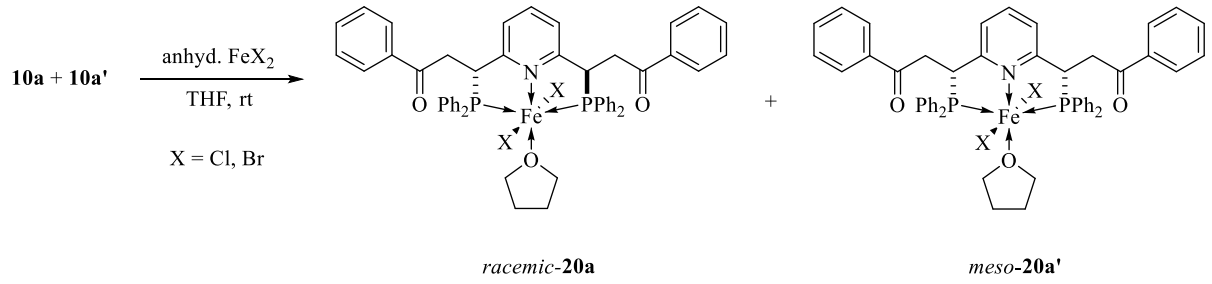

Scheme 3.10. Complexation trial using anhydrous iron(II) salts and the postulated products **20a** and **20a'**.

Upon mixing both diphosphines and metal precursor at room temperature, a distinct colour change from pale to darker yellow was observed within a few minutes. It must be noted that THF was used as solvent for reaction due to two primary reasons. Firstly, it is the only suitable solvent that allows the dissolution of both ligand and metal precursors to ensure homogeneity in the system for efficient occurrence of reaction. Secondly, in line with reported examples in the literature, we envisaged the generation of a 5-coordinate complex with just the affixation of the ligand.[25] More specifically, it is likely that the resultant coordinatively unsaturated complex which constitutes to an overall 16-electron iron(II) species, might be considerably unstable for an already electron deficient iron center and therefore present complications for straightforward characterization. Accordingly, the lack of electrons in conjunction with further coordinative accommodation would

render the species highly Lewis acidic.[26] Furthermore, in recognition of the oxophilicity of iron, THF was hence chosen as the optimal solvent of choice due to its coordinative ability to fulfill the abovementioned requirements for the formation of an electronically and coordinatively more stable complex illustrated by **20a** and **20a'**.

NMR analysis of the crude mixture after 1 hour reaction time revealed no apparent signals on the $^{31}P\{^{1}H\}$ NMR spectrum. The ^{1}H NMR spectrum also displayed broad and ill-defined signals which did not provide any significant peaks of noteworthy mention. Both observations signify evidently towards a product with paramagnetic property and hence likely a high spin d^6 iron(II) complex. The paramagnetism was subsequently verified via an Evans method of solution analysis, using NMR chemical shift comparisons between the crude against a standard solvent that the mixture is dissolved in (i.e. THF-d_8).[27] As seen from the spectrum obtained, two pairs of signals are observed, one corresponding to the reference solvent peaks from the standard, and the other corresponding to the magnetically shifted solvent peaks resulted from paramagnetic influence in the crude mixture (Figure 3.2).

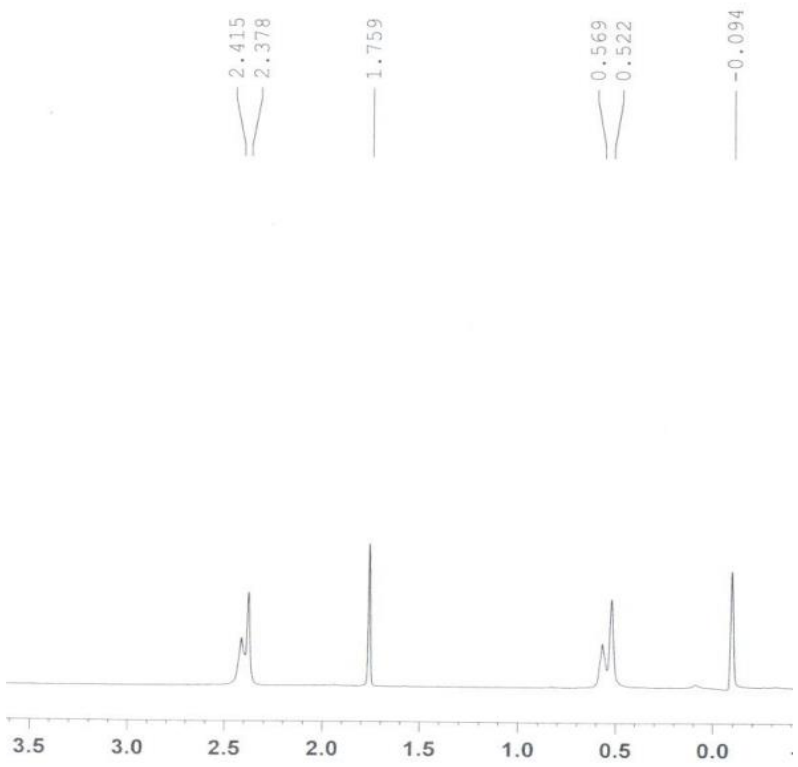

Figure 3.2. NMR representation of solvent shift resulted from paramagnetic influence.

The compounds formed visibly change upon exposure to open atmosphere, as indicated by an obvious colour shift from yellow to black over time. However, no conclusive identification of the chemically altered products could be performed similarly due to signal obscurity in the NMR spectrum of the exposed crude mixture. Further attempts to discern the complex structure of the initial products using liquid diffusion recrystallization under inert conditions failed to provide crystals of quality for X-ray analysis and as such, no confirmation or suggestions for their structural make-up could be provided.

In light of the results gathered from the above trials, the attention was next prompted towards the utilization of a suitable iron precursor that may be able to furnish a resultant complex which is diamagnetic so as to facilitate spectroscopic analysis via NMR. With the d^6 electronic configuration of iron(II), the most ideal formulation would be a typical octahedral shaped complex

with low spin characteristics. Additionally, the ligand field stabilization energy (LFSE) of iron is expectedly small in general with its situation in the 3d row of the periodic table. In relation to these considerations, the incorporation of appropriately strong field ligands is highly essential not just to satisfy a low spin configuration, but more importantly to accentuate the splitting energy of the metal d orbitals sufficiently enough for better realization of the low spin occurrence. To this end, it is imperative that ligands with high π-basicity should be avoided since these will reduce the LFSE and inherently lead to a higher probability for a high spin arrangement. In retrospect, the presence of halides which are strong π-donating ligands within the parent metal precursor could have directly translated and contributed to the paramagnetic display of the products in the previous trials. With this in mind, we thus averted from the use of halide containing iron(II) precursors and proceeded with an alternative replacement of the metal precursor to $Fe(BF_4)_2.6H_2O$ (Scheme 3.11).

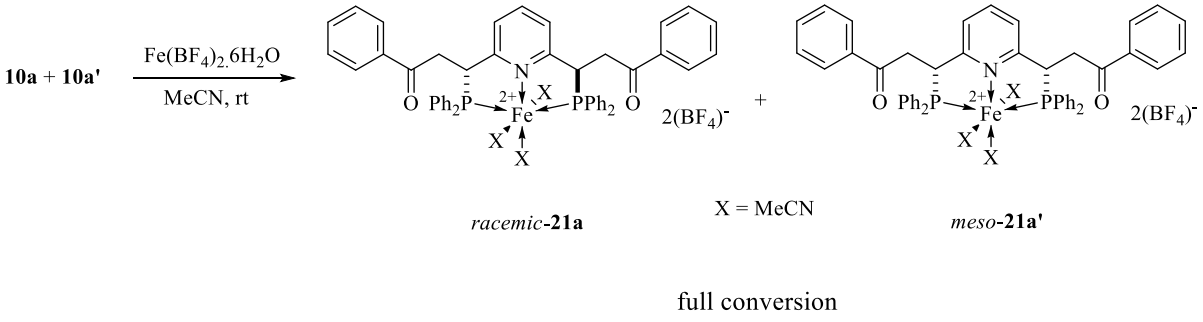

Scheme 3.11. Complexation trial using $Fe(BF_4)_2.6H_2O$ and the postulated products **21a** and **21a'**.

The anticipated product from this stoichiometric procedure was conceived to be a straightforward substitution of the PN(sp^2)P auxiliary with three corresponding displaced aqua ligands, leaving the other three remaining bound to form a coordinatively saturated, six coordinate iron(II) complex. Realizing the fact that the oxygen donors on H_2O can function as good π-donors, a deliberate choice was made to employ acetonitrile (MeCN) which is comparatively a weaker π-donor, as the solvent for reaction to perform a ligand exchange with the aqua ligands to furnish the

suggested complexes depicted by **21a** and **21a'**. At the same time, the stronger ligand field nature of MeCN would also better complement the similar strong field characteristics of the PN(sp^2)P ancillary, thereby generating an overall compounding effect to conjure a larger LFSE on the iron center.

Addition of excess MeCN to a reaction flask containing a portion of preformed, vacuumed dried solids of diphosphines **10a** and **10a'** at room temperature showed zero signs of solubilization of the ligand precursors. However upon subsequent addition of $Fe(BF_4)_2.6H_2O$ into the suspension, a clear orange solution was almost instantaneously resulted, with eventual complete dissolution of the PN(sp^2)P ligands. NMR analysis of the crude mixture was conducted after 1 hour into the reaction time, with the $^{31}P\{^1H\}$ NMR spectrum showing two sharp singlets having obvious coordination shifts at 73.3 ppm and 77.2 ppm. The two singlets are representative of the respective diastereomeric isomers and illustrates the chemical equivalence of the two phosphorus atoms pertaining to symmetrical products. Attempts to purify the crude mixture went unfounded due to the air sensitivity of the products. The crude products were also additionally found to be highly sensitive to different solvents, with immediate observation of a chemical change to form a black solution upon the addition of DCM even under inert conditions. As such, a separate experiment was specifically conducted with the use of Argon degassed deuterated MeCN for the purpose of running an air-excluded ^1H NMR analysis. The ^1H NMR spectrum was sufficiently resolved to provide a concise identification of the diastereomeric alkylic protons present on the ligand backbone, which correlates with the $^{31}P\{^1H\}$ NMR analysis to assert a successful metalation.

With conventional bench-open methods of purification rendered unsuitable for isolation and characterization of the products, a quick passing of the crude mixture through a Celite plug under inert atmosphere was performed using MeCN and the collected filtrate was subjected to

solvent layering with diethyl ether for liquid diffusion recrystallization. X-ray quality crystals were successfully obtained, and the diffraction analysis provided an interesting result of the resolved structure (Figure 3.3).

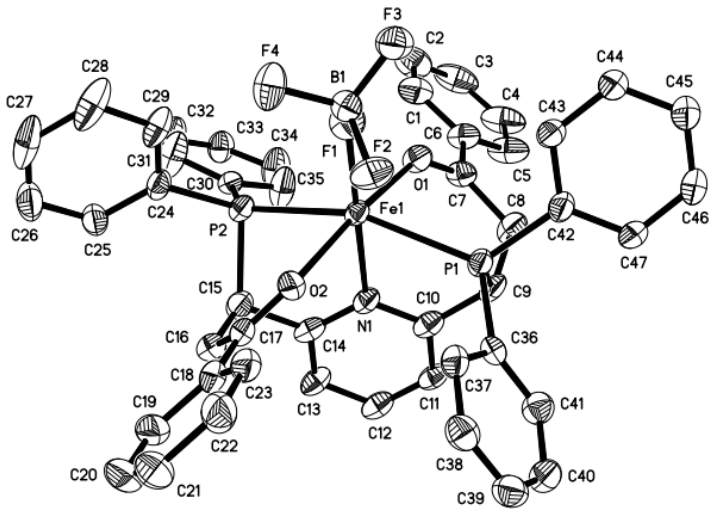

Figure 3.3. ORTEP representation of *racemic* PN(sp^2)P iron(II) complex **22** with thermal ellipsoids drawn at 50% probability level. Hydrogen atoms and the BF_4^- anion are omitted for clarity.

Contrary to the expected formation of a PN(sp^2)P iron(II) complex ligated with three MeCN co-ligands, X-ray resolutions illustrate a totally unexpected solid state structure with the PN(sp^2)P ligand coordinated in a pentadentate fashion, providing two additional donor contributions by the oxygen atoms present on the carbonyl functionality from the skeletal backbone. The final coordination site was also intriguingly occupied by a BF_4^- moiety bonded through one of its fluorine atoms. A closer scrutiny of the ORTEP diagram reveals a rather dissimilar structural elucidation between X-Ray and NMR analyses. To enable better observation and explanation of the structural intricacies of complex **22**, a few truncated but less convoluted representations of the crystal structure will be presented to highlight the main details of interest in the following section.

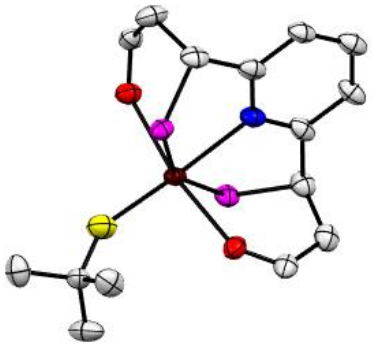

Figure 3.4. Truncated view of complex **22**. Colour identification for highlighted atoms as follows; Blue: N, Yellow: F, Red: O, Magenta: P, Brown: Fe.

As mentioned, the PN(sp^2)P auxiliary attaches itself to the iron center through the nitrogen, phosphorus, and oxygen atoms present on the ligand backbone. This conferred the formation of three chelates corresponding to a five, six and seven-membered chelate ring on each side of the iron center, which can be clearly seen in the truncated frontal view of complex **22** shown in Figure 3.4 above. Essentially, the complex consists of three formally different modes of ligand coordination namely, 1) a PNP meridional coordination, 2) an ONO meridional coordination and 3) an NOP facial coordination. In a further simplified exemplification of the structural architecture, it can be additionally realized that such a coordination pattern has led to the generation of chirality on the iron center itself (Figure 3.5).

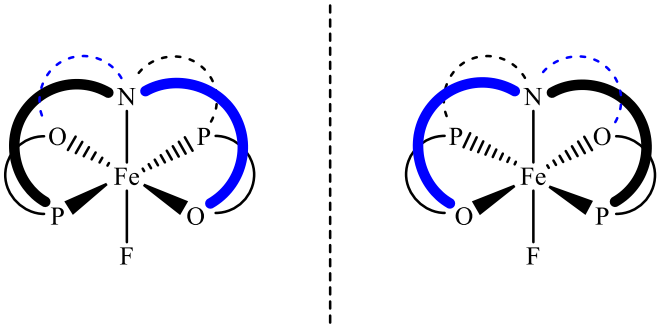

Figure 3.5. Simplified illustration of ligand coordination in complex **22**.

Figure 3.5 depicts the mirror images of complex **22**, with evident indication that both octahedral conformations are geometrical isomers that cannot be superimposed onto one another due to the presence of the multiple chelation. In turn, it may be possibly deduced that the complex could have existed differently in solution and solid states based on certain deviants between the NMR and X-ray results.

A major disparity associated to the abovementioned lies with the coupling interactions that the phosphorus atoms are involved in. Prior evaluation using $^{31}P\{^{1}H\}$ NMR has dictated only singular active signals corresponding to the chemically equivalent phosphorus donors from both isomeric products. This is validated with the observation of well-resolved sharp singlets displayed in the spectrum, which therefore indicates an absence of any coupling interactions between the phosphorus atoms to any other NMR active nuclei. However, a ligand conformation of that shown in complex **22** should reflect a splitting pattern corresponding to phosphorus-fluorine coupling and perhaps phosphorus-boron coupling as well. In turn, the $^{31}P\{^{1}H\}$ NMR spectrum should appear with more complex signals arising from multi-nuclei coupling interactions, or minimally two doublet signals from phosphorus-fluorine coupling. For further confirmation, a $^{19}F\{^{1}H\}$ NMR analysis was additionally done to reveal a well-resolved singlet in the spectrum at -152 ppm, which

is typical for the chemical shift of uncoordinated BF_4^- counter-anions.[28] The singlet signal also verifies the chemical equivalence of all fluorine atoms within the BF_4^- moieties present in each diastereomer, highlighting an absence of any form of fluorine bonding to other proximal NMR active nuclei aside from the boron atom. With these inferences drawn, it may therefore be affirmed that the solution state structure would not have incorporated the coordination of the tetrafluoroborate moiety, and hence exhibit a different configuration from that of the solid state structure.

It remains noteworthy that the weakly coordinating BF_4^- anion was assimilated into the complex structure despite the presence of larger amounts of competing coordinating ligands like MeCN and H_2O which have better coordination affinity with the iron(II) center.[29] On a separate note, this also signifies the stability of the compound within a hydrated environment since water is displaced out from the parent precursor. With reference to a related example in the literature, the similar employment of $Fe(BF_4)_2.6H_2O$ in acetonitrile with a PN(sp^2)P tridentate based on a 2,6-aminopyridine framework furnished the expected PN(sp^2)P iron(II) complex containing three MeCN co-ligands in both solid and solution states (Scheme 3.12).[30]

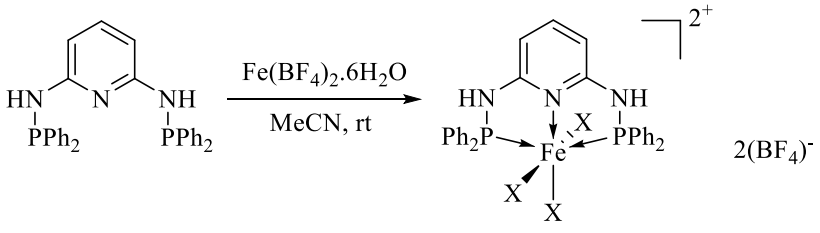

23

Scheme 3.12. Literature example of a PN(sp^2)P iron(II) complex with coordinated MeCN ligands.

Based on the example above, it is likely that complex **22** adopts a parallel coordinated arrangement as complex **23** in its solution state. This is in relation to the fact that MeCN is present in large excess and has good coordinative affinity to iron(II) as previously mentioned. On the other hand, the structural preservation observed in complex **23** in the solid state may be reasoned with resonance electron donating effects stemming from the NH spacer group, enhancing the electron density and donor characteristics of the pyridine moiety which in turn aids in the electronic stabilization of the metal core. Out of solution and in the absence of excess MeCN, it is probable that the comparatively more electron deficient iron center in complex **22** necessitates stronger electron donating moieties for the required stabilization and thus derives that from the strongly π-donating oxygen atoms which lie in close proximity, as well as an additional charged interaction with the BF_4^- anion that is available within the coordination environment. Accordingly, it may be considered that the MeCN ligands are relatively labile to allow for this observed substitution occurrence.

Complex **22** adopts a highly distorted octahedral geometry, which is clearly exemplified by the P1-Fe1-P2 bond that is stipulated at 156.04°. The observed bond angle is significantly much smaller than related PN(sp^2)P iron(II) pincer analogues in the literature with typical P-Fe-P bond angle values between 165° to 170°.[31] This can be in large attributed to the presence of multiple chelate rings above the P-Fe-P plane, which understandably causes an angular distortion upwards from the plane to reduce the magnitude of ring strain that is resulted. In accordance with this, the degree of angular distortion on the bond angles of different atoms is also directly related to the corresponding size of the chelate ring which the atoms are involved in bonding. For instance, one obvious comparison would be the O1-Fe1-O2 bond angle to the P1-Fe1-P2 bond angle, with the former having a value of 169.82° versus 156.04° for the latter. This aligns with the fact that the

P1-Fe1-P2 bond angle is distorted by two five-membered chelate rings, while the O1-Fe1-O2 bond angle is distorted by two seven-membered chelate rings which expectedly exhibit a larger extent of strain flexibility to accommodate a bigger bond angle. Similarly, the P1-Fe1-O1 bond angle is also much more acute than its adjacent P1-Fe1-O2 bond angle (81.73° versus 97.95°) by virtue of their involvement in a six-membered ring chelate compared to the free unrestricted angular formation of the latter bond angle.

The effects brought about by the extensive network of chelation are also extended to inducing distortion in the relative bond lengths of the complex. Most notably, the Fe-P bond lengths are at staggering values of 2.514 Å (for Fe1-P1) and 2.560 Å (for Fe1-P2) compared to typical literature values ranging between 2.20 Å to 2.23 Å.[31b] The Fe1-N1 bond length is also relatively longer at 2.192 Å compared to the usual values between 1.97 Å to 2.03 Å.[31b] Given that the fluorine donor from BF_4^- is not an exceptionally strong *trans* ligand, the source for the observed elongation of the Fe-N bond and correspondingly the Fe-P bonds should again revert back to easing of ring strain associated with the chelate rings. Particularly, the sizable increase in the Fe-P bond lengths may be attributed to a few contributing factors.

Firstly, the P atoms are concomitantly involved in bonding within two chelates of a five and six-membered ring. Expectedly, a short Fe-P bond length would introduce a highly constricted environment in the rigid structure with limited degrees of freedom. Secondly, with the chelation of the oxygen atoms from the carbonyl functionalities, the terminal phenyl substituents present on the ligand backbone are brought into a nearer spatial vicinity to the bulky PPh_2 groups as can be seen from the front view illustration of complex **22** (Figure 3.6).

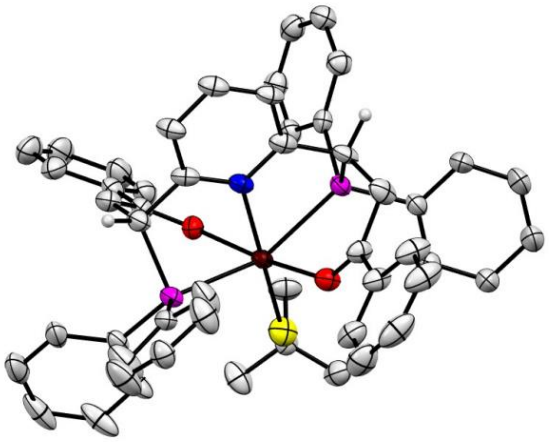

Figure 3.6. Front view illustration of complex **22**.

In addition, the chelation of the oxygen atoms also results in restricted bond flexibility about the C-C bonds along the ligand backbone which therefore presents limited orientation positions for the terminal phenyl substituents. Consequently, the only opportunity for steric relief between the phenyl moieties can only occur from elongation of the Fe-P bonds for further spatial distancing of these substituents. Thirdly, the natural strong *trans* effect of the phosphine ligands is also in effect to enhance the increase in bond distance as well. On the other hand, the Fe1-F1 bond length of 2.008 Å is rather short as compared to the literature bond length values that range from 1.96 Å to 2.26 Å for related η^1-coordinated BF_4^- iron complexes.[32] This also indicates that the pyridine moiety opposite to it exerts less significant of a *trans* effect.

In general, both F1-Fe-P bond angles are larger than the optimal value of 90°, which is a consequence of the upward distortion towards the pyridine moiety by the ring chelates as mentioned. However, the F1-Fe1-P1 bond angle of 104.07° is slightly larger than its F1-Fe1-P2 bond angle counterpart of 99.86°. This can be possibly rationalized by steric repulsion between the BF_4^- moiety with the phenyl ring comprised of C42-C47 atoms, both of which are pointing out of the plane towards the same direction. On the flipside, the F1-Fe1-O1 bond angle is slightly

smaller at 92.88° compared to its F1-Fe1-O2 bond angle equivalent at 97.05° likely because of steric repulsions between the phenyl moieties comprising of C36-C41 and C18-C23 atoms with the BF_4^- substituent.

With the extensive level of distortions present in the solid state structure of complex **22**, it may be justified that the resultant configurational stabilization is derived from the electronic fulfilment of the highly electrophilic iron(II) center since the coordination pattern was not observed in the solution state. Correspondingly, the coordination structure as suggested by NMR analysis propose a less sterically demanding structural arrangement, with a precondition of having suitable alternative ligands that are first able to stabilize the complex electronically. This essentially highlights complex **22** as a probable highly reactive species in solution, with good lability on the oxygen and BF_4^- coordination sites under appropriate electronic environments which satisfy the abovementioned condition. Ultimately, the structural analyses that were presented have offered plausible insights to the behavioral characteristics of the iron(II) center in relation to its electronic properties.

3.6. Ruthenium

Complexation via direct metalation often necessitates the use of metal precursors containing ancillaries that can be easily substituted for better regulation of the bonding process to facilitate ligand affixation. With respect to this, common ruthenium precursors intended for such use usually consist of labile triphenylphosphine (PPh_3) ligands that have been reportedly employed in the syntheses of a variety of ruthenium pincer complexes.[33] Apart from that, the NMR active characteristic of the PPh_3 moiety presents an added synthetic advantage where it can act as an internal probe for convenient assessment of the reaction progression. As such, complexation trials with ruthenium were commenced with readily prepared $RuCl_2(PPh_3)_3$ as the initial precursor of choice based on the benefits in synthetic analyses that it may provide (Scheme 3.13).

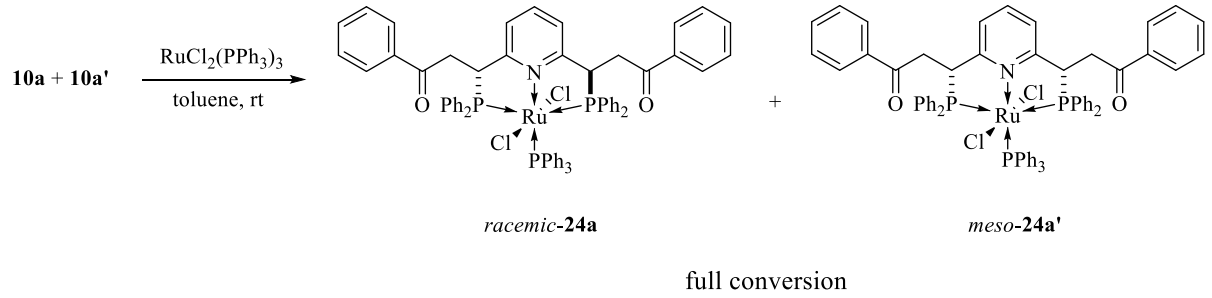

Scheme 3.13. Complexation trial using $RuCl_2(PPh_3)_3$.

Addition of the ruthenium(II) precursor into a toluene mixture of diphosphines **10a** and **10a'** at room temperature resulted in the formation of a yellow solution within a few minutes. The reaction mixture was left to stir for 1 hour before a crude NMR analysis was performed. The $^{31}P\{^{1}H\}$ crude NMR spectrum showed two sets of signals, each constituting of a mutually coupled doublet and triplet splitting pattern with coupling constants of 28.0 Hz and 29.6 Hz. These signals were respectively imaged at chemical shifts of 39.3 ppm (t), 47.7 ppm (d) for the first set and 43.4 ppm

(t), 59.1 ppm (d) for the second set, each of which corresponding to the diastereomeric *racemic* and *meso* isomer. Additionally, a sharp singlet located at -5.5 ppm indicates the presence of free uncoordinated PPh_3 correlating to their displacement from the parent precursor for metalation. Integration of the signals revealed a 2:1 ratio of phosphorus atoms between the doublet and triplet respectively, which convincingly validates the coordination of the PN(sp^2)P ligand together with an additional PPh_3 substituent on the metal center in an MX_2Y system. The observed chemical shifts also fall within range of related PN(sp^2)P coordinated ruthenium complexes bearing a PPh_3 co-ligand.[34]

Information drawn from the splitting patterns and integrals in the $^{31}P\{^1H\}$ NMR spectrum infer the chemical equivalence of the two phosphorus atoms on the PN(sp^2)P auxiliary, with the PPh_3 co-ligand positioned *cis* to both phosphorus donors from the tridentate as corroborated by the magnitude of the $^2J_{P\text{-}P}$ coupling constants.[34] In turn, this verifies the symmetricity of the furnished complexes with the ligand precursor coordinated in a meridional fashion and the PPh_3 substituent attached *trans* to the pyridine moiety as illustrated by **24a** and **24a'**. The products were ascertained to be unstable under atmospheric conditions, as portrayed by a distinct colour change of the solution from yellow to dark green over time upon exposure to air. The observed end state green colouration is indicative of typical ruthenium(III) compounds, suggesting that oxidation of the metal center had likely occurred. A discussion will be included in a later part of this section to narrate the related observations associated to this chemical change.

As a result of its instability, standard purification techniques were thus rendered unsuitable, and a rough purification was performed by passing the crude mixture through a short Celite plug under inert conditions. The collected filtrate was subsequently subjected to liquid diffusion recrystallization by layering degassed *n*-hexane on DCM in the cold, explicating that the products

are stable in varying solvents including reactive ones such as DCM. Suitable crystals of X-ray quality were successfully grown and a diffraction analysis of the *racemic* PN(sp^2)P ruthenium(II) complex **24a** is illustrated in the ORTEP representation below (Figure 3.7).

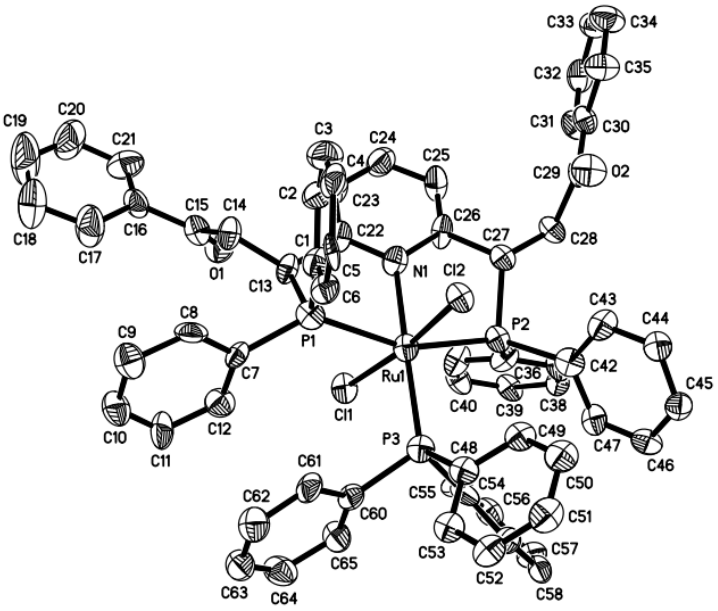

Figure 3.7. ORTEP representation of *racemic* PN(sp^2)P ruthenium(II) complex **24a** with thermal ellipsoids drawn at 50% probability level. Hydrogen atoms are omitted for clarity.

The X-ray diagram in Figure 3.7 displays a consistency in the structural depiction of complex **24a** with relation to the inferences drawn from NMR analyses that were mentioned above. In the same meaning, the complex retains its structural configuration in both solution and solid states. Based on the X-ray figure, it may be suggested that the PPh_3 substituent accommodated the *cis* position which is pseudo axial with reference to the PPh_2 groups, as the alternative situation in the pseudo equatorial *cis* position (where the Cl atoms are) would probably result in a configurationally unstable complex due to extensive steric overcrowding between all the projecting phenyl moieties.

In general, complex **24a** adopts a distorted octahedral conformation with all ligands *cis* to the PPh_3 substituent bent away from it resulting in an overall upward distortion towards the pyridine ring. This is evidently illustrated by the relatively small P1-Ru1-P2 bond angle of 157.75° as well as a partially diminished Cl1-Ru1-Cl2 bond angle of 172.91°. Prominently, the P2-Ru1-Cl1 bond angle is much bigger at 101.42° than the P2-Ru1-Cl2 bond angle of 84.34°, which could be likely caused by steric repulsion between Cl1 and the phenyl group comprised of C48-C53 atoms. In another notable comparison, the P1-Ru1-P3 bond angle is distinctly larger at 105.10° than the corresponding P2-Ru1-P3 bond angle of 96.60°, presumably due to repulsion between the phenyl group comprised of C7-C12 atoms and the entirety of the PPh_3 moiety. All in all, the major bond lengths of interest described in complex **24a** exhibit no significant deviations from literature reported values; Ru1-P bond lengths at 2.377 Å, 2.351 Å and 2.330 Å for Ru1-P1, Ru1-P2 and Ru1-P3 bonds respectively, Ru1-Cl bond lengths at 2.439 Å and 2.391 Å for Ru1-Cl1 and Ru1-Cl2 bonds respectively and the Ru1-N1 bond length at 2.155 Å.[34-35] The slightly shorter bond length observed for Ru1-P3 may be ascribed to the less intense *trans* effect from the pyridine donor compared to the other two phosphorus ligands that are mutually *trans* to each other.

Comparisons may also be made to the PN(sp^2)P iron(II) complex **22** with respect to the bond angle resulted from the five-membered ring chelate between the metal center to the chiral carbons through the phosphorus donors. For the case of complex **24a**, the relative Ru-P-C bond angles are between 98° to 99°. On the other hand, the relative Fe-P-C bond angles are between 91° to 93° in the case for complex **22,** which showcases the extent of constriction that the additional chelation in the complex has brought about. Additionally, the observed oxygen chelation by the carbonyl functionality on the ligand backbone in complex **22** does not occur in this case, probably due to steric encumberment from the chloride ligands which prevented its twisting approach.

Based on the descriptions of the major bond angles of complex **24a**, it may be discerned that the overall structure experiences an evident steric hindrance from the PPh_3 substituent with the apparent spatial deflection of all other bound ligands away from the bulky moiety. Going back to the chemical phenomenon as mentioned earlier, the instability of the complex that was observed may be accorded to a translational effect brought about by this sterically demanding conformation. $^{31}P\{^1H\}$ NMR analysis of the exposed dark green solution revealed the disappearance of the characteristic doublet and triplet signals associated with the structural representation of complexes **24**. A secondary observation that could also be made from the spectrum was a similar vanishment of the signal at -5.5 ppm corresponding to the substituted free PPh_3 ligands. Rather, a new signal denoted by a sharp singlet was observed at 27.1 ppm with it being the sole signal of significant observable intensity. On the other hand, the crude ^1H NMR spectrum showed up with a cluster of badly resolved signals that were too complicated to provide any definitive information, reminiscent of the presence of paramagnetic components within the sample.

An initial hypothesis made to associate the plausible identity of the newly formed signal on $^{31}P\{^1H\}$ NMR was pointed towards the concomitant decomplexation of the PN(sp^2)P auxiliary and re-coordination of the previously displaced PPh_3 ligands (presuming an existing equilibrium), which likely occurred due to the configurational instability of the structure in complexes **24**. Subsequent oxidation of the free diphosphines and ruthenium metal in solution led to the observed singlet corresponding to the diphosphine oxides and a paramagnetic ruthenium(III) byproduct which is masked from NMR appearance. This was in alignment with the understanding that PPh_3 is relatively stable against oxidation under atmospheric conditions while $RuCl_2(PPh_3)_3$ exhibits a relative degree of air sensitivity.[36] However, the postulation was eventually debunked by a series of experiments conducted to confirm the above. Firstly, a separate synthesis of the PN(sp^2)P

diphosphine oxides revealed a mismatch of their phosphorus chemical shift signal in the $^{31}P\{^{1}H\}$ NMR spectrum (coalesced at 33.2 ppm) within the same solvent as that for the exposed crude mixture (27.1 ppm). Secondly, in a bid to prevent the suggested ligand decomplexation pathway, a quick purification by passing the mixture through a short silica plug was performed under inert conditions using degassed DCM to remove the displaced PPh_3 from the crude mixture containing the complexed products. Interestingly, subsequent exposure of this purified mixture to open atmosphere resulted in the same outcome but with visibly much faster chemical change of the products and an exact replication of the crude $^{31}P\{^{1}H\}$ NMR spectrum showing a singlet at 27.1 ppm.

Judging from these correlations, the only possible remaining candidate which could fit the identity of the phosphorus species at 27.1 ppm would be triphenylphosphine oxide ($OPPh_3$). Indeed, this was later verified with a reference $^{31}P\{^{1}H\}$ NMR analysis of the pure compound within the same solvent. In accordance with this confirmation, it can be concluded from the second experimental trial above that the $OPPh_3$ formation can only be derived from the single existent PPh_3 source that is present and bound to the complexes itself. In other words, this implies a direct mediation by the ruthenium complex for the oxidation of PPh_3 in the presence of atmospheric oxygen. Retracing back a further step, it can also be inferred that the disappearance of the -5.5 ppm phosphorus peak in the unpurified crude mixture is a resultant of complete conversion of all the PPh_3 moieties to its oxide derivative. With no other visible phosphorus signals displayed, it can be further deduced that the PN(sp^2)P tridentate most likely remains chelated on the metal center without any signs of labilization or liberation.

While we were unable to ascertain the exact oxidation pathway for complexes **24**, related reports in the literature describe analogous observations which might shed some insights to what may have possibly happened (Scheme 3.14).[37]

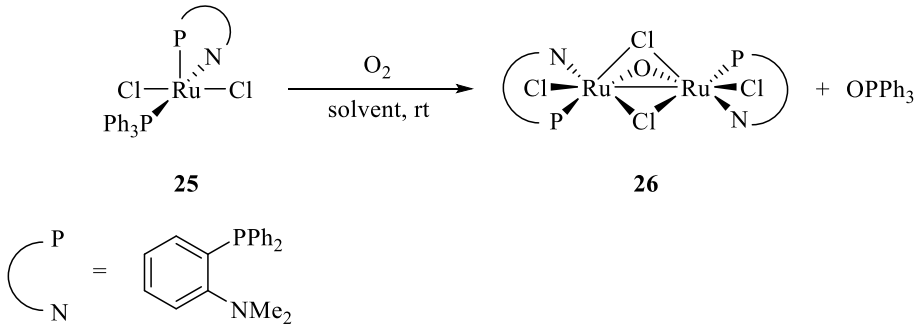

Scheme 3.14. Decomposition pathway of ruthenium(II) complex **25** in oxygen.

Scheme 3.14 depicts the atmospheric oxidation of PPh_3 that was initially present on complex **25**, which resulted in the detachment of the substituent to form $OPPh_3$ and an oxidized bimetallic ruthenium complex **26** incorporated with a bridging oxygen atom. A noteworthy point for the above reaction is that with supplementary addition of PPh_3 under O_2 atmosphere, complex **25** converts all the extra PPh_3 to $OPPh_3$ before any signs of complex **26** are detected. Linking this back to our previous experimental trial in removing the displaced PPh_3 ligands from the crude mixture, the consequential hastening in the rate of chemical change falls precisely in line with the abovementioned experimental observation. Furthermore, it has to be reiterated that the unpurified crude mixture containing the displaced PPh_3 ligands was also observed to show an eventual complete conversion of PPh_3 to its oxide on $^{31}P\{^1H\}$ NMR analysis.

With these in mind, a correlation may therefore be drawn whereby the PPh_3 moiety adopts a highly reactive state when coordinated to the ruthenium center. In our case, this may be a result of the spatial inadequacy of the ruthenium center which has been thoroughly described based on the bond angle distortions observed in its X-ray structure. It is likely that the consequence of steric

repulsion within the complex causes the Ru-PPh_3 bond to be less stable and thus renders a facile labilization of PPh_3 in the presence of coordinative oxygen molecules. Such ruthenium-oxo intermediates have been reported,[38] and in turn could have been the reactive species responsible for continuous reaction with the free PPh_3 in solution to generate $OPPh_3$. Ultimately once all the PPh_3 have reacted, the complex with oxygen in the replaced coordination site of PPh_3, oxidizes to form a related bimetallic oxo-bridged complex akin to complex **26** that contains a ruthenium(III) center with paramagnetic property.

Our next attempts were thus focused on the syntheses of a ruthenium(II) complex which has a better probability of being atmospherically stable, by replacing the PPh_3 substituent with other suitable choices of co-ligands. Aside from taking into account steric considerations, further deliberation was also made to include the use of electronically more compatible co-ligands with respect to the ruthenium(II) center, so that decomposition via ligand dissociation could be further prevented. To this end, we postulated that a nitrogen donor, which inherently possesses a harder donor characteristic compared to a phosphorus donor, would be electronically more favorable in its coordination to the ruthenium(II) center of borderline hardness.

Initial trials were conducted by mixing a pot of pre-synthesized complexes **24a** and **24a'** together in the presence of excess neat pyridine. The reaction vessel was first vacuumed dry for removal of the previous solvent prior to the in-situ addition of pyridine **(**Scheme 3.15).

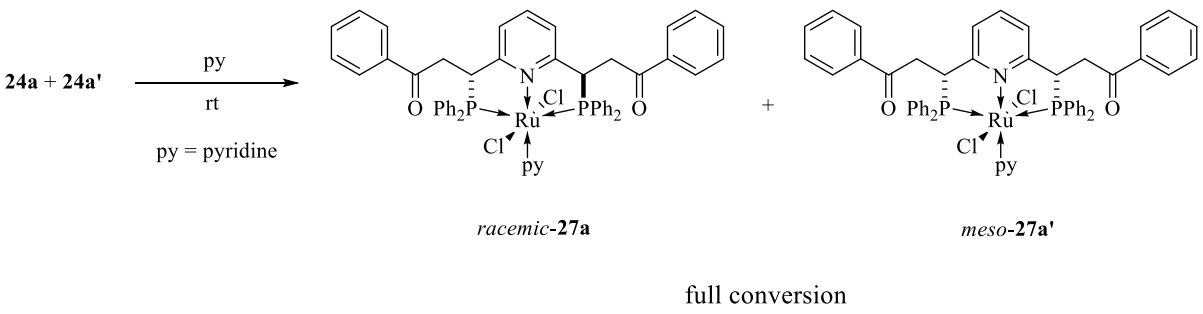

Scheme 3.15. Complexation trial of complexes **24a** and **24a'** using pyridine.

The resultant mixture was left to stir under room temperature for 1 hour during which a progressive colour alteration from yellow to dark yellow was observed. The mixture was left to stir for an additional 1 hour and analysis by $^{31}P\{^{1}H\}$ NMR of the crude mixture showed a complete disappearance of the doublet and triplet signals associated to complexes **24a** and **24a'**. Instead, a corresponding emergence of two singlets at 57.7 ppm and 58.2 ppm were observed, indicative of the dissociation of PPh_3. It has to be noted that an additional phosphorus peak was observed at -5.5 ppm as well, but does not provide conclusive evidence for the substitution of PPh_3 due to its pre-existence from $RuCl_2(PPh_3)_3$ displacement in the formation of complexes **24a** and **24a'**. The crude mixture proved to be stable under open atmosphere, with no visible degradation observed both physically and spectroscopically in solution even after several days of exposure. Purification of the crude mixture was subsequently performed using flash silica gel column chromatography, and the respective diastereomeric isomers **27a** and **27a'** were successfully separated as confirmed by ^{1}H NMR.

Based on the spectroscopic information provided by NMR, it may be established that the two singlets detected on the $^{31}P\{^{1}H\}$ NMR spectrum corresponds to the diastereomeric *racemic* and *meso* isomers. In conjunction with the spectroscopic assessments from ^{1}H NMR, the singlets also represent the successful ligand substitution reaction between pyridine and PPh_3, with the

complex bearing two chemically equivalent phosphorus atoms from the PN(sp^2)P auxiliary as presented by complexes **27a** and **27a'**. The ease of ligand substitution is exemplified in the mild reaction conditions employed and the quick reaction process, which further highlights the incompatibility of the PPh_3 substituent on the complex arising from configurational instability due to steric effects. Attempts to obtain a crystal sample for X-ray analysis via solvent recrystallization however led to the realization of the instability of complexes **27** in solution phase. In fact, the stability of the compounds seemed to drastically decrease after purification, with an evident colouration change from dark yellow to black within a day of exposure to air in solution. Crude NMR analysis of the black solution revealed no apparent signals on the $^{31}P\{^1H\}$ NMR spectrum as well as broad unresolved resonances in the ^1H NMR spectrum.

We hypothesized the instability of the compounds to be likely again ascribed to the dissociation of pyridine from the complex. This was verified in a second synthesis trial, but with intentional addition of a minute amount of pyridine into the isolated complexes after purification. Exposure of this resultant mixture proved the effectiveness of the added pyridine in stabilizing the complexes, with negligible indications of decomposition in solution under open atmospheric conditions even for extended periods of time. On hindsight, the relative display of higher stability exuded by the crude mixture in comparison to the isolated pure products also singles out the necessary presence of pyridine within the mixture for stabilization purposes. The observations as mentioned therefore testify towards the above decomposition hypothesis via a plausible pyridine dissociation pathway. Unfortunately, repeated attempts to obtain a crystal structure employing the abovementioned stabilization technique proceeded with no avail, and hence no solid state structural elucidations of the products could be provided. On the contrary, it was noticed that the

decomposition of the pure products accelerates only in solution state, with the corresponding pure solids of the compounds exhibiting good stability at ambient conditions.

To circumvent the hassle from having to undergo multiple synthetic steps, an alternative synthetic methodology to furnish complexes **27a** and **27a'** was performed by subjecting diphosphines **10a** and **10a'** to the easily synthesized precursor $RuCl_2(pyridine)_4$ (Scheme 3.16).

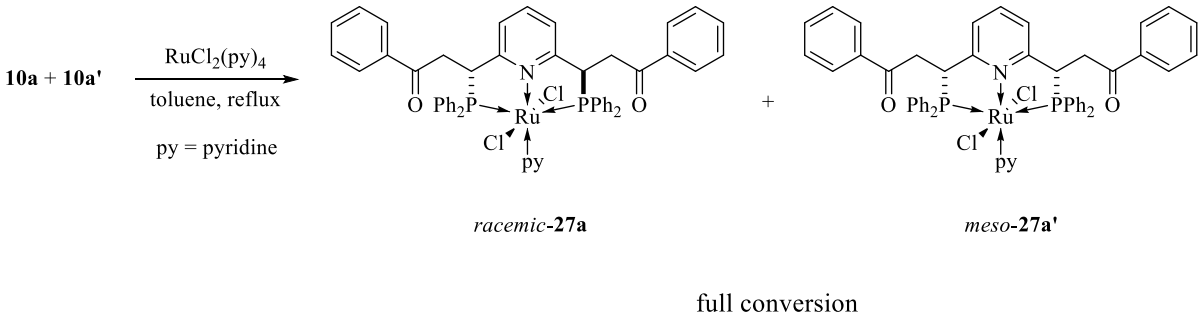

Scheme 3.16. Complexation trial using $RuCl_2(py)_4$.

Astonishingly, much to the contrast of all other complexation trials that have been mentioned thus far, the reaction was found to require reflux temperatures to enable the affixation of the tridentate ligand. Trials conducted at room temperature and mildly heated conditions displayed negligible to very slow reaction progression as monitored by $^{31}P\{^{1}H\}$ NMR, showing the enhanced coordination strength and corresponding lower lability of the pyridine ligands to the ruthenium(II) center. Accordingly, it may be presumed that the steric influences brought about by the PN(sp^2)P tridentate exhibit an immensely significant impact towards the penultimate coordination site of the ruthenium complex, which therefore results in a strong labilization effect in that direction even for an electronically compatible ligand.

3.7. Nickel

Complexation trials with nickel proceeded with use of $Ni(dme)Cl_2$ as the precursor (where dme = 1,2-dimethoxyethane) by virtue of the convenient accessibility from its commercial availability (Scheme 3.17).

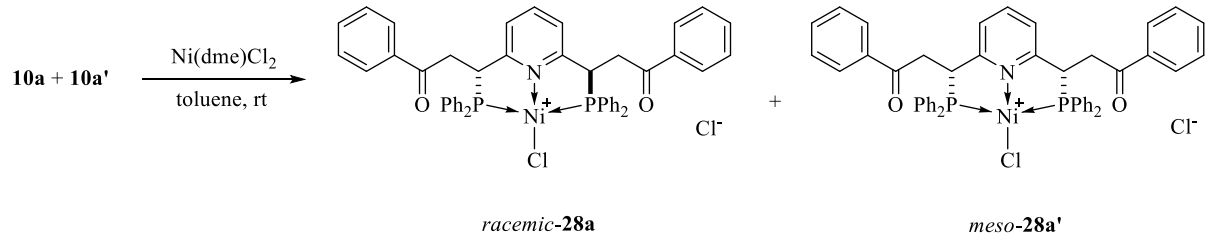

Scheme 3.17. Complexation trial using $Ni(dme)Cl_2$ and the postulated products **28a** and **28a'**.

Addition of the nickel(II) precursor into a toluene mixture of diphosphines **10a** and **10a'** at room temperature resulted in a quick transition of the mixture from a pale yellow suspension to a dark purple solution within a few minutes. The mixture was left to stir for 1 hour before a crude NMR analysis was performed to check on the reaction development. It must be noted that the metal precursor (which is a yellow solid) exhibits negligible solubility in toluene, and hence the observed end state of the crude mixture as a purple solution pointed towards an evident indication of a reaction occurrence.

Unfortunately, both $^{31}P\{^{1}H\}$ and ^{1}H NMR spectra revealed an absence of any visible signals for the former and broad undefined signals for the latter, which may be postulated to be attributed to a few plausible circumstances. 1) A successful metalation reaction results in the formation of complexes **28a** and **28a'**, which could be in a fixed tetrahedral conformation that would inherently demonstrate paramagnetism for a nickel(II) d^8 configuration. 2) Complexes **28a** and **28a'** exhibit conformational flexibility which causes them to exist as an equilibrium between

a square planar and tetrahedral arrangement in solution. The interconversion between these conformations thus results in spectral interferences on NMR which are contributed by the paramagnetic tetrahedral species. 3) The metalation resulted in purely a ligand affixation to generate a penta-coordinated nickel species without liberation of a chloride anion. In a similar aspect to the situation described previously for iron, the low LFSE of the first row 3d nickel metal in conjunction with two strong π-donating chloride ligands leads to a resultant high spin complex with paramagnetic display. Unfortunately, attempts to obtain crystals from this crude mixture were unsuccessful and no further characterizations could be made for structural identification of the generated products.

Subsequent efforts were therefore directed at quantifying the hypotheses that have been mentioned above. Firstly, an Evans solution method using ^{1}H NMR analysis confirmed the existence of paramagnetism within the furnished products as determined by a solvent shift within the spectrum. Secondly, an in-situ metathesis reaction was conducted with addition of sodium tetrafluoroborate ($NaBF_4$) into the crude mixture derived from the first step of metal and ligand addition (Scheme 3.18). The purpose for this reaction will be explained later in this section.

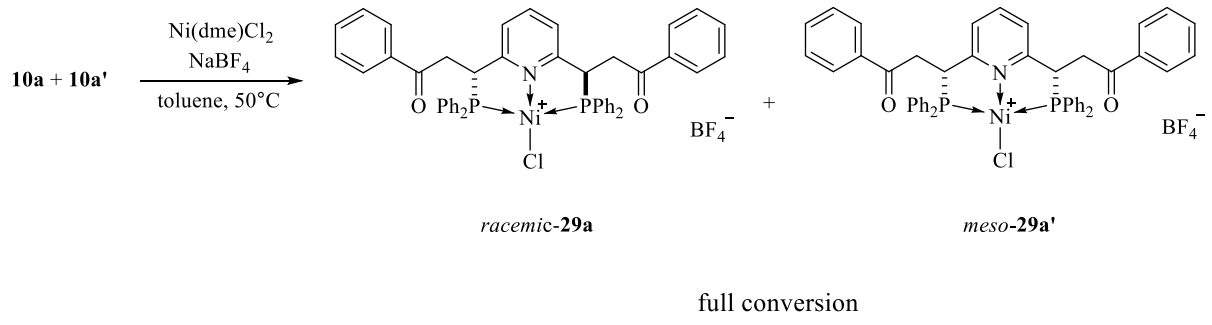

Scheme 3.18. Complexation trial using $Ni(dme)Cl_2$ with in-situ addition of $NaBF_4$.

Upon addition of one equivalence of $NaBF_4$ into the crude mixture, a gradual change from the original purple coloured crude solution to a slight reddish colouration was observed after a few hours at room temperature. Nevertheless, the mixture remained to be predominantly purple in colour despite the noticeable signs of change even after 12 hours into the reaction time. Assuming the sluggish progression was due to solubility issues related to the sodium salt, the mixture was thus subjected to a heated temperature of 50°C in a bid to increase its solubility and speed up the rate of reaction. An end state orange suspension with substantial amounts of precipitate was eventually resulted after 2 days, and a rough purification via filtration through a Celite plug was performed to remove the supposed NaCl byproduct formed in the reaction. The precipitate was tested to be soluble and stable in DCM, which was thus the solvent used for the Celite filtration as well as NMR analysis of the filtrate. On another note, when a separate complexation trial without addition of $NaBF_4$ was conducted under similar heated reaction conditions as that shown in Scheme 3.18, no observable changes of the initial purple coloured crude solution to an orange precipitate were made.

Spectroscopic analysis of the newly furnished crude mixture displayed two singlets on the $^{31}P\{^1H\}$ NMR spectrum, with coordination shifts at 32.6 ppm and 32.9 ppm that are representative of the diastereomeric isomers of *racemic* **29a** and *meso* **29a'**, as well as the chemical equivalence of the two phosphorus atoms present on the tridentate ligand. The ^1H NMR analysis also showed up with a comparatively better resolved spectrum, with obvious indications of the signals corresponding to the alkylic protons present on the ligand backbone. Exposure of the mixture to air revealed the stability of the products to ambient conditions, with no hints of chemical change in both solution and solid states as confirmed spectroscopically after several days. The recognized stability of the products enabled their convenient recrystallization and slow evaporation of the

crude mixture using DCM/*n*-hexane was fruitful in providing single crystals of X-ray quality for structural elucidation (Figure 3.8).

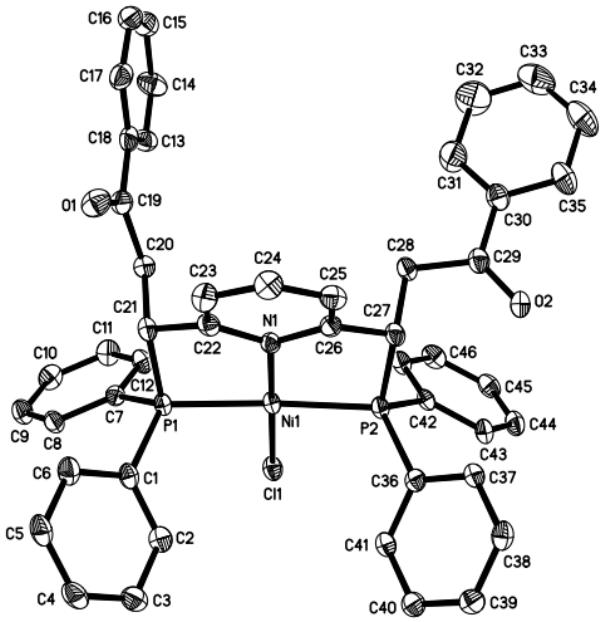

Figure 3.8. ORTEP representation of *meso* PN(sp^2)P nickel(II) complex **29a'** with thermal ellipsoids drawn at 50% probability level. Hydrogen atoms and the BF_4^- anion are omitted for clarity.

Complex **29a'** adopts an approximate square planar geometry with a slight angular distortion towards the pyridine ring as evidenced by the P1-Ni1-P2 bond angle of 169.07°. In general, the relative bond angles and bond lengths of the complex adhere consistently to related literature values,[28, 39] with the selected representations for each of them as follows. Bond angles: P1-Ni1-P2 = 169.07º, N1-Ni1-P1 = 86.36°, N1-Ni1-P2 = 87.21°, Cl1-Ni1-P1 = 93.35°, Cl1-Ni1-P2 = 92.80°. Bond lengths: Ni1-N1 = 1.905 Å, Ni1-P1 = 2.199 Å, Ni1-P2 = 2.203 Å, Ni1-Cl1 = 2.147 Å.

Based on the analytical information obtained, it can be justified that the postulation suggested above with regard to the possibility of a furnished tetrahedral complex is disproved since the generic framework between complexes **28** and **29** remains identical. Furthermore, the coherence between the X-ray diffraction and NMR data suggests retention of the structural integrity of complex **29a'** in both solid and solution states. In turn, this presents an unlikelihood of a conformational equilibrium resulting from geometrical interconversions of the complex structure in solution. This is additionally in accordance with the fact that the NMR signals display good resolution at room temperature analysis. With these in mind, the rationale behind the conduct of the in-situ metathesis reaction becomes explicitly clear as a test experiment to validate the hypothesis of a metalated five-coordinate dichloride nickel species. While no confirmation can be provided to ascertain the structural make-up of this proposed nickel intermediate, the contrasting observations both physically and spectroscopically made between the intrinsically similar complexes **28** and **29** suggests that complex **28** should most likely be adopting a distinctly dissimilar structural configuration instead, thereby highlighting a good probability that the proposed five-coordinate nickel species could exist. Attention has also got to be brought to the fact that similar employments of this metathesis reaction in the literature utilizing analogous metal and ligand precursors proceeded with milder conditions and faster reaction rates (Scheme 3.19).[28]

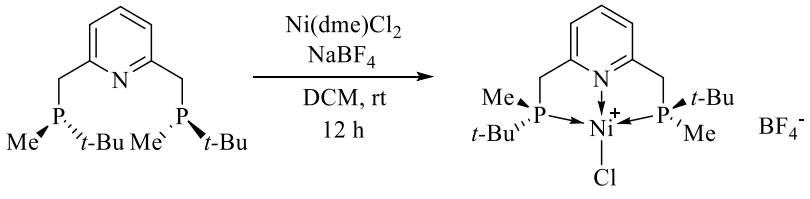

Scheme 3.19. $NaBF_4$ metathesis reaction for an analogous PN(sp^2)P nickel(II) complex.

Accordingly, the harsher reaction conditions required in our case may be associated with a harder substitution pathway that is suggestive of a non-displaced, ionic bonded chloride anion which necessitates stronger activation energy for displacement. Another possible reasoning for the difficult removal of the chloride anion could also be attributed to the phosphine groups which are directly involved in coordinative bonding to the metal center. A quick comparison to the literature reported example above shows an apparent electronic disparity between the substituents present on the phosphine ligands, with the PPh_2 group (for our case) paling in electronic donating propensity as compared to the alkyl functionalized phosphines in the reported work. Consequently, the comparative lack of electronic stabilization required for the charged nickel(II) center may have resulted in a stronger electrostatic interaction with the chloride anions, thereby withholding them from dissociating out from the metal core as easily.

3.8. Palladium

Complexation trials with palladium were adapted from our previous metalation experiments with the PC(sp^2)P pincer ligand analogue using the same palladium(II) precursor $PdCl_2(MeCN)_2$ (Scheme 3.20).[40]

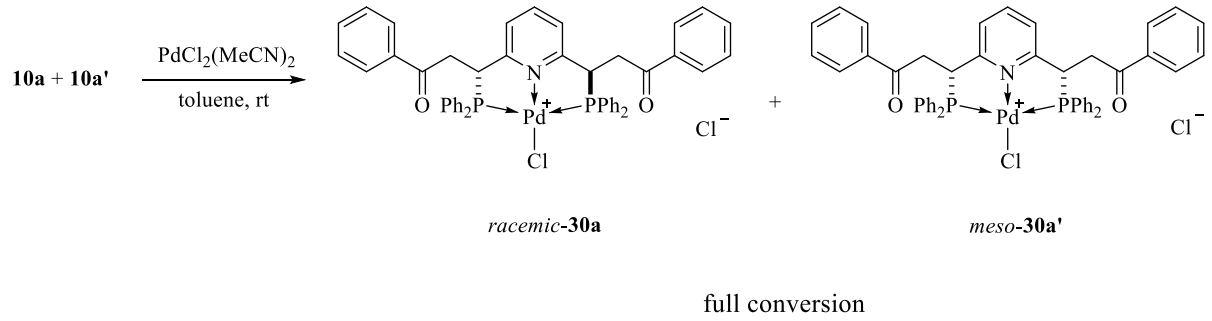

Scheme 3.20. Complexation trial using $PdCl_2(MeCN)_2$.

Addition of the metal precursor into a toluene mixture of diphosphines **10a** and **10a'** at room temperature resulted in an immediate formation of a yellow solution which was left to continue stirring for 1 hour. NMR analysis of the crude mixture provided two clear singlets on the $^{31}P\{^1H\}$ NMR spectrum at chemical shifts of 32.4 ppm and 37.2 ppm, characteristic of the two diastereomeric isomers **30a** and **30a'** bearing two chemically equivalent phosphorus atoms symbolizing their symmetrical geometries. The ^1H NMR spectrum also displayed the respective signals corroborating to the diastereomeric alkylic protons present on the ligand backbones of each isomeric complex. It is noteworthy that the reaction proceeds in a much milder fashion as compared to the complexation trial with nickel, re-suggesting the possible requirement for more extensive electronic stabilization on the less electron rich nickel(II) center by retention of the chloride anion that consequently resulted in stronger Ni-Cl bonding. Stability of the products in both solution and solid states were attested with their exposure to open atmosphere, showing no

evident indications of degradation even after an extended period of time. The stability of the products in solution was further realized to encompass most organic solvents as well. Attempts to obtain structural elucidations of the complexes were successfully conducted via slow evaporative recrystallization in DCM/*n*-hexane and the resolved X-ray structure is depicted in the ORTEP representation below (Figure 3.9).

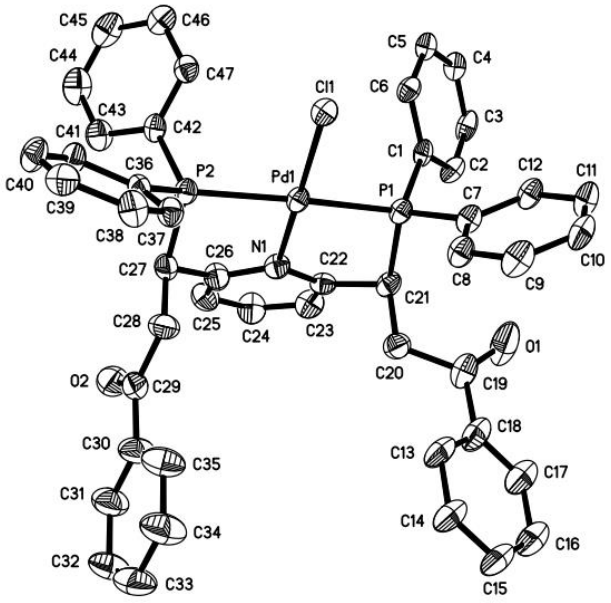

Figure 3.9. ORTEP representation of *meso* PN(sp^2)P palladium(II) complex **30a'** with thermal ellipsoids drawn at 50% probability level. Hydrogen atoms and the Cl^- anion are omitted for clarity.

Complex **30a'** takes up an approximate square planar arrangement with slight distortions towards the pyridine ring due to the formation of two fused five-membered chelate rings from ligand coordination. This is showcased by an acute bending of the P1-Pd1-P2 bond angle, which is stipulated at a value of 166.39°. Overall, the general bond lengths and bond angles of interest in complex **30a'** resemble closely to those found in related literature examples,[41] with the selected values of each respective component reported as follows.

Bond lengths: Pd1-N1 = 2.051 Å, Pd1-P1 = 2.284 Å, Pd1-P2 = 2.301 Å, Pd-Cl1 = 2.283 Å. Bond angles: P1-Pd1-P2 = 166.39°, N1-Pd1-P1 = 85.07º, N1-Pd1-P2 = 83.93º, Cl1-Pd1-P1 = 93.22º, Cl1-Pd1-P2 = 96.90º.

Comparisons made between complex **30a'** with its nickel(II) analogue complex **29a'** disclose certain associative trends with respect to several bond angle and bond length properties of the same type within the complexes. In particular, the differences observed in the P-M-P bond angles (where M refers to metal) of both complexes are directly implicated by the degree of distortion implemented by the subtending tridentate ligand and primarily affected by the respective N(aryl)-M bond lengths. In a general definition, this degree of distortion can be classified into two different modes of conformations (Figure 3.10).[6a]

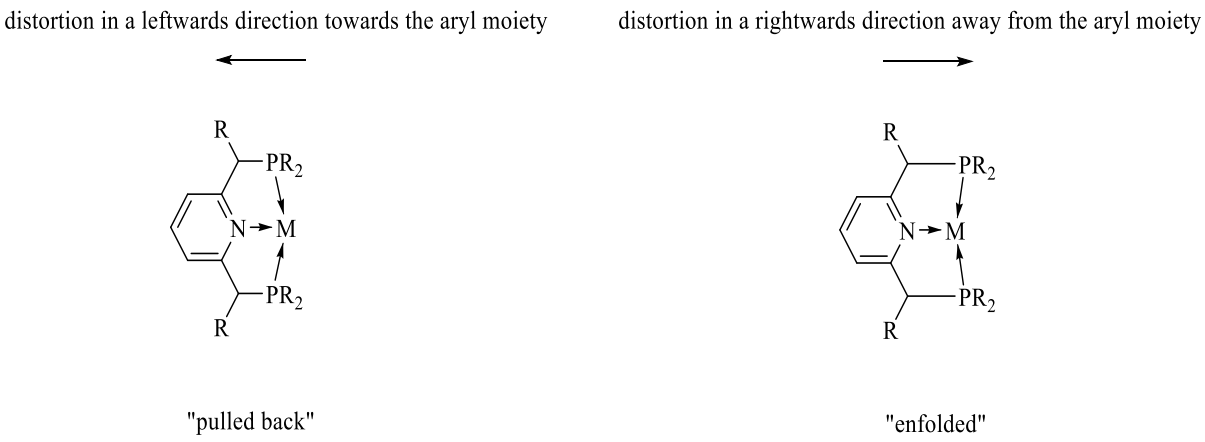

Figure 3.10. Modes of P-M-P angular distortion in a pincer complex.

Depending on the angular distortion caused by the ligand, the resultant pincer complex may adopt either a "pulled back" or "enfolded" arrangement as described in Figure 3.10. These distortions are typically affected by steric influences within the coordination sphere of the metal center, mainly generated by the ligand *trans* to the aryl ring as well as the steric occupancies of the phosphine moieties that are bonded immediately to the metal. With the same exact ligand

make-ups present in both complexes **29a'** and **30a'**, the abovementioned parameter for angular distortion of the complex structure is hence undifferentiated and not applicable as a means for comparison. In turn, the main contributing factor for the degree of P-M-P angular distortion lies with the relative values of the N(aryl)-M bond length, which is inherently dependent on the bonding radii provided by the respective metal centers. Based on the illustrations in Figure 3.10, it can be imagined that a complex with a shorter N(aryl)-M bond length would propel a better level of "enfolding" of the M-P bonds or in the same light, render a less extensive "pulled back" distortion effect. Given the smaller ionic radius of the nickel(II) center, the length of the N-Ni bond (1.905 Å) is expectedly shorter than the N-Pd bond (2.051 Å), thereby resulting in comparatively a larger extent of "enfolding" by the tridentate ligand onto the metal center. Consequently, this supports for the bigger P-M-P bond angle observed in complex **29a'** (169.07º) as compared to that of complex **30a'** (166.39º). In another comparison of complex **30a'** with its pyrrolyl counterpart complex **16b**, the observed Pd-Cl bond length is longer in the latter (2.283 Å versus 2.327 Å respectively) which highlights a stronger *trans* effect by the pyrrolyl nitrogen likely due to its greater extent of σ donating character as an anionic moiety.

3.9. Platinum

In a similar experimental approach to that of palladium, trials for the complexation of diphosphines **10a** and **10a'** to platinum followed an initial use of an analogous metal precursor $PtCl_2(MeCN)_2$. Unfortunately, the reaction proceeded to give a messy combination of products as determined by crude NMR analysis which was not further quantified to confirm for the intended product formation. Subsequent attempts therefore proceeded with the substitutional use of K_2PtCl_4, which proved to be a more compatible choice of metal precursor for the complexation reaction (Scheme 3.21).

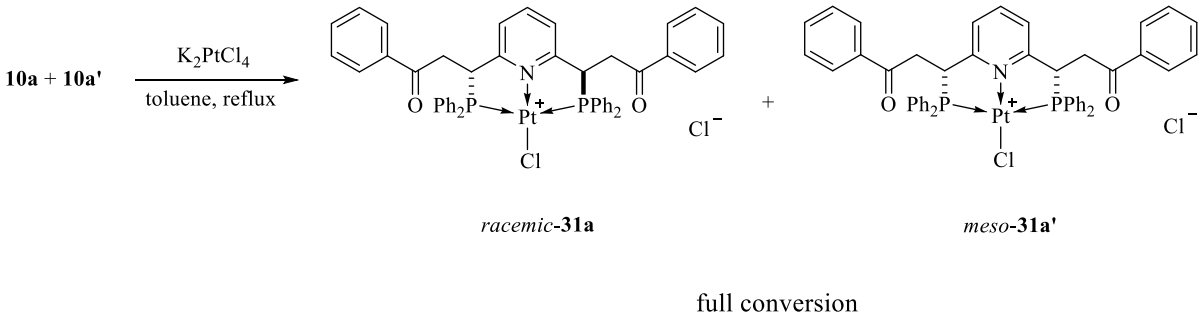

Scheme 3.21. Complexation trial using K_2PtCl_4.

Subjecting a toluene mixture of diphosphines **10a** and **10a'** together with K_2PtCl_4 under reflux resulted in a clean and complete coordination of the tridentate ligand to the platinum(II) center albeit with a prolonged reaction time of 7 days. Conducting the reaction under room temperature or mildly heated conditions displayed negligible amounts of product conversion as confirmed by visibly distinct chemical shifts corresponding to the free uncoordinated diphosphine precursors in the crude $^{31}P\{^1H\}$ NMR spectrum. This enhanced difficulty in reaction promotion may presumably be attributed to the larger and more diffused 5d orbitals of platinum which resulted in stronger

bonding interactions with the chloride moieties, thereby preventing a low energy substitution pathway.

The reaction progression was physically observable, with an obvious formation of a white suspension in conjunction with the concomitant disappearance of the red solids of K_2PtCl_4 over time. Dissolution of the suspension was achievable with the use of DCM, and the resultant solution was analyzed using NMR to provide for solution state characterizations of the furnished products. Analysis by $^{31}P\{^1H\}$ NMR showcased evident coordination shifts of the newly complexed adducts with two main singlets at 31.8 ppm and 33.7 ppm, respective of the diastereomeric isomers represented by complexes **31a** and **31a'**. This also indicates the chemical similarity between the two phosphorus atoms of the ligand, highlighting the formation of structurally symmetrical complexes. The associated platinum satellite peaks were also observed in the $^{31}P\{^1H\}$ NMR spectrum, with the corresponding $^1J_{Pt\text{-}P}$ coupling constant values of 1307.3 Hz and 1293.6 Hz that are typical of platinum based complexes bearing *trans* phosphorus ligands. Similarly, the signals respective of the diastereomeric alkylic protons belonging on the tridentate ligand backbone were also clearly identifiable on the ^1H NMR spectrum. Exposure of the crude mixture to open atmosphere revealed the complexes' stability to ambient conditions, and a slow fractional recrystallization using DCM/*n*-hexane was performed to obtain X-ray suitable crystals that were successfully resolved and reproduced in the ORTEP diagram below (Figure 3.11).

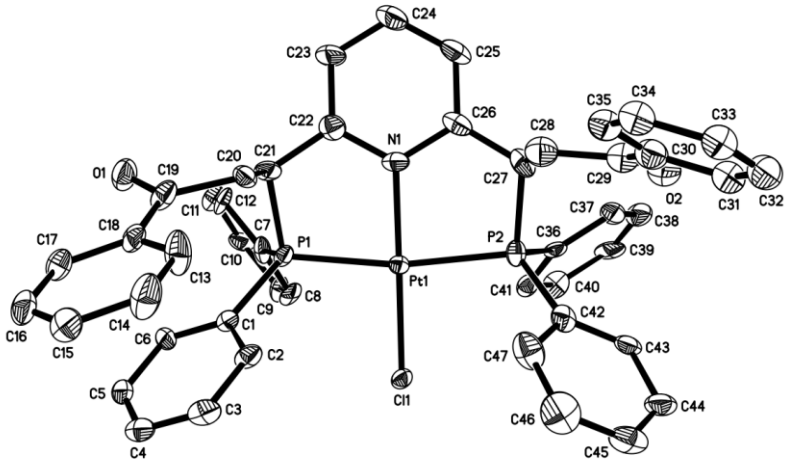

Figure 3.11. ORTEP representation of *meso* PN(sp^2)P platinum(II) complex **31a'** with thermal ellipsoids drawn at 50% probability level. Hydrogen atoms and the Cl^- anion are omitted for clarity.

Complex **31a'** adopts a relative square planar conformation with slight distortions towards the pyridine ring as depicted by the P1-Pt1-P2 bond angle of 169.60º. Interestingly, the bond angle value falls coincidentally similar to the P-Ni-P bond angle (169.07º) in complex **29a'** despite the fact that the platinum(II) center bears a larger ionic radius and would supposedly experience a less effective "enfolding" distortion by the ligand. On the other hand, the larger P-Pt-P bond angle value observed with respect to the P-Pd-P bond angle (166.39º) in complex **30a'** aligns with the understanding that the platinum(II) ionic radius is smaller by virtue of relativistic contractions within the platinum nucleus.[42] This is also illustrated by the slightly shorter N-Pt bond length of 2.027 Å as compared to the N-Pd bond length of 2.05 Å. The selected bond angles and bond lengths of complex **31a'** are indicated below, and no anomalies beyond the reported values of analogous literature examples were observed.[43] Bond lengths: Pt1-N1 = 2.027 Å, Pt1-P1 = 2.274 Å, Pt1-P2 = 2.279 Å, Pt1-Cl = 2.290 Å. Bond angles: P1-Pt1-P2 = 169.60º, N1-Pt1-P1 = 85.20º, N1-Pt1-P2 = 85.50º, P1-Pt1-Cl1 = 94.35º, P2-Pt1-Cl1 = 94.92º.

3.10. Rhodium

Complexation trials with rhodium were conducted with the use of the easily synthesized precursor $RhCl_3(MeCN)_3$. The choice of the precursor was in line with the consideration of a substitution reaction that could be mediated in a facile manner between the three existing labile MeCN ligands and the incoming neutral PNP tridentate (Scheme 3.22).

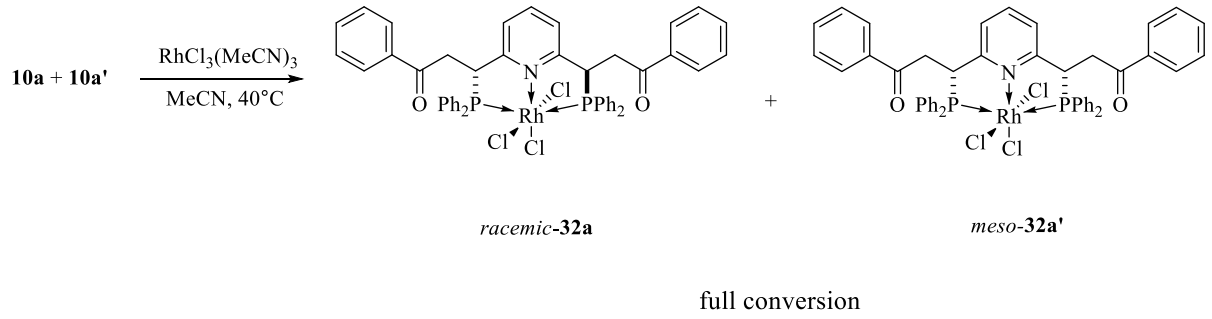

Scheme 3.22. Complexation trial using $RhCl_3(MeCN)_3$.

Reaction of $RhCl_3(MeCN)_3$ with a pot of pre-synthesized diphosphines **10a** and **10a'** in MeCN at 40ºC resulted in the preliminary formation of a clear yellow solution within a few minutes into the reaction. The mixture was left to continue stirring for another 5 hours with confirmation of reaction completion via a crude NMR analysis. Performing the reaction under room temperature conditions was also proven to be viable for reaction occurrence but with significantly slower progression rates. $^{31}P\{^1H\}$ NMR analysis of the crude mixture showed up a total of four singlets corresponding to two individual doublets with coordination shifts centered at 37.1 ppm and 39.6 ppm within the spectrum. These doublet signals were eventually identified to represent the diastereomeric isomers as illustrated by complexes **32a** and **32a'**, with both signals having $^1J_{Rh\text{-}P}$ coupling constant values of 89.0 Hz. This further denotes the chemical equivalence of the two phosphorus atoms within the complexes and signifies the structural symmetricity of the products. The small coupling constant

values observed corroborates to typical rhodium(III) complexes, but with much lower values in this case as compared to analogous PNP rhodium(III) complexes in the literature.[44] This deviation illustrates a rhodium center of lower electron density which could be possibly attributed to the lower basicity of the chloride moieties in complex **32** as compared to the co-ligands described in the literature examples (iodide and methyl). The crude ^{1}H NMR spectrum also displayed the distinct signals correlating to the diastereomeric alkylic protons present on the ligand backbone, affirming the successful coordination of the tridentate onto the metal center. The furnished products were tested to be highly stable under atmospheric conditions in solution state with most organic solvents, showing absolutely no signs of chemical degradation even after long periods of exposure as confirmed spectroscopically. In turn, this facilitated the convenient separation of the diastereomeric isomers using flash silica gel column chromatography with good purity and in almost quantitative yields. Slow evaporation of both purified complexes in DCM/*n*-hexane afforded single crystals of X-ray quality that were resolved to provide for their respective ORTEP representations as depicted below (Figures 3.12 and 3.13).

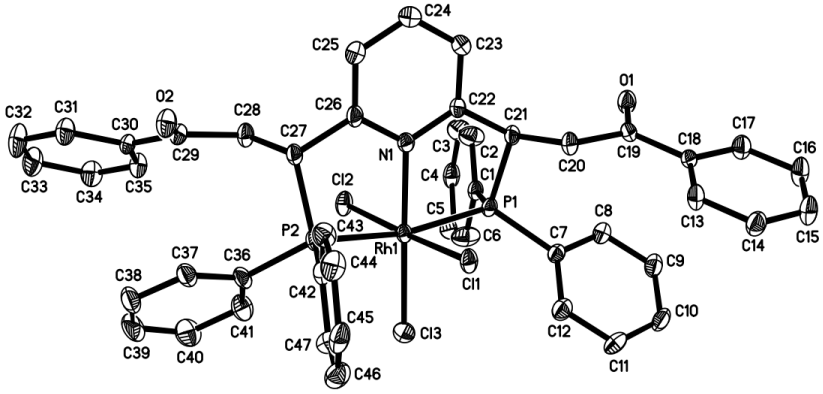

Figure 3.12. ORTEP representation of *racemic* PN(sp^2)P rhodium(III) complex **32a** with thermal ellipsoids drawn at 50% probability level. Hydrogen atoms are omitted for clarity.

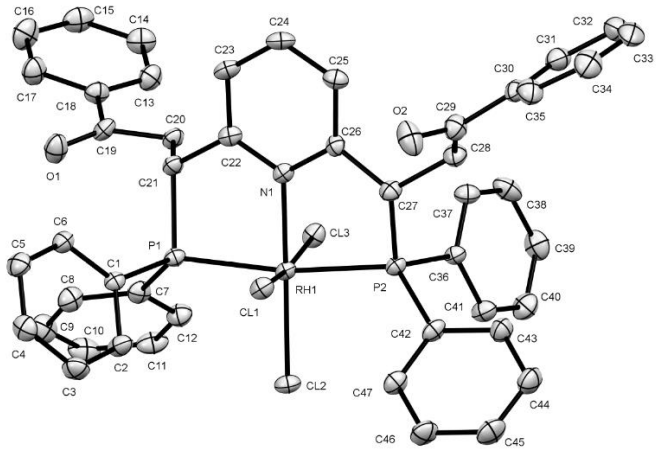

Figure 3.13. ORTEP representation of *meso* PN(sp^2)P rhodium(III) complex **32a'** with thermal ellipsoids drawn at 50% probability level. Hydrogen atoms are omitted for clarity.

For easier illustrative purposes, the selected bond lengths and bond angles of the complexes are summarized in the following table below (Table 3.1).

Bond lengths	Complex **32a**	Complex **32a'**
Rh-N	2.059 Å	2.041 Å
Rh-P	2.298 Å (for P1) 2.313 Å (for P2)	2.324 Å (for P1) 2.305 Å (for P2)
Rh-Cl (*trans* to N)	2.335 Å	2.362 Å
Rh-Cl (*trans* to Cl)	2.351 Å (for Cl1) 2.341 Å (for Cl2)	2.352 Å (for Cl1) 2.343 Å (for Cl3)
Bond angles	Complex **32a**	Complex **32a'**
P-Rh-P	168.47º	170.64º
Cl-Rh-Cl	177.15º	170.43º
N-Rh-P	84.57º (for P1) 83.91º (for P2)	85.20º (for P1) 85.45º (for P2)
P-Rh-Cl (*trans* to N)	93.74º (for P1) 97.79º (for P2)	94.35º (for P1) 95.00º (for P2)

Table 3.1. Selected bond lengths and bond angles for complexes **32a** and **32a'**.

In general, both complexes **32a** and **32a'** adopt an approximate octahedral geometry with slight distortions towards the pyridine ring. This is evidently showcased by an acute bending of the P-Rh-P bond angle in both complexes, each stipulated at values of less than the optimal 180º. The provision of both *racemic* and *meso* solid state structures of complex **32** allows for certain interesting structural comparisons to be made. Essentially, these would solely be influenced based on the physical architectural orientations of the substituents present on the ligand backbone since the electronical make-up of the complexes are effectively identical. One particularly noteworthy comparison is reflected in the apparent disparity of the Rh-Cl bond length for the chloride moiety that is *trans* to the pyridine ring (2.335 Å for *racemic* complex **32a** to 2.362 Å for *meso* complex **32a'**). Judging from the diagrammatical illustrations of both complexes above, it is likely that the bond elongation of the Rh-Cl bond experienced in complex **32a'** is a resultant effect of more extensive steric influence from the projecting bulky PPh_2 groups. This is further corroborated by a difference observed in the Cl-Rh-Cl bond angle, with complex **32a'** having a smaller relative angle of 170.64º compared to 177.15º for complex **32a**, indicating a greater upward distortion that could only be caused by steric repulsion between the Cl and PPh_2 moieties. Based on these correlations, it may be inferred that the relative steric occupancy of the PPh_2 substituents below the P-N-P plane in complex **32a'** is greater than that in complex **32a**, thereby conjuring stronger steric influences to distort the Cl-Rh-Cl bond axis away from the plane. In a similar effect, the chloride moiety *trans* to the pyridine ring which occupies the same spatial face as the PPh_2 groups would comparatively experience a greater steric hindrance in complex **32a'**. Consequently, the increase in bond length of the corresponding Rh-Cl (*trans* to N) bond may be assumed to have been resulted from this spatial limitation between the PPh_2 groups in accommodating the chloride moiety.

An additional possible reasoning to explain for the longer Rh-Cl bond may be surmised from the symmetricity of complex **32a'**. Given the presence of a vertical plane of symmetry in the *meso* configuration, the arrangements of the PPh_2 substituents are therefore inherently uniformly oriented in direction and space. In turn, this generates an approximately equal distribution of the steric requirements and occupancies of the PPh_2 groups within the spatial environment that they are localized in, as indicated by the marginal differences observed between the P-Rh-Cl (*trans* to N) bond angles (94.35º and 95.00º). In this case, it is likely that distortions of the Rh-Cl bond in a horizontal manner would be less favorable to prevent the surfacing of a steric imbalance within the structural configuration. Instead, a vertical distortion is resulted to ultimately cause the increase in length of the Rh-Cl (*trans* to N) bond. Overall however, the generic bond characteristics as noted in Table 3.1 concur fairly well to related PN(sp^2)P rhodium(III) complexes reported in the literature.[44-45] On a separate note, trials in replicating the above complexation using $IrCl_3(MeCN)_3$ were unsuccessful in forming the intended PN(sp^2)P iridium(III) complex, showing absolutely no indications of ligand coordination after extended periods of reaction time under reflux conditions.

3.11. Supplementary reaction trials

With the findings achieved from the abovementioned complexation trials on various metal precursors, supplementary experimental attempts were conducted in general and/or specifically to selected examples to explore the feasibility of furnishing potentially useful complexes for the intended goal of using them for application. These will be respectively illustrated in the ensuing sections.

3.11.1. Experimental attempts with borane protection-deprotection

An evident issue plaguing the access towards clean isolated complexes for the majority of the complexation trials described above can be accustomed to the formation of an inseparable diastereomeric mixture stemming from the ligand synthesis process. Aside from that, attempts to purify the complexed mixture are also hindered by the formation of highly air sensitive complexes, as in the cases for iron and ruthenium. In other examples with the group 10 congeners, formation of end state ionic complexes immediately negated any possibilities of purifications via standard chromatographic methods despite their stability under ambient conditions. Efforts in purification via slow fractional recrystallization were also posed with difficulty for clean separation due to the modest level of diastereoselectivity. In light of this, we sought to separate the diastereomeric mixture of the free ligands prior to complexation so that the eventual furnishment of the complexes would be isomerically pure. To this end, a borane protection-deprotection protocol served as the most viable option due to the inherent air sensitivity of the free diphosphine precursors (Scheme 3.23).

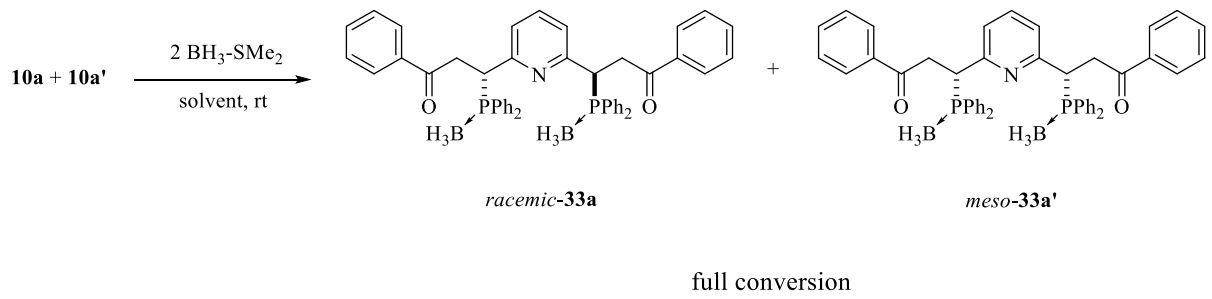

Scheme 3.23. Borane protection of ligand precursors using BH_3-SMe_2.

Reaction of the free diphosphine ligands **10a** and **10a'** with borane dimethylsulfide (BH_3-SMe_2) straightforwardly produced the borane protected diphosphine adducts, which could be conveniently separated on silica gel chromatography to give the diastereomerically pure diphosphine boranes **33a** and **33a'**. However, the separation process required a slow elution of the mobile phase which resulted in a significant loss in product yield likely due to adherence of the basic pyridyl moiety to the acidic stationary phase. Subsequent tries using basic or neutral alumina as well as triethylamine (NEt_3) deactivated silica were unsuccessful in allowing clean separation due to fast elution with all attempted eluent combinations. Nevertheless, we proceeded on with the deprotection trials to assert the feasibility of this protocol.

The deprotection of phosphine boranes conventionally proceeds via the addition of amines for transfer of the borane group.[46] Among the wide range of amines available, several candidates have been identified as effective deprotection partners depending on the electronics of the phosphine moiety.[46] Other than that, deliberate considerations are also required to be made with respect to an appropriate choice of the amine additive. With the intention of utilizing the in-situ generated free diphosphines for direct metalation, a critical factor of consideration involves the ease of removal of the amine borane side products which are known to be capable reducing agents of metals.[47] To circumvent such an occurrence, the use of an amine that would generate a

corresponding volatile amine borane adduct would be the best approach for its convenient removal under vacuum. Additionally in our case, care has to be taken to avert from using an overly nucleophilic amine so as to prevent plausible interactions with the reactive electrophilic carbonyl functionalities present on the ligand backbone.

Initial trials employing NEt_3 as the amine precursor failed to carry out the deprotection reaction even under reflux conditions likely due to its low nucleophilicity. Following assessments utilizing diethylamine and pyrrolidine provided positive indications of borane removal under room temperature conditions. Given the higher boiling points of their respective amine borane adducts, the crude mixture was subjected to evacuation under strong vacuum at heated temperatures of 120ºC for up to 12 hours. Despite this, complete removal of the amine borane side product was still unable to be accomplished as indicated by quick decomposition of $PdCl_2(MeCN)_2$ to palladium black in a preliminary complexation trial with the crude mixture. Unfortunately, the mobile interactions of both the free phosphine and amine borane adducts were similar on all stationary phases, thereby rendering purification of the mixture via a short plug unsuitable. In a final attempt with the deprotection methodology, a synthesis of an ionic derivative of [1,4-diazabicyclo[2.2.2]octane] (DABCO) via methylation with methyl triflate (MeOTf) was performed (Scheme 3.24).

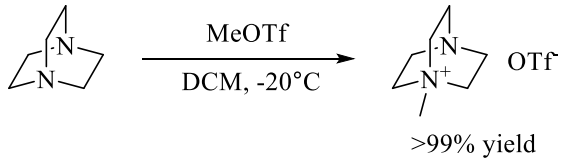

Scheme 3.24. Synthesis of ionic DABCO derivative.

The intention was to generate an ionic amine borane species after deprotection which would expectedly be immobile on silica, hence allowing its direct removal from the pure deprotected ligand under an inert short plug. Much to our dismal, the derivatized DABCO moiety showed no reactivity with the phosphine borane probably due to its reduced nucleophilicity from the introduction of a positive charge on the overall molecule. In a separate reaction trial, attempts at reduction of the purified phosphine sulfide isomers using Raney nickel were also met with no apparent reaction occurrence, with the sulfur remaining bound to the phosphine moieties despite severe reflux conditions.

3.11.2. Experimental attempts with PN(sp^2)P rhodium(III) complexes 32

We next shifted our attention towards the functionalization of the PN(sp^2)P rhodium(III) complexes **32** that could be synthesized with good yields and purity. In order to probe their plausible applicability, it was necessary to investigate the lability of the chloride ligands or the ease of their substitution with more labile ligands for the provision of vacant sites to mediate reactions. Initial attempts were conducted using standard methods of chloride substitution via metathesis with common silver additives. Specifically, silver salts comprised of weakly or non-coordinating anions namely silver acetate (AgOAc) and silver perchlorate ($AgClO_4$) were chosen for the reaction to fulfill the above stated motivation (Scheme 3.25).

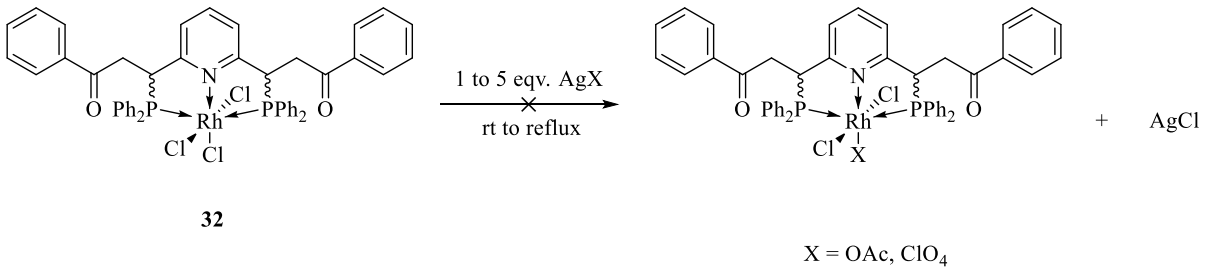

32

Scheme 3.25. Chloride substitution trials on complexes **32** using silver additives.

Surprisingly, treatment of the rhodium complexes with an equivalence of the silver salts resulted with no observable changes to the complex based on crude NMR analysis. Further subjecting the crude mixture under harsher reflux conditions were also fruitless in achieving chloride abstraction. More unexpectedly, addition of excess stoichiometry of the silver salt in up to five equivalences were returned with similar outcomes bearing no chloride substitution.

Without any promising leads with the metathesis reaction, we then directed our focus towards an alternative manner of complex activation via attempts to reduce the rhodium(III) center (Scheme 3.26).

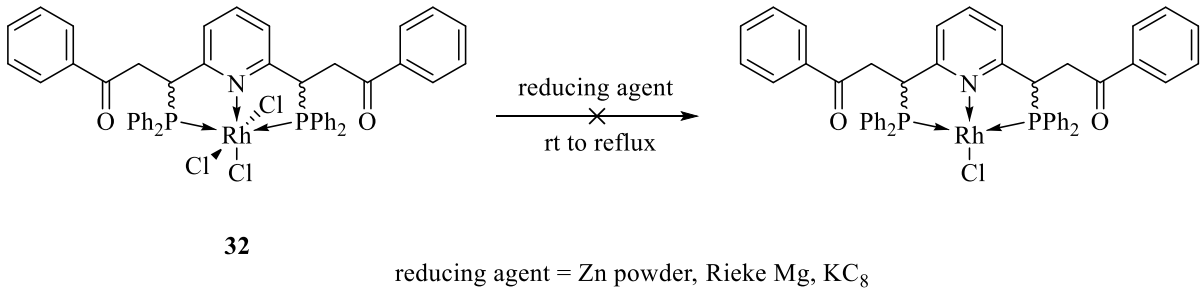

Scheme 3.26. Reduction trials on complexes **32** using illustrated reducing agents.

Reports in the literature for the reduction of analogous rhodium(III) centers involved in bonding within a complex were however seemingly rare, and our efforts could only be limited to the methods employed within the selected few examples that were found.[45, 48] Reacting complexes **32** with activated zinc powder under room temperature to refluxed temperatures did not yield the intended corresponding reduced complexes, which could be easily determined by $^{31}P\{^{1}H\}$ NMR analysis of the Rh-P coupling constant.[44] Additional trials were also conducted using highly activated Rieke magnesium by virtue of its lower reduction potential in comparison to zinc. Nonetheless, reactions done under similar conditions as that of the zinc trials proved futile in

instigating the desired reduction occurrence. In a last ditch effort, utilization of the strongly reducing potassium graphite (KC_8) reagent again under reflux conditions was equally ineffective for the reduction of complexes **32**.

Despite the uneventful outcomes observed, the reactions performed were noteworthy in shedding some insights towards the chemical resilience of the pincer scaffold. Of particular significance is the tolerability of the carbonyl functionalities under strong reducing conditions, displaying no evident reduction of the ketone group even with their concomitant exposure to elevated temperature conditions. Additionally, the electronic properties of the PN(sp^2)P tridentate were also illustrated in the metathesis reactions, with the chemical inertness of the Rh-Cl bond likely ascribed to a probable lack of electronic stabilization provided by the ligand onto the highly electron deficient rhodium(III) center. This may be justified with reference to literature reports in the similar employment of silver additives to coordinatively saturated rhodium(III) pincer complexes, which were successful in facilitating metal mediated reactions from the generation of a vacant site via chloride abstraction.[49]

3.12. Conclusion

In closing for this chapter, a thorough exploration towards the compatible affixation of the synthesized PN(sp^2)P tridentates **10a** and **10a'** to various metal centers belonging to Group 8, 9 and 10 was conducted to elucidate the structural characteristics of the corresponding furnished pincer complexes. These were extensively investigated and discussed based on solution and solid state characterizations, revealing certain associative trends and differences between complexed metallic congeners within the same periodic group. Additional comparisons were also made to related analogous PN(sp^2)P complexes in the literature, highlighting the probable causal effects brought about by the ligand properties of **10a** and **10a'** in affecting the ease of formation of the intended complexes as well as the consequential stability of the formed complexes.

Supplementary experimental efforts were also performed in a bid to overcome the synthetic issue relating to diastereomeric impurity. These were conducted with the higher motivation of furnishing isomerically pure complexes which could be further probed for reaction and/or catalytic applicability. Unfortunately, attempts in achieving this objective were met with both synthetic and reactivity difficulties, some of which were unexpected despite following similar reaction protocols employed in existing literature. Nevertheless, the trials executed provided interesting and valuable insights to the stability of the ligand auxiliary, which would be useful for its subsequent assessments in other possible reaction employments.

Experimental and Methods

General information

All experimental procedures follow the same necessary preparations and conducts as previously described in Chapter 2 unless otherwise stated. Laboratory equipment used also follow similarly to those represented in Chapter 2.

Materials

Syntheses of the metal precursors; $RuCl_2(PPh_3)_3$,[50] $RuCl_2(pyridine)_4$,[51] $PdCl_2(MeCN)_2$,[52] $RhCl_3(MeCN)_3$[53] were performed according to literature methods. All other reagents were procured from Sigma Aldrich and used directly as supplied.

General procedure for the preparation of *racemic* and *meso* diphosphines 10a and 10a'

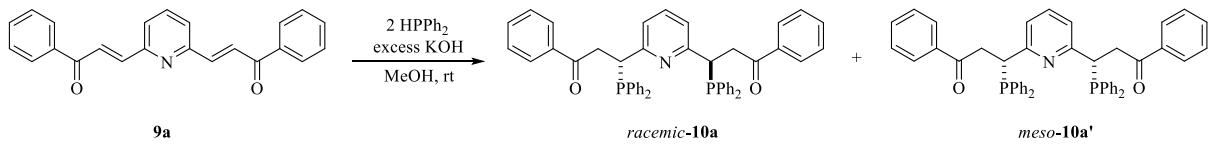

Scheme 3.27. Synthetic outline for preparation of *racemic* and *meso* diphosphines **10a** and **10a'**.

A 10 mL storage tube was charged with substrate **9a** (0.029 mmol, 1.0 equiv.) in methanol (1 mL) before diphenylphosphine (10.7 mg, 0.057 mmol, 2.0 equiv.) was added with washing using another portion of methanol (0.5-1 mL). A small pellet of KOH was tipped into the reaction vessel and the resultant mixture was left to stir overnight for 16 hours at room temperature, forming a white suspension with full conversion of diphenylphosphine. The reaction vessel was evacuated under vacuum for removal of methanol and the formed solids were subsequently redissolved with toluene (2 mL). Extraction via cannula was performed with toluene (3 x 2 mL) and washed using water (1 x 2 mL) to obtain a pale yellow solution of *racemic* and *meso* diphosphines **10a** and **10a'**. The toluene mixture can be immediately used for metalation or otherwise re-evacuated under reduced pressure for use with an alternative solvent.

General procedures for complexation trials with metal precursors

Complexation procedure with FeX_2 precursors

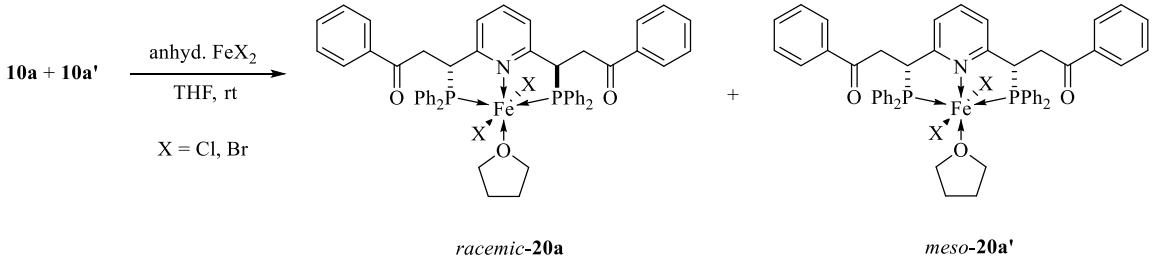

Scheme 3.28. Synthetic outline for complexation experiment using FeX_2 precursors with postulated products **20a** and **20a'**.

Following the above protocol to synthesize diphosphines **10a** and **10a'**, the extracted mixture was evacuated under vacuum to first remove toluene before being redissolved with THF (2 mL). The anhydrous iron(II) halide precursors (0.029 mmol, 1.0 equiv.) were added into a separate 10 mL storage flask under an inert environment within a glovebox and carefully sealed before being brought out for connection to the Schlenk line. Subsequent transfer of the THF solution containing the ligand precursors via cannula into the reaction vessel containing the metal precursor formed a resultant pale yellow solution which gradually turned darker yellow within a few minutes. Analysis of the crude mixture on NMR revealed the formation of a paramagnetic species which cannot be further characterized.

Complexation procedure with $Fe(BF_4)_2.6H_2O$

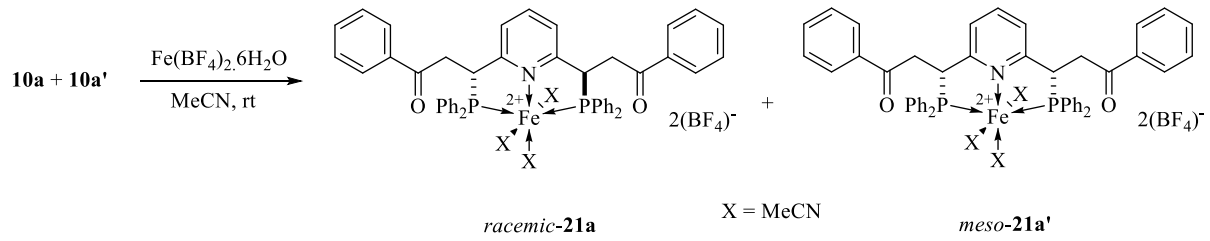

Scheme 3.29. Synthetic outline for complexation experiment using $Fe(BF_4)_2.6H_2O$ and the postulated solution state products **21a** and **21a'**.

Following the above protocol to synthesize diphosphines **10a** and **10a'**, the extracted mixture was evacuated under reduced pressure to first remove toluene before addition of acetonitrile (2 mL) to form an insoluble suspension. Subsequent addition of $Fe(BF_4)_2.6H_2O$ (0.029 mmol, 1.0 equiv.) into the mixture formed a resultant clear orange solution immediately, which was left to continue stirring for 1 hour at room temperature until reaction completion as confirmed by $^{31}P\{^1H\}$ NMR analysis. The furnished products were characterized as a diastereomeric mixture due to their instability in open atmosphere which disallowed further purifications of the crude mixture. Slow liquid diffusion recrystallization of the crude mixture in MeCN/diethyl ether managed to afford a single crystal representing *racemic* complex **22,** which is structurally different from the solution state configuration of the complex as postulated by complexes **21a** and **21a'**. NMR characterizations of the solution state mixture are thus represented without exact structural confirmation.

Complexation procedure with $RuCl_2(PPh_3)_3$

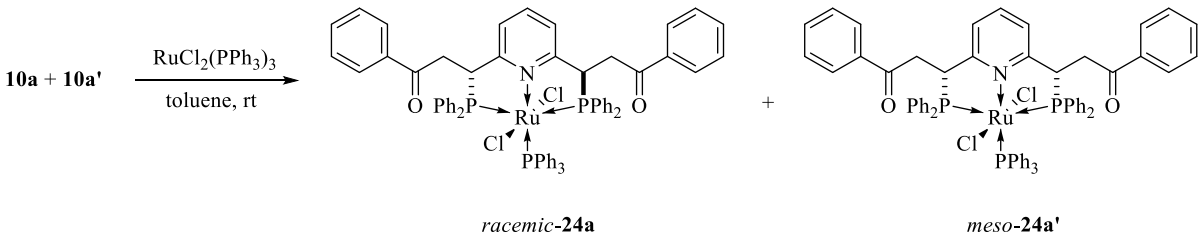

Scheme 3.30. Synthetic outline for complexation experiment using $RuCl_2(PPh_3)_3$.

Following the above protocol to synthesize diphosphines **10a** and **10a'**, the extracted toluene mixture was used directly with the in-situ addition of $RuCl_2(PPh_3)_3$ (0.029 mmol, 1.0 equiv.) and stirred at room temperature. Formation of a clear yellow solution was observed within a few minutes and the resultant mixture was left to continue stirring for 1 hour until reaction completion as confirmed by $^{31}P\{^1H\}$ NMR analysis. The furnished products were characterized as a diastereomeric mixture due to their instability in open atmosphere which disallowed further purifications of the crude mixture. Slow liquid diffusion recrystallization of the crude mixture in DCM/*n*-hexane managed to afford a single crystal representing *racemic* complex **24a**.

Complexation procedure with $RuCl_2(py)_4$

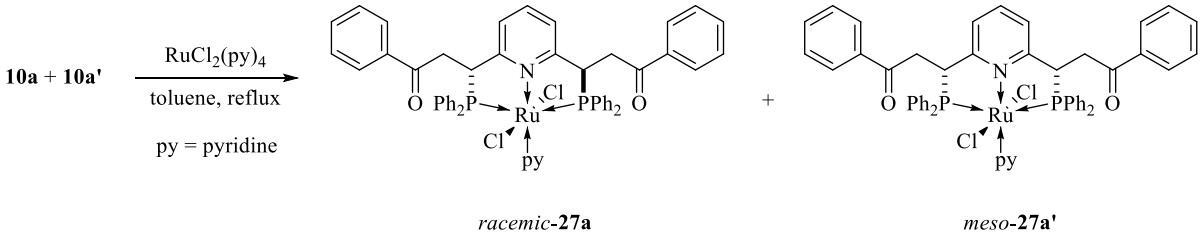

Scheme 3.31. Synthetic outline for complexation experiment using $RuCl_2(py)_4$.

Following the above protocol to synthesize diphosphines **10a** and **10a'**, the extracted toluene mixture was used directly with the in-situ addition of $RuCl_2(py)_4$ (0.029 mmol, 1.0 equiv.) and stirred under reflux. Formation of a clear dark yellow solution was observed within a few minutes and the resultant mixture was left to continue stirring for 6 hours until reaction completion as confirmed by $^{31}P\{^1H\}$ NMR analysis. Solvents were removed via rotary evaporation and the crude mixture was purified via a flash silica gel column chromatography in DCM/EA to afford the isomerically pure complexes **27a** and **27a'**.

For characterization purposes, a separate upscaled experimental conduct following the procedure as previously mentioned in Chapter 2 (page 111, Scheme 2.14) was performed. After complete consumption of the substrate as confirmed using TLC, the crude mixture was subjected to vacuum for the removal of acetone, before being redissolved with toluene (8 mL). $RuCl_2(py)_4$ (0.216 mmol, 1.0 equiv.) was then added and the resultant mixture was left to stir under reflux for 6 hours until reaction completion as confirmed by $^{31}P\{^1H\}$ NMR analysis. Solvents were removed via rotary evaporation and the crude mixture was purified via a flash silica gel column chromatography in DCM/EA to afford the isomerically pure complexes **27a** and **27a'**.

Complexation procedure with $NiCl_2$(dme)

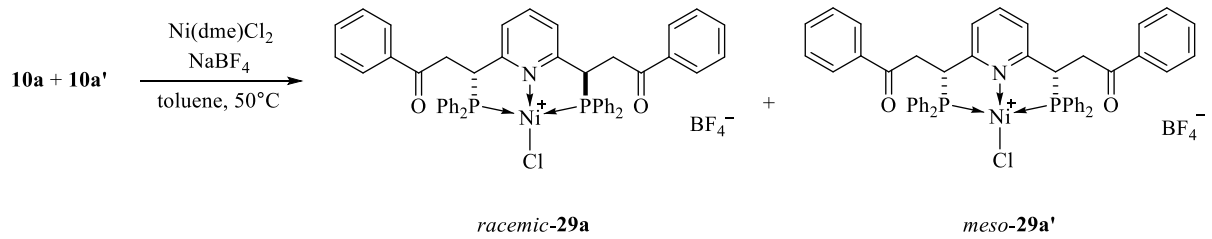

Scheme 3.32. Synthetic outline for complexation experiment using $NiCl_2$(dme).

Following the above protocol to synthesize diphosphines **10a** and **10a'**, the extracted toluene mixture was used directly with the in-situ addition of $NiCl_2$(dme) (0.029 mmol, 1.0 equiv.) and $NaBF_4$ (0.029 mmol, 1.0 equiv.) at room temperature to form a dark purple solution. The resultant mixture was stirred at 50ºC for 2 days until reaction completion as confirmed by $^{31}P\{^1H\}$ NMR analysis, forming an orange suspension. Solvents were removed via rotary evaporation and the products were redissolved in CD_2Cl_2 for characterization as a diastereomeric mixture due to their ionic nature which disallowed further purifications. Slow fractional recrystallization of the crude mixture in DCM/*n*-hexane managed to afford a single crystal representing *meso* complex **29a'**.

Complexation procedure with $PdCl_2(MeCN)_2$

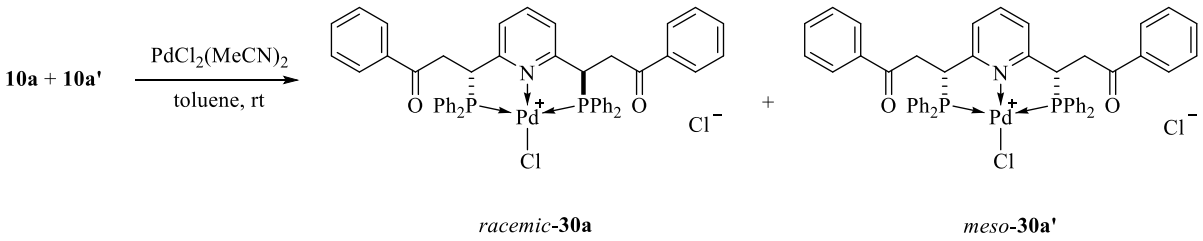

Scheme 3.33. Synthetic outline for complexation experiment using $PdCl_2(MeCN)_2$.

Following the above protocol to synthesize diphosphines **10a** and **10a'**, the extracted toluene mixture was used directly with the in-situ addition of $PdCl_2(MeCN)_2$ (0.029 mmol, 1.0 equiv.) and stirred at room temperature. Formation of a clear yellow solution was observed within a few minutes and the resultant mixture was left to continue stirring for 1 hour until reaction completion as confirmed by $^{31}P\{^1H\}$ NMR analysis. Solvents were removed via rotary evaporation and the products were redissolved in CD_2Cl_2 for characterization as a diastereomeric mixture due to their ionic nature which disallowed further purifications. Slow fractional recrystallization of the crude mixture in DCM/*n*-hexane managed to afford a single crystal representing *meso* complex **30a'**.

Complexation procedure with K_2PtCl_4

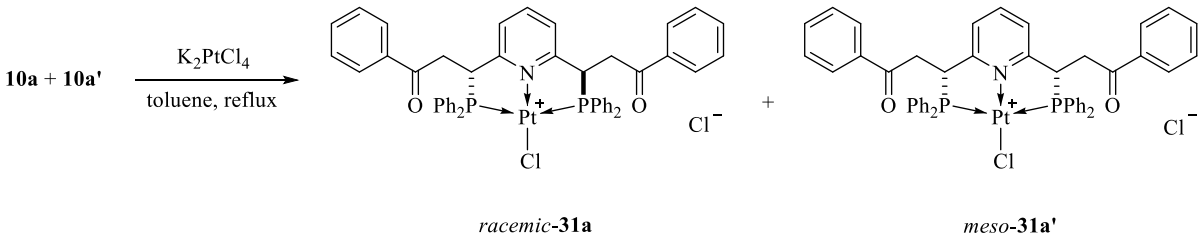

Scheme 3.34. Synthetic outline for complexation experiment using K_2PtCl_4.

Following the above protocol to synthesize diphosphines **10a** and **10a'**, the extracted toluene mixture was used directly with the in-situ addition of K_2PtCl_4 (0.029 mmol, 1.0 equiv.) and stirred under reflux. The resultant mixture was left to continue stirring for 7 days until reaction completion as confirmed by $^{31}P\{^1H\}$ NMR analysis, forming a white suspension. Solvents were removed via rotary evaporation and the products were redissolved in CD_2Cl_2 for characterization as a diastereomeric mixture due to their ionic nature which disallowed further purifications. Slow fractional recrystallization of the crude mixture in DCM/*n*-hexane managed to afford a single crystal representing *meso* complex **31a'**.

Complexation procedure with $RhCl_3(MeCN)_3$

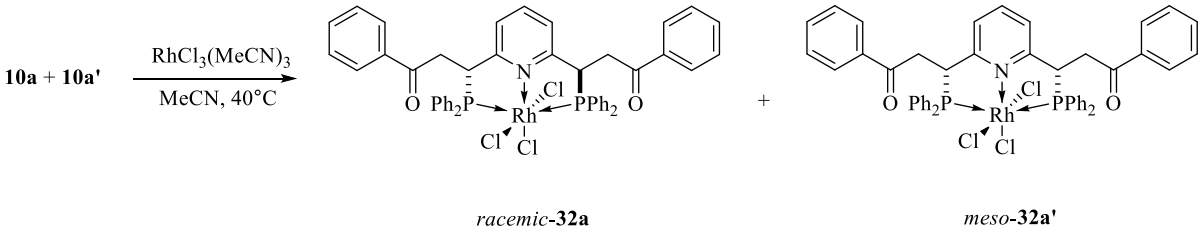

Scheme 3.35. Synthetic outline for complexation experiment using $RhCl_3(MeCN)_3$.

Following the above protocol to synthesize diphosphines **10a** and **10a'**, the extracted mixture was evacuated under reduced pressure to first remove toluene before addition of acetonitrile (2 mL) to form an insoluble suspension. Subsequent addition of $RhCl_3(MeCN)_3$ (0.029 mmol, 1.0 equiv.) into the mixture formed a resultant clear yellow solution within a few minutes, which was left to continue stirring for 5 hours at 40ºC until reaction completion as confirmed by $^{31}P\{^1H\}$ NMR analysis. Solvents were removed via rotary evaporation and the crude mixture was purified via a flash silica gel column chromatography in DCM to afford the isomerically pure complexes **32a** and **32a'**. Single crystals of both *racemic* complex **32a** and *meso* complex **32a'** were obtained from slow fractional recrystallization of the respective isolated compounds in DCM/*n*-hexane.

General procedure for phosphine borane protection

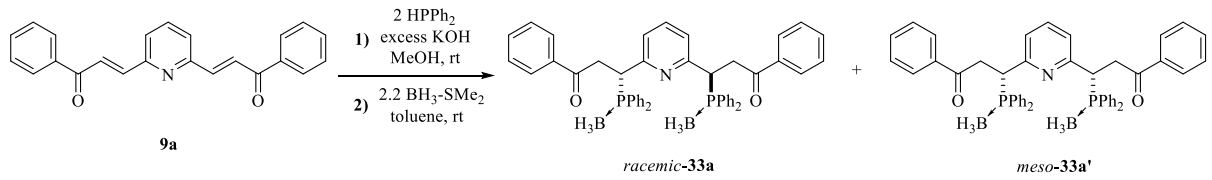

Scheme 3.36. Synthetic outline for borane protection using BH_3-SMe_2.

A 10 mL storage tube was charged with substrate **9a** (0.144 mmol, 1.0 equiv.) in methanol (3 mL) before diphenylphosphine (53.5 mg, 0.287 mmol, 2.0 equiv.) was added with washing using another portion of methanol (1 mL). A small pellet of KOH was tipped into the reaction vessel and the resultant mixture was left to stir overnight for 16 hours at room temperature, forming a white suspension. The reaction vessel was evacuated under vacuum for removal of methanol and the formed solids were subsequently redissolved with toluene (2 mL). Extraction via cannula was performed with toluene (3 x 2 mL) and washed using water (1 x 2 mL) to obtain a pale yellow solution of *racemic* and *meso* diphosphines **10a** and **10a'**. The toluene mixture was dried with stirring over $MgSO_4$ and thereafter filtered for immediate use in reaction with BH_3-SMe_2 (0.317 mmol 2.2 equiv.) at room temperature until complete conversion of the free phosphine as determined by $^{31}P\{^1H\}$ NMR analysis of the crude mixture. Solvents were removed via rotary evaporation and the crude mixture was purified via silica gel column chromatography in DCM/*n*-hexane to afford the isomerically pure phosphine borane adducts **33a** and **33a'**

Characterization data of PN(sp^2)P complexes

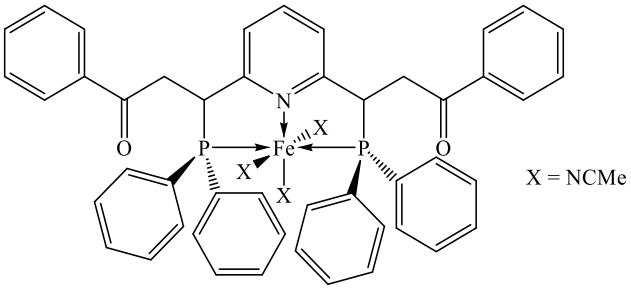

21a/21a' (reported as a diastereomeric mixture for solution state characterization). Orange solution. ^{1}H NMR (CD_3CN, 500 MHz): δ 1.97 (br s, C*H*$_3$CN), 2.25 (br s, C*H*$_3$CN), 2.82-2.93 (br m, PCHC*H*), 3.12-3.25 (br m, PCHC*H*), 3.67-3.85 (br m, overlap of 2 sets of PCHC*H*), 4.70-4.81 (br m, PC*H*), 5.56-5.67 (br m, PC*H*), 7.12-7.91 (m, Ar); ^{31}P{^{1}H} NMR (CD_3CN, 202 MHz): δ 73.3, 77.2.

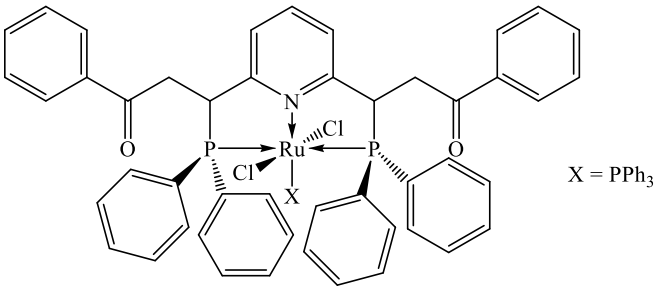

24a/24a' (reported as an inseparable diastereomeric mixture). Yellow solid. ^{1}H NMR (CD_2Cl_2, 400 MHz): δ 3.14-3.22 (m, overlap of 2 sets of PCHC*H*), 3.31-3.41 (m, PCHC*H*), 3.60-3.65 (m, PCHC*H*), 5.74-5.86 (m, PC*H*), 6.11-6.20 (m, PC*H*), 6.78-7.73 (m, Ar); ^{31}P{^{1}H} NMR (CD_2Cl_2, 162 MHz): δ 39.3 (t, $^{2}J_{PP}$ = 29.6 Hz), 43.4 (t, $^{2}J_{PP}$ = 28.2 Hz), 47.7 (d, $^{2}J_{PP}$ = 29.6 Hz), 59.1 (d, $^{2}J_{PP}$ = 27.8 Hz).

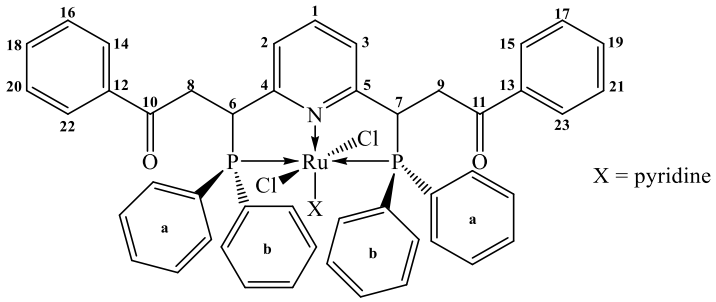

Figure 3.14. General labelling of carbon atoms for complexes **27**.

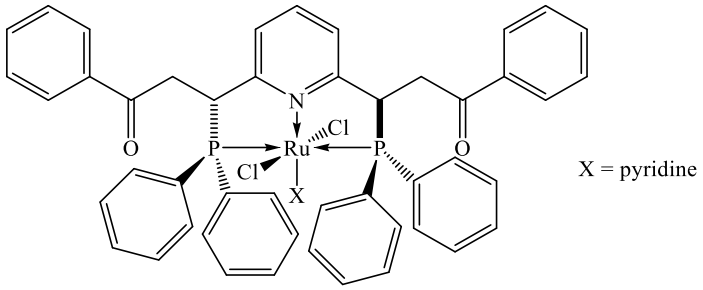

27a. Yellow solid. Yield: 79.0 mg, 0.082 mmol, 38%. $[\alpha]_D^{25}$ = -157.3 (*c* = 1.48, CH_2Cl_2). ^{1}H NMR (CD_2Cl_2, 400 MHz): δ 3.41-3.50 (m, 2H, PCHC*H*), 3.81-3.89 (m, 2H, PCHC*H*), 5.65-5.73 (m, 2H, PC*H*), 7.00-7.04 (m, 2H, Ar), 7.10-7.23 (m, 8H Ar), 7.29-7.55 (m, 22H, Ar), 7.62-7.69 (m, 4H, Ar), 8.92-9.02 (m, 2H, Ar); ^{31}P{^{1}H} NMR (CD_2Cl_2, 162 MHz): δ 58.2. ^{13}C{^{1}H} NMR (CD_2Cl_2, 100 MHz): δ 43.0 (s, 2C, C8 and C9), 48.2 (vt, 2C, $^1J_{CP}$ = 10.3 Hz, C6 and C7), 120.7 (vt, 2C, $^3J_{CP}$ = 5.2 Hz, C2 and C3), 123.6 (s, 2C, Cpy^{meta}) 128.08 (s, 1C, C1), 128.10 (s, 1C, Cpy^{para}), 128.5 (s, 4C, C16, C17, C20 and C21) 128.8 (s, 4C, C14, C15, C22 and C23), 129.5 (s, 4C, Ca^{meta}), 130.2 (s, 4C, Cb^{meta}), 130.9 (vt, 2C, $^1J_{CP}$ = 17.4 Hz, Ca^{ipso}), 133.5 (s, 2C, C18 and C19), 133.8 (vt, 4C, $^2J_{CP}$ = 5.1 Hz, Ca^{ortho}), 133.9 (vt, 2C, $^1J_{CP}$ = 17.5 Hz, Cb^{ipso}), 135.1 (s, 2C, Ca^{para}), 135.70 (vt, 4C, $^2J_{CP}$ = 5.2 Hz, Cb^{ortho}), 135.71 (s, 2C, Cb^{para}), 136.7 (s, 2C, C12 and C13), 156.9 (s, 2C, Cpy^{ortho}), 170.1 (vt, 2C, $^2J_{CP}$ = 5.8 Hz, C4 and C5), 198.3 (s, 2C, C10 and C11). HRMS (ESI) m/z: $(M + H)^+$ calcd for $C_{52}H_{45}Cl_2N_2O_2P_2Ru$, 962.1299; found, 962.1291.

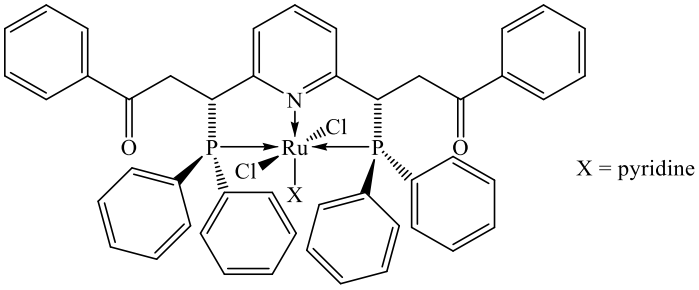

27a'. Yellow solid. Yield: 48.9 mg, 0.051 mmol, 24%. ^{1}H NMR (CD_2Cl_2, 400 MHz): δ 3.62-3.69 (m, 2H, PCHC*H*), 3.84-3.90 (m, 2H, PCHC*H*), 5.55-5.64 (m, 2H, PC*H*), 7.03-7.06 (m, 2H, Ar), 7.16-7.22 (m, 6H Ar), 7.25-7.38 (m, 15H, Ar), 7.41-7.57 (m, 9H, Ar), 7.64-7.71 (m, 4H, Ar), 8.99-9.08 (m, 2H, Ar); ^{31}P{^{1}H} NMR (CD_2Cl_2, 162 MHz): δ 57.7; ^{13}C{^{1}H} NMR (CD_2Cl_2, 100 MHz): δ 42.2 (s, 2C, C8 and C9), 48.3 (vt, 2C, $^{1}J_{CP}$ = 9.9 Hz, C6 and C7), 120.4 (vt, 2C, $^{3}J_{CP}$ = 5.1 Hz, C2 and C3), 123.7 (s, 2C, Cpy^{meta}) 128.1 (s, 1C, C1), 128.2 (s, 1C, Cpy^{para}), 128.5 (s, 4C, C16, C17, C20 and C21) 128.8 (s, 4C, C14, C15, C22 and C23), 129.7 (s, 4C, Ca^{meta}), 130.0 (s, 4C, Cb^{meta}), 131.2 (vt, 2C, $^{1}J_{CP}$ = 17.9 Hz, Ca^{ipso}), 133.5 (s, 2C, C18 and C19), 133.7 (vt, 2C, $^{1}J_{CP}$ = 17.9 Hz, Cb^{ipso}), 134.2 (vt, 4C, $^{2}J_{CP}$ = 5.2 Hz, Ca^{ortho}), 135.1 (s, 2C, Ca^{para}), 135.4 (vt, 4C, $^{2}J_{CP}$ = 5.4 Hz, Cb^{ortho}), 135.7 (s, 2C, Cb^{para}), 136.7 (s, 2C, C12 and C13), 157.0 (s, 2C, Cpy^{ortho}), 169.9 (vt, 2C, $^{2}J_{CP}$ = 6.1 Hz, C4 and C5), 198.2 (s, 2C, C10 and C11). HRMS (ESI) m/z: $(M + H)^+$ calcd for $C_{52}H_{45}Cl_2N_2O_2P_2Ru$, 962.1299; found, 962.1296.

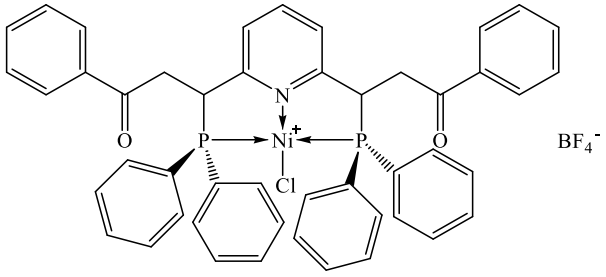

29a/29a' (reported as an inseparable diastereomeric mixture). Orange solid. ^{1}H NMR (CD_2Cl_2, 400 MHz): δ 3.27-3.49 (m, overlap of 2 sets of PCHC*H*), 3.55-3.67 (m, PCHC*H*), 4.12-4.23 (m, PCHC*H*), 4.33-4.46 (m, PC*H*), 4.51-4.64 (m, PC*H*), 6.75-8.17 (m, Ar); ^{31}P{^{1}H} NMR (CD_2Cl_2, 162 MHz): δ 32.6, 32.9. HRMS (ESI) m/z: $(M + H)^+$ calcd for $C_{47}H_{40}BClF_4NO_2P_2Ni$, 891.1528; found, 891.1531.

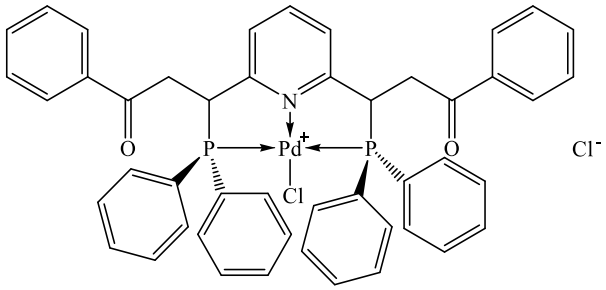

30a/30a' (reported as an inseparable diastereomeric mixture). Yellow solid. ^{1}H NMR (CD_2Cl_2, 400 MHz): δ 3.40-3.48 (m, PCHC*H*), 3.85-3.98 (m, overlap of 2 sets of PCHC*H*), 4.44-4.53 (m, PCHC*H*), 5.56-5.61 (m, PC*H*), 5.78-5.83 (m, PC*H*), 7.30-8.24 (m, Ar); ^{31}P{^{1}H} NMR (CD_2Cl_2, 162 MHz): δ 32.4, 37.2; HRMS (ESI) m/z: $(M + H)^+$ calcd for $C_{47}H_{40}Cl_2NO_2P_2Pd$, 852.1179; found, 852.1183.

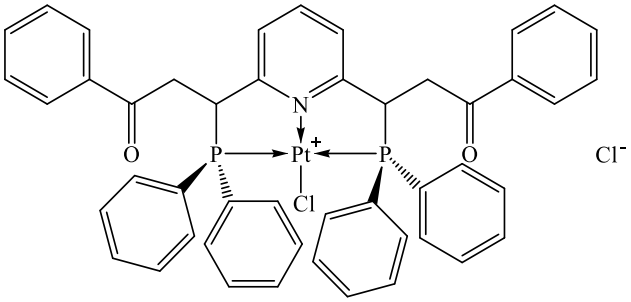

31a/31a' (reported as an inseparable diastereomeric mixture). Off-white solid. ^{1}H NMR (CD_2Cl_2, 400 MHz): δ 3.45-3.64 (m, PCHC*H*), 3.71-3.84 (m, PCHC*H*), 4.02-4.18 (m, PCHC*H*), 4.33-4.48 (m, PCHC*H*), 5.65-5.76 (m, PC*H*), 5.82-5.91 (m, PC*H*), 7.20-8.38 (m, Ar); ^{31}P{^{1}H} NMR (CD_2Cl_2, 162 MHz): δ 31.8, 33.7; HRMS (ESI) m/z: $(M + H)^+$ calcd for $C_{47}H_{40}Cl_2NO_2P_2Pt$, 976.1481; found, 976.1486.

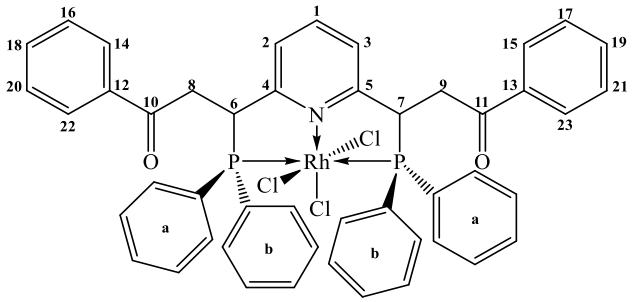

Figure 3.15. General labelling of carbon atoms for complexes **32a** and **32a'**.

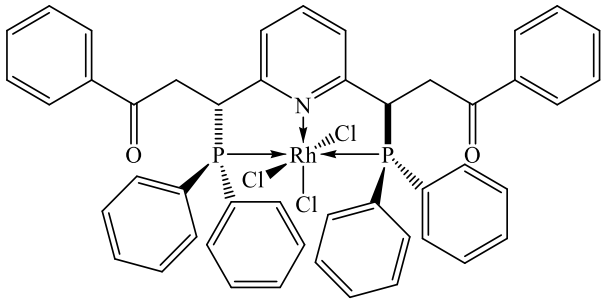

32a. Yellow solid. Yield: 12.3 mg, 13.3 µmol, 46%. ^{1}H NMR (CD_2Cl_2, 400 MHz): δ 3.33 (ddd, 2H, $^{2}J_{HH}$ = 19.5 Hz, $^{3}J_{HP}$ = 10.5 Hz, $^{3}J_{HH}$ = 5.3 Hz, PCHC*H*), 4.13 (ddd, 2H, $^{2}J_{HH}$ = 19.5 Hz, $^{3}J_{HH}$ = 12.5 Hz, $^{3}J_{HP}$ = 6.4 Hz, PCHC*H*), 5.98-6.03 (m, 2H, PC*H*), 7.19-7.28 (m, 10H, Ar), 7.45-7.56 (m, 12H, Ar), 7.61-7.67 (m, 6H, Ar), 7.76-7.80 (m, 1H, Ar), 8.07-8.11 (m, 4H, Ar); ^{31}P{^{1}H} NMR (CD_2Cl_2, 162 MHz): δ 37.1 (d, $^{1}J_{RhP}$ = 89.0 Hz); ^{13}C{^{1}H} NMR (CD_2Cl_2, 100 MHz): δ 45.4 (s, 2C, C8 and C9), 46.8 (vt, 2C, $^{1}J_{CP}$ = 12.3 Hz, C6 and C7), 123.7 (vt, 2C, $^{3}J_{CP}$ = 5.6 Hz, C2 and C3), 125.9 (vt, 2C, $^{1}J_{CP}$ = 25.4 Hz, Ca^{ipso}), 127.96 (s, 4C, C16, C17, C20 and C21), 128.03 (s, 4C, Ca^{meta}), 128.1 (s, 1C, C1), 128.4 (s, 4C, C14, C15, C22 and C23), 130.3 (s, 2C, C18 and C19), 130.5 (vt, 2C, $^{1}J_{CP}$ = 25.2 Hz, Cb^{ipso}), 131.5 (s, 2C, Ca^{para}), 133.0 (vt, 4C, $^{2}J_{CP}$ = 5.0 Hz, Ca^{ortho}), 133.5 (s, 4C, Cb^{meta}), 135.5 (s, 2C, Cb^{para}), 137.4 (vt, 4C, $^{2}J_{CP}$ = 6.1 Hz, Cb^{ortho}), 140.0 (s, 2C, C12 and C13), 168.6 (vt, 2C, $^{2}J_{CP}$ = 6.1 Hz, C4 and C5), 196.4 (s, 2C, C10 and C11). HRMS (ESI) m/z: $(M + H)^+$ calcd for $C_{47}H_{39}Cl_3NO_2P_2Rh$, 919.0577; found, 919.0581.

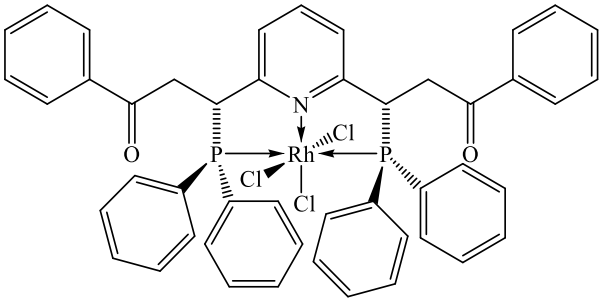

32a'. Yellow solid. Yield: 12.8 mg, 13.9 µmol, 48%. ^{1}H NMR (CD_2Cl_2, 400 MHz): δ 3.71 (pseudo ddd, 2H, $^{2}J_{HH}$ = 19.0 Hz, $^{3}J_{HP}$ = 10.5 Hz, $^{3}J_{HH}$ = 3.2 Hz, PCHC*H*), 3.94 (pseudo ddd, 2H, $^{2}J_{HH}$ = 18.9 Hz, $^{3}J_{HH}$ = 9.7 Hz, $^{3}J_{HP}$ = 5.8 Hz, PCHC*H*), 5.92-5.98 (m, 2H, PC*H*), 7.31-7.53 (m, 20H, Ar), 7.66-7.68 (m, 4H, Ar), 7.74-7.78 (m, 1H, Ar), 7.83-7.89 (m, 8H, Ar); ^{31}P{^{1}H} NMR (CD_2Cl_2, 162 MHz): δ 39.6 (d, $^{1}J_{RhP}$ = 89.0 Hz); ^{13}C{^{1}H} NMR (CD_2Cl_2, 100 MHz): δ 42.3 (s, 2C, C8 and C9), 46.8 (vt, 2C, $^{1}J_{CP}$ = 11.7 Hz, C6 and C7), 122.8 (vt, 2C, $^{3}J_{CP}$ = 5.4 Hz, C2 and C3), 126.4 (vt, 2C, $^{1}J_{CP}$ = 24.4 Hz, Ca^{ipso}), 128.1-128.2 (overlapped, 8C, C16, C17, C20, C21 and Ca^{meta}), 128.4 (s, 1C, C1), 128.6 (s, 4C, C14, C15, C22 and C23), 128.8 (vt, 2C, $^{1}J_{CP}$ = 25.1 Hz, Cb^{ipso}), 130.9 (s, 2C, Ca^{para}), 131.2 (s, 2C, Cb^{para}) 133.7 (s, 4C, Cb^{meta}), 134.1 (vt, 4C, $^{2}J_{CP}$ = 5.2 Hz, Ca^{ortho}), 135.6 (s, 2C, C18 and C19), 135.9 (vt, 4C, $^{2}J_{CP}$ = 5.6 Hz, Cb^{ortho}), 139.9 (s, 2C, C12 and C13), 167.4 (vt, 2C, $^{2}J_{CP}$ = 5.1 Hz, C4 and C5), 196.1 (s, 2C, C10 and C11). HRMS (ESI) m/z: $(M + H)^+$ calcd for $C_{47}H_{39}Cl_3NO_2P_2Rh$, 919.0577; found, 919.0575.

Characterization data of phosphine boranes 33

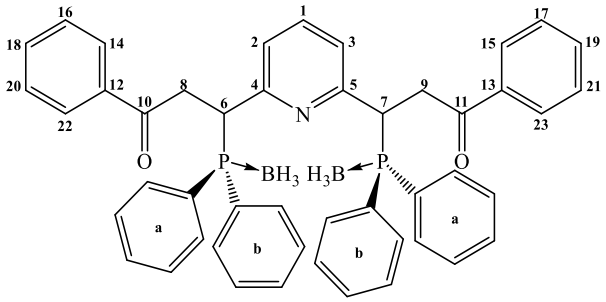

Figure 3.16. General labelling of carbon atoms for phosphine boranes **33a** and **33a'**.

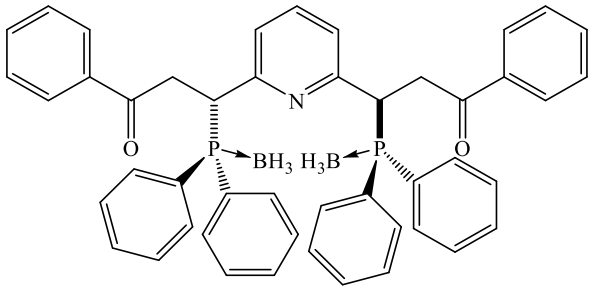

33a. White solid. Yield: 10.6 mg, 14.3 µmol, 10%. ^{1}H NMR (CD_2Cl_2, 400 MHz): δ 0.87-1.42 (br s, 6H, B*H*$_3$), 3.43-3.52 (m, 2H, PCHC*H*), 4.56-4.67 (m, 4H, overlap of PCHC*H* and PC*H*), 6.62 (pseudo d, 2H, $^{3}J_{HH}$ = 7.7 Hz, NCC*H*), 6.93 (t, 1H, $^{3}J_{HH}$ = 7.7 Hz, NCCHC*H*), 7.16-7.65 (m, 26H, Ar), 7.88-7.90 (m, 4H, Ar); ^{31}P{^{1}H} NMR (CD_2Cl_2, 162 MHz): δ 26.6; ^{13}C{^{1}H} NMR (CD_2Cl_2, 100 MHz): δ 39.5 (d, 2C, $^{2}J_{CP}$ = 5.3 Hz, C8 and C9), 40.6 (d, 2C, $^{1}J_{CP}$ = 32.6 Hz, C6 and C7), 124.5 (s, 2C, C2 and C3), 128.3 (d, 2C, $^{1}J_{CP}$ = 53.8 Hz, Ca^{ipso}), 128.5 (d, 2C, $^{1}J_{CP}$ = 50.3 Hz, Cb^{ipso}) 128.6 (s, 4C, C16, C17, C20 and C21), 128.7 (d, 4C, $^{3}J_{CP}$ = 10.0 Hz, Ca^{meta}), 128.9 (s, 4C, C14, C15, C22 and C23), 129.1 (d, 4C, $^{3}J_{CP}$ = 9.6 Hz, Cb^{meta}), 131.4 (d, 2C, $^{4}J_{CP}$ = 2.3 Hz, Ca^{para}), 131.6 (d, 2C, $^{4}J_{CP}$ = 2.2 Hz, Cb^{para}), 133.0 (d, 4C, $^{2}J_{CP}$ = 8.7 Hz, Ca^{ortho}), 133.4 (d, 4C, $^{2}J_{CP}$ = 8.9 Hz, Cb^{ortho}), 133.7 (s, 2C, C18 and C19), 135.9 (s, 1C, C1), 136.6 (s, 2C, C12 and C13), 156.6 (d, 2C,

$^{2}J_{CP}$ = 5.9 Hz, C4 and C5), 196.9 (d, 2C, $^{3}J_{CP}$ = 12.5 Hz, C10 and C11). HRMS (ESI) m/z: $(M + H)^{+}$ calcd for $C_{47}H_{46}B_2NO_2P_2$, 739.3112; found, 739.3114.

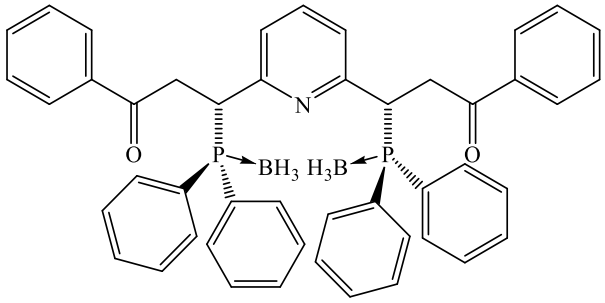

33a'. White solid. Yield: 22.3 mg, 30.0 µmol, 21%. ^{1}H NMR (CD_2Cl_2, 400 MHz): δ 0.61-1.34 (br s, 6H, B*H*$_3$), 3.31 (ddd, 2H, $^{2}J_{HH}$ = 18.2 Hz, $^{3}J_{HP}$ = 11.2 Hz, $^{3}J_{HH}$ = 2.5 Hz, PCHC*H*), 3.88 (ddd, 2H, $^{2}J_{HH}$ = 18.1 Hz, $^{3}J_{HH}$ = 10.3 Hz, $^{3}J_{HP}$ = 4.7 Hz, PCHC*H*), 4.66-4.72 (pseudo ddd, 2H, $^{2}J_{HP}$ = 13.5 Hz, $^{3}J_{HH}$ = 10.5 Hz, $^{3}J_{HH}$ = 2.4 Hz, PC*H*), 6.71 (d, 2H, $^{3}J_{HP}$ = 7.8 Hz, NCC*H*) 7.07 (t, 1H, $^{3}J_{HH}$ = 7.8 Hz, NCCHC*H*), 7.24-7.77 (m, 30H, Ar); ^{31}P{^{1}H} NMR (CD_2Cl_2, 162 MHz): δ 25.9; ^{13}C{^{1}H} NMR (CD_2Cl_2, 100 MHz): δ 38.5 (d, 2C, $^{2}J_{CP}$ = 5.3 Hz, C8 and C9), 39.8 (d, 2C, $^{1}J_{CP}$ = 31.7 Hz, C6 and C7), 123.6 (s, 2C, C2 and C3), 127.8 (d, 2C, $^{1}J_{CP}$ = 50.6 Hz, Ca^{ipso}), 128.3 (s, 4C, C16, C17, C20 and C21), 128.4 (d, 2C, $^{1}J_{CP}$ = 50.0 Hz, Cb^{ipso}) 128.8 (d, 4C, $^{3}J_{CP}$ = 10.1 Hz, Ca^{meta}), 128.9 (s, 4C, C14, C15, C22 and C23), 129.1 (d, 4C, $^{3}J_{CP}$ = 10.0 Hz, Cb^{meta}), 131.7 (d, 2C, $^{4}J_{CP}$ = 2.3 Hz, Ca^{para}), 131.8 (d, 2C, $^{4}J_{CP}$ = 2.4 Hz, Cb^{para}), 133.4 (d, 4C, $^{2}J_{CP}$ = 8.8 Hz, Ca^{ortho}), 133.5 (s, 2C, C18 and C19), 133.9 (d, 4C, $^{2}J_{CP}$ = 9.1 Hz, Cb^{ortho}), 136.0 (s, 1C, C1), 136.6 (s, 2C, C12 and C13), 156.1 (d, 2C, $^{2}J_{CP}$ = 6.0 Hz, C4 and C5), 196.7 (d, 2C, $^{3}J_{CP}$ = 12.3 Hz, C10 and C11). HRMS (ESI) m/z: $(M + H)^{+}$ calcd for $C_{47}H_{46}B_2NO_2P_2$, 739.3112; found, 739.3117.

References

[1] Moulton, C. J.; Shaw, B. L., Transition metal–carbon bonds. Part XLII. Complexes of nickel, palladium, platinum, rhodium and iridium with the tridentate ligand 2, 6-bis [(di-t-butylphosphino) methyl] phenyl. *Journal of the Chemical Society, Dalton Transactions* **1976**, (11), 1020-1024.

[2] a) Albrecht, M.; van Koten, G., Platinum group organometallics based on "pincer" complexes: sensors, switches, and catalysts. *Angew. Chem. Int. Ed.* **2001**, *40* (20), 3750-3781; b) Van Koten, G.; Milstein, D., *Organometallic pincer chemistry*. Springer: 2012; Vol. 40; c) Van Koten, G.; Gossage, R. A., *The privileged pincer-metal platform: Coordination chemistry & applications*. Springer: 2015; Vol. 54; d) Lawrence, M. A.; Green, K.-A.; Nelson, P. N.; Lorraine, S. C., Pincer ligands—Tunable, versatile and applicable. *Polyhedron* **2018**, *143*, 11-27; e) Morales-Morales, D., *Pincer Compounds: Chemistry and Applications*. Elsevier: 2018.

[3] a) Albrecht, M.; Lutz, M.; Schreurs, A. M.; Lutz, E. T.; Spek, A. L.; van Koten, G., Self-assembled organoplatinum (II) supermolecules as crystalline, SO 2 gas-triggered switches. *J. Chem. Soc., Dalton Trans.* **2000**, (21), 3797-3804; b) Albrecht, M.; Lutz, M.; Spek, A. L.; van Koten, G., Organoplatinum crystals for gas-triggered switches. *Nature* **2000**, *406* (6799), 970-974; c) Meijer, M. D.; Gebbink, R.; van Koten, G., Solid-gas interactions between small gaseous molecules and transition metals in the solid state. Toward sensor applications. Perspect. *Supramol. Chem* **2003**, *7*, 375-386; d) Wieczorek, B.; Dijkstra, H. P.; Egmond, M. R.; Gebbink, R. J. K.; van Koten, G., Incorporating ECE-pincer metal complexes as functional building blocks in semisynthetic metalloenzymes, supramolecular polypeptide hybrids, tamoxifen derivatives, biomarkers and sensors. *J. Organomet. Chem.* **2009**, *694* (6), 812-822; e) Bryant, M.; Skelton, J.; Hatcher, L.; Stubbs, C.; Madrid, E.; Pallipurath, A. R.; Thomas, L.; Woodall, C.; Christensen, J.; Fuertes, S., A rapidly-reversible absorptive and emissive vapochromic Pt (II) pincer-based

chemical sensor. *Nature communications* **2017**, *8* (1), 1-9; f) Tabrizi, L.; Chiniforoshan, H., High-performance room temperature gas sensor based on gold (III) pincer complex with high sensitivity for NH3. *Sensors and Actuators B: Chemical* **2017**, *245*, 815-820.

[4] a) Beletskaya, I. P.; Chuchurjukin, A. V.; Dijkstra, H. P.; van Klink, G. P.; van Koten, G., Conjugated G0 metallo-dendrimers, functionalized with tridentate 'pincer'-type ligands. *Tetrahedron Lett.* **2000**, *41* (7), 1081-1085; b) Chase, P. A.; Gebbink, R. J. K.; van Koten, G., Where organometallics and dendrimers merge: the incorporation of organometallic species into dendritic molecules. *J. Organomet. Chem.* **2004**, *689* (24), 4016-4054; c) Berger, A.; Gebbink, R. J. K.; van Koten, G., Transition metal dendrimer catalysts. In *Dendrimer catalysis*, Springer: 2006; pp 1-38; d) Machado, K.; Mishra, J.; Suzuki, S.; Mishra, G. S., Synthesis of superparamagnetic carbon nanotubes immobilized Pt and Pd pincer complexes: highly active and selective catalysts towards cyclohexane oxidation with dioxygen. *Dalton Transactions* **2014**, *43* (46), 17475-17482; e) Jerome, P.; Kausalya, G.; Thangadurai, T. D.; Karvembu, R., Green synthesis of CuO nanoflakes from copper pincer complex for effective N-arylation of benzimidazole. *Catal. Commun.* **2016**, *75*, 50-54.

[5] a) Van Der Boom, M. E.; Milstein, D., Cyclometalated phosphine-based pincer complexes: mechanistic insight in catalysis, coordination, and bond activation. *Chem. Rev.* **2003**, *103* (5), 1759-1792; b) Morales-Morales, D., Pincer Complexes: Applications in Catalysis. *Revista de la Sociedad Química de México* **2004**, *48* (4), 338-346; c) Peris, E.; Crabtree, R. H., Recent homogeneous catalytic applications of chelate and pincer N-heterocyclic carbenes. *Coord. Chem. Rev.* **2004**, *248* (21-24), 2239-2246; d) Nishiyama, H., Synthesis and use of bisoxazolinyl-phenyl pincers. *Chem. Soc. Rev.* **2007**, *36* (7), 1133-1141; e) Gunanathan, C.; Milstein, D., Bond activation and catalysis by ruthenium pincer complexes. *Chem. Rev.* **2014**, *114* (24), 12024-12087;

f) O'Reilly, M. E.; Veige, A. S., Trianionic pincer and pincer-type metal complexes and catalysts. *Chem. Soc. Rev.* **2014**, *43* (17), 6325-6369; g) Szabo, K. J.; Wendt, O. F., *Pincer and pincer-type complexes: applications in organic synthesis and catalysis*. John Wiley & Sons: 2014; h) Asay, M.; Morales-Morales, D., Non-symmetric pincer ligands: complexes and applications in catalysis. *Dalton Transactions* **2015**, *44* (40), 17432-17447; i) Bauer, G.; Hu, X., Recent developments of iron pincer complexes for catalytic applications. *Inorganic Chemistry Frontiers* **2016**, *3* (6), 741-765; j) Garbe, M.; Junge, K.; Beller, M., Homogeneous catalysis by manganese-based pincer complexes. *Eur. J. Org. Chem.* **2017**, *2017* (30), 4344-4362.

[6] a) Roddick, D. M., Tuning of PCP pincer ligand electronic and steric properties. In *Organometallic Pincer Chemistry*, Springer: 2013; pp 49-88; b) van Koten, G.; Jastrzebski, J. T.; Noltes, J. G.; Spek, A. L.; Schoone, J. C., Triorganotin cations stabilized by intramolecular Sn□ N coordination; synthesis and characterization of {C, N, N′-2, 6-bis [(dimethylamino) methyl] phenyl} diorganotin bromides. *J. Organomet. Chem.* **1978**, *148* (3), 233-245; c) vAN KoTEN, G.; Timmer, K.; Noltes, J. G.; Spek, A. L., A novel type of Pt–C interaction and a model for the final stage in reductive elimination processes involving C–C coupling at Pt; synthesis and molecular geometry of [1, N, N′-η-2, 6-bis {(dimethylamino) methyl}-toluene] iodoplatinum (II) tetrafluoroborate. *J. Chem. Soc., Chem. Commun.* **1978**, (6), 250-252; d) Errington, J.; McDonald, W. S.; Shaw, B. L., Cyclopalladation of C 6 H 4 (CH 2 SBu t) 2-1, 3 and the crystal structure of [PdCl {C 6 H 3 (CH 2 SBu t) 2-2, 6}]. *J. Chem. Soc., Dalton Trans.* **1980**, (11), 2312-2314.

[7] a) Peris, E.; Crabtree, R. H., Key factors in pincer ligand design. *Chem. Soc. Rev.* **2018**, *47* (6), 1959-1968; b) Maser, L.; Vondung, L.; Langer, R., The ABC in pincer chemistry–From amine-to borylene-and carbon-based pincer-ligands. *Polyhedron* **2018**, *143*, 28-42.

[8] a) Benito-Garagorri, D.; Kirchner, K., Modularly designed transition metal PNP and PCP pincer complexes based on aminophosphines: synthesis and catalytic applications. *Acc. Chem. Res.* **2008**, *41* (2), 201-213; b) Serrano-Becerra, J. M.; Morales-Morales, D., Applications in catalysis and organic transformations mediated by platinum group PCP and PNP aromatic-based pincer complexes: recent advances. *Current Organic Synthesis* **2009**, *6* (2), 169-192; c) van der Vlugt, J. I.; Reek, J. N., Neutral Tridentate PNP Ligands and Their Hybrid Analogues: Versatile Non-Innocent Scaffolds for Homogeneous Catalysis. *Angew. Chem. Int. Ed.* **2009**, *48* (47), 8832-8846; d) Murugesan, S.; Kirchner, K., Non-precious metal complexes with an anionic PCP pincer architecture. *Dalton Transactions* **2016**, *45* (2), 416-439; e) Bauer, R. C.; Gloaguen, Y.; Lutz, M.; Reek, J. N.; de Bruin, B.; van der Vlugt, J. I., Pincer ligands with an all-phosphorus donor set: subtle differences between rhodium and palladium. *Dalton Transactions* **2011**, *40* (35), 8822-8829; f) Liang, L.-C., Metal complexes of chelating diarylamido phosphine ligands. *Coord. Chem. Rev.* **2006**, *250* (9-10), 1152-1177.

[9] Jensen, C., Iridium PCP pincer complexes: highly active and robust catalysts for novel homogeneous aliphatic dehydrogenations. *Chem. Commun.* **1999**, (24), 2443-2449.

[10] a) Mohammadnezhad, G.; Abad, S.; Farrokhpour, H., Theoretical studies on the thermodynamics and kinetics of one-pot synthesis of aromatic PCP and PNP pincer ligands. *Struct. Chem.* **2018**, *29* (1), 81-88; b) Lease, N.; Pelczar, E. M.; Zhou, T.; Malakar, S.; Emge, T. J.; Hasanayn, F.; Krogh-Jespersen, K.; Goldman, A. S., PNP-Pincer Complexes of Osmium: Comparison with Isoelectronic (PCP) Ir and (PNP) Ir+ Units. *Organometallics* **2018**, *37* (3), 314-326; c) Zhu, G.; Terry, M.; Zhang, X., Asymmetric hydrosilylation of ketones catalyzed by ruthenium complexes with chiral tridentate ligands. *J. Organomet. Chem.* **1997**, *547* (1), 97-101.

[11] Alzamly, A.; Gambarotta, S.; Korobkov, I., Polymer-free ethylene oligomerization using a pyridine-based pincer PNP-type of ligand. *Organometallics* **2013**, *32* (23), 7204-7212.

[12] Crabtree, R. H., *The organometallic chemistry of the transition metals*. John Wiley & Sons: 2009.

[13] a) Cucciolito, M. E.; D'Amor, A.; Vitagliano, A., Catalytic coupling of ethylene and internal olefins by dicationic palladium (II) and platinum (II) complexes: Switching from hydrovinylation to cyclopropane ring formation. *Organometallics* **2005**, *24* (14), 3359-3361; b) Michael, F. E.; Cochran, B. M., Room temperature palladium-catalyzed intramolecular hydroamination of unactivated alkenes. *J. Am. Chem. Soc.* **2006**, *128* (13), 4246-4247; c) Cochran, B. M.; Michael, F. E., Synthesis of 2, 6-disubstituted piperazines by a diastereoselective palladium-catalyzed hydroamination reaction. *Org. Lett.* **2008**, *10* (2), 329-332; d) Hahn, C.; Morvillo, P.; Vitagliano, A., Olefins Coordinated at a Highly Electrophilic Site− Dicationic Palladium (II) Complexes and Their Equilibrium Reactions with Nucleophiles. *Eur. J. Inorg. Chem.* **2001**, *2001* (2), 419-429; e) Hahn, C.; Cucciolito, M. E.; Vitagliano, A., Coordinated olefins as incipient carbocations: catalytic codimerization of ethylene and internal olefins by a dicationic Pt (II)− ethylene complex. *J. Am. Chem. Soc.* **2002**, *124* (31), 9038-9039; f) Hahn, C.; Morvillo, P.; Herdtweck, E.; Vitagliano, A., Coordination of alkenes at a highly electrophilic site. New dicationic platinum (II) complexes: Synthesis, structure, and reactions with nucleophiles. *Organometallics* **2002**, *21* (9), 1807-1818.

[14] Milstein, D., Discovery of environmentally benign catalytic reactions of alcohols catalyzed by pyridine-based pincer Ru complexes, based on metal–ligand cooperation. *Top. Catal.* **2010**, *53* (13), 915-923.

[15] Milstein, D., Metal–ligand cooperation by aromatization–dearomatization as a tool in single bond activation. *Philosophical Transactions of the Royal Society A: Mathematical, Physical and Engineering Sciences* **2015**, *373* (2037), 20140189.

[16] Gunanathan, C.; Milstein, D., Metal–ligand cooperation by aromatization–dearomatization: a new paradigm in bond activation and "Green" catalysis. *Acc. Chem. Res.* **2011**, *44* (8), 588-602.

[17] a) Gunanathan, C.; Milstein, D., Applications of acceptorless dehydrogenation and related transformations in chemical synthesis. *Science* **2013**, *341* (6143); b) Zhang, J.; Gandelman, M.; Shimon, L. J.; Rozenberg, H.; Milstein, D., Electron-rich, bulky ruthenium PNP-type complexes. Acceptorless catalytic alcohol dehydrogenation. *Organometallics* **2004**, *23* (17), 4026-4033.

[18] Zell, T.; Milstein, D., Hydrogenation and dehydrogenation iron pincer catalysts capable of metal–ligand cooperation by aromatization/dearomatization. *Acc. Chem. Res.* **2015**, *48* (7), 1979-1994.

[19] a) Schwartsburd, L.; Iron, M. A.; Konstantinovski, L.; Ben-Ari, E.; Milstein, D., A Dearomatized anionic PNP pincer rhodium complex: C–H and H–H bond activation by metal–ligand cooperation and inhibition by dinitrogen. *Organometallics* **2011**, *30* (10), 2721-2729; b) Anaby, A.; Feller, M.; Ben-David, Y.; Leitus, G.; Diskin-Posner, Y.; Shimon, L. J.; Milstein, D., Bottom-up construction of a CO2-based cycle for the photocarbonylation of benzene, promoted by a rhodium (I) pincer complex. *J. Am. Chem. Soc.* **2016**, *138* (31), 9941-9950.

[20] a) Hermann, D.; Gandelman, M.; Rozenberg, H.; Shimon, L. J.; Milstein, D., Synthesis, Structure, and Reactivity of New Rhodium and Iridium Complexes, Bearing a Highly Electron-Donating PNP System. Iridium-Mediated Vinylic C− H Bond Activation. *Organometallics* **2002**, *21* (5), 812-818; b) Schwartsburd, L.; Iron, M. A.; Konstantinovski, L.; Diskin-Posner, Y.; Leitus, G.; Shimon, L. J.; Milstein, D., Synthesis and Reactivity of an Iridium (I) Acetonyl PNP Complex.

Experimental and Computational Study of Metal− Ligand Cooperation in H− H and C− H Bond Activation via Reversible Ligand Dearomatization. *Organometallics* **2010**, *29* (17), 3817-3827; c) Ben-Ari, E.; Cohen, R.; Gandelman, M.; Shimon, L. J.; Martin, J. M.; Milstein, D., ortho C− H Activation of Haloarenes and Anisole by an Electron-Rich Iridium (I) Complex: Mechanism and Origin of Regio-and Chemoselectivity. An Experimental and Theoretical Study. *Organometallics* **2006**, *25* (13), 3190-3210; d) Feller, M.; Gellrich, U.; Anaby, A.; Diskin-Posner, Y.; Milstein, D., Reductive cleavage of CO2 by metal–ligand-cooperation mediated by an iridium pincer complex. *J. Am. Chem. Soc.* **2016**, *138* (20), 6445-6454.

[21] a) Vogt, M.; Rivada-Wheelaghan, O.; Iron, M. A.; Leitus, G.; Diskin-Posner, Y.; Shimon, L. J.; Ben-David, Y.; Milstein, D., Anionic Nickel (II) complexes with doubly deprotonated PNP pincer-type ligands and their reactivity toward CO2. *Organometallics* **2013**, *32* (1), 300-308; b) Oren, D.; Diskin-Posner, Y.; Avram, L.; Feller, M.; Milstein, D., Metal–Ligand Cooperation as Key in Formation of Dearomatized NiII–H Pincer Complexes and in Their Reactivity toward CO and CO2. *Organometallics* **2018**, *37* (14), 2217-2221.

[22] a) van der Vlugt, J. I.; Pidko, E. A.; Bauer, R. C.; Gloaguen, Y.; Rong, M. K.; Lutz, M., Dinuclear copper (I) thiolate complexes with a bridging noninnocent PNP ligand. *Chemistry–A European Journal* **2011**, *17* (14), 3850-3854; b) van der Vlugt, J. I.; Pidko, E. A.; Vogt, D.; Lutz, M.; Spek, A. L., CuI complexes with a noninnocent PNP ligand: selective dearomatization and electrophilic addition reactivity. *Inorg. Chem.* **2009**, *48* (16), 7513-7515; c) de Boer, S. Y.; Gloaguen, Y.; Lutz, M.; van der Vlugt, J. I., CuI click catalysis with cooperative noninnocent pyridylphosphine ligands. *Inorg. Chim. Acta* **2012**, *380*, 336-342.

[23] a) Sablong, R.; Osborn, J. A., The asymmetric hydrogenation of imines using tridentate C2 diphosphine complexes of iridium (I) and rhodium (I). *Tetrahedron Lett.* **1996**, *37* (28), 4937-4940;

b) Sablong, R.; Newton, C.; Dierkes, P.; Osborn, J. A., Chiral tridentate C2 diphosphine ligands for enantioselective catalysis. *Tetrahedron Lett.* **1996**, *37* (28), 4933-4936; c) Jiang, Q.; Van Plew, D.; Murtuza, S.; Zhang, X., Synthesis of (1R, 1R′)-2, 6-bis [1-(diphenylphosphino) ethyl] pyridine and its application in asymmetric transfer hydrogenation. *Tetrahedron Lett.* **1996**, *37* (6), 797-800; d) Zhu, G.; Terry, M.; Zhang, X., Asymmetric allylic alkylation catalyzed by palladium complexes with new chiral ligands. *Tetrahedron Lett.* **1996**, *37* (26), 4475-4478.

[24] Huber, R.; Passera, A.; Mezzetti, A., Iron (II)-catalyzed hydrogenation of acetophenone with a chiral, pyridine-based PNP pincer ligand: support for an outer-sphere mechanism. *Organometallics* **2018**, *37* (3), 396-405.

[25] Dahlhoff, W.; Nelson, S., Studies on the magnetic cross-over in five-co-ordinate complexes of iron (II), cobalt (II), and nickel (II). Part II. *Journal of the Chemical Society A: Inorganic, Physical, Theoretical* **1971,** 2184-2190.

[26] Hamon, P.; Toupet, L.; Hamon, J.-R.; Lapinte, C., Syntheses and X-ray Crystal Structures of Five-and Six-Coordinated Iron (I) and Iron (II) Complexes with the Same (η5-C5Me5) Fe (dppe) Framework. *Organometallics* **1996**, *15* (1), 10-12.

[27] Evans, D., 400. The determination of the paramagnetic susceptibility of substances in solution by nuclear magnetic resonance. *Journal of the Chemical Society (Resumed)* **1959**, 2003-2005.

[28] Yang, Z.; Liu, D.; Liu, Y.; Sugiya, M.; Imamoto, T.; Zhang, W., Synthesis and structural characterization of nickel complexes possessing P-stereogenic pincer scaffolds and their application in asymmetric Aza-Michael reactions. *Organometallics* **2015**, *34* (7), 1228-1237.

[29] Jacobsen, G. M.; Shoemaker, R. K.; McNevin, M. J.; Rakowski DuBois, M.; DuBois, D. L., Syntheses and structural characterizations of iron (II) complexes containing cyclic diphosphine ligands with positioned pendant nitrogen bases. *Organometallics* **2007**, *26* (20), 5003-5009.

[30] Benito-Garagorri, D.; Becker, E.; Wiedermann, J.; Lackner, W.; Pollak, M.; Mereiter, K.; Kisala, J.; Kirchner, K., Achiral and chiral transition metal complexes with modularly designed tridentate PNP pincer-type ligands based on N-heterocyclic diamines. *Organometallics* **2006**, *25* (8), 1900-1913.

[31] a) Langer, R.; Iron, M. A.; Konstantinovski, L.; Diskin-Posner, Y.; Leitus, G.; Ben-David, Y.; Milstein, D., Iron borohydride pincer complexes for the efficient hydrogenation of ketones under mild, base-free conditions: synthesis and mechanistic insight. *Chemistry–A European Journal* **2012**, *18* (23), 7196-7209; b) Glatz, M.; Schröder-Holzhacker, C.; Bichler, B.; Stöger, B.; Mereiter, K.; Veiros, L. F.; Kirchner, K., Synthesis and characterization of cationic dicarbonyl Fe (II) PNP pincer complexes. *Monatshefte für Chemie-Chemical Monthly* **2016**, *147* (10), 1713-1719.

[32] Spiridonova, Y. S.; Nikolaeva, Y. A.; Balueva, A. S.; Musina, E. I.; Litvinov, I. A.; Strelnik, I. D.; Khrizanforova, V. V.; Budnikova, Y. G.; Karasik, A. A., Synthesis and Structure of Iron (II) Complexes of Functionalized 1, 5-Diaza-3, 7-Diphosphacyclooctanes. *Molecules* **2020**, *25* (17), 3775.

[33] Younus, H. A.; Ahmad, N.; Su, W.; Verpoort, F., Ruthenium pincer complexes: ligand design and complex synthesis. *Coord. Chem. Rev.* **2014**, *276*, 112-152.

[34] Barloy, L.; Ku, S. Y.; Osborn, J. A.; De Clan, A.; Fischer, J., Synthesis and structure of new 2, 6-(diphenylphosphinomethyl) pyridine ruthenium (II) complexes. *Polyhedron* **1997**, *16* (2), 291-295.

[35] Jia, G.; Lee, H. M.; Williams, I. D.; Lau, C. P.; Chen, Y., Synthesis, Characterization, and Acidity Properties of [MCl (H2)(L)(PMP)] BF4 (M= Ru, L= PPh3, CO; M= Os, L= PPh3; PMP= 2, 6-(Ph2PCH2) 2C5H3N). *Organometallics* **1997**, *16* (18), 3941-3949.

[36] Hallman, P.; Stephenson, T.; Wilkinson, G., Tetrakis (triphenylphosphine) dichlororuthenium (II) and Tris (triphenylphosphine) dichlororuthenium (II). *Inorg. Synth.* **1970**, *12*, 237-240.

[37] Ma, E. S.; Rettig, S. J.; Patrick, B. O.; James, B. R., Ruthenium (II) thiol and H2S complexes: synthesis, characterization, and thermodynamic properties. *Inorg. Chem.* **2012**, *51* (9), 5427-5434.

[38] Yu, H.; Fu, Y.; Guo, Q.; Lin, Z., DFT studies on reactions of transition metal complexes with O2. *Organometallics* **2009**, *28* (15), 4443-4451.

[39] a) van der Vlugt, J. I.; Lutz, M.; Pidko, E. A.; Vogt, D.; Spek, A. L., Cationic and neutral Ni II complexes containing a non-innocent PNP ligand: formation of alkyl and thiolate species. *Dalton Transactions* **2009**, (6), 1016-1023; b) Lapointe, S.; Khaskin, E.; Fayzullin, R. R.; Khusnutdinova, J. R., Stable nickel (I) complexes with electron-rich, sterically-hindered, innocent PNP pincer ligands. *Organometallics* **2019**, *38* (7), 1581-1594.

[40] a) Huang, Y.; Chew, R. J.; Li, Y.; Pullarkat, S. A.; Leung, P.-H., Direct synthesis of chiral tertiary diphosphines via Pd (II)-catalyzed asymmetric hydrophosphination of dienones. *Org. Lett.* **2011**, *13* (21), 5862-5865; b) Yang, X.-Y.; Tay, W. S.; Li, Y.; Pullarkat, S. A.; Leung, P.-H., Versatile Syntheses of Optically Pure PCE Pincer Ligands: Facile Modifications of the Pendant Arms and Ligand Backbones. *Organometallics* **2015**, *34* (8), 1582-1588.

[41] Cochran, B. M.; Michael, F. E., Mechanistic studies of a palladium-catalyzed intramolecular hydroamination of unactivated alkenes: protonolysis of a stable palladium alkyl complex is the turnover-limiting step. *J. Am. Chem. Soc.* **2008**, *130* (9), 2786-2792.

[42] Bond, G. C., Relativistic Phenomena in the chemistry of the platinum group metals. *Platinum Met. Rev.* **2000**, *44* (4), 146-155.

[43] Feller, M.; Ben-Ari, E.; Iron, M. A.; Diskin-Posner, Y.; Leitus, G.; Shimon, L. J.; Konstantinovski, L.; Milstein, D., Cationic, Neutral, and Anionic PNP PdII and PtII Complexes: Dearomatization by Deprotonation and Double-Deprotonation of Pincer Systems. *Inorg. Chem.* **2010**, *49* (4), 1615-1625.

[44] Hahn, C.; Spiegler, M.; Herdtweck, E.; Taube, R., Oxidative Addition Reactions of Organorhodium (I) Complexes Containing the Tridentate Ligand 2, 6-Bis (diphenylphosphanylmethyl) pyridine [Rh (PNP) R](R= CH3, C6H5) with Iodine and Methyl Iodide and Investigation of the Reductive Elimination. *Eur. J. Inorg. Chem.* **1999**, *1999* (3), 435-440.

[45] Parker, G. L.; Lau, S.; Leforestier, B.; Chaplin, A. B., Probing the Donor Properties of Pincer Ligands Using Rhodium Carbonyl Fragments: An Experimental and Computational Case Study. *Eur. J. Inorg. Chem.* **2019**, *2019* (33), 3791.

[46] Lloyd-Jones, G. C.; Taylor, N. P., Mechanism of phosphine borane deprotection with amines: The effects of phosphine, solvent and amine on rate and efficiency. *Chemistry–A European Journal* **2015**, *21* (14), 5423-5428.

[47] Babu Kalidindi, S.; Sanyal, U.; Jagirdar, B. R., Chemical synthesis of metal nanoparticles using amine–boranes. *ChemSusChem* **2011**, *4* (3), 317-324.

[48] Kawakami, R.; Kuriyama, S.; Tanaka, H.; Arashiba, K.; Konomi, A.; Nakajima, K.; Yoshizawa, K.; Nishibayashi, Y., Catalytic reduction of dinitrogen to tris (trimethylsilyl) amine using rhodium complexes with a pyrrole-based PNP-type pincer ligand. *Chem. Commun.* **2019**, *55* (99), 14886-14889.

[49] Nishiyama, H.; Sakaguchi, H.; Nakamura, T.; Horihata, M.; Kondo, M.; Itoh, K., Chiral and C2-symmetrical bis (oxazolinylpyridine) rhodium (III) complexes: effective catalysts for asymmetric hydrosilylation of ketones. *Organometallics* **1989**, *8* (3), 846-848.

[50] Stephenson, T.; Wilkinson, G., New complexes of ruthenium (II) and (III) with triphenylphosphine, triphenylarsine, trichlorostannate, pyridine and other ligands. *J. Inorg. Nucl. Chem.* **1966**, *28* (4), 945-956.

[51] Coe, B. J., Syntheses and Characterization of Ruthenium (II) Tetrakis (Pyridine) Complexes. An Advanced Coordination Chemistry Experiment or Mini-Project. *J. Chem. Educ.* **2004**, *81* (5), 718.

[52] Luu, H.-T.; Wiesler, S.; Frey, G.; Streuff, J., A titanium (III)-catalyzed reductive umpolung reaction for the synthesis of 1, 1-disubstituted tetrahydroisoquinolines. *Org. Lett.* **2015**, *17* (10), 2478-2481.

[53] Catsikis, B.; Good, M. L., The preparation and identification of 1, 2, 3-RhCl3 (CH3CN) 3. *Inorganic and Nuclear Chemistry Letters* **1968**, *4* (9), 529-531.

Chapter 4

Conclusions and Future Work

In closure, this chapter entails a concise summary of the research motivations considered and work performed thus far in this thesis. The summarized portions serve to provide a retelling of the significant accomplishments made in the course of the research project, and how they went about to satisfy the aims and objectives that were initially proposed to bridge the existing gaps and limitations in the research area. A brief outline for future work will also be illustrated, highlighting several plausible outlooks that may be ventured upon to expand current results as well as to extend the scope of applicability for the newly furnished synthons. These were otherwise unable to be conducted due to limitations in the duration of the research stint.

4.1. The chemical relevance of chiral tertiary phosphines

The beginning of the thesis saw the introduction of chiral tertiary phosphines as versatile and effective ligand auxiliaries in a multitude of reaction applications. These were mainly centered on their utilizations in metal catalyzed processes, with extensive illustrations on the different modes of their incorporations onto metal centers. Progressive developments in the modulation of these moieties saw the transition of chiral tertiary phosphine utility from simple monondentates to structurally more resounding multidentates that were increasingly more adept towards facilitating applications with specific reaction requirements. In turn, this established the chemical relevance and significance of chiral tertiary phosphines as well as the notion for continual efforts to expand their molecular library.

4.2. Access to chiral PN(sp^2)P tertiary diphosphine adducts

With the fundamental research aim backed by the synthetic motivations behind furnishing new chiral tertiary phosphine adducts, the research was kickstarted with the exploration in the syntheses of pyridyl based PN(sp^2)P moieties that have been generally less exemplified in the literature. Based on recognized efficiencies of the catalytic asymmetric hydrophosphination reaction, the protocol was employed in the first section, to furnish the intended chiral tertiary diphosphine products **10** with excellent conversions and enantioselectivities (up to >99% for both). A series of functionalized pyridyl trans chalcones **9a-f** were well tolerated, except for the tetra ester substituted derivative **9f** which was rationalized by control experiments to have undergone a catalyst excluded reaction pathway to provide adducts of low selectivity. The modest levels of diastereoselectivity obtained were ascertained to be highly temperature dependent, but were unfortunately unable to be further improved on due to reduced substrate reactivities at lowered temperatures. This pointed towards a probable need for better catalytic systems to render enhanced degrees of stereochemical differentiation. Proposals based on understood catalyst properties and behaviors were included to conceptualize a reaction mechanism as well as origins of the underlying stereoselective addition processes.

In the second section, the scope of reaction was extended to a preliminary testing with the use of electronically more challenging pyrrolyl based substrates. The increased difficulty in reaction promotion was immediately realized with the use of **14a**, which barely showed any appreciable levels of conversion despite intensified reaction conditions. The lack of reactivity was surmised to have resulted from the inherent reduced electrophilicity of the β-carbon, and a substitutional use of substrate **14b** was implemented to confirm the above conjecture. Reaction trials with **14b** proceeded with improved conversions, and initial screenings afforded a satisfactory

observation with modest conversions and enantioselectivity (51% and 70% respectively). Further attempts with improving reaction selectivity were again accorded with poor reactivities at decreased reaction temperatures. A preliminary complexation trial was also performed to discern the compatibility of such synthons as ligand auxiliaries. Successful formation of complexes **16** paved the research direction towards investigations using the comparatively better furnished pyridyl diphosphines as ligand partners in subsequent complexation reactions.

4.3. Access to PN(sp^2)P pincer complexes

Successive attempts were carried out in complexation trials using diphosphines **10a** and **10a'** with various metal precursors from Group 8, 9 and 10. The construction of these complexes were definitively affirmed via NMR spectroscopy as well as X-ray crystallography (wherever possible). Comprehensive discussions were made to compare and postulate for the differences observed within individual complexes with analogous examples from the literature as well as among other congeners formed. These include differences in structural characteristics existing immediately to the coordination sphere of the metal center and how interactions between the main PN(sp^2)P ligand framework with other co-ligands affect the overall stability and coordination patterns of the generated complexes. In relation to that, the most notable example stem from the complexation trials with iron, which provided an unprecedented and unexpected solid state structure incorporating the carbonyl functionalities from the PN(sp^2)P auxiliary. Additional trials in modulating the complexation conditions for ruthenium also revealed interesting effects brought about by the sterics and electronics of both ligand and metal in affecting the structural stability of the resultant complexes. Overall, the compatibility of the pyridyl PN(sp^2)P tridentate as a potential ligand precursor was extensively explored and remarkably displayed in its effective association to various metal centers.

4.4. Supplementary experimental attempts

Additional experimental efforts were placed to resolve the inherent issue related to diastereomeric inseparability surfaced from the ligand synthesis step. Protection-deprotection attempts with BH_3-SMe_2 were successful in allowing clean separation of the borane protected diastereomers, but were accosted with low isolated yields due to a necessary slow elution of the mobile phase. Subsequent deprotection reactions were however interfered with the presence of the amine borane side product, which was attested to be a capable reducing agent on metals. Complete removal of the side product was unable to be achieved and the protocol was eventually sidelined due to this disruption.

In other efforts, trials to activate the diastereomerically pure rhodium(III) complexes **32** were conducted via separate attempts with chloride abstraction and reduction of the rhodium(III) center. Metathesis reactions using silver additives were unaccomplished with regard to the former, highlighting the chemical inertness of the Rh-Cl bond likely due to insufficient electronic stabilization by the PN(sp^2)P ligand. In the case of the latter, reduction reactions following literature reported methods were similarly unsuccessful in providing a rhodium(I) complex as determined by NMR analysis. Intriguingly, the reactive carbonyl functionalities were found to be unaffected by the strong reducing conditions employed. While the abovementioned experimental trials did not proceed as intended to provide for the desired outcomes, several noteworthy insights were obtained with respect to the chemical nature of the pincer backbone which can serve as valuable information for further tinkering of the ligand precursor and/or associated complexes in future supplementary reaction tests.

4.5. Fulfilment of research aims and objectives

In conclusion, the compilation of experimental trials conducted and results obtained have culminated to fulfill the research aims and objectives in the following ways. Firstly, the successful syntheses of chiral PN(sp^2)P tertiary phosphines were portrayed, significantly contributing to the expansion of the library of chiral tertiary phosphines as well as for this particular class of compounds which has been to the best of our knowledge, extremely rare in the literature. Secondly, the furnishment of these adducts were conveniently performed via a highly effective and sustainable asymmetric hydrophosphination protocol, which provides for a direct one-pot reaction process under mild conditions with absolute atom economy. These benefits thoroughly surpass conventional methods for the preparation of related PN(sp^2)P analogues, which has been an apparent limitation and deterrence for the synthetic access towards such synthons. Thirdly, successful complexation trials performed using a variety of metal precursors asserted the compatibility of the synthesized PN(sp^2)P adducts as feasible coordination auxiliaries, showcasing their useful functionality as potential ligand precursors.

4.6. Future work

With the experimental findings and accomplishments gathered from this thesis, the next plausible research direction can be focused on the utility of the associated PN(sp^2)P complexes in application reactions. In this aspect, the synthesis of chiral ruthenium complex **27a** presents the greatest potential by virtue of the experimental possibility in generating the complex as a diastereomerically pure entity. Furthermore, the decomposition phenomenon observed with complexes **27** in solution suggests an apparent level of reactivity that they possess. To this end, the application trials should be targeted towards base promoted reactions, leveraging upon preliminary verifications that the decomposition was likely due to dissociation of the pyridine co-ligand. In turn, this presents an opportunity to test out the compatibility of *chiral*-**27a** in the catalytic asymmetric hydrophosphination reaction as an initial starting point and proof of concept to deduce its potentials as a catalyst.

In light of the reaction pathways that have been established with related palladacycles[1] as well as for other metals in general with respect to the catalytic hydrophosphination reaction,[2] employments of *chiral*-**27a** may be mechanistically proposed to mediate the reaction in analogous fashions. For instance, in comparison to the working mechanism behind (*S*,*S*)-**8**, the functionality of pyridine dissociation would concur with the behavior of the OAc ligand to act as an internal base for reaction promotion (Scheme 4.1). This is also in line with the fact that the relative basicity of both pyridine as well as the acetate moiety lies fairly close to each other (pK_a values of their conjugate acids are 5.23 and 4.76 respectively).[3]

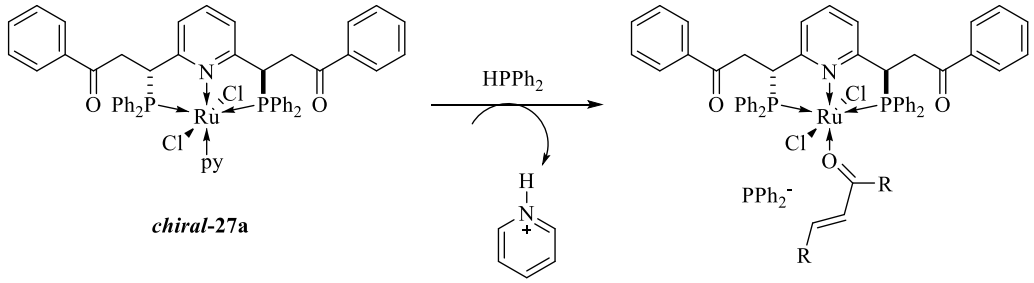

Scheme 4.1. Postulated reaction intermediate for AHP reaction with *chiral* Ru(II) complex **27a**.

In another approach, addition of a silver additive may also be performed to emulate the reaction pathway mediated by (*S*)-**2** via an intermolecular addition route (Scheme 4.2). Furthermore, representative examples in the literature have also demonstrated the reactive capability of ruthenium-phosphido intermediates to undergo nucleophilic phosphine addition to alkenes via inner sphere pathways.[4]

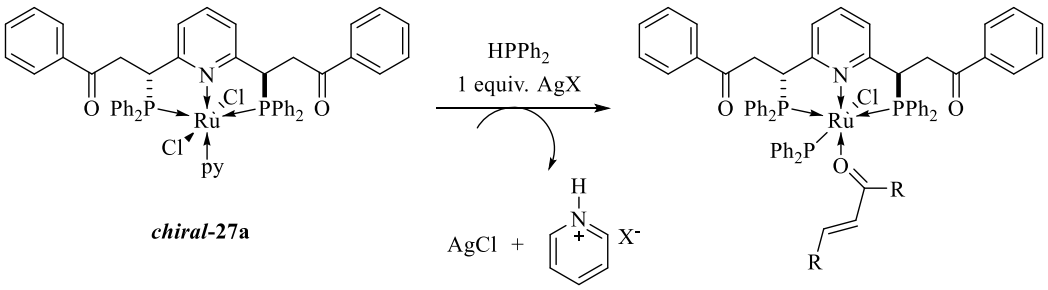

Scheme 4.2. Postulated reaction intermediate for AHP reaction with *chiral* Ru(II) complex **27a** in the presence of a silver additive.

In the case of successful reaction, the scope of substrate compatibility may also be explored with regard to reactivity differences that complex **27** may imbue based on its sensitivity to steric conditions as discussed in Chapter 3. The general labilizing effect observed at the position *trans* to the chelated pyridine, which would effectively be the vacant site, poises the complex for activation of sterically compatible substrates and thereafter facile product elimination upon

addition of a bulky phosphine moiety. Comparisons may also be made with the structurally analogous palladium(II) complexes (*S*,*S*)-**5** and (*S*,*S*)-**6** to further elucidate reactivity differences based on the inherent electronic disparities of the metal center as well as electronic influences from the ligand auxiliary. It may be plausible that the moderately harder ruthenium(II) center would be comparatively more suitable to facilitate the activation of electronically less activated substrates, which in turn provides a measure of possibility for reinvestigation of the hydrophosphination reaction onto the pyrrolyl based substrates **14** as a subsequent future endeavor.

The above ideas serve as a non-exhaustive list of suggestions for future work. With the promising identification of the synthesized, enantiomerically pure PN(sp^2)P diphosphine adducts as compatible ligand precursors, further application of the associated pincer complexes as potential catalysts would be the ultimate accomplishment for the entirety of this research project.

References

[1] Yang, X.-Y.; Jia, Y.-X.; Tay, W. S.; Li, Y.; Pullarkat, S. A.; Leung, P.-H., Mechanistic insights into the role of PC-and PCP-type palladium catalysts in asymmetric hydrophosphination of activated alkenes incorporating potential coordinating heteroatoms. *Dalton Transactions* **2016**, *45* (34), 13449-13455.

[2] Rosenberg, L., Mechanisms of metal-catalyzed hydrophosphination of alkenes and alkynes. *ACS Catalysis* **2013**, *3* (12), 2845-2855.

[3] a) Casasnovas, R.; Frau, J.; Ortega-Castro, J.; Salvà, A.; Donoso, J.; Muñoz, F., Absolute and relative pKa calculations of mono and diprotic pyridines by quantum methods. *Journal of Molecular Structure: THEOCHEM* **2009**, *912* (1-3), 5-12; b) Saracino, G. A.; Improta, R.; Barone, V., Absolute pKa determination for carboxylic acids using density functional theory and the polarizable continuum model. *Chem. Phys. Lett.* **2003**, *373* (3-4), 411-415.

[4] a) Derrah, E. J.; Pantazis, D. A.; McDonald, R.; Rosenberg, L., Concerted [2+ 2] Cycloaddition of Alkenes to a Ruthenium–Phosphorus Double Bond. *Angew. Chem.* **2010**, *122* (19), 3439-3442; b) Belli, R. G.; Burton, K. M.; Rufh, S. A.; McDonald, R.; Rosenberg, L., Inner-and outer-sphere roles of ruthenium phosphido complexes in the hydrophosphination of alkenes. *Organometallics* **2015**, *34* (23), 5637-5646.

Appendix (Crystallographic data)

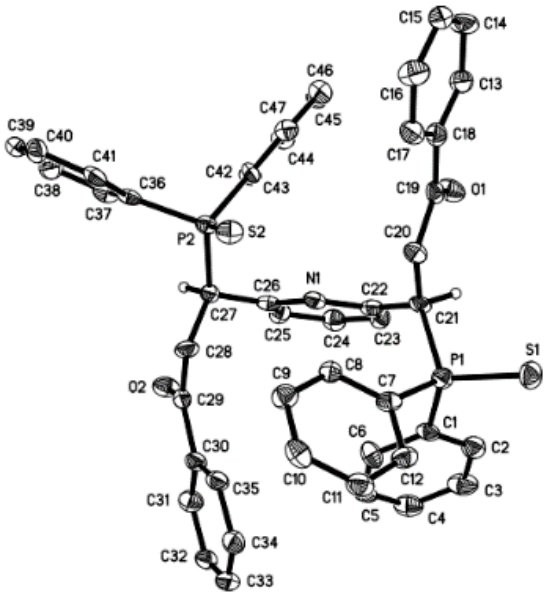

A colourless plate-like specimen of $C_{47}H_{39}NO_2P_2S_2$, approximate dimensions 0.020 mm x 0.060 mm x 0.160 mm, was used for the X-ray crystallographic analysis. The X-ray intensity data were measured (λ = 0.71073 Å). A total of 385 frames were collected. The total exposure time was 1.07 hours. The frames were integrated with the Bruker SAINT software package using a narrow-frame algorithm. The integration of the data using a triclinic unit cell yielded a total of 17983 reflections to a maximum θ angle of 27.92° (0.76 Å resolution), of which 17983 were independent (average redundancy 1.000, completeness = 96.8%, Rsig = 36.96%) and 10638 (59.16%) were greater than 2σ(F2). The final cell constants of a = 9.3403(12) Å, b = 10.2748(12) Å, c = 21.133(3) Å, α = 87.105(4)°, β = 79.895(4)°, γ = 86.008(4)°, volume = 1990.3(4) Å3, are based upon the refinement of the XYZ-centroids of 5888 reflections above 20 σ(I) with 5.151° < 2θ < 52.65°. Data were corrected for absorption effects using the Multi-Scan method (SADABS). The ratio of minimum to maximum apparent transmission was 0.767. The calculated minimum and maximum

transmission coefficients (based on crystal size) are 0.9600 and 0.9950. The structure was solved and refined using the Bruker SHELXTL Software Package, using the space group P 1, with Z = 2 for the formula unit, $C_{47}H_{39}NO_2P_2S_2$. The final anisotropic full-matrix least-squares refinement on F2 with 805 variables converged at R1 = 8.37%, for the observed data and wR2 = 18.98% for all data. The goodness-of-fit was 1.006. The largest peak in the final difference electron density synthesis was 0.622 e-/Å3 and the largest hole was -0.614 e-/Å3 with an RMS deviation of 0.090 e-/Å3. On the basis of the final model, the calculated density was 1.295 g/cm3 and F(000), 812 e-.

Table 1. Sample and crystal data for Compound 10a.

Identification code	leung1171m_0m_4	
Chemical formula	$C_{47}H_{39}NO_2P_2S_2$	
Formula weight	775.85 g/mol	
Temperature	100(2) K	
Wavelength	0.71073 Å	
Crystal size	0.020 x 0.060 x 0.160 mm	
Crystal habit	colourless plate	
Crystal system	triclinic	
Space group	P 1	
Unit cell dimensions	a = 9.3403(12) Å	α = 87.105(4)°
	b = 10.2748(12) Å	β = 79.895(4)°
	c = 21.133(3) Å	γ = 86.008(4)°
Volume	1990.3(4) $Å^3$	
Z	2	
Density (calculated)	1.295 g/cm^3	
Absorption coefficient	0.255 mm^{-1}	
F(000)	812	

Table 2. Data collection and structure refinement for Compound 10a.

Theta range for data collection	2.27 to 27.92°	
Index ranges	-12<=h<=12, -13<=k<=13, -27<=l<=27	
Reflections collected	17983	
Coverage of independent reflections	96.8%	
Absorption correction	Multi-Scan	
Max. and min. transmission	0.9950 and 0.9600	
Structure solution technique	direct methods	
Structure solution program	XT, VERSION 2014/5	
Refinement method	Full-matrix least-squares on F^2	
Refinement program	SHELXL-2018/3 (Sheldrick, 2018)	
Function minimized	$\Sigma\ w(F_o^2 - F_c^2)^2$	
Data / restraints / parameters	17983 / 3 / 805	
Goodness-of-fit on F^2	1.006	
Final R indices	10638 data; $I>2\sigma(I)$	R1 = 0.0837, wR2 = 0.1665
	all data	R1 = 0.1616, wR2 = 0.1898
Weighting scheme	$w=1/[\sigma^2(F_o^2)+(0.0801P)^2]$ where $P=(F_o^2+2F_c^2)/3$	
Absolute structure parameter	0.01(8)	
Largest diff. peak and hole	0.622 and -0.614 eÅ^{-3}	
R.M.S. deviation from mean	0.090 eÅ^{-3}	

Table 3. Bond lengths (Å) for Compound 10a.

C1-C2	1.39	C1-C6	1.39
C1-P1	1.804(4)	C2-C3	1.39
C2-H2	0.95	C3-C4	1.39
C3-H3	0.95	C4-C5	1.39
C4-H4	0.95	C5-C6	1.39
C5-H5	0.95	C6-H6	0.95
C7-C8	1.39	C7-C12	1.39
C7-P1	1.816(4)	C8-C9	1.39
C8-H8	0.95	C9-C10	1.39
C9-H9	0.95	C10-C11	1.39
C10-H10	0.95	C11-C12	1.39
C11-H11	0.95	C12-H12	0.95
C13-C14	1.39	C13-C18	1.39
C13-H13	0.95	C14-C15	1.39
C14-H14	0.95	C15-C16	1.39
C15-H15	0.95	C16-C17	1.39
C16-H16	0.95	C17-C18	1.39
C17-H17	0.95	C18-C19	1.502(9)
C19-O1	1.209(9)	C19-C20	1.516(11)
C20-C21	1.518(11)	C20-H20A	0.99
C20-H20B	0.99	C21-C22	1.470(8)
C21-P1	1.846(7)	C21-H21	1.0
C22-C23	1.39	C22-N1	1.39
C23-C24	1.39	C23-H23	0.95
C24-C25	1.39	C24-H24	0.95
C25-C26	1.39	C25-H25	0.95
C26-N1	1.39	C26-C27	1.465(8)
C27-C28	1.546(11)	C27-P2	1.857(8)
C27-H27	1.0	C28-C29	1.533(11)
C28-H28A	0.99	C28-H28B	0.99
C29-O2	1.213(9)	C29-C30	1.502(8)
C30-C31	1.39	C30-C35	1.39
C31-C32	1.39	C31-H31	0.95
C32-C33	1.39	C32-H32	0.95
C33-C34	1.39	C33-H33	0.95
C34-C35	1.39	C34-H34	0.95

C35-H35	0.95	C36-C37	1.39
C36-C41	1.39	C36-P2	1.832(4)
C37-C38	1.39	C37-H37	0.95
C38-C39	1.39	C38-H38	0.95
C39-C40	1.39	C39-H39	0.95
C40-C41	1.39	C40-H40	0.95
C41-H41	0.95	C42-C43	1.39
C42-C47	1.39	C42-P2	1.814(5)
C43-C44	1.39	C43-H43	0.95
C44-C45	1.39	C44-H44	0.95
C45-C46	1.39	C45-H45	0.95
C46-C47	1.39	C46-H46	0.95
C47-H47	0.95	C48-C49	1.39
C48-C53	1.39	C48-P3	1.826(4)
C49-C50	1.39	C49-H49	0.95
C50-C51	1.39	C50-H50	0.95
C51-C52	1.39	C51-H51	0.95
C52-C53	1.39	C52-H52	0.95
C53-H53	0.95	C54-C55	1.39
C54-C59	1.39	C54-P3	1.817(4)
C55-C56	1.39	C55-H55	0.95
C56-C57	1.39	C56-H56	0.95
C57-C58	1.39	C57-H57	0.95
C58-C59	1.39	C58-H58	0.95
C59-H59	0.95	C60-C61	1.39
C60-C65	1.39	C60-H60	0.95
C61-C62	1.39	C61-H61	0.95
C62-C63	1.39	C62-H62	0.95
C63-C64	1.39	C63-H63	0.95
C64-C65	1.39	C64-H64	0.95
C65-C66	1.493(9)	C66-O3	1.215(9)
C66-C67	1.502(11)	C67-C68	1.530(11)
C67-H67A	0.99	C67-H67B	0.99
C68-C69	1.494(8)	C68-P3	1.837(8)
C68-H68	1.0	C69-C70	1.39
C69-N2	1.39	C70-C71	1.39
C70-H70	0.95	C71-C72	1.39
C71-H71	0.95	C72-C73	1.39

C72-H72	0.95	C73-N2	1.39
C73-C74	1.467(8)	C74-C75	1.546(11)
C74-P4	1.845(8)	C74-H74	1.0
C75-C76	1.512(11)	C75-H75A	0.99
C75-H75B	0.99	C76-O4	1.223(9)
C76-C77	1.490(9)	C77-C78	1.39
C77-C82	1.39	C78-C79	1.39
C78-H78	0.95	C79-C80	1.39
C79-H79	0.95	C80-C81	1.39
C80-H80	0.95	C81-C82	1.39
C81-H81	0.95	C82-H82	0.95
C83-C84	1.39	C83-C88	1.39
C83-P4	1.813(4)	C84-C85	1.39
C84-H84	0.95	C85-C86	1.39
C85-H85	0.95	C86-C87	1.39
C86-H86	0.95	C87-C88	1.39
C87-H87	0.95	C88-H88	0.95
C89-C90	1.39	C89-C94	1.39
C89-P4	1.824(4)	C90-C91	1.39
C90-H90	0.95	C91-C92	1.39
C91-H91	0.95	C92-C93	1.39
C92-H92	0.95	C93-C94	1.39
C93-H93	0.95	C94-H94	0.95
P1-S1	1.956(3)	P2-S2	1.951(3)
P3-S3	1.947(3)	P4-S4	1.957(3)

Table 4. Bond angles (°) for Compound 10a.

C2-C1-C6	120.0	C2-C1-P1	119.2(3)
C6-C1-P1	120.8(3)	C1-C2-C3	120.0
C1-C2-H2	120.0	C3-C2-H2	120.0
C4-C3-C2	120.0	C4-C3-H3	120.0
C2-C3-H3	120.0	C5-C4-C3	120.0
C5-C4-H4	120.0	C3-C4-H4	120.0
C6-C5-C4	120.0	C6-C5-H5	120.0
C4-C5-H5	120.0	C5-C6-C1	120.0
C5-C6-H6	120.0	C1-C6-H6	120.0
C8-C7-C12	120.0	C8-C7-P1	122.6(3)
C12-C7-P1	117.0(3)	C7-C8-C9	120.0
C7-C8-H8	120.0	C9-C8-H8	120.0
C10-C9-C8	120.0	C10-C9-H9	120.0
C8-C9-H9	120.0	C9-C10-C11	120.0
C9-C10-H10	120.0	C11-C10-H10	120.0
C12-C11-C10	120.0	C12-C11-H11	120.0
C10-C11-H11	120.0	C11-C12-C7	120.0
C11-C12-H12	120.0	C7-C12-H12	120.0
C14-C13-C18	120.0	C14-C13-H13	120.0
C18-C13-H13	120.0	C15-C14-C13	120.0
C15-C14-H14	120.0	C13-C14-H14	120.0
C14-C15-C16	120.0	C14-C15-H15	120.0
C16-C15-H15	120.0	C17-C16-C15	120.0
C17-C16-H16	120.0	C15-C16-H16	120.0
C16-C17-C18	120.0	C16-C17-H17	120.0
C18-C17-H17	120.0	C17-C18-C13	120.0
C17-C18-C19	122.3(5)	C13-C18-C19	117.7(5)
O1-C19-C18	121.0(7)	O1-C19-C20	121.0(7)
C18-C19-C20	118.0(6)	C19-C20-C21	112.8(6)
C19-C20-H20A	109.0	C21-C20-H20A	109.0
C19-C20-H20B	109.0	C21-C20-H20B	109.0
H20A-C20-H20B	107.8	C22-C21-C20	115.4(6)
C22-C21-P1	115.4(5)	C20-C21-P1	111.9(5)
C22-C21-H21	104.1	C20-C21-H21	104.1
P1-C21-H21	104.1	C23-C22-N1	120.0
C23-C22-C21	124.8(4)	N1-C22-C21	115.2(4)

C24-C23-C22	120.0	C24-C23-H23	120.0
C22-C23-H23	120.0	C25-C24-C23	120.0
C25-C24-H24	120.0	C23-C24-H24	120.0
C24-C25-C26	120.0	C24-C25-H25	120.0
C26-C25-H25	120.0	N1-C26-C25	120.0
N1-C26-C27	115.4(4)	C25-C26-C27	124.6(4)
C26-N1-C22	120.0	C26-C27-C28	110.9(6)
C26-C27-P2	111.3(5)	C28-C27-P2	111.4(5)
C26-C27-H27	107.7	C28-C27-H27	107.7
P2-C27-H27	107.7	C29-C28-C27	108.7(7)
C29-C28-H28A	109.9	C27-C28-H28A	109.9
C29-C28-H28B	109.9	C27-C28-H28B	109.9
H28A-C28-H28B	108.3	O2-C29-C30	119.7(7)
O2-C29-C28	119.7(7)	C30-C29-C28	120.5(6)
C31-C30-C35	120.0	C31-C30-C29	117.5(4)
C35-C30-C29	122.5(4)	C32-C31-C30	120.0
C32-C31-H31	120.0	C30-C31-H31	120.0
C31-C32-C33	120.0	C31-C32-H32	120.0
C33-C32-H32	120.0	C32-C33-C34	120.0
C32-C33-H33	120.0	C34-C33-H33	120.0
C35-C34-C33	120.0	C35-C34-H34	120.0
C33-C34-H34	120.0	C34-C35-C30	120.0
C34-C35-H35	120.0	C30-C35-H35	120.0
C37-C36-C41	120.0	C37-C36-P2	121.6(3)
C41-C36-P2	118.2(3)	C38-C37-C36	120.0
C38-C37-H37	120.0	C36-C37-H37	120.0
C39-C38-C37	120.0	C39-C38-H38	120.0
C37-C38-H38	120.0	C40-C39-C38	120.0
C40-C39-H39	120.0	C38-C39-H39	120.0
C39-C40-C41	120.0	C39-C40-H40	120.0
C41-C40-H40	120.0	C40-C41-C36	120.0
C40-C41-H41	120.0	C36-C41-H41	120.0
C43-C42-C47	120.0	C43-C42-P2	120.6(3)
C47-C42-P2	119.4(3)	C42-C43-C44	120.0
C42-C43-H43	120.0	C44-C43-H43	120.0
C45-C44-C43	120.0	C45-C44-H44	120.0
C43-C44-H44	120.0	C44-C45-C46	120.0
C44-C45-H45	120.0	C46-C45-H45	120.0

C47-C46-C45	120.0	C47-C46-H46	120.0
C45-C46-H46	120.0	C46-C47-C42	120.0
C46-C47-H47	120.0	C42-C47-H47	120.0
C49-C48-C53	120.0	C49-C48-P3	121.5(3)
C53-C48-P3	118.3(3)	C48-C49-C50	120.0
C48-C49-H49	120.0	C50-C49-H49	120.0
C49-C50-C51	120.0	C49-C50-H50	120.0
C51-C50-H50	120.0	C50-C51-C52	120.0
C50-C51-H51	120.0	C52-C51-H51	120.0
C53-C52-C51	120.0	C53-C52-H52	120.0
C51-C52-H52	120.0	C52-C53-C48	120.0
C52-C53-H53	120.0	C48-C53-H53	120.0
C55-C54-C59	120.0	C55-C54-P3	120.7(3)
C59-C54-P3	119.1(3)	C56-C55-C54	120.0
C56-C55-H55	120.0	C54-C55-H55	120.0
C55-C56-C57	120.0	C55-C56-H56	120.0
C57-C56-H56	120.0	C58-C57-C56	120.0
C58-C57-H57	120.0	C56-C57-H57	120.0
C57-C58-C59	120.0	C57-C58-H58	120.0
C59-C58-H58	120.0	C58-C59-C54	120.0
C58-C59-H59	120.0	C54-C59-H59	120.0
C61-C60-C65	120.0	C61-C60-H60	120.0
C65-C60-H60	120.0	C60-C61-C62	120.0
C60-C61-H61	120.0	C62-C61-H61	120.0
C63-C62-C61	120.0	C63-C62-H62	120.0
C61-C62-H62	120.0	C64-C63-C62	120.0
C64-C63-H63	120.0	C62-C63-H63	120.0
C65-C64-C63	120.0	C65-C64-H64	120.0
C63-C64-H64	120.0	C64-C65-C60	120.0
C64-C65-C66	121.4(4)	C60-C65-C66	118.6(4)
O3-C66-C65	120.0(7)	O3-C66-C67	121.5(7)
C65-C66-C67	118.4(6)	C66-C67-C68	111.4(7)
C66-C67-H67A	109.4	C68-C67-H67A	109.4
C66-C67-H67B	109.4	C68-C67-H67B	109.4
H67A-C67-H67B	108.0	C69-C68-C67	111.6(6)
C69-C68-P3	113.0(5)	C67-C68-P3	110.0(5)
C69-C68-H68	107.4	C67-C68-H68	107.4
P3-C68-H68	107.4	C70-C69-N2	120.0

C70-C69-C68	124.6(4)	N2-C69-C68	115.2(4)
C71-C70-C69	120.0	C71-C70-H70	120.0
C69-C70-H70	120.0	C70-C71-C72	120.0
C70-C71-H71	120.0	C72-C71-H71	120.0
C71-C72-C73	120.0	C71-C72-H72	120.0
C73-C72-H72	120.0	N2-C73-C72	120.0
N2-C73-C74	115.8(4)	C72-C73-C74	123.7(4)
C73-N2-C69	120.0	C73-C74-C75	112.2(6)
C73-C74-P4	120.6(5)	C75-C74-P4	109.6(5)
C73-C74-H74	104.2	C75-C74-H74	104.2
P4-C74-H74	104.2	C76-C75-C74	113.0(6)
C76-C75-H75A	109.0	C74-C75-H75A	109.0
C76-C75-H75B	109.0	C74-C75-H75B	109.0
H75A-C75-H75B	107.8	O4-C76-C77	121.3(7)
O4-C76-C75	120.8(7)	C77-C76-C75	117.9(7)
C78-C77-C82	120.0	C78-C77-C76	121.3(5)
C82-C77-C76	118.7(5)	C79-C78-C77	120.0
C79-C78-H78	120.0	C77-C78-H78	120.0
C78-C79-C80	120.0	C78-C79-H79	120.0
C80-C79-H79	120.0	C79-C80-C81	120.0
C79-C80-H80	120.0	C81-C80-H80	120.0
C82-C81-C80	120.0	C82-C81-H81	120.0
C80-C81-H81	120.0	C81-C82-C77	120.0
C81-C82-H82	120.0	C77-C82-H82	120.0
C84-C83-C88	120.0	C84-C83-P4	120.4(3)
C88-C83-P4	119.5(3)	C85-C84-C83	120.0
C85-C84-H84	120.0	C83-C84-H84	120.0
C84-C85-C86	120.0	C84-C85-H85	120.0
C86-C85-H85	120.0	C87-C86-C85	120.0
C87-C86-H86	120.0	C85-C86-H86	120.0
C88-C87-C86	120.0	C88-C87-H87	120.0
C86-C87-H87	120.0	C87-C88-C83	120.0
C87-C88-H88	120.0	C83-C88-H88	120.0
C90-C89-C94	120.0	C90-C89-P4	123.2(3)
C94-C89-P4	116.5(3)	C89-C90-C91	120.0
C89-C90-H90	120.0	C91-C90-H90	120.0
C92-C91-C90	120.0	C92-C91-H91	120.0
C90-C91-H91	120.0	C91-C92-C93	120.0

C91-C92-H92	120.0	C93-C92-H92	120.0
C92-C93-C94	120.0	C92-C93-H93	120.0
C94-C93-H93	120.0	C93-C94-C89	120.0
C93-C94-H94	120.0	C89-C94-H94	120.0
C1-P1-C7	103.8(3)	C1-P1-C21	105.7(3)
C7-P1-C21	111.2(3)	C1-P1-S1	113.1(2)
C7-P1-S1	113.7(2)	C21-P1-S1	109.0(3)
C42-P2-C36	104.1(3)	C42-P2-C27	104.4(3)
C36-P2-C27	105.2(3)	C42-P2-S2	113.9(2)
C36-P2-S2	111.8(2)	C27-P2-S2	116.3(3)
C54-P3-C48	105.7(3)	C54-P3-C68	101.3(3)
C48-P3-C68	107.0(3)	C54-P3-S3	113.1(2)
C48-P3-S3	113.2(2)	C68-P3-S3	115.5(3)
C83-P4-C89	103.6(3)	C83-P4-C74	107.2(3)
C89-P4-C74	112.0(3)	C83-P4-S4	113.37(19)
C89-P4-S4	111.6(2)	C74-P4-S4	109.0(3)

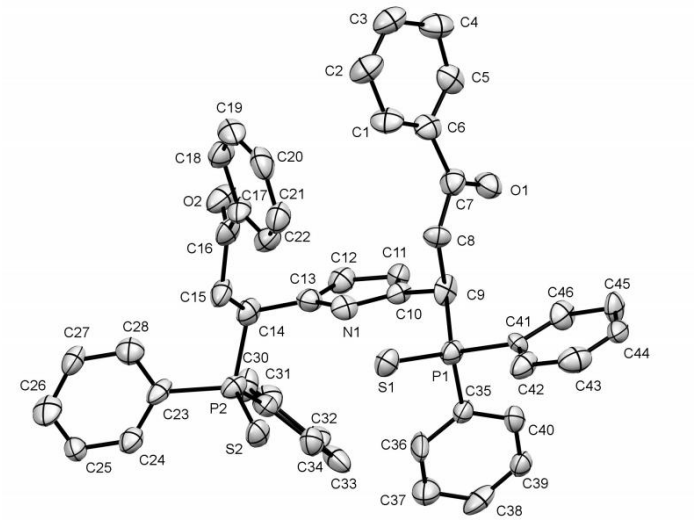

A colourless block-like specimen of $C_{46}H_{39}NO_2P_2S_2$, approximate dimensions 0.060 mm x 0.140 mm x 0.180 mm, was used for the X-ray crystallographic analysis. The X-ray intensity data were measured (λ = 1.54178 Å). A total of 779 frames were collected. The total exposure time was 1.35 hours. The frames were integrated with the Bruker SAINT software package using a narrow-frame algorithm. The integration of the data using a monoclinic unit cell yielded a total of 9851 reflections to a maximum θ angle of 66.60° (0.84 Å resolution), of which 3473 were independent (average redundancy 2.836, completeness = 99.4%, Rint = 5.81%, Rsig = 7.14%) and 2634 (75.84%) were greater than $2\sigma(F2)$. The final cell constants of a = 25.5717(13) Å, b = 12.0220(7) Å, c = 14.6121(7) Å, β = 118.779(4)°, volume = 3937.2(4) Å3, are based upon the refinement of the XYZ-centroids of 4550 reflections above 20 $\sigma(I)$ with 7.889° < 2θ < 133.0°. Data were corrected for absorption effects using the Multi-Scan method (SADABS). The ratio of minimum to maximum apparent transmission was 0.356. The calculated minimum and maximum transmission coefficients (based on crystal size) are 0.6820 and 0.8740.

The structure was solved and refined using the Bruker SHELXTL Software Package, using the space group C 1 2/c 1, with Z = 4 for the formula unit, $C_{46}H_{39}NO_2P_2S_2$. The final anisotropic full-matrix least-squares refinement on F2 with 240 variables converged at R1 = 7.45%, for the observed data and wR2 = 22.79% for all data. The goodness-of-fit was 1.092. The largest peak in the final difference electron density synthesis was 1.005 e-/Å3 and the largest hole was -0.432 e-/Å3 with an RMS deviation of 0.082 e-/Å3. On the basis of the final model, the calculated density was 1.289 g/cm3 and F(000), 1600 e-.

Table 5. Sample and crystal data for Compound 15a'.

Identification code	leung1207s	
Chemical formula	$C_{46}H_{39}NO_2P_2S_2$	
Formula weight	763.84 g/mol	
Temperature	100(2) K	
Wavelength	1.54178 Å	
Crystal size	0.060 x 0.140 x 0.180 mm	
Crystal habit	colourless block	
Crystal system	monoclinic	
Space group	C 1 2/c 1	
Unit cell dimensions	a = 25.5717(13) Å	α = 90°
	b = 12.0220(7) Å	β = 118.779(4)°
	c = 14.6121(7) Å	γ = 90°
Volume	3937.2(4) $Å^3$	
Z	4	
Density (calculated)	1.289 g/cm^3	
Absorption coefficient	2.300 mm^{-1}	
F(000)	1600	

Table 6. Data collection and structure refinement for Compound 15a'.

Theta range for data collection	3.94 to 66.60°	
Index ranges	-30<=h<=22, -14<=k<=12, -17<=l<=17	
Reflections collected	9851	
Independent reflections	3473 [R(int) = 0.0581]	
Coverage of independent reflections	99.4%	
Absorption correction	Multi-Scan	
Max. and min. transmission	0.8740 and 0.6820	
Structure solution technique	direct methods	
Structure solution program	XT, VERSION 2014/5	
Refinement method	Full-matrix least-squares on F^2	
Refinement program	SHELXL-2018/3 (Sheldrick, 2018)	
Function minimized	$\Sigma\ w(F_o^2 - F_c^2)^2$	
Data / restraints / parameters	3473 / 0 / 240	
Goodness-of-fit on F^2	1.092	
Final R indices	2634 data; $I>2\sigma(I)$	R1 = 0.0745, wR2 = 0.2124
	all data	R1 = 0.0917, wR2 = 0.2279
Weighting scheme	$w=1/[\sigma^2(F_o^2)+(0.1288P)^2+3.9593P]$ where $P=(F_o^2+2F_c^2)/3$	
Largest diff. peak and hole	1.005 and -0.432 $eÅ^{-3}$	
R.M.S. deviation from mean	0.082 $eÅ^{-3}$	

Table 7. Bond lengths (Å) for Compound 15a'.

C1-C6	1.378(6)	C1-C2	1.403(6)
C1-H1	0.95	C2-C3	1.377(7)
C2-H2	0.95	C3-C4	1.393(8)
C3-H3	0.95	C4-C5	1.388(7)
C4-H4	0.95	C5-C6	1.392(6)
C5-H5	0.95	C6-C7	1.498(6)
C7-O1	1.196(5)	C7-C8	1.531(6)
C8-C9	1.533(5)	C8-H8A	0.99
C8-H8B	0.99	C9-C10	1.501(5)
C9-P1	1.841(4)	C9-H9	1.0
C10-C11	1.362(6)	C10-N1	1.379(5)
C11-C11	1.406(7)	C11-H11	0.95
C12-C13	1.378(7)	C12-C17	1.378(6)
C12-P1	1.823(4)	C13-C14	1.380(8)
C13-H13	0.95	C14-C15	1.378(8)
C14-H14	0.95	C15-C16	1.378(7)
C15-H15	0.95	C16-C17	1.394(6)
C16-H16	0.95	C17-H17	0.95
C18-C19	1.388(6)	C18-C23	1.397(6)
C18-P1	1.809(4)	C19-C20	1.385(6)
C19-H19	0.95	C20-C21	1.384(7)
C20-H20	0.95	C21-C22	1.367(7)
C21-H21	0.95	C22-C23	1.380(7)
C22-H22	0.95	C23-H23	0.95
N1-H1A	0.88	P1-S1	1.9587(15)

Table 8. Bond angles (°) for Compound 15a'.

C6-C1-C2	120.4(4)	C6-C1-H1	119.8
C2-C1-H1	119.8	C3-C2-C1	119.4(5)
C3-C2-H2	120.3	C1-C2-H2	120.3
C2-C3-C4	120.4(4)	C2-C3-H3	119.8
C4-C3-H3	119.8	C5-C4-C3	119.9(5)
C5-C4-H4	120.0	C3-C4-H4	120.0
C4-C5-C6	119.8(5)	C4-C5-H5	120.1
C6-C5-H5	120.1	C1-C6-C5	120.0(4)
C1-C6-C7	121.6(4)	C5-C6-C7	118.4(4)
O1-C7-C6	121.1(4)	O1-C7-C8	122.2(3)
C6-C7-C8	116.7(4)	C7-C8-C9	112.8(3)
C7-C8-H8A	109.0	C9-C8-H8A	109.0
C7-C8-H8B	109.0	C9-C8-H8B	109.0
H8A-C8-H8B	107.8	C10-C9-C8	113.2(3)
C10-C9-P1	112.9(3)	C8-C9-P1	107.3(3)
C10-C9-H9	107.7	C8-C9-H9	107.7
P1-C9-H9	107.7	C11-C10-N1	107.5(3)
C11-C10-C9	130.2(3)	N1-C10-C9	122.3(4)
C10-C11-C11	107.9(2)	C10-C11-H11	126.0
C11-C11-H11	126.0	C13-C12-C17	119.8(4)
C13-C12-P1	118.7(4)	C17-C12-P1	121.3(3)
C12-C13-C14	120.5(5)	C12-C13-H13	119.7
C14-C13-H13	119.7	C15-C14-C13	120.1(5)
C15-C14-H14	120.0	C13-C14-H14	120.0
C14-C15-C16	119.7(4)	C14-C15-H15	120.1
C16-C15-H15	120.1	C15-C16-C17	120.2(5)
C15-C16-H16	119.9	C17-C16-H16	119.9
C12-C17-C16	119.7(4)	C12-C17-H17	120.2
C16-C17-H17	120.2	C19-C18-C23	118.4(4)
C19-C18-P1	120.4(3)	C23-C18-P1	120.8(3)
C20-C19-C18	120.5(4)	C20-C19-H19	119.8
C18-C19-H19	119.8	C21-C20-C19	120.4(4)
C21-C20-H20	119.8	C19-C20-H20	119.8
C22-C21-C20	119.4(4)	C22-C21-H21	120.3
C20-C21-H21	120.3	C21-C22-C23	120.9(4)
C21-C22-H22	119.6	C23-C22-H22	119.6

C22-C23-C18	120.4(4)	C22-C23-H23	119.8
C18-C23-H23	119.8	C10-N1-C10	109.1(5)
C10-N1-H1A	125.5	C10-N1-H1A	125.5
C18-P1-C12	108.52(19)	C18-P1-C9	108.34(19)
C12-P1-C9	101.64(18)	C18-P1-S1	112.25(14)
C12-P1-S1	113.19(15)	C9-P1-S1	112.28(14)

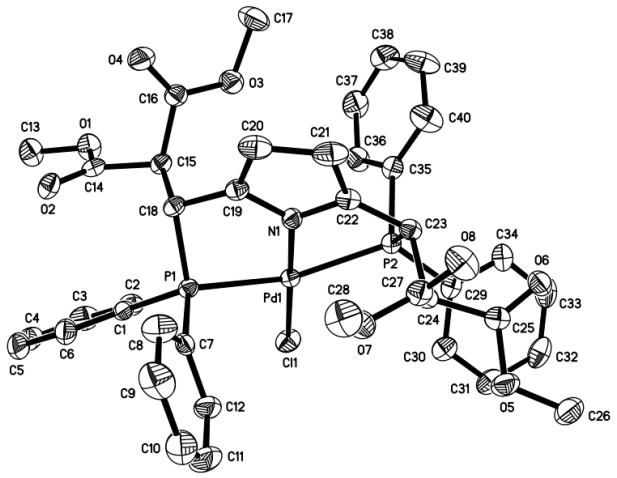

A yellow plate-like specimen of $C_{40}H_{38}ClNO_8P_2Pd$, approximate dimensions 0.040 mm x 0.120 mm x 0.200 mm, was used for the X-ray crystallographic analysis. The X-ray intensity data were measured (λ = 0.71073 Å). A total of 520 frames were collected. The total exposure time was 0.77 hours. The frames were integrated with the Bruker SAINT software package using a narrow-frame algorithm. The integration of the data using a triclinic unit cell yielded a total of 37574 reflections to a maximum θ angle of 31.61° (0.68 Å resolution), of which 12605 were independent (average redundancy 2.981, completeness = 99.2%, Rint = 6.84%, Rsig = 8.57%) and 9715 (77.07%) were greater than 2σ(F2). The final cell constants of a = 10.2484(10) Å, b = 10.3076(10) Å, c = 18.5331(18) Å, α = 101.405(3)°, β = 99.467(4)°, γ = 90.041(3)°, volume = 1891.9(3) Å3, are based upon the refinement of the XYZ-centroids of 9818 reflections above 20 σ(I) with 4.548° < 2θ < 63.08°. Data were corrected for absorption effects using the Multi-Scan method (SADABS). The ratio of minimum to maximum apparent transmission was 0.721. The calculated minimum and maximum transmission coefficients (based on crystal size) are 0.8730 and 0.9730. The structure was solved and refined using the Bruker SHELXTL Software Package, using the space group P -1, with Z = 2 for the formula unit, $C_{40}H_{38}ClNO_8P_2Pd$. The final anisotropic full-matrix least-squares refinement on F2 with 483 variables converged at R1 = 6.29%, for the observed data and

wR2 = 14.68% for all data. The goodness-of-fit was 1.071. The largest peak in the final difference electron density synthesis was 2.512 e-/Å3 and the largest hole was -0.821 e-/Å3 with an RMS deviation of 0.133 e-/Å3. On the basis of the final model, the calculated density was 1.518 g/cm3 and F(000), 884 e-.

Table 9. Sample and crystal data for Complex 16b.

Identification code	leung1226m	
Chemical formula	$C_{40}H_{38}ClNO_8P_2Pd$	
Formula weight	864.50 g/mol	
Temperature	100(2) K	
Wavelength	0.71073 Å	
Crystal size	0.040 x 0.120 x 0.200 mm	
Crystal habit	yellow plate	
Crystal system	triclinic	
Space group	P -1	
Unit cell dimensions	a = 10.2484(10) Å	α = 101.405(3)°
	b = 10.3076(10) Å	β = 99.467(4)°
	c = 18.5331(18) Å	γ = 90.041(3)°
Volume	1891.9(3) $Å^3$	
Z	2	
Density (calculated)	1.518 g/cm^3	
Absorption coefficient	0.700 mm^{-1}	
F(000)	884	

Table 10. Data collection and structure refinement for Complex 16b.

Theta range for data collection	2.02 to 31.61°	
Index ranges	-15<=h<=15, -11<=k<=15, -27<=l<=27	
Reflections collected	37574	
Independent reflections	12605 [R(int) = 0.0684]	
Coverage of independent reflections	99.2%	
Absorption correction	Multi-Scan	
Max. and min. transmission	0.9730 and 0.8730	
Structure solution technique	direct methods	
Structure solution program	XT, VERSION 2018/2	
Refinement method	Full-matrix least-squares on F^2	
Refinement program	SHELXL-2018/3 (Sheldrick, 2018)	
Function minimized	$\Sigma\ w(F_o^2 - F_c^2)^2$	
Data / restraints / parameters	12605 / 0 / 483	
Goodness-of-fit on F^2	1.071	
Δ/σ_{max}	0.001	
Final R indices	9715 data; I>2σ(I)	R1 = 0.0629, wR2 = 0.1308
	all data	R1 = 0.0902, wR2 = 0.1468
Weighting scheme	$w=1/[\sigma^2(F_o^2)+(0.0368P)^2+6.0874P]$ where $P=(F_o^2+2F_c^2)/3$	
Largest diff. peak and hole	2.512 and -0.821 eÅ^{-3}	
R.M.S. deviation from mean	0.133 eÅ^{-3}	

Table 11. Bond lengths (Å) for Complex 16b.

C1-C2	1.391(6)	C1-C6	1.397(6)
C1-P1	1.812(4)	C2-C3	1.393(6)
C3-C4	1.396(8)	C4-C5	1.371(8)
C5-C6	1.385(6)	C7-C8	1.390(6)
C7-C12	1.390(6)	C7-P1	1.804(4)
C8-C9	1.391(7)	C9-C10	1.376(9)
C10-C11	1.361(9)	C11-C12	1.390(7)
C13-O1	1.436(5)	C14-O2	1.202(5)
C14-O1	1.336(5)	C14-C15	1.518(6)
C15-C16	1.515(6)	C15-C18	1.561(5)
C16-O4	1.200(5)	C16-O3	1.329(5)
C17-O3	1.456(6)	C18-C19	1.496(6)
C18-P1	1.847(4)	C19-C20	1.371(6)
C19-N1	1.381(5)	C20-C21	1.484(7)
C21-C22	1.383(6)	C22-N1	1.372(5)
C22-C23	1.498(6)	C23-C24	1.557(5)
C23-P2	1.862(4)	C24-C25	1.523(6)
C24-C27	1.527(6)	C25-O6	1.194(5)
C25-O5	1.348(5)	C26-O5	1.444(6)
C27-O8	1.200(5)	C27-O7	1.322(5)
C28-O7	1.447(6)	C29-C30	1.394(6)
C29-C34	1.399(6)	C29-P2	1.810(4)
C30-C31	1.400(6)	C31-C32	1.393(8)
C32-C33	1.376(8)	C33-C34	1.403(7)
C35-C36	1.382(6)	C35-C40	1.387(7)
C35-P2	1.812(4)	C36-C37	1.399(7)
C37-C38	1.357(8)	C38-C39	1.366(7)
C39-C40	1.392(7)	Cl1-Pd1	2.3269(10)
N1-Pd1	1.984(3)	P1-Pd1	2.3114(11)
P2-Pd1	2.3141(11)		

Table 12. Bond angles (°) for Complex 16b.

C2-C1-C6	120.5(4)	C2-C1-P1	119.0(3)
C6-C1-P1	120.5(3)	C1-C2-C3	119.1(5)
C2-C3-C4	119.9(5)	C5-C4-C3	120.8(4)
C4-C5-C6	120.0(5)	C5-C6-C1	119.8(5)
C8-C7-C12	119.5(4)	C8-C7-P1	124.1(3)
C12-C7-P1	116.3(3)	C7-C8-C9	119.8(5)
C10-C9-C8	119.6(5)	C11-C10-C9	121.2(5)
C10-C11-C12	119.9(5)	C11-C12-C7	119.9(5)
O2-C14-O1	124.0(4)	O2-C14-C15	125.6(4)
O1-C14-C15	110.4(3)	C16-C15-C14	108.2(3)
C16-C15-C18	110.0(3)	C14-C15-C18	111.4(3)
O4-C16-O3	125.9(4)	O4-C16-C15	123.9(4)
O3-C16-C15	110.2(4)	C19-C18-C15	113.5(3)
C19-C18-P1	103.1(3)	C15-C18-P1	108.9(3)
C20-C19-N1	109.1(4)	C20-C19-C18	134.1(4)
N1-C19-C18	116.8(3)	C19-C20-C21	105.3(4)
C22-C21-C20	107.6(4)	N1-C22-C21	107.3(4)
N1-C22-C23	117.2(3)	C21-C22-C23	135.5(4)
C22-C23-C24	112.0(3)	C22-C23-P2	102.8(3)
C24-C23-P2	109.4(3)	C25-C24-C27	107.6(3)
C25-C24-C23	111.0(3)	C27-C24-C23	109.5(3)
O6-C25-O5	124.3(4)	O6-C25-C24	126.1(4)
O5-C25-C24	109.5(4)	O8-C27-O7	125.0(4)
O8-C27-C24	123.6(4)	O7-C27-C24	111.5(4)
C30-C29-C34	120.6(4)	C30-C29-P2	118.3(3)
C34-C29-P2	121.2(4)	C29-C30-C31	119.8(4)
C32-C31-C30	119.5(5)	C33-C32-C31	120.7(4)
C32-C33-C34	120.6(5)	C29-C34-C33	118.9(5)
C36-C35-C40	118.5(4)	C36-C35-P2	118.4(3)
C40-C35-P2	123.0(3)	C35-C36-C37	120.5(5)
C38-C37-C36	119.9(5)	C37-C38-C39	120.6(5)
C38-C39-C40	120.0(5)	C35-C40-C39	120.4(5)
C22-N1-C19	110.7(3)	C22-N1-Pd1	124.6(3)
C19-N1-Pd1	124.7(3)	C14-O1-C13	115.1(3)
C16-O3-C17	114.0(4)	C25-O5-C26	114.7(4)
C27-O7-C28	115.2(4)	C7-P1-C1	104.70(19)

C7-P1-C18	106.50(19)	C1-P1-C18	109.25(18)
C7-P1-Pd1	109.17(13)	C1-P1-Pd1	126.03(14)
C18-P1-Pd1	99.90(13)	C29-P2-C35	107.2(2)
C29-P2-C23	110.47(18)	C35-P2-C23	103.98(19)
C29-P2-Pd1	123.67(15)	C35-P2-Pd1	110.34(14)
C23-P2-Pd1	99.39(13)	N1-Pd1-P1	78.10(10)
N1-Pd1-P2	78.36(10)	P1-Pd1-P2	156.41(4)
N1-Pd1-Cl1	179.51(11)	P1-Pd1-Cl1	101.98(4)
P2-Pd1-Cl1	101.57(4)		

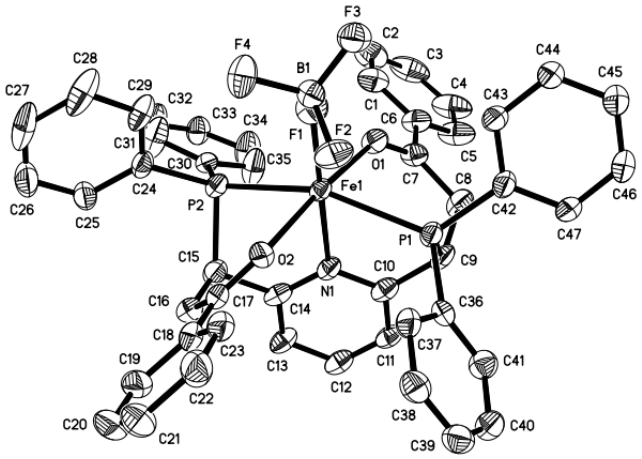

An orange block-like specimen of $C_{48}H_{41}B_2Cl_2F_8FeNO_2P_2$, approximate dimensions 0.140 mm x 0.200 mm x 0.220 mm, was used for the X-ray crystallographic analysis. The X-ray intensity data were measured (λ = 0.71073 Å). A total of 148 frames were collected. The total exposure time was 0.41 hours. The frames were integrated with the Bruker SAINT software package using a narrow-frame algorithm. The integration of the data using a monoclinic unit cell yielded a total of 24544 reflections to a maximum θ angle of 28.75° (0.74 Å resolution), of which 11183 were independent (average redundancy 2.195, completeness = 99.5%, Rint = 7.22%, Rsig = 10.70%) and 7984 (71.39%) were greater than $2\sigma(F2)$. The final cell constants of a = 20.2186(15) Å, b = 14.1922(9) Å, c = 18.6246(11) Å, β = 122.249(2)°, volume = 4519.8(5) Å3, are based upon the refinement of the XYZ-centroids of 5398 reflections above 20 $\sigma(I)$ with $5.213° < 2\theta < 57.07°$. Data were corrected for absorption effects using the Multi-Scan method (SADABS). The ratio of minimum to maximum apparent transmission was 0.699. The calculated minimum and maximum transmission coefficients (based on crystal size) are 0.8800 and 0.9210. The structure was solved and refined using the Bruker SHELXTL Software Package, using the space group C 1 c 1, with Z = 4 for the formula unit, $C_{48}H_{41}B_2Cl_2F_8FeNO_2P_2$. The final anisotropic full-matrix least-squares refinement on F2 with 595 variables converged at R1 = 6.23%, for the observed data and wR2 =

16.63% for all data. The goodness-of-fit was 1.009. The largest peak in the final difference electron density synthesis was 0.991 e-/Å3 and the largest hole was -0.630 e-/Å3 with an RMS deviation of 0.093 e-/Å3. On the basis of the final model, the calculated density was 1.508 g/cm3 and F(000), 2096 e-.

Table 13. Sample and crystal data for Complex 22.

Identification code	leung1135m	
Chemical formula	$C_{48}H_{41}B_2Cl_2F_8FeNO_2P_2$	
Formula weight	1026.13 g/mol	
Temperature	100(2) K	
Wavelength	0.71073 Å	
Crystal size	0.140 x 0.200 x 0.220 mm	
Crystal habit	orange block	
Crystal system	monoclinic	
Space group	C 1 c 1	
Unit cell dimensions	a = 20.2186(15) Å	α = 90°
	b = 14.1922(9) Å	β = 122.249(2)°
	c = 18.6246(11) Å	γ = 90°
Volume	4519.8(5) $Å^3$	
Z	4	
Density (calculated)	1.508 g/cm^3	
Absorption coefficient	0.598 mm^{-1}	
F(000)	2096	

Table 14. Data collection and structure refinement for Complex 22.

Theta range for data collection	2.41 to 28.75°	
Index ranges	-27<=h<=27, -19<=k<=17, -24<=l<=25	
Reflections collected	24544	
Independent reflections	11183 [R(int) = 0.0722]	
Coverage of independent reflections	99.5%	
Absorption correction	Multi-Scan	
Max. and min. transmission	0.9210 and 0.8800	
Structure solution technique	direct methods	
Structure solution program	XT, VERSION 2014/5	
Refinement method	Full-matrix least-squares on F^2	
Refinement program	SHELXL-2017/1 (Sheldrick, 2017)	
Function minimized	$\Sigma\ w(F_o^2 - F_c^2)^2$	
Data / restraints / parameters	11183 / 2 / 595	
Goodness-of-fit on F^2	1.009	
Final R indices	7984 data; I>2σ(I)	R1 = 0.0623, wR2 = 0.1444
	all data	R1 = 0.0974, wR2 = 0.1663
Weighting scheme	$w=1/[\sigma^2(F_o^2)+(0.0847P)^2]$ where $P=(F_o^2+2F_c^2)/3$	
Absolute structure parameter	0.012(14)	
Largest diff. peak and hole	0.991 and -0.630 eÅ^{-3}	
R.M.S. deviation from mean	0.093 eÅ^{-3}	

Table 15. Bond lengths (Å) for Complex 22.

B1-F3	1.381(9)	B1-F2	1.388(9)
B1-F4	1.403(8)	B1-F1	1.471(9)
B2-F8	1.342(12)	B2-F6	1.342(11)
B2-F7	1.367(12)	B2-F5	1.418(11)
C1-C2	1.379(12)	C1-C6	1.397(12)
C1-H1	0.95	C2-C3	1.386(14)
C2-H2	0.95	C3-C4	1.386(15)
C3-H3	0.95	C4-C5	1.375(12)
C4-H4	0.95	C5-C6	1.400(10)
C5-H5	0.95	C6-C7	1.479(10)
C7-O1	1.243(8)	C7-C8	1.491(10)
C8-C9	1.553(10)	C8-H8A	0.99
C8-H8B	0.99	C9-C10	1.518(11)
C9-P1	1.856(8)	C9-H9	1.0
C10-N1	1.352(8)	C10-C11	1.388(10)
C11-C12	1.366(11)	C11-H11	0.95
C12-C13	1.392(10)	C12-H12	0.95
C13-C14	1.387(10)	C13-H13	0.95
C14-N1	1.350(10)	C14-C15	1.512(9)
C15-C16	1.515(11)	C15-P2	1.882(8)
C15-H15	1.0	C16-C17	1.513(11)
C16-H16A	0.99	C16-H16B	0.99
C17-O2	1.235(9)	C17-C18	1.474(11)
C18-C23	1.399(12)	C18-C19	1.410(11)
C19-C20	1.390(13)	C19-H19	0.95
C20-C21	1.350(15)	C20-H20	0.95
C21-C22	1.418(13)	C21-H21	0.95
C22-C23	1.390(11)	C22-H22	0.95
C23-H23	0.95	C24-C29	1.379(12)
C24-C25	1.402(10)	C24-P2	1.816(7)
C25-C26	1.385(12)	C25-H25	0.95
C26-C27	1.382(16)	C26-H26	0.95
C27-C28	1.376(15)	C27-H27	0.95
C28-C29	1.368(10)	C28-H28	0.95
C29-H29	0.95	C30-C35	1.374(11)
C30-C31	1.407(11)	C30-P2	1.822(8)

C31-C32	1.372(15)	C31-H31	0.95
C32-C33	1.360(12)	C32-H32	0.95
C33-C34	1.364(12)	C33-H33	0.95
C34-C35	1.382(13)	C34-H34	0.95
C35-H35	0.95	C36-C37	1.397(9)
C36-C41	1.405(10)	C36-P1	1.817(7)
C37-C38	1.389(11)	C37-H37	0.95
C38-C39	1.382(11)	C38-H38	0.95
C39-C40	1.384(11)	C39-H39	0.95
C40-C41	1.374(11)	C40-H40	0.95
C41-H41	0.95	C42-C43	1.375(10)
C42-C47	1.394(10)	C42-P1	1.821(8)
C43-C44	1.398(10)	C43-H43	0.95
C44-C45	1.386(11)	C44-H44	0.95
C45-C46	1.349(13)	C45-H45	0.95
C46-C47	1.392(12)	C46-H46	0.95
C47-H47	0.95	C48-Cl1	1.767(7)
C48-Cl2	1.774(9)	C48-H48A	0.99
C48-H48B	0.99	F1-Fe1	2.008(5)
Fe1-O2	2.161(5)	Fe1-N1	2.192(6)
Fe1-O1	2.218(5)	Fe1-P1	2.5143(19)
Fe1-P2	2.560(2)		

Table 16. Bond angles (°) for Complex 22.

F3-B1-F2	110.8(6)	F3-B1-F4	108.3(6)
F2-B1-F4	110.4(6)	F3-B1-F1	109.4(6)
F2-B1-F1	108.5(6)	F4-B1-F1	109.4(6)
F8-B2-F6	108.1(9)	F8-B2-F7	114.5(10)
F6-B2-F7	105.4(8)	F8-B2-F5	112.8(8)
F6-B2-F5	106.7(8)	F7-B2-F5	108.7(8)
C2-C1-C6	120.4(9)	C2-C1-H1	119.8
C6-C1-H1	119.8	C1-C2-C3	119.4(10)
C1-C2-H2	120.3	C3-C2-H2	120.3
C4-C3-C2	120.5(8)	C4-C3-H3	119.7
C2-C3-H3	119.7	C5-C4-C3	120.5(9)
C5-C4-H4	119.8	C3-C4-H4	119.8
C4-C5-C6	119.4(9)	C4-C5-H5	120.3
C6-C5-H5	120.3	C1-C6-C5	119.7(7)
C1-C6-C7	117.8(7)	C5-C6-C7	122.3(7)
O1-C7-C6	119.1(6)	O1-C7-C8	121.9(6)
C6-C7-C8	119.0(6)	C7-C8-C9	116.6(5)
C7-C8-H8A	108.1	C9-C8-H8A	108.1
C7-C8-H8B	108.1	C9-C8-H8B	108.1
H8A-C8-H8B	107.3	C10-C9-C8	111.8(6)
C10-C9-P1	108.9(4)	C8-C9-P1	114.4(5)
C10-C9-H9	107.1	C8-C9-H9	107.1
P1-C9-H9	107.1	N1-C10-C11	120.5(7)
N1-C10-C9	117.7(6)	C11-C10-C9	121.7(6)
C12-C11-C10	120.4(6)	C12-C11-H11	119.8
C10-C11-H11	119.8	C11-C12-C13	118.4(7)
C11-C12-H12	120.8	C13-C12-H12	120.8
C14-C13-C12	120.0(7)	C14-C13-H13	120.0
C12-C13-H13	120.0	N1-C14-C13	120.3(6)
N1-C14-C15	118.8(6)	C13-C14-C15	120.9(7)
C14-C15-C16	110.4(6)	C14-C15-P2	109.9(5)
C16-C15-P2	115.1(5)	C14-C15-H15	107.0
C16-C15-H15	107.0	P2-C15-H15	107.0
C17-C16-C15	117.8(6)	C17-C16-H16A	107.9
C15-C16-H16A	107.9	C17-C16-H16B	107.9
C15-C16-H16B	107.9	H16A-C16-H16B	107.2

O2-C17-C18	118.7(7)	O2-C17-C16	123.0(7)
C18-C17-C16	118.3(6)	C23-C18-C19	119.8(7)
C23-C18-C17	118.5(7)	C19-C18-C17	121.7(8)
C20-C19-C18	119.2(9)	C20-C19-H19	120.4
C18-C19-H19	120.4	C21-C20-C19	121.4(8)
C21-C20-H20	119.3	C19-C20-H20	119.3
C20-C21-C22	120.4(8)	C20-C21-H21	119.8
C22-C21-H21	119.8	C23-C22-C21	119.3(9)
C23-C22-H22	120.3	C21-C22-H22	120.3
C22-C23-C18	119.8(8)	C22-C23-H23	120.1
C18-C23-H23	120.1	C29-C24-C25	118.1(7)
C29-C24-P2	118.2(5)	C25-C24-P2	123.8(7)
C26-C25-C24	121.3(9)	C26-C25-H25	119.3
C24-C25-H25	119.3	C27-C26-C25	118.7(8)
C27-C26-H26	120.7	C25-C26-H26	120.7
C28-C27-C26	120.3(8)	C28-C27-H27	119.8
C26-C27-H27	119.8	C29-C28-C27	120.7(10)
C29-C28-H28	119.7	C27-C28-H28	119.7
C28-C29-C24	120.9(8)	C28-C29-H29	119.6
C24-C29-H29	119.6	C35-C30-C31	117.1(8)
C35-C30-P2	118.8(6)	C31-C30-P2	124.0(6)
C32-C31-C30	120.9(9)	C32-C31-H31	119.6
C30-C31-H31	119.6	C33-C32-C31	120.8(9)
C33-C32-H32	119.6	C31-C32-H32	119.6
C32-C33-C34	119.2(8)	C32-C33-H33	120.4
C34-C33-H33	120.4	C33-C34-C35	120.9(8)
C33-C34-H34	119.5	C35-C34-H34	119.5
C30-C35-C34	121.0(8)	C30-C35-H35	119.5
C34-C35-H35	119.5	C37-C36-C41	118.7(7)
C37-C36-P1	116.4(5)	C41-C36-P1	124.9(5)
C38-C37-C36	120.4(7)	C38-C37-H37	119.8
C36-C37-H37	119.8	C39-C38-C37	120.6(7)
C39-C38-H38	119.7	C37-C38-H38	119.7
C38-C39-C40	118.7(7)	C38-C39-H39	120.7
C40-C39-H39	120.7	C41-C40-C39	122.0(8)
C41-C40-H40	119.0	C39-C40-H40	119.0
C40-C41-C36	119.6(7)	C40-C41-H41	120.2
C36-C41-H41	120.2	C43-C42-C47	119.4(7)

C43-C42-P1	118.1(5)	C47-C42-P1	122.4(6)
C42-C43-C44	120.7(6)	C42-C43-H43	119.6
C44-C43-H43	119.6	C45-C44-C43	119.3(8)
C45-C44-H44	120.3	C43-C44-H44	120.3
C46-C45-C44	119.6(8)	C46-C45-H45	120.2
C44-C45-H45	120.2	C45-C46-C47	122.3(7)
C45-C46-H46	118.9	C47-C46-H46	118.9
C46-C47-C42	118.6(8)	C46-C47-H47	120.7
C42-C47-H47	120.7	Cl1-C48-Cl2	111.4(4)
Cl1-C48-H48A	109.3	Cl2-C48-H48A	109.3
Cl1-C48-H48B	109.3	Cl2-C48-H48B	109.3
H48A-C48-H48B	108.0	B1-F1-Fe1	132.0(4)
F1-Fe1-O2	97.05(18)	F1-Fe1-N1	175.6(2)
O2-Fe1-N1	86.5(2)	F1-Fe1-O1	92.88(18)
O2-Fe1-O1	169.8(2)	N1-Fe1-O1	83.5(2)
F1-Fe1-P1	104.07(15)	O2-Fe1-P1	97.95(15)
N1-Fe1-P1	77.83(16)	O1-Fe1-P1	81.73(14)
F1-Fe1-P2	99.86(14)	O2-Fe1-P2	80.09(15)
N1-Fe1-P2	78.22(16)	O1-Fe1-P2	96.03(15)
P1-Fe1-P2	156.04(7)	C14-N1-C10	120.2(6)
C14-N1-Fe1	119.6(4)	C10-N1-Fe1	120.1(5)
C7-O1-Fe1	137.4(5)	C17-O2-Fe1	140.1(5)
C36-P1-C42	106.0(3)	C36-P1-C9	102.5(3)
C42-P1-C9	104.2(3)	C36-P1-Fe1	121.1(2)
C42-P1-Fe1	124.6(2)	C9-P1-Fe1	93.2(2)
C24-P2-C30	105.0(3)	C24-P2-C15	105.2(3)
C30-P2-C15	101.9(3)	C24-P2-Fe1	118.8(3)
C30-P2-Fe1	128.8(2)	C15-P2-Fe1	91.4(2)

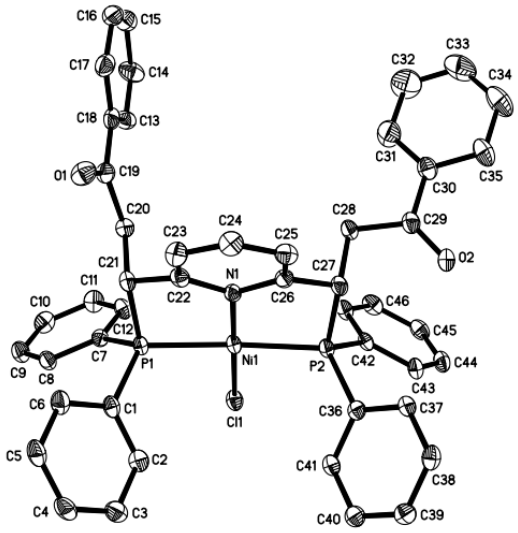

A red needle-like specimen of $C_{50}H_{45}BClF_4NNiO_3P_2$, approximate dimensions 0.020 mm x 0.040 mm x 0.280 mm, was used for the X-ray crystallographic analysis. The X-ray intensity data were measured (λ = 0.71073 Å). A total of 894 frames were collected. The total exposure time was 1.24 hours. The frames were integrated with the Bruker SAINT software package using a narrow-frame algorithm. The integration of the data using a monoclinic unit cell yielded a total of 69923 reflections to a maximum θ angle of 27.11° (0.78 Å resolution), of which 9770 were independent (average redundancy 7.157, completeness = 99.9%, Rint = 14.84%, Rsig = 8.32%) and 6465 (66.17%) were greater than 2σ(F2). The final cell constants of a = 40.340(3) Å, b = 9.5724(5) Å, c = 23.5603(15) Å, β = 103.664(2)°, volume = 8840.3(9) Å3, are based upon the refinement of the XYZ-centroids of 5630 reflections above 20 σ(I) with 4.525° < 2θ < 49.72°. Data were corrected for absorption effects using the Multi-Scan method (SADABS). The ratio of minimum to maximum apparent transmission was 0.867. The calculated minimum and maximum transmission coefficients (based on crystal size) are 0.8430 and 0.9870. The structure was solved and refined using the Bruker SHELXTL Software Package, using the space group C 1 2/c 1, with Z = 8 for the

formula unit, $C_{50}H_{45}BClF_4NNiO_3P_2$. The final anisotropic full-matrix least-squares refinement on F2 with 609 variables converged at R1 = 4.92%, for the observed data and wR2 = 12.36% for all data. The goodness-of-fit was 1.036. The largest peak in the final difference electron density synthesis was 0.649 e-/Å3 and the largest hole was -0.644 e-/Å3 with an RMS deviation of 0.091 e-/Å3. On the basis of the final model, the calculated density was 1.429 g/cm3 and F(000), 3936 e-.

Table 17. Sample and crystal data for Complex 29a'.

Identification code	leung1199m	
Chemical formula	$C_{50}H_{45}BClF_4NNiO_3P_2$	
Formula weight	950.78 g/mol	
Temperature	100(2) K	
Wavelength	0.71073 Å	
Crystal size	0.020 x 0.040 x 0.280 mm	
Crystal habit	red needle	
Crystal system	monoclinic	
Space group	C 1 2/c 1	
Unit cell dimensions	a = 40.340(3) Å	α = 90°
	b = 9.5724(5) Å	β = 103.664(2)°
	c = 23.5603(15) Å	γ = 90°
Volume	8840.3(9) $Å^3$	
Z	8	
Density (calculated)	1.429 g/cm^3	
Absorption coefficient	0.634 mm^{-1}	
F(000)	3936	

Table 18. Data collection and structure refinement for Complex 29a'.

Theta range for data collection	1.78 to 27.11°	
Index ranges	-51<=h<=51, -12<=k<=10, -30<=l<=30	
Reflections collected	69923	
Independent reflections	9770 [R(int) = 0.1484]	
Coverage of independent reflections	99.9%	
Absorption correction	Multi-Scan	
Max. and min. transmission	0.9870 and 0.8430	
Structure solution technique	direct methods	
Structure solution program	XT, VERSION 2018/2	
Refinement method	Full-matrix least-squares on F^2	
Refinement program	SHELXL-2018/3 (Sheldrick, 2018)	
Function minimized	$\Sigma\ w(F_o^2 - F_c^2)^2$	
Data / restraints / parameters	9770 / 137 / 609	
Goodness-of-fit on F^2	1.036	
Δ/σ_{max}	0.001	
Final R indices	6465 data; $I>2\sigma(I)$	R1 = 0.0492, wR2 = 0.1021
	all data	R1 = 0.0990, wR2 = 0.1236
Weighting scheme	$w=1/[\sigma^2(F_o^2)+(0.0419P)^2+14.0249P]$ where $P=(F_o^2+2F_c^2)/3$	
Largest diff. peak and hole	0.649 and -0.644 eÅ^{-3}	
R.M.S. deviation from mean	0.091 eÅ^{-3}	

Table 19. Bond lengths (Å) for Complex 29a'.

B1-F1	1.366(6)	B1-F4	1.369(5)
B1-F2	1.384(5)	B1-F3	1.404(5)
C1-C2	1.395(5)	C1-C6	1.398(4)
C1-P1	1.814(3)	C2-C3	1.392(4)
C3-C4	1.380(5)	C4-C5	1.379(5)
C5-C6	1.381(5)	C7-C12	1.391(4)
C7-C8	1.393(4)	C7-P1	1.808(3)
C8-C9	1.387(4)	C9-C10	1.386(5)
C10-C11	1.378(5)	C11-C12	1.389(4)
C13-C14	1.385(5)	C13-C18	1.387(5)
C14-C15	1.383(5)	C15-C16	1.389(5)
C16-C17	1.381(5)	C17-C18	1.389(5)
C18-C19	1.493(5)	C19-O1	1.221(4)
C19-C20	1.517(5)	C20-C21	1.533(4)
C21-C22	1.509(4)	C21-P1	1.844(3)
C22-N1	1.372(4)	C22-C23	1.380(4)
C23-C24	1.380(5)	C24-C25	1.373(5)
C25-C26	1.382(4)	C26-N1	1.362(4)
C26-C27	1.510(4)	C27-C28	1.546(4)
C27-P2	1.839(3)	C28-C29	1.509(4)
C29-O2	1.219(4)	C29-C30	1.491(5)
C30-C31	1.383(5)	C30-C35	1.391(5)
C31-C32	1.395(5)	C32-C33	1.369(6)
C33-C34	1.371(6)	C34-C35	1.382(5)
C36-C37	1.401(4)	C36-C41	1.405(4)
C36-P2	1.811(3)	C37-C38	1.380(4)
C38-C39	1.386(5)	C39-C40	1.387(4)
C40-C41	1.386(4)	C42-C47	1.391(4)
C42-C43	1.393(4)	C42-P2	1.807(3)
C43-C44	1.384(4)	C44-C45	1.384(5)
C45-C46	1.387(5)	C46-C47	1.383(5)
C48-C49	1.489(8)	C49-O3	1.218(10)
C49-C50	1.495(8)	C48A-C49A	1.494(8)
C49A-O3A	1.211(10)	C49A-C50A	1.489(8)
Cl1-Ni1	2.1471(9)	N1-Ni1	1.905(3)

Table 20. Bond angles (°) for Complex 29a'.

F1-B1-F4	111.2(4)	F1-B1-F2	111.7(4)
F4-B1-F2	108.7(3)	F1-B1-F3	108.0(3)
F4-B1-F3	109.6(4)	F2-B1-F3	107.6(4)
C2-C1-C6	119.1(3)	C2-C1-P1	119.2(2)
C6-C1-P1	121.8(3)	C3-C2-C1	119.9(3)
C4-C3-C2	120.1(3)	C5-C4-C3	120.5(3)
C4-C5-C6	119.9(3)	C5-C6-C1	120.5(3)
C12-C7-C8	120.0(3)	C12-C7-P1	118.0(2)
C8-C7-P1	122.1(2)	C9-C8-C7	119.9(3)
C10-C9-C8	119.7(3)	C11-C10-C9	120.6(3)
C10-C11-C12	120.0(3)	C11-C12-C7	119.7(3)
C14-C13-C18	120.3(3)	C15-C14-C13	119.8(3)
C14-C15-C16	120.1(3)	C17-C16-C15	120.0(3)
C16-C17-C18	120.2(3)	C13-C18-C17	119.6(3)
C13-C18-C19	122.0(3)	C17-C18-C19	118.3(3)
O1-C19-C18	121.3(3)	O1-C19-C20	121.0(3)
C18-C19-C20	117.8(3)	C19-C20-C21	113.2(3)
C22-C21-C20	110.1(3)	C22-C21-P1	104.8(2)
C20-C21-P1	111.4(2)	N1-C22-C23	121.2(3)
N1-C22-C21	116.2(3)	C23-C22-C21	122.4(3)
C24-C23-C22	119.5(3)	C25-C24-C23	119.6(3)
C24-C25-C26	119.3(3)	N1-C26-C25	121.8(3)
N1-C26-C27	117.2(3)	C25-C26-C27	121.0(3)
C26-C27-C28	108.9(3)	C26-C27-P2	106.2(2)
C28-C27-P2	114.1(2)	C29-C28-C27	112.1(3)
O2-C29-C30	121.1(3)	O2-C29-C28	121.1(3)
C30-C29-C28	117.7(3)	C31-C30-C35	119.4(3)
C31-C30-C29	122.6(3)	C35-C30-C29	117.9(3)
C30-C31-C32	119.9(4)	C33-C32-C31	120.0(4)
C32-C33-C34	120.3(4)	C33-C34-C35	120.4(4)
C34-C35-C30	119.9(4)	C37-C36-C41	119.0(3)
C37-C36-P2	121.6(2)	C41-C36-P2	119.4(2)
C38-C37-C36	120.3(3)	C37-C38-C39	120.5(3)
C38-C39-C40	119.7(3)	C41-C40-C39	120.6(3)
C40-C41-C36	119.9(3)	C47-C42-C43	119.6(3)
C47-C42-P2	118.8(2)	C43-C42-P2	121.6(2)

C44-C43-C42	120.0(3)	C45-C44-C43	120.0(3)
C44-C45-C46	120.3(3)	C47-C46-C45	119.9(3)
C46-C47-C42	120.2(3)	O3-C49-C48	121.0(7)
O3-C49-C50	120.8(7)	C48-C49-C50	118.1(8)
O3A-C49A-C50A	121.7(9)	O3A-C49A-C48A	121.3(8)
C50A-C49A-C48A	116.9(9)	C26-N1-C22	117.9(3)
C26-N1-Ni1	120.2(2)	C22-N1-Ni1	120.6(2)
N1-Ni1-Cl1	178.18(8)	N1-Ni1-P1	86.36(8)
Cl1-Ni1-P1	93.35(3)	N1-Ni1-P2	87.21(8)
Cl1-Ni1-P2	92.80(3)	P1-Ni1-P2	169.07(4)
C7-P1-C1	107.98(14)	C7-P1-C21	107.89(14)
C1-P1-C21	104.75(15)	C7-P1-Ni1	122.27(11)
C1-P1-Ni1	112.50(11)	C21-P1-Ni1	99.69(10)
C42-P2-C36	106.26(15)	C42-P2-C27	110.91(14)
C36-P2-C27	104.65(14)	C42-P2-Ni1	118.82(10)
C36-P2-Ni1	115.91(10)	C27-P2-Ni1	99.24(11)

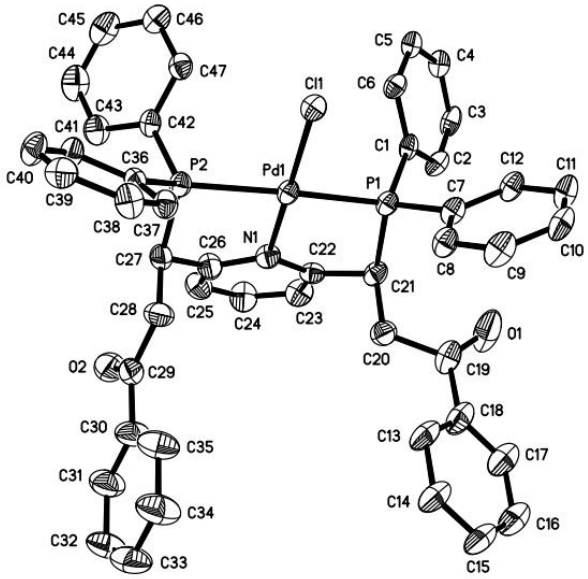

A yellow needle-like specimen of $C_{50}H_{48}Cl_2NO_3P_2Pd$, approximate dimensions 0.010 mm x 0.020 mm x 0.220 mm, was used for the X-ray crystallographic analysis. The X-ray intensity data were measured (λ = 0.71073 Å). A total of 219 frames were collected. The total exposure time was 0.85 hours. The frames were integrated with the Bruker SAINT software package using a narrow-frame algorithm. The integration of the data using a monoclinic unit cell yielded a total of 57247 reflections to a maximum θ angle of 28.72° (0.74 Å resolution), of which 11160 were independent (average redundancy 5.130, completeness = 99.8%, Rint = 16.59%, Rsig = 11.82%) and 6491 (58.16%) were greater than $2\sigma(F2)$. The final cell constants of a = 40.803(3) Å, b = 9.1948(5) Å, c = 23.6108(12) Å, β = 103.177(2)°, volume = 8625.0(8) Å3, are based upon the refinement of the XYZ-centroids of 4488 reflections above 20 $\sigma(I)$ with 4.794° < 2θ < 51.30°. Data were corrected for absorption effects using the Multi-Scan method (SADABS). The ratio of minimum to maximum apparent transmission was 0.682. The calculated minimum and maximum transmission coefficients (based on crystal size) are 0.8660 and 0.9930. The structure was solved and refined using the Bruker SHELXTL Software Package, using the space group C 1 2/c 1, with Z = 8 for the

formula unit, $C_{50}H_{48}Cl_2NO_3P_2Pd$. The final anisotropic full-matrix least-squares refinement on F2 with 622 variables converged at R1 = 6.90%, for the observed data and wR2 = 18.82% for all data. The goodness-of-fit was 1.045. The largest peak in the final difference electron density synthesis was 1.573 e-/Å3 and the largest hole was -1.565 e-/Å3 with an RMS deviation of 0.144 e-/Å3. On the basis of the final model, the calculated density was 1.463 g/cm3 and F(000), 3912 e-.

Table 21. Sample and crystal data for Complex 30a'.

Identification code	leung1170m	
Chemical formula	$C_{50}H_{48}Cl_2NO_3P_2Pd$	
Formula weight	950.13 g/mol	
Temperature	100(2) K	
Wavelength	0.71073 Å	
Crystal size	0.010 x 0.020 x 0.220 mm	
Crystal habit	yellow needle	
Crystal system	monoclinic	
Space group	C 1 2/c 1	
Unit cell dimensions	a = 40.803(3) Å	α = 90°
	b = 9.1948(5) Å	β = 103.177(2)°
	c = 23.6108(12) Å	γ = 90°
Volume	8625.0(8) $Å^3$	
Z	8	
Density (calculated)	1.463 g/cm^3	
Absorption coefficient	0.673 mm^{-1}	
F(000)	3912	

Table 22. Data collection and structure refinement for Complex 30a'.

Theta range for data collection	2.27 to 28.72°	
Index ranges	-51<=h<=54, -12<=k<=12, -31<=l<=31	
Reflections collected	57247	
Independent reflections	11160 [R(int) = 0.1659]	
Coverage of independent reflections	99.8%	
Absorption correction	Multi-Scan	
Max. and min. transmission	0.9930 and 0.8660	
Structure solution technique	direct methods	
Structure solution program	XT, VERSION 2014/5	
Refinement method	Full-matrix least-squares on F^2	
Refinement program	SHELXL-2018/3 (Sheldrick, 2018)	
Function minimized	$\Sigma\, w(F_o^2 - F_c^2)^2$	
Data / restraints / parameters	11160 / 614 / 622	
Goodness-of-fit on F^2	1.045	
Δ/σ_{max}	0.001	
Final R indices	6491 data; I>2σ(I)	R1 = 0.0690, wR2 = 0.1489
	all data	R1 = 0.1398, wR2 = 0.1882
Weighting scheme	$w=1/[\sigma^2(F_o^2)+(0.0731P)^2+26.6622P]$ where $P=(F_o^2+2F_c^2)/3$	
Largest diff. peak and hole	1.573 and -1.565 eÅ^{-3}	
R.M.S. deviation from mean	0.144 eÅ^{-3}	

Table 23. Bond lengths (Å) for Complex 30a'.

C1-C6	1.399(8)	C1-C2	1.404(7)
C1-P1	1.812(5)	C2-C3	1.382(8)
C2-H2	0.95	C3-C4	1.379(8)
C3-H3	0.95	C4-C5	1.396(7)
C4-H4	0.95	C5-C6	1.379(8)
C5-H5	0.95	C6-H6	0.95
C7-C12	1.392(8)	C7-C8	1.401(8)
C7-P1	1.804(6)	C8-C9	1.388(8)
C8-H8	0.95	C9-C10	1.383(9)
C9-H9	0.95	C10-C11	1.388(9)
C10-H10	0.95	C11-C12	1.390(8)
C11-H11	0.95	C12-H12	0.95
C13-C14	1.39	C13-C18	1.39
C13-H13	0.95	C14-C15	1.39
C14-H14	0.95	C15-C16	1.39
C15-H15	0.95	C16-C17	1.39
C16-H16	0.95	C17-C18	1.39
C17-H17	0.95	C18-C19	1.501(7)
C13A-C14A	1.39	C13A-C18A	1.39
C13A-H13A	0.95	C14A-C15A	1.39
C14A-H14A	0.95	C15A-C16A	1.39
C15A-H15A	0.95	C16A-C17A	1.39
C16A-H16A	0.95	C17A-C18A	1.39
C17A-H17A	0.95	C18A-C19	1.482(8)
C19-O1	1.226(8)	C19-C20	1.502(8)
C20-C21	1.541(8)	C20-H20A	0.99
C20-H20B	0.99	C21-C22	1.511(8)
C21-P1	1.843(6)	C21-H21	1.0
C22-N1	1.349(7)	C22-C23	1.393(8)
C23-C24	1.368(8)	C23-H23	0.95
C24-C25	1.381(9)	C24-H24	0.95
C25-C26	1.382(8)	C25-H25	0.95
C26-N1	1.361(7)	C26-C27	1.503(8)
C27-C28	1.554(8)	C27-P2	1.848(6)
C27-H27	1.0	C28-C29	1.515(9)
C28-H28A	0.99	C28-H28B	0.99

C29-O2	1.213(8)	C29-C30	1.466(7)
C29-C30A	1.514(8)	C30-C31	1.39
C30-C35	1.39	C31-C32	1.39
C31-H31	0.95	C32-C33	1.39
C32-H32	0.95	C33-C34	1.39
C33-H33	0.95	C34-C35	1.39
C34-H34	0.95	C35-H35	0.95
C30A-C31A	1.39	C30A-C35A	1.39
C31A-C32A	1.39	C31A-H31A	0.95
C32A-C33A	1.39	C32A-H32A	0.95
C33A-C34A	1.39	C33A-H33A	0.95
C34A-C35A	1.39	C34A-H34A	0.95
C35A-H35A	0.95	C36-C41	1.395(7)
C36-C37	1.399(7)	C36-P2	1.800(6)
C37-C38	1.387(8)	C37-H37	0.95
C38-C39	1.389(8)	C38-H38	0.95
C39-C40	1.378(8)	C39-H39	0.95
C40-C41	1.393(8)	C40-H40	0.95
C41-H41	0.95	C42-C47	1.397(8)
C42-C43	1.402(7)	C42-P2	1.805(5)
C43-C44	1.375(9)	C43-H43	0.95
C44-C45	1.379(10)	C44-H44	0.95
C45-C46	1.376(9)	C45-H45	0.95
C46-C47	1.391(8)	C46-H46	0.95
C47-H47	0.95	C48-C49	1.636(17)
C48-H48A	0.98	C48-H48B	0.98
C48-H48C	0.98	C49-C50	1.412(13)
C49-H49A	0.99	C49-H49B	0.99
C50-C51	1.415(12)	C50-H50A	0.99
C50-H50B	0.99	C51-C52	1.337(14)
C51-H51A	0.99	C51-H51B	0.99
C52-C53	1.655(13)	C52-H52A	0.99
C52-H52B	0.99	C53-H53A	0.98
C53-H53B	0.98	C53-H53C	0.98
Cl1-Pd1	2.2831(14)	N1-Pd1	2.051(5)
O3-H1O	0.969	O3-H2O	0.9493
P1-Pd1	2.2840(14)	P2-Pd1	2.3011(14)

Table 24. Bond angles (°) for Complex 30a'.

C6-C1-C2	119.7(5)	C6-C1-P1	118.4(4)
C2-C1-P1	121.9(4)	C3-C2-C1	119.4(5)
C3-C2-H2	120.3	C1-C2-H2	120.3
C4-C3-C2	120.6(5)	C4-C3-H3	119.7
C2-C3-H3	119.7	C3-C4-C5	120.5(5)
C3-C4-H4	119.8	C5-C4-H4	119.8
C6-C5-C4	119.6(5)	C6-C5-H5	120.2
C4-C5-H5	120.2	C5-C6-C1	120.2(5)
C5-C6-H6	119.9	C1-C6-H6	119.9
C12-C7-C8	120.0(5)	C12-C7-P1	120.8(4)
C8-C7-P1	119.2(4)	C9-C8-C7	119.3(5)
C9-C8-H8	120.4	C7-C8-H8	120.4
C10-C9-C8	120.5(6)	C10-C9-H9	119.8
C8-C9-H9	119.8	C9-C10-C11	120.6(5)
C9-C10-H10	119.7	C11-C10-H10	119.7
C10-C11-C12	119.5(6)	C10-C11-H11	120.3
C12-C11-H11	120.3	C11-C12-C7	120.2(5)
C11-C12-H12	119.9	C7-C12-H12	119.9
C14-C13-C18	120.0	C14-C13-H13	120.0
C18-C13-H13	120.0	C13-C14-C15	120.0
C13-C14-H14	120.0	C15-C14-H14	120.0
C16-C15-C14	120.0	C16-C15-H15	120.0
C14-C15-H15	120.0	C17-C16-C15	120.0
C17-C16-H16	120.0	C15-C16-H16	120.0
C16-C17-C18	120.0	C16-C17-H17	120.0
C18-C17-H17	120.0	C17-C18-C13	120.0
C17-C18-C19	120.3(9)	C13-C18-C19	119.7(10)
C14A-C13A-C18A	120.0	C14A-C13A-H13A	120.0
C18A-C13A-H13A	120.0	C13A-C14A-C15A	120.0
C13A-C14A-H14A	120.0	C15A-C14A-H14A	120.0
C16A-C15A-C14A	120.0	C16A-C15A-H15A	120.0
C14A-C15A-H15A	120.0	C17A-C16A-C15A	120.0
C17A-C16A-H16A	120.0	C15A-C16A-H16A	120.0
C16A-C17A-C18A	120.0	C16A-C17A-H17A	120.0
C18A-C17A-H17A	120.0	C17A-C18A-C13A	120.0
C17A-C18A-C19	114.1(17)	C13A-C18A-C19	125.3(17)

O1-C19-C18A	118.4(13)	O1-C19-C18	123.0(8)
O1-C19-C20	120.6(5)	C18A-C19-C20	120.9(14)
C18-C19-C20	116.3(8)	C19-C20-C21	114.3(5)
C19-C20-H20A	108.7	C21-C20-H20A	108.7
C19-C20-H20B	108.7	C21-C20-H20B	108.7
H20A-C20-H20B	107.6	C22-C21-C20	106.8(5)
C22-C21-P1	107.8(4)	C20-C21-P1	112.8(4)
C22-C21-H21	109.8	C20-C21-H21	109.8
P1-C21-H21	109.8	N1-C22-C23	120.7(5)
N1-C22-C21	116.7(5)	C23-C22-C21	122.3(5)
C24-C23-C22	119.0(5)	C24-C23-H23	120.5
C22-C23-H23	120.5	C23-C24-C25	119.5(6)
C23-C24-H24	120.3	C25-C24-H24	120.3
C24-C25-C26	120.4(6)	C24-C25-H25	119.8
C26-C25-H25	119.8	N1-C26-C25	119.3(5)
N1-C26-C27	116.3(5)	C25-C26-C27	124.4(5)
C26-C27-C28	109.8(5)	C26-C27-P2	107.5(4)
C28-C27-P2	110.0(4)	C26-C27-H27	109.9
C28-C27-H27	109.9	P2-C27-H27	109.9
C29-C28-C27	113.0(5)	C29-C28-H28A	109.0
C27-C28-H28A	109.0	C29-C28-H28B	109.0
C27-C28-H28B	109.0	H28A-C28-H28B	107.8
O2-C29-C30	119.2(6)	O2-C29-C30A	124.2(8)
O2-C29-C28	121.4(6)	C30-C29-C28	119.4(6)
C30A-C29-C28	113.8(8)	C31-C30-C35	120.0
C31-C30-C29	117.5(6)	C35-C30-C29	122.5(6)
C30-C31-C32	120.0	C30-C31-H31	120.0
C32-C31-H31	120.0	C31-C32-C33	120.0
C31-C32-H32	120.0	C33-C32-H32	120.0
C34-C33-C32	120.0	C34-C33-H33	120.0
C32-C33-H33	120.0	C33-C34-C35	120.0
C33-C34-H34	120.0	C35-C34-H34	120.0
C34-C35-C30	120.0	C34-C35-H35	120.0
C30-C35-H35	120.0	C31A-C30A-C35A	120.0
C31A-C30A-C29	120.4(10)	C35A-C30A-C29	119.6(10)
C30A-C31A-C32A	120.0	C30A-C31A-H31A	120.0
C32A-C31A-H31A	120.0	C33A-C32A-C31A	120.0
C33A-C32A-H32A	120.0	C31A-C32A-H32A	120.0

C34A-C33A-C32A	120.0	C34A-C33A-H33A	120.0
C32A-C33A-H33A	120.0	C33A-C34A-C35A	120.0
C33A-C34A-H34A	120.0	C35A-C34A-H34A	120.0
C34A-C35A-C30A	120.0	C34A-C35A-H35A	120.0
C30A-C35A-H35A	120.0	C41-C36-C37	119.8(5)
C41-C36-P2	121.7(4)	C37-C36-P2	118.5(4)
C38-C37-C36	119.7(5)	C38-C37-H37	120.1
C36-C37-H37	120.1	C37-C38-C39	120.3(5)
C37-C38-H38	119.9	C39-C38-H38	119.9
C40-C39-C38	120.1(5)	C40-C39-H39	119.9
C38-C39-H39	119.9	C39-C40-C41	120.4(5)
C39-C40-H40	119.8	C41-C40-H40	119.8
C40-C41-C36	119.7(5)	C40-C41-H41	120.2
C36-C41-H41	120.2	C47-C42-C43	118.7(5)
C47-C42-P2	118.6(4)	C43-C42-P2	122.6(5)
C44-C43-C42	120.4(6)	C44-C43-H43	119.8
C42-C43-H43	119.8	C43-C44-C45	120.1(6)
C43-C44-H44	119.9	C45-C44-H44	119.9
C46-C45-C44	120.7(6)	C46-C45-H45	119.6
C44-C45-H45	119.6	C45-C46-C47	119.6(6)
C45-C46-H46	120.2	C47-C46-H46	120.2
C46-C47-C42	120.4(5)	C46-C47-H47	119.8
C42-C47-H47	119.8	C49-C48-H48A	109.5
C49-C48-H48B	109.5	H48A-C48-H48B	109.5
C49-C48-H48C	109.5	H48A-C48-H48C	109.5
H48B-C48-H48C	109.5	C50-C49-C48	112.2(11)
C50-C49-H49A	109.2	C48-C49-H49A	109.2
C50-C49-H49B	109.2	C48-C49-H49B	109.2
H49A-C49-H49B	107.9	C49-C50-C51	128.1(13)
C49-C50-H50A	105.3	C51-C50-H50A	105.3
C49-C50-H50B	105.3	C51-C50-H50B	105.3
H50A-C50-H50B	106.0	C52-C51-C50	139.0(16)
C52-C51-H51A	102.3	C50-C51-H51A	102.3
C52-C51-H51B	102.3	C50-C51-H51B	102.3
H51A-C51-H51B	104.9	C51-C52-C53	115.2(12)
C51-C52-H52A	108.5	C53-C52-H52A	108.5
C51-C52-H52B	108.5	C53-C52-H52B	108.5
H52A-C52-H52B	107.5	C52-C53-H53A	109.5

C52-C53-H53B	109.5	H53A-C53-H53B	109.5
C52-C53-H53C	109.5	H53A-C53-H53C	109.5
H53B-C53-H53C	109.5	C22-N1-C26	120.4(5)
C22-N1-Pd1	117.9(4)	C26-N1-Pd1	119.3(4)
H1O-O3-H2O	106.3	C7-P1-C1	106.6(3)
C7-P1-C21	111.0(3)	C1-P1-C21	106.1(3)
C7-P1-Pd1	119.27(19)	C1-P1-Pd1	114.64(16)
C21-P1-Pd1	98.40(18)	C36-P2-C42	106.4(2)
C36-P2-C27	109.2(3)	C42-P2-C27	105.6(3)
C36-P2-Pd1	122.34(18)	C42-P2-Pd1	113.26(17)
C27-P2-Pd1	98.68(18)	N1-Pd1-Cl1	174.01(14)
N1-Pd1-P1	85.07(13)	Cl1-Pd1-P1	93.22(5)
N1-Pd1-P2	83.93(13)	Cl1-Pd1-P2	96.90(5)
P1-Pd1-P2	166.39(5)		

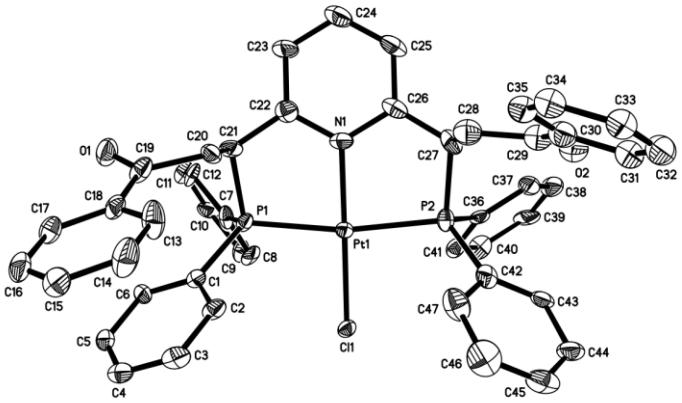

A colourless plate-like specimen of $C_{47}H_{39}Cl_2NO_2P_2Pt$, approximate dimensions 0.020 mm x 0.120 mm x 0.240 mm, was used for the X-ray crystallographic analysis. The X-ray intensity data were measured (λ = 0.71073 Å). A total of 245 frames were collected. The total exposure time was 0.68 hours. The frames were integrated with the Bruker SAINT software package using a narrow-frame algorithm. The integration of the data using a triclinic unit cell yielded a total of 56284 reflections to a maximum θ angle of 29.62° (0.72 Å resolution), of which 24509 were independent (average redundancy 2.296, completeness = 98.6%, Rint = 9.27%, Rsig = 16.31%) and 14695 (59.96%) were greater than $2\sigma(F2)$. The final cell constants of a = 9.1847(8) Å, b = 16.8496(14) Å, c = 28.854(2) Å, α = 81.344(2)°, β = 89.506(2)°, γ = 87.573(3)°, volume = 4410.6(6) Å3, are based upon the refinement of the XYZ-centroids of 8854 reflections above 20 $\sigma(I)$ with 4.895° < 2θ < 51.62°. Data were corrected for absorption effects using the Multi-Scan method (SADABS). The ratio of minimum to maximum apparent transmission was 0.691. The calculated minimum and maximum transmission coefficients (based on crystal size) are 0.4950 and 0.9350. The structure was solved and refined using the Bruker SHELXTL Software Package, using the space group P -1, with Z = 4 for the formula unit, $C_{47}H_{39}Cl_2NO_2P_2Pt$. The final anisotropic full-matrix least-squares refinement on F2 with 1355 variables converged at R1 = 11.22%, for the observed data and wR2 = 23.60% for all data. The goodness-of-fit was 1.135. The largest peak in the final

difference electron density synthesis was 3.309 e-/Å3 and the largest hole was -4.750 e-/Å3 with an RMS deviation of 0.262 e-/Å3. On the basis of the final model, the calculated density was 1.472 g/cm3 and F(000), 1944 e-.

Table 25. Sample and crystal data for Complex 31a'.

Identification code	leung1198m_sq	
Chemical formula	$C_{47}H_{39}Cl_2NO_2P_2Pt$	
Formula weight	977.72 g/mol	
Temperature	100(2) K	
Wavelength	0.71073 Å	
Crystal size	0.020 x 0.120 x 0.240 mm	
Crystal habit	Colou rless plate	
Crystal system	triclinic	
Space group	P -1	
Unit cell dimensions	a = 9.1847(8) Å	α = 81.344(2)°
	b = 16.8496(14) Å	β = 89.506(2)°
	c = 28.854(2) Å	γ = 87.573(3)°
Volume	4410.6(6) $Å^3$	
Z	4	
Density (calculated)	1.472 g/cm^3	
Absorption coefficient	3.412 mm^{-1}	
F(000)	1944	

Table 26. Data collection and structure refinement for Complex 31a'.

Theta range for data collection	2.02 to 29.62°	
Index ranges	-10<=h<=12, -23<=k<=23, -40<=l<=40	
Reflections collected	56284	
Independent reflections	24509 [R(int) = 0.0927]	
Coverage of independent reflections	98.6%	
Absorption correction	Multi-Scan	
Max. and min. transmission	0.9350 and 0.4950	
Structure solution technique	direct methods	
Structure solution program	XT, VERSION 2014/5	
Refinement method	Full-matrix least-squares on F^2	
Refinement program	SHELXL-2018/3 (Sheldrick, 2018)	
Function minimized	$\Sigma\, w(F_o^2 - F_c^2)^2$	
Data / restraints / parameters	24509 / 4271 / 1355	
Goodness-of-fit on F^2	1.135	
Δ/σ_{max}	0.004	
Final R indices	14695 data; I>2σ(I)	R1 = 0.1122, wR2 = 0.2112
	all data	R1 = 0.1778, wR2 = 0.2360
Weighting scheme	$w=1/[\sigma^2(F_o^2)+(0.0339P)^2+124.2488P]$ where $P=(F_o^2+2F_c^2)/3$	
Largest diff. peak and hole	3.309 and -4.750 eÅ^{-3}	
R.M.S. deviation from mean	0.262 eÅ^{-3}	

Table 27. Bond lengths (Å) for Complex 31a'.

C1-C2	1.39	C1-C6	1.39
C1-P1	1.794(6)	C2-C3	1.39
C2-H2	0.95	C3-C4	1.39
C3-H3	0.95	C4-C5	1.39
C4-H4	0.95	C5-C6	1.39
C5-H5	0.95	C6-H6	0.95
C7-C8	1.39	C7-C12	1.39
C7-P1	1.804(6)	C8-C9	1.39
C8-H8	0.95	C9-C10	1.39
C9-H9	0.95	C10-C11	1.39
C10-H10	0.95	C11-C12	1.39
C11-H11	0.95	C12-H12	0.95
C13-C14	1.39	C13-C18	1.39
C13-H13	0.95	C14-C15	1.39
C14-H14	0.95	C15-C16	1.39
C15-H15	0.95	C16-C17	1.39
C16-H16	0.95	C17-C18	1.39
C17-H17	0.95	C18-C19	1.498(15)
C19-O1	1.204(15)	C19-C20	1.527(18)
C20-C21	1.531(17)	C20-H20A	0.99
C20-H20B	0.99	C21-C22	1.500(14)
C21-P1	1.832(13)	C21-H21	1.0
C22-C23	1.39	C22-N1	1.39
C23-C24	1.39	C23-H23	0.95
C24-C25	1.39	C24-H24	0.95
C25-C26	1.39	C25-H25	0.95
C26-N1	1.39	C26-C27	1.494(15)
N1-Pt1	2.027(6)	C27-C28	1.51(2)
C27-C28A	1.51(2)	C27-P2	1.853(15)
C27-H27A	1.0	C27-H27	1.0
O2-C29	1.24(2)	C28-C29	1.49(2)
C28-H28A	0.99	C28-H28B	0.99
C29-C30	1.490(19)	C30-C31	1.39
C30-C35	1.39	C31-C32	1.39
C31-H31	0.95	C32-C33	1.39
C32-H32	0.95	C33-C34	1.39
C33-H33	0.95	C34-C35	1.39

C34-H34	0.95	C35-H35	0.95
O2A-C29A	1.24(2)	C28A-C29A	1.49(2)
C28A-H28C	0.99	C28A-H28D	0.99
C29A-C30A	1.492(19)	C30A-C35A	1.388(9)
C30A-C31A	1.393(9)	C31A-C32A	1.392(9)
C31A-H31A	0.95	C32A-C33A	1.391(9)
C32A-H32A	0.95	C33A-C34A	1.392(9)
C33A-H33A	0.95	C34A-C35A	1.393(9)
C34A-H34A	0.95	C35A-H35A	0.95
C36-C37	1.39	C36-C41	1.39
C36-P2	1.810(6)	C37-C38	1.39
C37-H37	0.95	C38-C39	1.39
C38-H38	0.95	C39-C40	1.39
C39-H39	0.95	C40-C41	1.39
C40-H40	0.95	C41-H41	0.95
C42-C43	1.39	C42-C47	1.39
C42-P2	1.805(7)	C43-C44	1.39
C43-H43	0.95	C44-C45	1.39
C44-H44	0.95	C45-C46	1.39
C45-H45	0.95	C46-C47	1.39
C46-H46	0.95	C47-H47	0.95
C48-C49	1.39	C48-C53	1.39
C48-P3	1.789(8)	C49-C50	1.39
C49-H49	0.95	C50-C51	1.39
C50-H50	0.95	C51-C52	1.39
C51-H51	0.95	C52-C53	1.39
C52-H52	0.95	C53-H53	0.95
C54-C55	1.39	C54-C59	1.39
C54-P3	1.807(8)	C55-C56	1.39
C55-H55	0.95	C56-C57	1.39
C56-H56	0.95	C57-C58	1.39
C57-H57	0.95	C58-C59	1.39
C58-H58	0.95	C59-H59	0.95
C60-C61	1.39	C60-C65	1.39
C60-H60	0.95	C61-C62	1.39
C61-H61	0.95	C62-C63	1.39
C62-H62	0.95	C63-C64	1.39
C63-H63	0.95	C64-C65	1.39

C64-H64	0.95	C65-C66	1.479(16)
C66-O3	1.211(18)	C66-C67	1.55(2)
C67-C68	1.523(19)	C67-H67A	0.99
C67-H67B	0.99	C68-C69	1.476(16)
C68-P3	1.883(16)	C68-H68	1.0
C69-C70	1.39	C69-N2	1.39
C70-C71	1.39	C70-H70	0.95
C71-C72	1.39	C71-H71	0.95
C72-C73	1.39	C72-H72	0.95
C73-N2	1.39	C73-C74	1.509(18)
N2-Pt2	2.013(9)	C74-C75	1.54(3)
C74-P4	1.87(2)	C74-H74	1.0
C75-C76	1.51(3)	C75-H75A	0.99
C75-H75B	0.99	C76-O4	1.22(2)
C76-C77	1.46(2)	C77-C78	1.39
C77-C82	1.39	C78-C79	1.39
C78-H78	0.95	C79-C80	1.39
C79-H79	0.95	C80-C81	1.39
C80-H80	0.95	C81-C82	1.39
C81-H81	0.95	C82-H82	0.95
C83-C84	1.39	C83-C88	1.39
C83-P4	1.811(9)	C84-C85	1.39
C84-H84	0.95	C85-C86	1.39
C85-H85	0.95	C86-C87	1.39
C86-H86	0.95	C87-C88	1.39
C87-H87	0.95	C88-H88	0.95
C89-C90	1.39	C89-C94	1.39
C89-P4	1.834(8)	C90-C91	1.39
C90-H90	0.95	C91-C92	1.39
C91-H91	0.95	C92-C93	1.39
C92-H92	0.95	C93-C94	1.39
C93-H93	0.95	C94-H94	0.95
P3-Pt2	2.272(5)	P4-Pt2	2.281(6)
Cl2-Pt2	2.303(7)	C48A-C49A	1.39
C48A-C53A	1.39	C48A-P3A	1.789(8)
C49A-C50A	1.39	C49A-H49A	0.95
C50A-C51A	1.39	C50A-H50A	0.95
C51A-C52A	1.39	C51A-H51A	0.95

C52A-C53A	1.39	C52A-H52A	0.95
C53A-H53A	0.95	C54A-C55A	1.39
C54A-C59A	1.39	C54A-P3A	1.811(8)
C55A-C56A	1.39	C55A-H55A	0.95
C56A-C57A	1.39	C56A-H56A	0.95
C57A-C58A	1.39	C57A-H57A	0.95
C58A-C59A	1.39	C58A-H58A	0.95
C59A-H59A	0.95	C60A-C61A	1.39
C60A-C65A	1.39	C60A-H60A	0.95
C61A-C62A	1.39	C61A-H61A	0.95
C62A-C63A	1.39	C62A-H62A	0.95
C63A-C64A	1.39	C63A-H63A	0.95
C64A-C65A	1.39	C64A-H64A	0.95
C65A-C66A	1.482(16)	C66A-O3A	1.212(18)
C66A-C67A	1.55(2)	C67A-C68A	1.525(19)
C67A-H67C	0.99	C67A-H67D	0.99
C68A-C69A	1.480(16)	C68A-P3A	1.881(16)
C68A-H68A	1.0	C69A-C70A	1.39
C69A-N2A	1.39	C70A-C71A	1.39
C70A-H70A	0.95	C71A-C72A	1.39
C71A-H71A	0.95	C72A-C73A	1.39
C72A-H72A	0.95	C73A-N2A	1.39
C73A-C74A	1.510(19)	C73A-H73A	1.0
N2A-Pt2A	2.017(9)	C74A-C75A	1.53(3)
C74A-P4A	1.88(2)	C74A-H74A	1.0
C75A-C76A	1.51(3)	C75A-H75C	0.99
C75A-H75D	0.99	C76A-O4A	1.22(2)
C76A-C77A	1.46(2)	C77A-C78A	1.39
C77A-C82A	1.39	C78A-C79A	1.39
C78A-H78A	0.95	C79A-C80A	1.39
C79A-H79A	0.95	C80A-C81A	1.39
C80A-H80A	0.95	C81A-C82A	1.39
C81A-H81A	0.95	C83A-C84A	1.39
C83A-C88A	1.39	C83A-P4A	1.808(9)
C84A-C85A	1.39	C84A-H84A	0.95
C85A-C86A	1.39	C85A-H85A	0.95
C86A-C87A	1.39	C86A-H86A	0.95
C87A-C88A	1.39	C87A-H87A	0.95

C88A-H88A	0.95	C89A-C90A	1.39
C89A-C94A	1.39	C89A-P4A	1.831(8)
C90A-C91A	1.39	C90A-H90A	0.95
C91A-C92A	1.39	C91A-H91A	0.95
C92A-C93A	1.39	C92A-H92A	0.95
C93A-C94A	1.39	C93A-H93A	0.95
C94A-H94A	0.95	P3A-Pt2A	2.271(6)
P4A-Pt2A	2.280(6)	Cl2A-Pt2A	2.296(7)
Cl1-Pt1	2.290(3)	P1-Pt1	2.274(3)
P2-Pt1	2.279(3)		

Table 28. Bond angles (°) for Complex 31a'.

C2-C1-C6	120.0	C2-C1-P1	118.1(4)
C6-C1-P1	121.9(4)	C1-C2-C3	120.0
C1-C2-H2	120.0	C3-C2-H2	120.0
C4-C3-C2	120.0	C4-C3-H3	120.0
C2-C3-H3	120.0	C3-C4-C5	120.0
C3-C4-H4	120.0	C5-C4-H4	120.0
C4-C5-C6	120.0	C4-C5-H5	120.0
C6-C5-H5	120.0	C5-C6-C1	120.0
C5-C6-H6	120.0	C1-C6-H6	120.0
C8-C7-C12	120.0	C8-C7-P1	117.7(4)
C12-C7-P1	122.2(4)	C7-C8-C9	120.0
C7-C8-H8	120.0	C9-C8-H8	120.0
C8-C9-C10	120.0	C8-C9-H9	120.0
C10-C9-H9	120.0	C11-C10-C9	120.0
C11-C10-H10	120.0	C9-C10-H10	120.0
C10-C11-C12	120.0	C10-C11-H11	120.0
C12-C11-H11	120.0	C11-C12-C7	120.0
C11-C12-H12	120.0	C7-C12-H12	120.0
C14-C13-C18	120.0	C14-C13-H13	120.0
C18-C13-H13	120.0	C13-C14-C15	120.0
C13-C14-H14	120.0	C15-C14-H14	120.0
C16-C15-C14	120.0	C16-C15-H15	120.0
C14-C15-H15	120.0	C15-C16-C17	120.0
C15-C16-H16	120.0	C17-C16-H16	120.0
C18-C17-C16	120.0	C18-C17-H17	120.0
C16-C17-H17	120.0	C17-C18-C13	120.0
C17-C18-C19	117.9(8)	C13-C18-C19	122.1(8)
O1-C19-C18	121.5(12)	O1-C19-C20	118.8(13)
C18-C19-C20	119.7(10)	C19-C20-C21	112.5(11)
C19-C20-H20A	109.1	C21-C20-H20A	109.1
C19-C20-H20B	109.1	C21-C20-H20B	109.1
H20A-C20-H20B	107.8	C22-C21-C20	111.2(10)
C22-C21-P1	109.0(8)	C20-C21-P1	111.0(8)
C22-C21-H21	108.5	C20-C21-H21	108.5
P1-C21-H21	108.5	C23-C22-N1	120.0
C23-C22-C21	123.0(7)	N1-C22-C21	116.3(7)

C22-C23-C24	120.0	C22-C23-H23	120.0
C24-C23-H23	120.0	C25-C24-C23	120.0
C25-C24-H24	120.0	C23-C24-H24	120.0
C24-C25-C26	120.0	C24-C25-H25	120.0
C26-C25-H25	120.0	C25-C26-N1	120.0
C25-C26-C27	122.7(8)	N1-C26-C27	115.9(8)
C26-N1-C22	120.0	C26-N1-Pt1	118.9(4)
C22-N1-Pt1	118.8(4)	C26-C27-C28	110.(2)
C26-C27-C28A	109.(2)	C26-C27-P2	109.8(9)
C28-C27-P2	118.(4)	C28A-C27-P2	114.(4)
C26-C27-H27A	107.8	C28A-C27-H27A	107.8
P2-C27-H27A	107.8	C26-C27-H27	106.3
C28-C27-H27	106.3	P2-C27-H27	106.3
C29-C28-C27	113.1(18)	C29-C28-H28A	109.0
C27-C28-H28A	109.0	C29-C28-H28B	109.0
C27-C28-H28B	109.0	H28A-C28-H28B	107.8
O2-C29-C30	121.8(16)	O2-C29-C28	120.9(16)
C30-C29-C28	117.0(15)	C31-C30-C35	120.0
C31-C30-C29	118.0(11)	C35-C30-C29	122.0(11)
C30-C31-C32	120.0	C30-C31-H31	120.0
C32-C31-H31	120.0	C33-C32-C31	120.0
C33-C32-H32	120.0	C31-C32-H32	120.0
C32-C33-C34	120.0	C32-C33-H33	120.0
C34-C33-H33	120.0	C35-C34-C33	120.0
C35-C34-H34	120.0	C33-C34-H34	120.0
C34-C35-C30	120.0	C34-C35-H35	120.0
C30-C35-H35	120.0	C29A-C28A-C27	116.6(18)
C29A-C28A-H28C	108.1	C27-C28A-H28C	108.1
C29A-C28A-H28D	108.1	C27-C28A-H28D	108.1
H28C-C28A-H28D	107.3	O2A-C29A-C28A	120.7(16)
O2A-C29A-C30A	121.4(16)	C28A-C29A-C30A	117.7(15)
C35A-C30A-C31A	120.3(10)	C35A-C30A-C29A	122.3(12)
C31A-C30A-C29A	117.0(13)	C32A-C31A-C30A	119.7(11)
C32A-C31A-H31A	120.1	C30A-C31A-H31A	120.1
C33A-C32A-C31A	119.6(12)	C33A-C32A-H32A	120.2
C31A-C32A-H32A	120.2	C32A-C33A-C34A	120.5(12)
C32A-C33A-H33A	119.7	C34A-C33A-H33A	119.7
C33A-C34A-C35A	119.4(11)	C33A-C34A-H34A	120.3

C35A-C34A-H34A	120.3	C30A-C35A-C34A	120.0(11)
C30A-C35A-H35A	120.0	C34A-C35A-H35A	120.0
C37-C36-C41	120.0	C37-C36-P2	121.4(5)
C41-C36-P2	118.6(5)	C36-C37-C38	120.0
C36-C37-H37	120.0	C38-C37-H37	120.0
C39-C38-C37	120.0	C39-C38-H38	120.0
C37-C38-H38	120.0	C40-C39-C38	120.0
C40-C39-H39	120.0	C38-C39-H39	120.0
C39-C40-C41	120.0	C39-C40-H40	120.0
C41-C40-H40	120.0	C40-C41-C36	120.0
C40-C41-H41	120.0	C36-C41-H41	120.0
C43-C42-C47	120.0	C43-C42-P2	121.9(5)
C47-C42-P2	117.5(5)	C44-C43-C42	120.0
C44-C43-H43	120.0	C42-C43-H43	120.0
C45-C44-C43	120.0	C45-C44-H44	120.0
C43-C44-H44	120.0	C44-C45-C46	120.0
C44-C45-H45	120.0	C46-C45-H45	120.0
C47-C46-C45	120.0	C47-C46-H46	120.0
C45-C46-H46	120.0	C46-C47-C42	120.0
C46-C47-H47	120.0	C42-C47-H47	120.0
C49-C48-C53	120.0	C49-C48-P3	117.9(6)
C53-C48-P3	122.0(6)	C48-C49-C50	120.0
C48-C49-H49	120.0	C50-C49-H49	120.0
C51-C50-C49	120.0	C51-C50-H50	120.0
C49-C50-H50	120.0	C50-C51-C52	120.0
C50-C51-H51	120.0	C52-C51-H51	120.0
C53-C52-C51	120.0	C53-C52-H52	120.0
C51-C52-H52	120.0	C52-C53-C48	120.0
C52-C53-H53	120.0	C48-C53-H53	120.0
C55-C54-C59	120.0	C55-C54-P3	117.7(6)
C59-C54-P3	122.1(6)	C56-C55-C54	120.0
C56-C55-H55	120.0	C54-C55-H55	120.0
C55-C56-C57	120.0	C55-C56-H56	120.0
C57-C56-H56	120.0	C56-C57-C58	120.0
C56-C57-H57	120.0	C58-C57-H57	120.0
C59-C58-C57	120.0	C59-C58-H58	120.0
C57-C58-H58	120.0	C58-C59-C54	120.0
C58-C59-H59	120.0	C54-C59-H59	120.0

C61-C60-C65	120.0	C61-C60-H60	120.0
C65-C60-H60	120.0	C62-C61-C60	120.0
C62-C61-H61	120.0	C60-C61-H61	120.0
C61-C62-C63	120.0	C61-C62-H62	120.0
C63-C62-H62	120.0	C64-C63-C62	120.0
C64-C63-H63	120.0	C62-C63-H63	120.0
C65-C64-C63	120.0	C65-C64-H64	120.0
C63-C64-H64	120.0	C64-C65-C60	120.0
C64-C65-C66	116.3(10)	C60-C65-C66	123.7(10)
O3-C66-C65	122.3(15)	O3-C66-C67	118.4(15)
C65-C66-C67	118.5(13)	C68-C67-C66	111.2(14)
C68-C67-H67A	109.4	C66-C67-H67A	109.4
C68-C67-H67B	109.4	C66-C67-H67B	109.4
H67A-C67-H67B	108.0	C69-C68-C67	113.8(13)
C69-C68-P3	106.5(9)	C67-C68-P3	110.0(12)
C69-C68-H68	108.8	C67-C68-H68	108.8
P3-C68-H68	108.8	C70-C69-N2	120.0
C70-C69-C68	121.8(9)	N2-C69-C68	117.7(9)
C69-C70-C71	120.0	C69-C70-H70	120.0
C71-C70-H70	120.0	C72-C71-C70	120.0
C72-C71-H71	120.0	C70-C71-H71	120.0
C73-C72-C71	120.0	C73-C72-H72	120.0
C71-C72-H72	120.0	C72-C73-N2	120.0
C72-C73-C74	120.5(11)	N2-C73-C74	118.9(11)
C73-N2-C69	120.0	C73-N2-Pt2	118.1(6)
C69-N2-Pt2	118.3(6)	C73-C74-C75	110.2(14)
C73-C74-P4	106.8(11)	C75-C74-P4	110.5(15)
C73-C74-H74	109.8	C75-C74-H74	109.8
P4-C74-H74	109.8	C76-C75-C74	113.1(17)
C76-C75-H75A	109.0	C74-C75-H75A	109.0
C76-C75-H75B	109.0	C74-C75-H75B	109.0
H75A-C75-H75B	107.8	O4-C76-C77	122.2(17)
O4-C76-C75	119.(2)	C77-C76-C75	119.1(15)
C78-C77-C82	120.0	C78-C77-C76	121.0(11)
C82-C77-C76	119.0(11)	C77-C78-C79	120.0
C77-C78-H78	120.0	C79-C78-H78	120.0
C80-C79-C78	120.0	C80-C79-H79	120.0
C78-C79-H79	120.0	C81-C80-C79	120.0

C81-C80-H80	120.0	C79-C80-H80	120.0
C80-C81-C82	120.0	C80-C81-H81	120.0
C82-C81-H81	120.0	C81-C82-C77	120.0
C81-C82-H82	120.0	C77-C82-H82	120.0
C84-C83-C88	120.0	C84-C83-P4	117.3(7)
C88-C83-P4	122.4(7)	C85-C84-C83	120.0
C85-C84-H84	120.0	C83-C84-H84	120.0
C86-C85-C84	120.0	C86-C85-H85	120.0
C84-C85-H85	120.0	C85-C86-C87	120.0
C85-C86-H86	120.0	C87-C86-H86	120.0
C88-C87-C86	120.0	C88-C87-H87	120.0
C86-C87-H87	120.0	C87-C88-C83	120.0
C87-C88-H88	120.0	C83-C88-H88	120.0
C90-C89-C94	120.0	C90-C89-P4	118.7(7)
C94-C89-P4	121.2(7)	C89-C90-C91	120.0
C89-C90-H90	120.0	C91-C90-H90	120.0
C92-C91-C90	120.0	C92-C91-H91	120.0
C90-C91-H91	120.0	C91-C92-C93	120.0
C91-C92-H92	120.0	C93-C92-H92	120.0
C92-C93-C94	120.0	C92-C93-H93	120.0
C94-C93-H93	120.0	C93-C94-C89	120.0
C93-C94-H94	120.0	C89-C94-H94	120.0
C48-P3-C54	109.4(6)	C48-P3-C68	110.5(7)
C54-P3-C68	107.2(7)	C48-P3-Pt2	116.2(5)
C54-P3-Pt2	114.0(5)	C68-P3-Pt2	98.8(5)
C83-P4-C89	107.5(7)	C83-P4-C74	112.5(8)
C89-P4-C74	105.0(8)	C83-P4-Pt2	116.5(5)
C89-P4-Pt2	114.2(5)	C74-P4-Pt2	100.6(6)
N2-Pt2-P3	85.4(3)	N2-Pt2-P4	85.7(4)
P3-Pt2-P4	168.6(3)	N2-Pt2-Cl2	177.6(7)
P3-Pt2-Cl2	94.0(3)	P4-Pt2-Cl2	94.5(3)
C49A-C48A-C53A	120.0	C49A-C48A-P3A	118.8(7)
C53A-C48A-P3A	121.2(7)	C48A-C49A-C50A	120.0
C48A-C49A-H49A	120.0	C50A-C49A-H49A	120.0
C51A-C50A-C49A	120.0	C51A-C50A-H50A	120.0
C49A-C50A-H50A	120.0	C50A-C51A-C52A	120.0
C50A-C51A-H51A	120.0	C52A-C51A-H51A	120.0
C51A-C52A-C53A	120.0	C51A-C52A-H52A	120.0

C53A-C52A-H52A	120.0	C52A-C53A-C48A	120.0
C52A-C53A-H53A	120.0	C48A-C53A-H53A	120.0
C55A-C54A-C59A	120.0	C55A-C54A-P3A	116.6(7)
C59A-C54A-P3A	123.4(7)	C56A-C55A-C54A	120.0
C56A-C55A-H55A	120.0	C54A-C55A-H55A	120.0
C55A-C56A-C57A	120.0	C55A-C56A-H56A	120.0
C57A-C56A-H56A	120.0	C58A-C57A-C56A	120.0
C58A-C57A-H57A	120.0	C56A-C57A-H57A	120.0
C57A-C58A-C59A	120.0	C57A-C58A-H58A	120.0
C59A-C58A-H58A	120.0	C58A-C59A-C54A	120.0
C58A-C59A-H59A	120.0	C54A-C59A-H59A	120.0
C61A-C60A-C65A	120.0	C61A-C60A-H60A	120.0
C65A-C60A-H60A	120.0	C60A-C61A-C62A	120.0
C60A-C61A-H61A	120.0	C62A-C61A-H61A	120.0
C63A-C62A-C61A	120.0	C63A-C62A-H62A	120.0
C61A-C62A-H62A	120.0	C62A-C63A-C64A	120.0
C62A-C63A-H63A	120.0	C64A-C63A-H63A	120.0
C65A-C64A-C63A	120.0	C65A-C64A-H64A	120.0
C63A-C64A-H64A	120.0	C64A-C65A-C60A	120.0
C64A-C65A-C66A	115.7(10)	C60A-C65A-C66A	124.2(10)
O3A-C66A-C65A	121.9(15)	O3A-C66A-C67A	118.9(15)
C65A-C66A-C67A	119.1(13)	C68A-C67A-C66A	112.7(14)
C68A-C67A-H67C	109.0	C66A-C67A-H67C	109.0
C68A-C67A-H67D	109.0	C66A-C67A-H67D	109.0
H67C-C67A-H67D	107.8	C69A-C68A-C67A	113.2(14)
C69A-C68A-P3A	106.9(9)	C67A-C68A-P3A	110.2(12)
C69A-C68A-H68A	108.8	C67A-C68A-H68A	108.8
P3A-C68A-H68A	108.8	C70A-C69A-N2A	120.0
C70A-C69A-C68A	121.5(9)	N2A-C69A-C68A	117.1(9)
C69A-C70A-C71A	120.0	C69A-C70A-H70A	120.0
C71A-C70A-H70A	120.0	C70A-C71A-C72A	120.0
C70A-C71A-H71A	120.0	C72A-C71A-H71A	120.0
C73A-C72A-C71A	120.0	C73A-C72A-H72A	120.0
C71A-C72A-H72A	120.0	C72A-C73A-N2A	120.0
C72A-C73A-C74A	120.6(11)	N2A-C73A-C74A	118.0(11)
C72A-C73A-H73A	94.0	N2A-C73A-H73A	94.0
C74A-C73A-H73A	94.0	C73A-N2A-C69A	120.0
C73A-N2A-Pt2A	118.7(6)	C69A-N2A-Pt2A	119.1(6)

C73A-C74A-C75A	110.5(15)	C73A-C74A-P4A	105.8(11)
C75A-C74A-P4A	109.3(15)	C73A-C74A-H74A	110.4
C75A-C74A-H74A	110.4	P4A-C74A-H74A	110.4
C76A-C75A-C74A	113.8(18)	C76A-C75A-H75C	108.8
C74A-C75A-H75C	108.8	C76A-C75A-H75D	108.8
C74A-C75A-H75D	108.8	H75C-C75A-H75D	107.7
O4A-C76A-C77A	121.4(18)	O4A-C76A-C75A	120.(2)
C77A-C76A-C75A	118.2(16)	C78A-C77A-C82A	120.0
C78A-C77A-C76A	120.4(11)	C82A-C77A-C76A	119.5(11)
C77A-C78A-C79A	120.0	C77A-C78A-H78A	120.0
C79A-C78A-H78A	120.0	C80A-C79A-C78A	120.0
C80A-C79A-H79A	120.0	C78A-C79A-H79A	120.0
C79A-C80A-C81A	120.0	C79A-C80A-H80A	120.0
C81A-C80A-H80A	120.0	C82A-C81A-C80A	120.0
C82A-C81A-H81A	120.0	C80A-C81A-H81A	120.0
C81A-C82A-C77A	120.0	C84A-C83A-C88A	120.0
C84A-C83A-P4A	118.3(7)	C88A-C83A-P4A	121.7(7)
C83A-C84A-C85A	120.0	C83A-C84A-H84A	120.0
C85A-C84A-H84A	120.0	C86A-C85A-C84A	120.0
C86A-C85A-H85A	120.0	C84A-C85A-H85A	120.0
C85A-C86A-C87A	120.0	C85A-C86A-H86A	120.0
C87A-C86A-H86A	120.0	C88A-C87A-C86A	120.0
C88A-C87A-H87A	120.0	C86A-C87A-H87A	120.0
C87A-C88A-C83A	120.0	C87A-C88A-H88A	120.0
C83A-C88A-H88A	120.0	C90A-C89A-C94A	120.0
C90A-C89A-P4A	119.0(7)	C94A-C89A-P4A	121.0(7)
C89A-C90A-C91A	120.0	C89A-C90A-H90A	120.0
C91A-C90A-H90A	120.0	C92A-C91A-C90A	120.0
C92A-C91A-H91A	120.0	C90A-C91A-H91A	120.0
C91A-C92A-C93A	120.0	C91A-C92A-H92A	120.0
C93A-C92A-H92A	120.0	C94A-C93A-C92A	120.0
C94A-C93A-H93A	120.0	C92A-C93A-H93A	120.0
C93A-C94A-C89A	120.0	C93A-C94A-H94A	120.0
C89A-C94A-H94A	120.0	C48A-P3A-C54A	108.4(7)
C48A-P3A-C68A	110.0(7)	C54A-P3A-C68A	108.6(7)
C48A-P3A-Pt2A	117.2(5)	C54A-P3A-Pt2A	112.6(5)
C68A-P3A-Pt2A	99.5(6)	C83A-P4A-C89A	107.6(7)
C83A-P4A-C74A	110.9(8)	C89A-P4A-C74A	103.8(8)

C83A-P4A-Pt2A	118.6(6)	C89A-P4A-Pt2A	114.6(5)
C74A-P4A-Pt2A	100.1(6)	N2A-Pt2A-P3A	85.0(4)
N2A-Pt2A-P4A	85.3(4)	P3A-Pt2A-P4A	169.4(3)
N2A-Pt2A-Cl2A	178.4(8)	P3A-Pt2A-Cl2A	94.9(3)
P4A-Pt2A-Cl2A	94.9(3)	C1-P1-C7	107.2(4)
C1-P1-C21	109.9(5)	C7-P1-C21	108.6(5)
C1-P1-Pt1	118.0(3)	C7-P1-Pt1	113.3(3)
C21-P1-Pt1	99.3(4)	C42-P2-C36	107.4(4)
C42-P2-C27	112.9(6)	C36-P2-C27	106.0(5)
C42-P2-Pt1	115.1(3)	C36-P2-Pt1	115.9(3)
C27-P2-Pt1	99.1(4)	N1-Pt1-P1	85.2(2)
N1-Pt1-P2	85.5(2)	P1-Pt1-P2	169.60(12)
N1-Pt1-Cl1	179.5(2)	P1-Pt1-Cl1	94.35(11)
P2-Pt1-Cl1	94.92(12)		

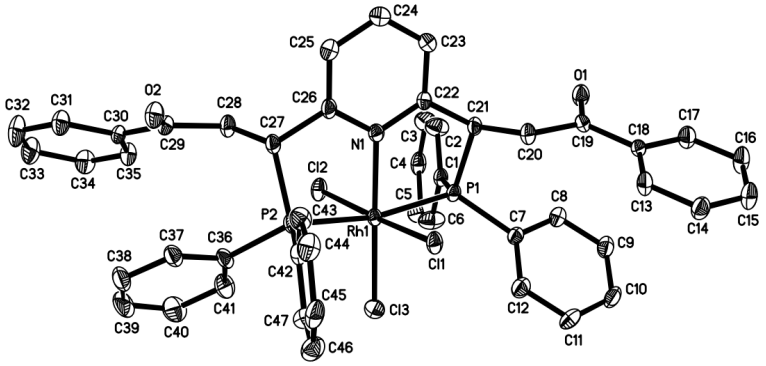

An orange prism-like specimen of $C_{47}H_{39}Cl_3NO_2P_2Rh$, approximate dimensions 0.040 mm x 0.080 mm x 0.160 mm, was used for the X-ray crystallographic analysis. The X-ray intensity data were measured (λ = 0.71073 Å). A total of 402 frames were collected. The total exposure time was 1.12 hours. The frames were integrated with the Bruker SAINT software package using a narrow-frame algorithm. The integration of the data using a monoclinic unit cell yielded a total of 69060 reflections to a maximum θ angle of 31.03° (0.69 Å resolution), of which 18648 were independent (average redundancy 3.703, completeness = 97.2%, Rint = 6.11%, Rsig = 5.97%) and 13726 (73.61%) were greater than $2\sigma(F2)$. The final cell constants of a = 37.8690(11) Å, b = 13.5343(4) Å, c = 27.4698(9) Å, β = 121.4089(12)°, volume = 12016.1(6) Å3, are based upon the refinement of the XYZ-centroids of 9873 reflections above 20 $\sigma(I)$ with $4.832° < 2\theta < 61.96°$. Data were corrected for absorption effects using the Multi-Scan method (SADABS). The ratio of minimum to maximum apparent transmission was 0.857. The calculated minimum and maximum transmission coefficients (based on crystal size) are 0.8900 and 0.9710. The structure was solved and refined using the Bruker SHELXTL Software Package, using the space group C 1 2/c 1, with Z = 12 for the formula unit, $C_{47}H_{39}Cl_3NO_2P_2Rh$. The final anisotropic full-matrix least-squares refinement on F2 with 759 variables converged at R1 = 4.60%, for the observed data and wR2 = 11.03% for all data. The goodness-of-fit was 1.047. The largest peak in the final difference electron

density synthesis was 1.009 e-/Å3 and the largest hole was -1.041 e-/Å3 with an RMS deviation of 0.118 e-/Å3. On the basis of the final model, the calculated density was 1.527 g/cm3 and F(000), 5640 e-.

Table 29. Sample and crystal data for Complex 32a.

Identification code	leung1196m	
Chemical formula	$C_{47}H_{39}Cl_3NO_2P_2Rh$	
Formula weight	920.99 g/mol	
Temperature	100(2) K	
Wavelength	0.71073 Å	
Crystal size	0.040 x 0.080 x 0.160 mm	
Crystal habit	orange prism	
Crystal system	monoclinic	
Space group	C 1 2/c 1	
Unit cell dimensions	a = 37.8690(11) Å	α = 90°
	b = 13.5343(4) Å	β = 121.4089(12)°
	c = 27.4698(9) Å	γ = 90°
Volume	12016.1(6) $Å^3$	
Z	12	
Density (calculated)	1.527 g/cm^3	
Absorption coefficient	0.748 mm^{-1}	
F(000)	5640	

Table 30. Data collection and structure refinement for Complex 32a.

Theta range for data collection	1.52 to 31.03°	
Index ranges	-53<=h<=54, -18<=k<=19, -39<=l<=38	
Reflections collected	69060	
Independent reflections	18648 [R(int) = 0.0611]	
Coverage of independent reflections	97.2%	
Absorption correction	Multi-Scan	
Max. and min. transmission	0.9710 and 0.8900	
Structure solution technique	direct methods	
Structure solution program	XT, VERSION 2014/5	
Refinement method	Full-matrix least-squares on F^2	
Refinement program	SHELXL-2018/3 (Sheldrick, 2018)	
Function minimized	$\Sigma\ w(F_o^2 - F_c^2)^2$	
Data / restraints / parameters	18648 / 0 / 759	
Goodness-of-fit on F^2	1.047	
Δ/σ_{max}	0.003	
Final R indices	13726 data; I>2σ(I)	R1 = 0.0460, wR2 = 0.0938
	all data	R1 = 0.0772, wR2 = 0.1103
Weighting scheme	$w=1/[\sigma^2(F_o^2)+(0.0211P)^2+53.1815P]$ where $P=(F_o^2+2F_c^2)/3$	
Largest diff. peak and hole	1.009 and -1.041 $eÅ^{-3}$	
R.M.S. deviation from mean	0.118 $eÅ^{-3}$	

Table 31. Bond lengths (Å) for Complex 32a.

C1-C2	1.379(4)	C1-C6	1.386(4)
C1-P1	1.811(3)	C2-C3	1.391(4)
C2-H2	0.95	C3-C4	1.372(5)
C3-H3	0.95	C4-C5	1.377(5)
C4-H4	0.95	C5-C6	1.386(4)
C5-H5	0.95	C6-H6	0.95
C7-C12	1.391(4)	C7-C8	1.399(4)
C7-P1	1.823(3)	C8-C9	1.387(4)
C8-H8	0.95	C9-C10	1.379(4)
C9-H9	0.95	C10-C11	1.385(5)
C10-H10	0.95	C11-C12	1.396(4)
C11-H11	0.95	C12-H12	0.95
C13-C14	1.385(4)	C13-C18	1.392(4)
C13-H13	0.95	C14-C15	1.380(4)
C14-H14	0.95	C15-C16	1.391(4)
C15-H15	0.95	C16-C17	1.388(4)
C16-H16	0.95	C17-C18	1.396(4)
C17-H17	0.95	C18-C19	1.490(4)
C19-O1	1.213(3)	C19-C20	1.516(4)
C20-C21	1.547(4)	C20-H20A	0.99
C20-H20B	0.99	C21-C22	1.517(4)
C21-P1	1.872(3)	C21-H21	1.0
C22-N1	1.357(3)	C22-C23	1.393(4)
C23-C24	1.383(4)	C23-H23	0.95
C24-C25	1.382(4)	C24-H24	0.95
C25-C26	1.383(4)	C25-H25	0.95
C26-N1	1.360(4)	C26-C27	1.518(4)
C27-C28	1.545(4)	C27-P2	1.861(3)
C27-H27	1.0	C28-C29	1.513(4)
C28-H28A	0.99	C28-H28B	0.99
C29-O2	1.214(3)	C29-C30	1.492(4)
C30-C35	1.393(4)	C30-C31	1.396(4)
C31-C32	1.379(4)	C31-H31	0.95
C32-C33	1.392(5)	C32-H32	0.95
C33-C34	1.376(4)	C33-H33	0.95
C34-C35	1.375(4)	C34-H34	0.95

C35-H35	0.95	C36-C41	1.388(4)
C36-C37	1.395(4)	C36-P2	1.809(3)
C37-C38	1.388(4)	C37-H37	0.95
C38-C39	1.373(5)	C38-H38	0.95
C39-C40	1.389(5)	C39-H39	0.95
C40-C41	1.398(4)	C40-H40	0.95
C41-H41	0.95	C42-C43	1.375(4)
C42-C47	1.402(4)	C42-P2	1.815(3)
C43-C44	1.390(4)	C43-H43	0.95
C44-C45	1.378(5)	C44-H44	0.95
C45-C46	1.391(5)	C45-H45	0.95
C46-C47	1.386(4)	C46-H46	0.95
C47-H47	0.95	C48-C53	1.387(4)
C48-C49	1.399(4)	C48-P3	1.814(3)
C49-C50	1.386(4)	C49-H49	0.95
C50-C51	1.374(4)	C50-H50	0.95
C51-C52	1.383(5)	C51-H51	0.95
C52-C53	1.401(4)	C52-H52	0.95
C53-H53	0.95	C54-C55	1.388(4)
C54-C59	1.392(4)	C54-P3	1.813(3)
C55-C56	1.388(4)	C55-H55	0.95
C56-C57	1.382(4)	C56-H56	0.95
C57-C58	1.378(4)	C57-H57	0.95
C58-C59	1.392(4)	C58-H58	0.95
C59-H59	0.95	C60-C65	1.390(4)
C60-C61	1.392(4)	C60-H60	0.95
C61-C62	1.374(5)	C61-H61	0.95
C62-C63	1.386(4)	C62-H62	0.95
C63-C64	1.382(4)	C63-H63	0.95
C64-C65	1.388(4)	C64-H64	0.95
C65-C66	1.485(4)	C66-O3	1.220(3)
C66-C67	1.512(4)	C67-C68	1.544(4)
C67-H67A	0.99	C67-H67B	0.99
C68-C69	1.518(4)	C68-P3	1.863(3)
C68-H68	1.0	C69-N2	1.359(3)
C69-C70	1.382(4)	C70-C71	1.382(4)
C70-H70	0.95	C71-H71	0.95
Cl1-Rh1	2.3506(7)	Cl2-Rh1	2.3412(7)

Cl3-Rh1	2.3349(7)	Cl4-Rh2	2.3508(6)
Cl5-Rh2	2.3347(10)	N1-Rh1	2.059(2)
N2-Rh2	2.066(3)	P1-Rh1	2.2980(8)
P2-Rh1	2.3127(8)	P3-Rh2	2.3087(7)

Table 32. Bond angles (°) for Complex 32a.

C2-C1-C6	118.5(3)	C2-C1-P1	124.9(2)
C6-C1-P1	116.4(2)	C1-C2-C3	120.4(3)
C1-C2-H2	119.8	C3-C2-H2	119.8
C4-C3-C2	120.7(3)	C4-C3-H3	119.6
C2-C3-H3	119.6	C3-C4-C5	119.4(3)
C3-C4-H4	120.3	C5-C4-H4	120.3
C4-C5-C6	120.0(3)	C4-C5-H5	120.0
C6-C5-H5	120.0	C1-C6-C5	121.0(3)
C1-C6-H6	119.5	C5-C6-H6	119.5
C12-C7-C8	119.8(3)	C12-C7-P1	121.5(2)
C8-C7-P1	118.7(2)	C9-C8-C7	120.2(3)
C9-C8-H8	119.9	C7-C8-H8	119.9
C10-C9-C8	119.8(3)	C10-C9-H9	120.1
C8-C9-H9	120.1	C9-C10-C11	120.3(3)
C9-C10-H10	119.9	C11-C10-H10	119.9
C10-C11-C12	120.5(3)	C10-C11-H11	119.7
C12-C11-H11	119.7	C7-C12-C11	119.2(3)
C7-C12-H12	120.4	C11-C12-H12	120.4
C14-C13-C18	120.6(3)	C14-C13-H13	119.7
C18-C13-H13	119.7	C15-C14-C13	120.2(3)
C15-C14-H14	119.9	C13-C14-H14	119.9
C14-C15-C16	120.3(3)	C14-C15-H15	119.9
C16-C15-H15	119.9	C17-C16-C15	119.3(3)
C17-C16-H16	120.3	C15-C16-H16	120.3
C16-C17-C18	121.0(3)	C16-C17-H17	119.5
C18-C17-H17	119.5	C13-C18-C17	118.6(3)
C13-C18-C19	123.5(3)	C17-C18-C19	117.9(3)
O1-C19-C18	121.0(3)	O1-C19-C20	120.4(3)
C18-C19-C20	118.6(2)	C19-C20-C21	112.0(2)
C19-C20-H20A	109.2	C21-C20-H20A	109.2
C19-C20-H20B	109.2	C21-C20-H20B	109.2

H20A-C20-H20B	107.9	C22-C21-C20	111.4(2)
C22-C21-P1	110.19(18)	C20-C21-P1	112.05(18)
C22-C21-H21	107.7	C20-C21-H21	107.7
P1-C21-H21	107.7	N1-C22-C23	120.8(3)
N1-C22-C21	120.6(2)	C23-C22-C21	118.6(2)
C24-C23-C22	119.8(3)	C24-C23-H23	120.1
C22-C23-H23	120.1	C25-C24-C23	118.9(3)
C25-C24-H24	120.5	C23-C24-H24	120.5
C24-C25-C26	119.8(3)	C24-C25-H25	120.1
C26-C25-H25	120.1	N1-C26-C25	121.2(3)
N1-C26-C27	120.4(2)	C25-C26-C27	118.4(3)
C26-C27-C28	111.6(2)	C26-C27-P2	109.39(19)
C28-C27-P2	112.58(19)	C26-C27-H27	107.7
C28-C27-H27	107.7	P2-C27-H27	107.7
C29-C28-C27	112.4(2)	C29-C28-H28A	109.1
C27-C28-H28A	109.1	C29-C28-H28B	109.1
C27-C28-H28B	109.1	H28A-C28-H28B	107.9
O2-C29-C30	120.8(3)	O2-C29-C28	120.1(3)
C30-C29-C28	119.1(2)	C35-C30-C31	118.3(3)
C35-C30-C29	123.8(3)	C31-C30-C29	117.9(3)
C32-C31-C30	120.9(3)	C32-C31-H31	119.5
C30-C31-H31	119.5	C31-C32-C33	119.7(3)
C31-C32-H32	120.2	C33-C32-H32	120.2
C34-C33-C32	119.8(3)	C34-C33-H33	120.1
C32-C33-H33	120.1	C35-C34-C33	120.5(3)
C35-C34-H34	119.8	C33-C34-H34	119.8
C34-C35-C30	120.8(3)	C34-C35-H35	119.6
C30-C35-H35	119.6	C41-C36-C37	120.1(3)
C41-C36-P2	121.2(2)	C37-C36-P2	118.7(2)
C38-C37-C36	120.3(3)	C38-C37-H37	119.9
C36-C37-H37	119.9	C39-C38-C37	119.5(3)
C39-C38-H38	120.3	C37-C38-H38	120.3
C38-C39-C40	121.0(3)	C38-C39-H39	119.5
C40-C39-H39	119.5	C39-C40-C41	119.7(3)
C39-C40-H40	120.1	C41-C40-H40	120.1
C36-C41-C40	119.3(3)	C36-C41-H41	120.4
C40-C41-H41	120.4	C43-C42-C47	119.2(3)
C43-C42-P2	124.5(2)	C47-C42-P2	116.2(2)

C42-C43-C44	120.8(3)	C42-C43-H43	119.6
C44-C43-H43	119.6	C45-C44-C43	120.2(3)
C45-C44-H44	119.9	C43-C44-H44	119.9
C44-C45-C46	119.5(3)	C44-C45-H45	120.2
C46-C45-H45	120.2	C47-C46-C45	120.4(3)
C47-C46-H46	119.8	C45-C46-H46	119.8
C46-C47-C42	119.8(3)	C46-C47-H47	120.1
C42-C47-H47	120.1	C53-C48-C49	120.3(3)
C53-C48-P3	121.3(2)	C49-C48-P3	118.3(2)
C50-C49-C48	119.9(3)	C50-C49-H49	120.1
C48-C49-H49	120.1	C51-C50-C49	119.6(3)
C51-C50-H50	120.2	C49-C50-H50	120.2
C50-C51-C52	121.2(3)	C50-C51-H51	119.4
C52-C51-H51	119.4	C51-C52-C53	119.7(3)
C51-C52-H52	120.2	C53-C52-H52	120.2
C48-C53-C52	119.2(3)	C48-C53-H53	120.4
C52-C53-H53	120.4	C55-C54-C59	118.8(3)
C55-C54-P3	123.2(2)	C59-C54-P3	117.9(2)
C56-C55-C54	120.6(3)	C56-C55-H55	119.7
C54-C55-H55	119.7	C57-C56-C55	120.1(3)
C57-C56-H56	119.9	C55-C56-H56	119.9
C58-C57-C56	119.8(3)	C58-C57-H57	120.1
C56-C57-H57	120.1	C57-C58-C59	120.3(3)
C57-C58-H58	119.8	C59-C58-H58	119.8
C58-C59-C54	120.2(3)	C58-C59-H59	119.9
C54-C59-H59	119.9	C65-C60-C61	120.2(3)
C65-C60-H60	119.9	C61-C60-H60	119.9
C62-C61-C60	120.1(3)	C62-C61-H61	119.9
C60-C61-H61	119.9	C61-C62-C63	120.1(3)
C61-C62-H62	120.0	C63-C62-H62	120.0
C64-C63-C62	119.9(3)	C64-C63-H63	120.1
C62-C63-H63	120.1	C63-C64-C65	120.8(3)
C63-C64-H64	119.6	C65-C64-H64	119.6
C64-C65-C60	118.9(3)	C64-C65-C66	118.7(3)
C60-C65-C66	122.3(3)	O3-C66-C65	120.5(3)
O3-C66-C67	121.4(3)	C65-C66-C67	118.1(2)
C66-C67-C68	112.0(2)	C66-C67-H67A	109.2
C68-C67-H67A	109.2	C66-C67-H67B	109.2

C68-C67-H67B	109.2	H67A-C67-H67B	107.9
C69-C68-C67	111.4(2)	C69-C68-P3	109.24(18)
C67-C68-P3	113.73(19)	C69-C68-H68	107.4
C67-C68-H68	107.4	P3-C68-H68	107.4
N2-C69-C70	121.0(3)	N2-C69-C68	120.2(2)
C70-C69-C68	118.8(3)	C69-C70-C71	119.9(3)
C69-C70-H70	120.1	C71-C70-H70	120.1
C70#1-C71-C70	118.8(4)	C70#1-C71-H71	120.6
C70-C71-H71	120.6	C22-N1-C26	119.5(2)
C22-N1-Rh1	120.19(18)	C26-N1-Rh1	120.29(18)
C69#1-N2-C69	119.3(3)	C69#1-N2-Rh2	120.33(17)
C69-N2-Rh2	120.33(16)	C1-P1-C7	101.61(13)
C1-P1-C21	108.83(13)	C7-P1-C21	106.82(12)
C1-P1-Rh1	115.13(9)	C7-P1-Rh1	123.95(9)
C21-P1-Rh1	99.78(9)	C36-P2-C42	101.72(13)
C36-P2-C27	105.55(13)	C42-P2-C27	107.11(13)
C36-P2-Rh1	125.17(10)	C42-P2-Rh1	116.15(9)
C27-P2-Rh1	99.65(9)	C54-P3-C48	101.29(13)
C54-P3-C68	105.49(13)	C48-P3-C68	106.24(13)
C54-P3-Rh2	117.39(9)	C48-P3-Rh2	124.98(10)
C68-P3-Rh2	99.62(9)	N1-Rh1-P1	84.57(7)
N1-Rh1-P2	83.91(7)	P1-Rh1-P2	168.47(3)
N1-Rh1-Cl3	178.14(7)	P1-Rh1-Cl3	93.74(3)
P2-Rh1-Cl3	97.79(3)	N1-Rh1-Cl2	89.18(6)
P1-Rh1-Cl2	91.61(3)	P2-Rh1-Cl2	88.24(3)
Cl3-Rh1-Cl2	90.10(3)	N1-Rh1-Cl1	88.02(6)
P1-Rh1-Cl1	88.63(3)	P2-Rh1-Cl1	90.95(3)
Cl3-Rh1-Cl1	92.71(3)	Cl2-Rh1-Cl1	177.15(3)
N2-Rh2-P3#1	83.491(18)	N2-Rh2-P3	83.491(18)
P3#1-Rh2-P3	166.98(4)	N2-Rh2-Cl5	180.0
P3#1-Rh2-Cl5	96.509(18)	P3-Rh2-Cl5	96.509(18)
N2-Rh2-Cl4#1	89.583(18)	P3#1-Rh2-Cl4#1	91.05(2)
P3-Rh2-Cl4#1	88.85(2)	Cl5-Rh2-Cl4#1	90.417(18)
N2-Rh2-Cl4	89.584(18)	P3#1-Rh2-Cl4	88.85(2)
P3-Rh2-Cl4	91.06(2)	Cl5-Rh2-Cl4	90.416(18)
Cl4#1-Rh2-Cl4	179.17(4)		

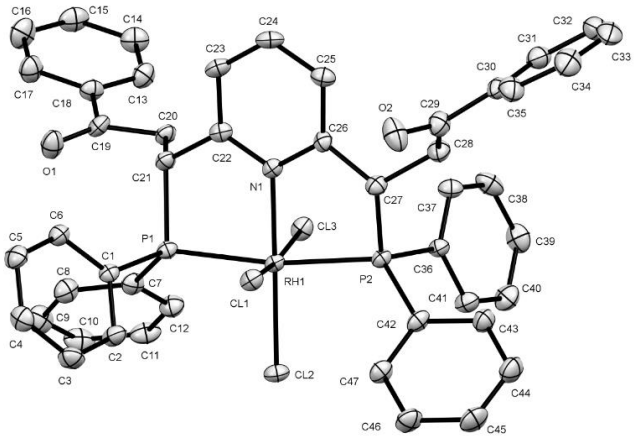

An orange plate-like specimen of $C_{47.50}H_{40}Cl_4NO_2P_2Rh$, approximate dimensions 0.020 mm x 0.220 mm x 0.280 mm, was used for the X-ray crystallographic analysis. The X-ray intensity data were measured ($\lambda = 0.71073$ Å). A total of 317 frames were collected. The total exposure time was 0.70 hours. The frames were integrated with the Bruker SAINT software package using a narrow-frame algorithm. The integration of the data using a monoclinic unit cell yielded a total of 79425 reflections to a maximum θ angle of 31.00° (0.69 Å resolution), of which 26899 were independent (average redundancy 2.953, completeness = 99.6%, Rint = 8.31%, Rsig = 10.37%) and 17992 (66.89%) were greater than $2\sigma(F2)$. The final cell constants of a = 30.9189(11) Å, b = 17.2300(8) Å, c = 16.3601(5) Å, $\beta = 103.6549(12)°$, volume = 8469.2(6) Å3, are based upon the refinement of the XYZ-centroids of 9832 reflections above 20 $\sigma(I)$ with $4.876° < 2\theta < 61.19°$. Data were corrected for absorption effects using the Multi-Scan method (SADABS). The ratio of minimum to maximum apparent transmission was 0.692. The calculated minimum and maximum transmission coefficients (based on crystal size) are 0.8130 and 0.9850. The structure was solved and refined using the Bruker SHELXTL Software Package, using the space group P 1 21/c 1, with Z = 8 for the formula unit, $C_{47.50}H_{40}Cl_4NO_2P_2Rh$. The final anisotropic full-matrix least-squares refinement on F2 with 1036 variables converged at R1 = 6.17%, for the observed data and wR2 =

15.87% for all data. The goodness-of-fit was 1.041. The largest peak in the final difference electron density synthesis was 1.616 e-/Å3 and the largest hole was -2.422 e-/Å3 with an RMS deviation of 0.144 e-/Å3. On the basis of the final model, the calculated density was 1.511 g/cm3 and F(000), 3928 e-.

Table 33. Sample and crystal data for Complex 32a'.

Identification code	leung1195m	
Chemical formula	$C_{47.50}H_{40}Cl_4NO_2P_2Rh$	
Formula weight	963.45 g/mol	
Temperature	100(2) K	
Wavelength	0.71073 Å	
Crystal size	0.020 x 0.220 x 0.280 mm	
Crystal habit	orange plate	
Crystal system	monoclinic	
Space group	P 1 21/c 1	
Unit cell dimensions	a = 30.9189(11) Å	α = 90°
	b = 17.2300(8) Å	β = 103.6549(12)°
	c = 16.3601(5) Å	γ = 90°
Volume	8469.2(6) $Å^3$	
Z	8	
Density (calculated)	1.511 g/cm^3	
Absorption coefficient	0.772 mm^{-1}	
F(000)	3928	

Table 34. Data collection and structure refinement for Complex 32a'.

Theta range for data collection	1.80 to 31.00°	
Index ranges	-44<=h<=44, -24<=k<=20, -18<=l<=23	
Reflections collected	79425	
Independent reflections	26899 [R(int) = 0.0831]	
Coverage of independent reflections	99.6%	
Absorption correction	Multi-Scan	
Max. and min. transmission	0.9850 and 0.8130	
Structure solution technique	direct methods	
Structure solution program	XT, VERSION 2014/5	
Refinement method	Full-matrix least-squares on F^2	
Refinement program	SHELXL-2018/3 (Sheldrick, 2018)	
Function minimized	$\Sigma\ w(F_o^2 - F_c^2)^2$	
Data / restraints / parameters	26899 / 0 / 1036	
Goodness-of-fit on F^2	1.041	
Δ/σ_{max}	0.002	
Final R indices	17992 data; $I>2\sigma(I)$	R1 = 0.0617, wR2 = 0.1359
	all data	R1 = 0.1046, wR2 = 0.1587
Weighting scheme	$w=1/[\sigma^2(F_o^2)+(0.0622P)^2+5.0575P]$ where $P=(F_o^2+2F_c^2)/3$	
Largest diff. peak and hole	1.616 and -2.422 eÅ^{-3}	
R.M.S. deviation from mean	0.144 eÅ^{-3}	

Table 35. Bond lengths (Å) for Complex 32a'.

C1-C6	1.380(5)	C1-C2	1.406(4)
C1-P1	1.816(4)	C2-C3	1.375(5)
C2-H2	0.95	C3-C4	1.389(6)
C3-H3	0.95	C4-C5	1.389(5)
C4-H4	0.95	C5-C6	1.384(5)
C5-H5	0.95	C6-H6	0.95
C7-C12	1.387(6)	C7-C8	1.403(5)
C7-P1	1.827(4)	C8-C9	1.390(6)
C8-H8	0.95	C9-C10	1.386(6)
C9-H9	0.95	C10-C11	1.389(6)
C10-H10	0.95	C11-C12	1.392(5)
C11-H11	0.95	C12-H12	0.95
C13-C18	1.386(5)	C13-C14	1.387(5)
C13-H13	0.95	C14-C15	1.387(6)
C14-H14	0.95	C15-C16	1.368(6)
C15-H15	0.95	C16-C17	1.389(6)
C16-H16	0.95	C17-C18	1.388(5)
C17-H17	0.95	C18-C19	1.499(5)
C19-O1	1.213(4)	C19-C20	1.511(5)
C20-C21	1.531(5)	C20-H20A	0.99
C20-H20B	0.99	C21-C22	1.518(5)
C21-P1	1.865(3)	C21-H21	1.0
C22-N1	1.354(4)	C22-C23	1.387(5)
C23-C24	1.376(5)	C23-H23	0.95
C24-C25	1.386(5)	C24-H24	0.95
C25-C26	1.380(5)	C25-H25	0.95
C26-N1	1.356(4)	C26-C27	1.514(5)
C27-C28	1.530(5)	C27-P2	1.847(4)
C27-H27	1.0	C28-C29	1.512(6)
C28-H28A	0.99	C28-H28B	0.99
C29-O2	1.225(5)	C29-C30	1.502(5)
C30-C35	1.382(6)	C30-C31	1.390(6)
C31-C32	1.403(5)	C31-H31	0.95
C32-C33	1.385(7)	C32-H32	0.95
C33-C34	1.387(6)	C33-H33	0.95
C34-C35	1.388(5)	C34-H34	0.95

C35-H35	0.95	C36-C41	1.391(5)
C36-C37	1.397(5)	C36-P2	1.808(4)
C37-C38	1.370(6)	C37-H37	0.95
C38-C39	1.383(6)	C38-H38	0.95
C39-C40	1.391(5)	C39-H39	0.95
C40-C41	1.375(6)	C40-H40	0.95
C41-H41	0.95	C42-C47	1.389(5)
C42-C43	1.398(5)	C42-P2	1.826(3)
C43-C44	1.398(5)	C43-H43	0.95
C44-C45	1.381(6)	C44-H44	0.95
C45-C46	1.386(6)	C45-H45	0.95
C46-C47	1.391(5)	C46-H46	0.95
C47-H47	0.95	C48-C53	1.389(5)
C48-C49	1.399(5)	C48-P3	1.826(3)
C49-C50	1.393(5)	C49-H49	0.95
C50-C51	1.371(6)	C50-H50	0.95
C51-C52	1.385(6)	C51-H51	0.95
C52-C53	1.395(6)	C52-H52	0.95
C53-H53	0.95	C54-C55	1.396(5)
C54-C59	1.406(5)	C54-P3	1.811(4)
C55-C56	1.380(6)	C55-H55	0.95
C56-C57	1.384(6)	C56-H56	0.95
C57-C58	1.391(6)	C57-H57	0.95
C58-C59	1.382(6)	C58-H58	0.95
C59-H59	0.95	C60-C61	1.391(5)
C60-C65	1.398(6)	C60-H60	0.95
C61-C62	1.385(6)	C61-H61	0.95
C62-C63	1.378(6)	C62-H62	0.95
C63-C64	1.394(5)	C63-H63	0.95
C64-C65	1.376(5)	C64-H64	0.95
C65-C66	1.500(5)	C66-O3	1.215(5)
C66-C67	1.508(5)	C67-C68	1.547(4)
C67-H67A	0.99	C67-H67B	0.99
C68-C69	1.515(5)	C68-P3	1.857(4)
C68-H68	1.0	C69-N2	1.361(5)
C69-C70	1.390(5)	C70-C71	1.370(5)
C70-H70	0.95	C71-C72	1.379(6)
C71-H71	0.95	C72-C73	1.394(5)

C72-H72	0.95	C73-N2	1.358(4)
C73-C74	1.516(5)	C74-C75	1.536(5)
C74-P4	1.859(3)	C74-H74	1.0
C75-C76	1.511(5)	C75-H75A	0.99
C75-H75B	0.99	C76-O4	1.214(5)
C76-C77	1.497(5)	C77-C82	1.379(6)
C77-C78	1.396(5)	C78-C79	1.379(6)
C78-H78	0.95	C79-C80	1.375(7)
C79-H79	0.95	C80-C81	1.392(6)
C80-H80	0.95	C81-C82	1.390(6)
C81-H81	0.95	C82-H82	0.95
C83-C88	1.392(6)	C83-C84	1.397(5)
C83-P4	1.817(4)	C84-C85	1.374(6)
C84-H84	0.95	C85-C86	1.395(6)
C85-H85	0.95	C86-C87	1.390(6)
C86-H86	0.95	C87-C88	1.387(6)
C87-H87	0.95	C88-H88	0.95
C89-C90	1.389(5)	C89-C94	1.408(5)
C89-P4	1.803(4)	C90-C91	1.380(6)
C90-H90	0.95	C91-C92	1.391(5)
C91-H91	0.95	C92-C93	1.379(6)
C92-H92	0.95	C93-C94	1.381(5)
C93-H93	0.95	C94-H94	0.95
C95-Cl9	1.744(6)	C95-Cl8	1.762(5)
C95-H95A	0.99	C95-H95B	0.99
Cl1-Rh1	2.3516(9)	Cl2-Rh1	2.3624(9)
Cl3-Rh1	2.3428(9)	Cl4-Rh2	2.3540(9)
Cl5-Rh2	2.3518(8)	Cl6-Rh2	2.3400(9)
N1-Rh1	2.041(3)	N2-Rh2	2.045(3)
P1-Rh1	2.3240(9)	P2-Rh1	2.3048(9)
P3-Rh2	2.3133(9)	P4-Rh2	2.2995(9)

Table 36. Bond angles (°) for Complex 32a'.

C6-C1-C2	118.7(3)	C6-C1-P1	124.8(3)
C2-C1-P1	116.4(3)	C3-C2-C1	120.3(4)
C3-C2-H2	119.8	C1-C2-H2	119.8
C2-C3-C4	120.4(3)	C2-C3-H3	119.8
C4-C3-H3	119.8	C5-C4-C3	119.6(4)
C5-C4-H4	120.2	C3-C4-H4	120.2
C6-C5-C4	119.9(4)	C6-C5-H5	120.1
C4-C5-H5	120.1	C1-C6-C5	121.1(3)
C1-C6-H6	119.4	C5-C6-H6	119.4
C12-C7-C8	119.2(4)	C12-C7-P1	121.0(3)
C8-C7-P1	119.7(3)	C9-C8-C7	119.7(4)
C9-C8-H8	120.2	C7-C8-H8	120.2
C10-C9-C8	120.7(4)	C10-C9-H9	119.6
C8-C9-H9	119.6	C9-C10-C11	119.7(4)
C9-C10-H10	120.1	C11-C10-H10	120.1
C10-C11-C12	119.9(4)	C10-C11-H11	120.1
C12-C11-H11	120.1	C7-C12-C11	120.7(4)
C7-C12-H12	119.6	C11-C12-H12	119.6
C18-C13-C14	120.2(4)	C18-C13-H13	119.9
C14-C13-H13	119.9	C15-C14-C13	119.3(4)
C15-C14-H14	120.4	C13-C14-H14	120.4
C16-C15-C14	120.7(4)	C16-C15-H15	119.7
C14-C15-H15	119.7	C15-C16-C17	120.4(4)
C15-C16-H16	119.8	C17-C16-H16	119.8
C18-C17-C16	119.3(4)	C18-C17-H17	120.3
C16-C17-H17	120.3	C13-C18-C17	120.1(3)
C13-C18-C19	122.4(3)	C17-C18-C19	117.5(3)
O1-C19-C18	120.8(3)	O1-C19-C20	121.6(3)
C18-C19-C20	117.5(3)	C19-C20-C21	112.3(3)
C19-C20-H20A	109.1	C21-C20-H20A	109.1
C19-C20-H20B	109.1	C21-C20-H20B	109.1
H20A-C20-H20B	107.9	C22-C21-C20	110.2(3)
C22-C21-P1	110.6(2)	C20-C21-P1	114.0(3)
C22-C21-H21	107.3	C20-C21-H21	107.3
P1-C21-H21	107.3	N1-C22-C23	120.7(3)
N1-C22-C21	120.7(3)	C23-C22-C21	118.6(3)

C24-C23-C22	119.5(3)	C24-C23-H23	120.3
C22-C23-H23	120.3	C23-C24-C25	119.2(3)
C23-C24-H24	120.4	C25-C24-H24	120.4
C26-C25-C24	119.9(3)	C26-C25-H25	120.1
C24-C25-H25	120.1	N1-C26-C25	120.3(3)
N1-C26-C27	118.1(3)	C25-C26-C27	121.4(3)
C26-C27-C28	114.5(3)	C26-C27-P2	111.6(2)
C28-C27-P2	117.9(3)	C26-C27-H27	103.6
C28-C27-H27	103.6	P2-C27-H27	103.6
C29-C28-C27	113.1(3)	C29-C28-H28A	109.0
C27-C28-H28A	109.0	C29-C28-H28B	109.0
C27-C28-H28B	109.0	H28A-C28-H28B	107.8
O2-C29-C30	120.2(4)	O2-C29-C28	121.2(3)
C30-C29-C28	118.4(3)	C35-C30-C31	119.9(3)
C35-C30-C29	117.7(4)	C31-C30-C29	122.3(4)
C30-C31-C32	120.3(4)	C30-C31-H31	119.9
C32-C31-H31	119.9	C33-C32-C31	118.5(4)
C33-C32-H32	120.8	C31-C32-H32	120.8
C32-C33-C34	121.6(4)	C32-C33-H33	119.2
C34-C33-H33	119.2	C33-C34-C35	119.0(4)
C33-C34-H34	120.5	C35-C34-H34	120.5
C30-C35-C34	120.6(4)	C30-C35-H35	119.7
C34-C35-H35	119.7	C41-C36-C37	118.6(3)
C41-C36-P2	118.3(3)	C37-C36-P2	122.7(3)
C38-C37-C36	120.2(4)	C38-C37-H37	119.9
C36-C37-H37	119.9	C37-C38-C39	120.9(3)
C37-C38-H38	119.5	C39-C38-H38	119.5
C38-C39-C40	119.4(4)	C38-C39-H39	120.3
C40-C39-H39	120.3	C41-C40-C39	119.8(4)
C41-C40-H40	120.1	C39-C40-H40	120.1
C40-C41-C36	121.0(3)	C40-C41-H41	119.5
C36-C41-H41	119.5	C47-C42-C43	119.1(3)
C47-C42-P2	119.9(3)	C43-C42-P2	120.9(3)
C44-C43-C42	120.0(3)	C44-C43-H43	120.0
C42-C43-H43	120.0	C45-C44-C43	120.5(4)
C45-C44-H44	119.8	C43-C44-H44	119.8
C44-C45-C46	119.6(3)	C44-C45-H45	120.2
C46-C45-H45	120.2	C45-C46-C47	120.4(4)

C45-C46-H46	119.8	C47-C46-H46	119.8
C42-C47-C46	120.4(3)	C42-C47-H47	119.8
C46-C47-H47	119.8	C53-C48-C49	118.5(3)
C53-C48-P3	121.2(3)	C49-C48-P3	120.1(3)
C50-C49-C48	120.1(3)	C50-C49-H49	120.0
C48-C49-H49	120.0	C51-C50-C49	120.8(4)
C51-C50-H50	119.6	C49-C50-H50	119.6
C50-C51-C52	119.8(4)	C50-C51-H51	120.1
C52-C51-H51	120.1	C51-C52-C53	119.9(4)
C51-C52-H52	120.0	C53-C52-H52	120.0
C48-C53-C52	120.9(4)	C48-C53-H53	119.6
C52-C53-H53	119.6	C55-C54-C59	118.5(4)
C55-C54-P3	120.1(3)	C59-C54-P3	121.3(3)
C56-C55-C54	120.8(4)	C56-C55-H55	119.6
C54-C55-H55	119.6	C55-C56-C57	120.2(4)
C55-C56-H56	119.9	C57-C56-H56	119.9
C56-C57-C58	120.0(4)	C56-C57-H57	120.0
C58-C57-H57	120.0	C59-C58-C57	120.1(4)
C59-C58-H58	120.0	C57-C58-H58	120.0
C58-C59-C54	120.4(4)	C58-C59-H59	119.8
C54-C59-H59	119.8	C61-C60-C65	119.4(4)
C61-C60-H60	120.3	C65-C60-H60	120.3
C62-C61-C60	120.6(4)	C62-C61-H61	119.7
C60-C61-H61	119.7	C63-C62-C61	119.7(4)
C63-C62-H62	120.2	C61-C62-H62	120.2
C62-C63-C64	120.1(4)	C62-C63-H63	120.0
C64-C63-H63	120.0	C65-C64-C63	120.4(4)
C65-C64-H64	119.8	C63-C64-H64	119.8
C64-C65-C60	119.7(3)	C64-C65-C66	122.2(3)
C60-C65-C66	118.1(3)	O3-C66-C65	120.6(3)
O3-C66-C67	121.8(3)	C65-C66-C67	117.6(3)
C66-C67-C68	114.0(3)	C66-C67-H67A	108.7
C68-C67-H67A	108.7	C66-C67-H67B	108.7
C68-C67-H67B	108.7	H67A-C67-H67B	107.6
C69-C68-C67	113.8(3)	C69-C68-P3	111.6(2)
C67-C68-P3	114.7(3)	C69-C68-H68	105.2
C67-C68-H68	105.2	P3-C68-H68	105.2
N2-C69-C70	120.9(3)	N2-C69-C68	119.1(3)

C70-C69-C68	119.8(3)	C71-C70-C69	119.7(4)
C71-C70-H70	120.1	C69-C70-H70	120.1
C70-C71-C72	119.7(3)	C70-C71-H71	120.1
C72-C71-H71	120.1	C71-C72-C73	119.3(3)
C71-C72-H72	120.3	C73-C72-H72	120.3
N2-C73-C72	121.0(3)	N2-C73-C74	120.6(3)
C72-C73-C74	118.4(3)	C73-C74-C75	110.8(3)
C73-C74-P4	109.7(2)	C75-C74-P4	114.3(3)
C73-C74-H74	107.2	C75-C74-H74	107.2
P4-C74-H74	107.2	C76-C75-C74	112.6(3)
C76-C75-H75A	109.1	C74-C75-H75A	109.1
C76-C75-H75B	109.1	C74-C75-H75B	109.1
H75A-C75-H75B	107.8	O4-C76-C77	121.0(3)
O4-C76-C75	120.8(4)	C77-C76-C75	118.2(3)
C82-C77-C78	118.9(4)	C82-C77-C76	123.4(3)
C78-C77-C76	117.7(4)	C79-C78-C77	121.0(4)
C79-C78-H78	119.5	C77-C78-H78	119.5
C80-C79-C78	119.4(4)	C80-C79-H79	120.3
C78-C79-H79	120.3	C79-C80-C81	120.7(4)
C79-C80-H80	119.7	C81-C80-H80	119.7
C82-C81-C80	119.3(4)	C82-C81-H81	120.3
C80-C81-H81	120.3	C77-C82-C81	120.6(4)
C77-C82-H82	119.7	C81-C82-H82	119.7
C88-C83-C84	118.7(4)	C88-C83-P4	122.4(3)
C84-C83-P4	118.9(3)	C85-C84-C83	120.8(4)
C85-C84-H84	119.6	C83-C84-H84	119.6
C84-C85-C86	120.5(4)	C84-C85-H85	119.8
C86-C85-H85	119.8	C87-C86-C85	119.2(4)
C87-C86-H86	120.4	C85-C86-H86	120.4
C88-C87-C86	120.3(4)	C88-C87-H87	119.8
C86-C87-H87	119.8	C87-C88-C83	120.6(4)
C87-C88-H88	119.7	C83-C88-H88	119.7
C90-C89-C94	118.7(3)	C90-C89-P4	124.5(3)
C94-C89-P4	116.5(3)	C91-C90-C89	121.0(3)
C91-C90-H90	119.5	C89-C90-H90	119.5
C90-C91-C92	120.0(4)	C90-C91-H91	120.0
C92-C91-H91	120.0	C93-C92-C91	119.5(4)
C93-C92-H92	120.3	C91-C92-H92	120.3

C92-C93-C94	121.0(3)	C92-C93-H93	119.5
C94-C93-H93	119.5	C93-C94-C89	119.8(4)
C93-C94-H94	120.1	C89-C94-H94	120.1
Cl9-C95-Cl8	111.4(3)	Cl9-C95-H95A	109.3
Cl8-C95-H95A	109.3	Cl9-C95-H95B	109.3
Cl8-C95-H95B	109.3	H95A-C95-H95B	108.0
C22-N1-C26	120.2(3)	C22-N1-Rh1	120.0(2)
C26-N1-Rh1	119.8(2)	C73-N2-C69	119.3(3)
C73-N2-Rh2	119.8(2)	C69-N2-Rh2	120.8(2)
C1-P1-C7	102.52(16)	C1-P1-C21	107.02(16)
C7-P1-C21	109.48(16)	C1-P1-Rh1	117.63(11)
C7-P1-Rh1	121.11(13)	C21-P1-Rh1	98.29(11)
C36-P2-C42	102.77(17)	C36-P2-C27	110.53(16)
C42-P2-C27	107.62(17)	C36-P2-Rh1	117.61(12)
C42-P2-Rh1	121.01(12)	C27-P2-Rh1	96.80(11)
C54-P3-C48	106.12(17)	C54-P3-C68	106.45(16)
C48-P3-C68	102.89(17)	C54-P3-Rh2	118.97(12)
C48-P3-Rh2	121.17(11)	C68-P3-Rh2	98.62(11)
C89-P4-C83	103.44(17)	C89-P4-C74	107.63(17)
C83-P4-C74	107.08(17)	C89-P4-Rh2	113.31(11)
C83-P4-Rh2	124.91(13)	C74-P4-Rh2	99.37(11)
N1-Rh1-P2	85.45(8)	N1-Rh1-P1	85.20(8)
P2-Rh1-P1	170.64(3)	N1-Rh1-Cl3	86.31(8)
P2-Rh1-Cl3	88.95(3)	P1-Rh1-Cl3	89.96(3)
N1-Rh1-Cl1	84.44(8)	P2-Rh1-Cl1	87.88(3)
P1-Rh1-Cl1	91.70(3)	Cl3-Rh1-Cl1	170.43(3)
N1-Rh1-Cl2	179.45(9)	P2-Rh1-Cl2	95.00(3)
P1-Rh1-Cl2	94.35(3)	Cl3-Rh1-Cl2	94.01(3)
Cl1-Rh1-Cl2	95.26(3)	N2-Rh2-P4	84.93(9)
N2-Rh2-P3	84.81(8)	P4-Rh2-P3	169.74(3)
N2-Rh2-Cl6	88.31(9)	P4-Rh2-Cl6	87.45(3)
P3-Rh2-Cl6	92.54(3)	N2-Rh2-Cl5	178.07(9)
P4-Rh2-Cl5	93.48(3)	P3-Rh2-Cl5	96.76(3)
Cl6-Rh2-Cl5	92.73(3)	N2-Rh2-Cl4	85.95(9)
P4-Rh2-Cl4	91.58(3)	P3-Rh2-Cl4	87.40(3)
Cl6-Rh2-Cl4	174.24(3)	Cl5-Rh2-Cl4	93.00(3)